Analyse théorique des distorsions dans la bande et en dehors de la bande de transmission pour les signaux à porteuses multiples : Impact conjoint des non-linéarités de l'amplificateur de puissance et effets de mémoire et prédistorsion

Ali Cheaito

Thèse

UNIVERSITE BRETAGNE LOIRE

THESE INSA Rennes
sous le sceau de l'Université Bretagne Loire
pour obtenir le titre de
DOCTEUR DE L'INSA RENNES
Spécialité : Electronique et Télécommunications

présentée par
Ali CHEAITO
ECOLE DOCTORALE : ***MATISSE***
LABORATOIRE : ***IETR***

Analytical analysis of in-band and out-of-band distortions for multicarrier signals: impact of non-linear amplification, memory effects and predistortion

Thèse soutenue le 10.03.2017
devant le jury composé de :

Raymond QUERE
Professeur à l'Université de Limoges / *Président*
Inbar FIJALKOW
Professeur à l'Université de Cergy-Pontoise / *Rapporteur*
Laurent ROS
Maître de Conférences à l'INP Grenoble / *Rapporteur*
Geneviève BAUDOUIN
Professeur à l'ESIEE Noisy Le Grand / *Examinateur*
Yves LOUËT
Professeur à CentraleSupélec Cesson-sévigné / *Co-encadrant de thèse*
Matthieu CRUSSIERE
Maître de Conférence à l'INSA Rennes / *Co-encadrant de thèse*
Jean-François HELARD
Professeur à l'INSA Rennes / *Directeur de thèse*

Analytical analysis of in-band and out-of-band distortions for multicarrier signals: impact of non-linear amplification, memory effects and predistortion

Ali CHEAITO

En partenariat avec

The man of knowledge is the one who recognizes that what is known is very little compared to what is not known, and as a result he considers himself ignorant, and accordingly he increases his efforts to know more by going out in search of knoCNCwledge.

—Nahj al-Balagha

Dedicated to my beloved parents and family . . .

Acknowledgement

First and foremost, I would like to thank God, whose many blessings have made me who I am today.

I wish to express my sincere gratitude to the persons who helped to make my three year's PhD a valuable experience and a pleasing journey that I will never forget.

I am truly grateful to my thesis advisor, Prof. Jean-François Hélard, and to my supervisors, Dr. Matthieu Crussière and Prof. Yves Louët, for all their help throughout my PhD studies. Their positive outlook and constant guidance helped me in all the time of research and writing of this dissertation.

I would like to thank the jury members, Prof. Inbar Fijalkow, Prof. Laurent Ros, Prof. Geneviève Baudouin, Prof. Raymond Quere, for reviewing and discussing my dissertation.

My thanks also go to all my colleagues and friends at IETR, where I passed three years of daily enriching interaction with each one of them. I mention H. Kdouh, M. Maaz, M. Zalghout, Hadi, Imad, Hiba, M. Rihani, Rida, Aurore, Pascal, Alaa, H. Srour, Ferdaouss, Ali Mokh, Ahmad and others.

My sincere feelings of gratitude to my parents, Houssein and Wafaa, my brothers, Hassan and Mohamad, and my sisters, Walaa and Maysaa for their support and valuable prayers. I salute you all for the selfless love, care, pain and sacrifice you did to shape my life. I would never be able to pay back your love and affection.

Finally, I take this opportunity to express my heartiest thanks to my beloved wife, Soumaya, for her love, patience and encouragement throughout my life. Also, I don't forget our always positive and joyful little girl, Ayah. Her smiles encourage me to efficiently overcome the difficulties. She is a powerful source of inspiration and energy.

Ali

Rennes, 18 May 2017

Résumé étendu

Après son invention, le télégramme a pris 90 ans pour se propager aux quatre cinquièmes des pays en développement. Cependant, pour le téléphone cellulaire, la diffusion comparable a été faite en 16 ans. En fait, le premier appel téléphonique mobile utilisant la seconde génération de téléphonie mobile (GSM) a eu lieu en 1991 en Finlande. Puis, 15 ans plus tard, il y avait plus de deux milliards d'abonnés mobiles. Aujourd'hui, plus de la moitié de la population de la planète ont déjà un abonnement mobile. Grâce aux réseaux de données mobiles à très haut débit, tels que la 4^e génération de téléphonie mobile (4G), les utilisateurs sont des consommateurs intensifs d'internet, y compris le streaming vidéo, le stockage en nuage, mais aussi jouent à des jeux en ligne et surfent sur les réseaux sociaux (Facebook, Twitter, etc), etc. Cette demande continue de haute vitesse de transmission de données sans fil et d'accès omniprésent, vient au prix d'une empreinte carbone considérable et d'une énorme consommation d'énergie. Par conséquent, on estime que l'ensemble des Technologies de l'Information et de la Communication (TIC) a généré 2 % de l'émission mondiale de CO_2 en 2007, ce qui équivaut à l'émission de l'industrie aéronautique. De même, cette quantité d'émission de CO_2 équivaut à un quart des émissions de tous les véhicules du monde [Gro08]. En outre, si rien n'est fait, l'empreinte globale des TIC pourrait presque tripler entre 2007 et 2020 [FFMB11]. Par ailleurs, le secteur des TIC représente plus de 2 % de la consommation mondiale d'énergie primaire. Par conséquent, la consommation d'énergie des TIC devient une préoccupation cruciale au niveau mondial ce que les industriels et les laboratoires de recherche tentent de réduire. Ainsi, les métriques vertes devraient être respectées dans les futurs systèmes de communications sans fil afin de réduire aussi bien la consommation d'énergie, que l'émission de CO_2 associée. Actuellement, l'un des plus grands défis est de réduire la consommation d'énergie des stations de base qui représentent jusqu'à 80% de la consommation totale d'énergie de l'infrastructure cellulaire. En particulier, l'efficacité énergétique de l'Amplificateur de Puissance (AP) joue un rôle clé dans l'efficacité énergétique de l'ensemble de la chaîne d'émetteurs puisque l'AP est l'une des composantes les plus consommatrices d'énergie. Par exemple, l'AP représente 55-60 % de la consommation d'énergie totale dans une station de base LTE de type macro [IP12] à pleine charge. D'autre part, bien que l'efficacité énergétique de l'AP soit la métrique de conception principale, elle est contradictoire avec d'autres paramètres traditionnels tels que la linéarité qui assurent la qualité du signal

transmis. En considérant les caractéristiques de l'AP et son efficacité énergétique, on peut remarquer que lorsque la linéarité de l'AP augmente, l'efficacité de l'AP diminue et vice versa. Par conséquent, un compromis entre l'efficacité de l'AP et la linéarité doit être soigneusement considéré surtout lorsque les modulations multiporteuses sont utilisées. En fait, les signaux à porteuses multiples, qui sont utilisés dans la plupart des systèmes de communications modernes tels que la 4G, le WiFi, le DVB, etc, se caractérisent par des fluctuations de puissance élevées, mesurées par le Peak to Average Power Ratio (PAPR). Une grande valeur de PAPR empêche les concepteurs de radiofréquences d'alimenter le signal au point optimal des caractéristiques de l'AP ce qui réduit l'efficacité d'énergie.

Dans la littérature, les techniques de réduction de PAPR et de linéarisation de l'amplificateur sont les principales approches pour résoudre le problème du PAPR et le problème des non-linéarités et la faible efficacité de l'AP. D'une part, les techniques de réduction de PAPR visent à réduire la dynamique du signal transmis, de sorte que le signal peut être alimenté au point optimal ce qui augmente l'efficacité de l'AP. D'autre part, les techniques de linéarisation tentent à compenser la non-linéarité de l'AP pour maintenir la qualité du signal en satisfaisant les exigences de linéarité. Bien que les techniques de réduction du PAPR et de linéarisation fonctionnent de manière complémentaire, elles ont été conçues séparément et appliquées d'une manière indépendante dans les systèmes classiques. Cependant, on peut remarquer que chacune de ces deux méthodes affecte à la fois la linéarité et l'efficacité de l'AP. Par conséquent, l'optimisation de chaque technique séparément n'offrira pas nécessairement une linéarité et une efficacité optimales de l'AP, car une technique peut dégrader la performance de l'autre. Par conséquent, l'impact conjoint de la réduction du PAPR et des techniques de linéarisation sur la linéarité et l'efficacité de l'AP doit être soigneusement étudié. Dans cette thèse, nous proposons d'aller au-delà de l'approche conventionnelle en introduisant une nouvelle approche adaptative pour les futurs systèmes de communications.

L'approche adaptative consiste à contrôler les techniques de réduction du PAPR et de la linéarisation d'une façon flexible et souple en fonction de certains paramètres prédéfinis et des conditions de transmission de sorte qu'ils deviennent adaptatifs et autoconfigurables. Notre objectif est de maximiser l'efficacité énergétique de l'AP tout en respectant des exigences de linéarité. On peut imaginer une implémentation d'émetteur qui contrôle ces deux étapes pour répondre à divers paramètres liés à différentes qualités de services. Donc, notre objectif est de créer un modèle d'émetteur flexible capable de mettre à jour ses paramètres en fonction des besoins afin de maximiser son efficacité énergétique autant que possible tout en respectant la contrainte de linéarité.

Ce travail constitue donc une étape importante dans l'étude de l'optimisation globale de l'efficacité et de la linéarité de l'émetteur. Dans cette perspective, nous avons développé dans cette thèse une dérivation analytique de l'EVM (Error vector Magnitude) et de l'ACPR (Adjacent Chanel Power Ratio) de signaux à porteuses multiples. L'EVM et l'ACPR sont des facteurs de mérite très utilisés dans les spécifications des systèmes de

communications sans fil, pour évaluer la qualité des systèmes de communications. D'une part, l'EVM mesure les distorsions dans la bande de transmission, et d'autre part l'ACPR mesure les distorsions en dehors de la bande de transmission.

Cette thèse fait partie du projet TEPN (Toward Energy Proportional Networks) qui est l'un des projets du laboratoire d'excellence CominLabs [1]. Le projet TEPN comprend différents partenaires, des universités et des instituts tels que l'INSA Rennes, Centralesupélec, TelecomBretagne, INRIA, etc. Ce projet vise à rendre la consommation d'énergie du réseau proportionnelle à la charge réelle de ce réseau. Un tel réseau peut être conçu en prenant des décisions intelligentes basées sur diverses contraintes et métriques dont notre approche adaptative proposée est une mise en œuvre de ce concept.

Chapitre 1

Le chapitre 1 est consacré à l'introduction du concept de modulation à porteuses multiples, en particulier la technique OFDM (Orthogonal Frequency Division Multiplexing). En effet, les avantages et les limitations de l'OFDM sont présentés. Ensuite, le problème du PAPR de tels signaux est abordé et certaines techniques de réduction du PAPR, comme l'écrêtage et le Tone Reservation (TR), sont discutées. Enfin, les critères de sélection des techniques de réduction du PAPR sont énumérés.

Chapitre 2

Le chapitre 2 traite l'amplificateur de puissance non linéaire. En effet, les caractéristiques de l'AP, les effets de mémoire et l'efficacité de l'AP sont discutés. Certains modèles d'amplificateurs de puissance sont présentés tels que le modèle de Rapp et les modèles polynomiaux avec et sans mémoire. En outre, dans ce chapitre, nous abordons plusieurs facteurs de mérite comme l'EVM ou Error Vector Magnitude qui mesure les distorsions dans la bande de transmission et l'ACPR ou Adjacent Chanel Power Ratio qui mesure les distorsions en dehors de la bande de transmission. Ces facteurs de mérite sont utilisés par la plupart des standards de communications tels que le LTE et le DVB pour caractériser l'effet des non-linéarités sur les performances des systèmes de communications. Ensuite, plusieurs techniques de linéarisation, comme la prédistorsion, sont détaillées. Plus tard, différentes approches, existantes dans la littérature, combinant la réduction du PAPR et la linéarisation sont présentées. Enfin, nous proposons notre approche globale qui contrôle la réduction du PAPR et la linéarisation de manière flexible à l'aide d'un moteur de décision et en fonction des conditions de transmission. Dans cette perspective, nous menons dans cette thèse des travaux sur la dérivation analytique de l'EVM et de l'ACPR des signaux à porteuses multiples.

1. www.tepn.cominlabs.ueb.eu

Chapitre 3

Dans le chapitre 3, la distribution d'amplitude du signal OFDM est rappelée. Ensuite, on étudie l'impact de certaines techniques de réduction du PAPR sur la distribution de l'amplitude. Puis, l'expression de l'EVM pour des signaux à porteuses multiples amplifiés utilisant le modèle d'amplificateur de Rapp est dérivée. Nous dérivons l'expression de l'EVM en tenant compte de la réduction du PAPR en utilisant une technique d'écrêtage. Puis, l'impact de la technique de prédistorsion, utilisée comme technique de linéarisation, est analysée.

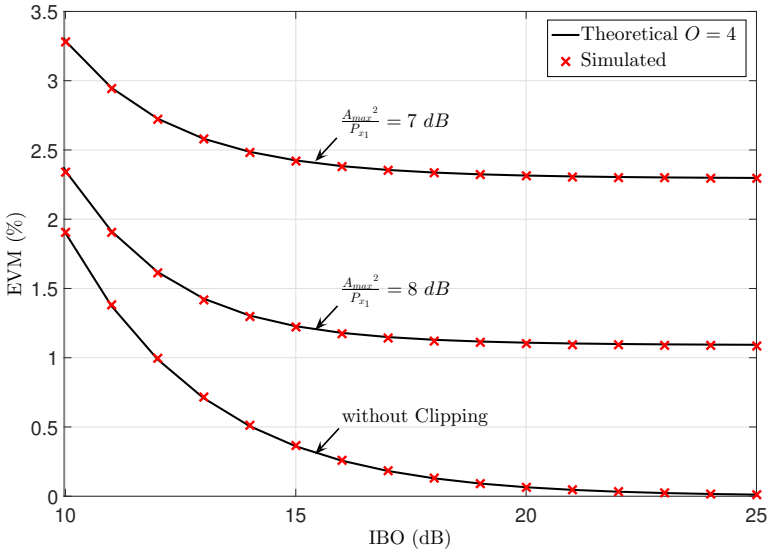

FIGURE 1 – EVM théorique et simulé avec écrêtage et sans prédistorsion (b = 1,5).

Les Fig. 1 et Fig. 2 comparent les résultats de l'EVM simulée numériquement à partir de véritables signaux OFDM et de l'EVM théorique donnée par les expressions analytiques dérivées dans les deux cas avec et sans prédistorsion en limitant la série à un ordre $\mathcal{O}$ donné. Dans les deux cas, sans et avec prédistorsion, les simulations sont effectuées en prenant en compte ou non l'utilisation de l'écrêtage, comme une technique de réduction du PAPR avec un seuil d'écrêtâge $\frac{A^2}{P_{r_1}}$ donné. Pour les simulations, on considère 10^6 symboles OFDM générés aléatoirement et comprenant 1024 sous-porteuses modulées avec une constellation de type 16-QAM. Les Figures donnent les variations des différentes mesures d'EVM, dans les 2 cas sans et avec prédistorsion, pour un facteur de transition de l'amplificateur $b = 1.5$ et de prédistorsion $a = 1.6$. Les courbes sont données en fonction du recul de puissance ou l'IBO (Input Back-Off).

Une première analyse des courbes montre que le modèle théorique basé sur la distribution de Rayleigh est parfaitement fidèle aux simulations OFDM. Ensuite, on constate que les résultats de l'EVM théorique approximée proposée correspondent parfaitement aux ré-

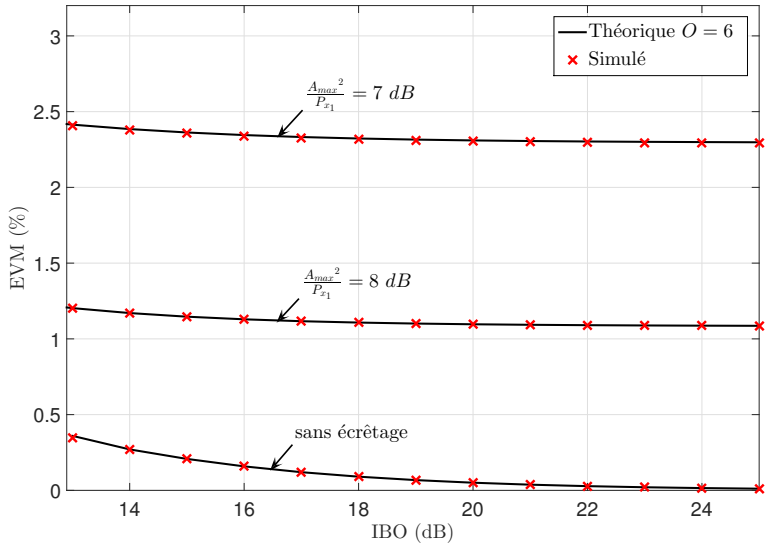

FIGURE 2 – EVM théorique et simulé avec écrêtage et prédistorsion (a = 1,6, b = 1,5).

sultats pour un ordre $\mathcal{O}$ raisonnable. Sans prédistorsion, (cf. Figure 1) la correspondance est très bonne dès $\mathcal{O} = 4$. Avec prédistorsion, (cf. Figure 2), une précision suffisante est obtenue pour $\mathcal{O} = 6$. Par ailleurs, à partir des courbes des Fig. 1 et Fig. 2, il peut être vérifié que l'EVM augmente lorsque le seuil d'écrêtage diminue.

Enfin, quelques scénarios pratiques sont présentés dans ce chapitre pour prouver l'importance de nos expressions proposées dans le contrôle des techniques de pré-distorsion et d'écrêtage afin d'optimiser l'efficacité de l'AP tout en respectant les contraintes de linéarité.

Chapitre 4

Dans le chapitre précédent, nous avons dérivé les expressions de l'EVM en utilisant le modèle de Rapp. En fait, ces expressions analytiques ne sont pas valables dans la zone de compression où l'efficacité de l'AP est très élevée. Cependant, il existe un besoin constant d'évaluer l'EVM à la fois dans les zones linéaires et dans les zones de compression de l'amplificateur pour pouvoir optimiser le compromis linéarité/efficacité de l'amplificateur de puissance. Par conséquent, nous adoptons dans ce chapitre le modèle polynomial avec et sans mémoire. Ainsi, nous dérivons les expressions de l'EVM avec ou sans les techniques d'écrêtage et/ou de prédistorsion.

Les coefficients polynomiaux de la fonction de l'AP ont été obtenus par identification de la caractéristique AM/AM d'un d'amplificateur utilisé pour le Digital Video Brodcasting-Terrestrial (DVB-T) [Tec10].

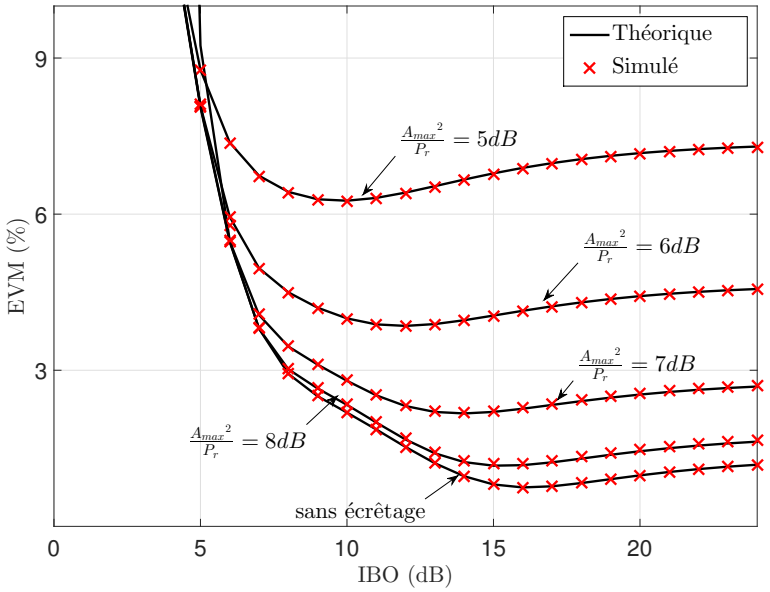

FIGURE 3 – EVM théorique et simulé sans prédistorsion en fonction de l'IBO, lorsque l'écrêtage est activé ou non,en utilisant un modèle d'AP de DVB-T [Tec10].

Les Fig. 3 et Fig. 4 comparent les résultats de l'EVM théorique donnée par les expressions analytiques dérivées et l'EVM simulée en utilisant le modèle polynomial, sans et avec prédistorsion, respectivement, lorsque l'écrêtage est activé ou non. En comparant l'EVM obtenu en utilisant le modèle de Rapp (Fig. 1, chapitre 3) et le modèle d'un amplificateur de signaux DVB-T (Fig. 3), on peut remarquer que l'EVM tend vers zéro pour un IBO élevé lorsque l'écrêtage est désactivé en utilisant le modèle de Rapp. Cependant, un tel comportement n'est pas observé dans le cas de l'amplificateur DVB-T. Cela est dû aux caractéristiques non linéaires de l'amplificateur DVB-T même dans la région linéaire, ce qui entraîne des distorsions supplémentaires. En outre, on peut remarquer que les résultats de l'EVM théorique sont toujours précis même dans la zone de compression avec un faible recul de puissance (petite valeur d'IBO).

Comme indiqué précédemment, maximiser l'efficacité de l'amplificateur est équivalant à minimiser l'IBO. Par conséquent, nous cherchons l'IBO minimum et le seuil d'écrêtage correspondant par rapport à une contrainte EVM spécifique. De la Fig. 4 nous remarquons que l'EVM du signal est constant si le IBO>PAPR du signal après écrêtage, cependant, il augmente rapidement lorsque le IBO <PAPR.

D'après ces résultats et en accord avec [GL12a], nous pouvons proposer que l'IBO doit être égal au PAPR du signal après la réduction du PAPR afin d'obtnir le maximum d'efficacité énergétique de l'AP. Par conséquent, on peut déduire l'expression analytique qui donne l'IBO optimale pour maximiser l'efficacité de l'AP en remplaçant le PAPR du

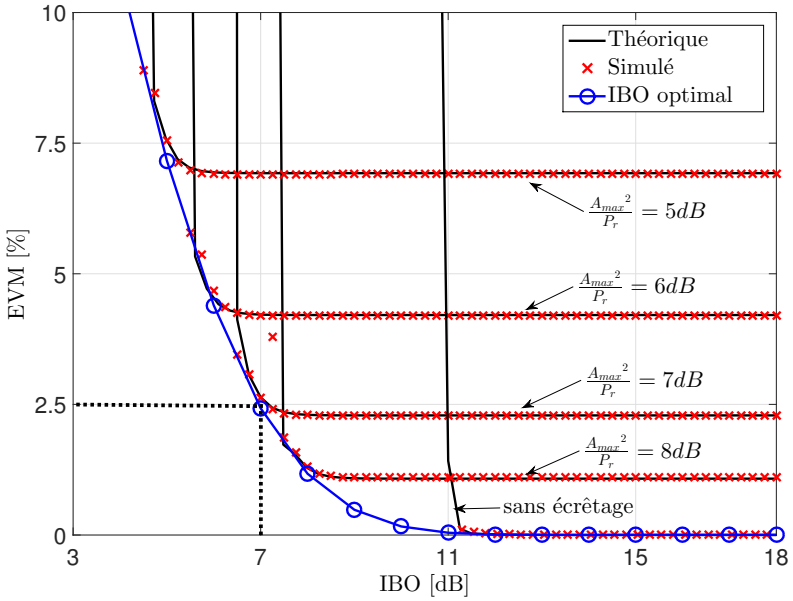

FIGURE 4 – EVM théorique et simulé avec prédistorsion en fonction de l'IBO, lorsque l'écrêtage est activé ou non, en utilisant un modèle d'AP de DVB-T [Tec10].

signal après l'écrêtage par l'IBO dans notre expression analytique de l'EVM.

Comme le montre la Fig. 4, l'équation analytique obtenue fournit exactement l'IBO optimal tout en évitant la saturation de l'AP. Ainsi, supposons maintenant que l'on vise l'efficacité énergétique maximale de l'AP et que l'on veut identifier quel IBO est le meilleur. Il existe deux stratégies pour choisir l'IBO optimal. La première stratégie vise à amplifier le signal d'émission sans distorsion, ce qui signifie que l'EVM doit tendre vers zéro. Dans ce cas, à partir de la courbe donnée par la Fig. 4, on remarque que l'IBO optimal qui maximise l'efficacité de l'AP et garantit un EVM nul est de 11 dB. Ainsi, le seuil d'écrêtage doit également être égal à 11 dB. D'autre part, la deuxième stratégie est de profiter du degré de liberté de l'EVM exigée du signal transmis afin d'améliorer l'efficacité de l'AP. Par conséquent, l'idée est de gérer soigneusement les distorsions, de sorte que nous restons dans les limites spécifiées dans les normes de communications. Par exemple, si la contrainte d'EVM du système de communications est égale à 2,5 %, à partir de la courbe donnée par la Fig. 4, on remarque que l'IBO optimal est de 7 dB. Le seuil d'écrêtage alors doit également être égal à 7 dB. En se référant aux caractéristiques de l'AP DVB-T utilisé, on peut affirmer que l'efficacité augmente de 19,5 % à 31 % [Tec10] en utilisant la deuxième stratégie au lieu de la première. Le gain d'efficacité énergétique est donc égal à 11,5%, ce qui est significatif.

Ensuite, la complexité de la technique de prédistorsion a été étudiée dans le but de la réduire. Par ailleurs, une analyse théorique du compromis entre la linéarité et l'efficacité

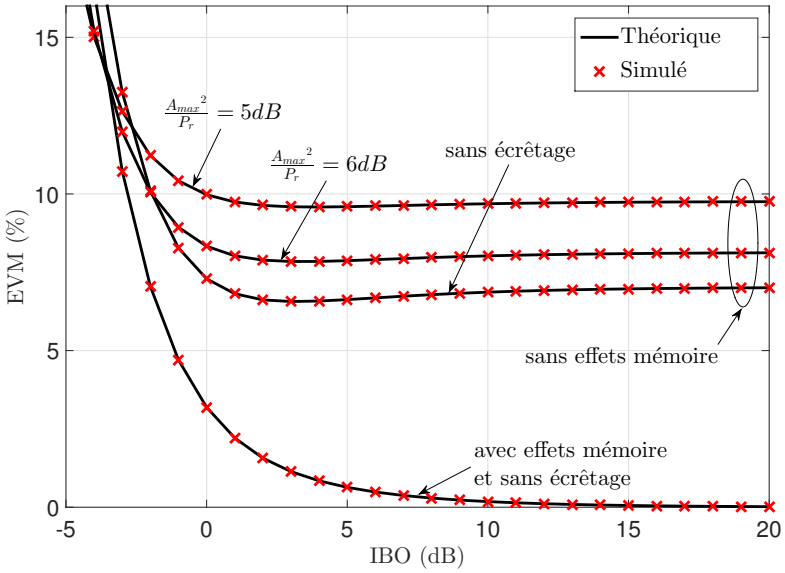

FIGURE 5 – EVM théorique et simulé en fonction de l'IBO, lorsque l'écrêtage est activé ou non, amplifié en utilisant le modèle polynomial sans et avec mémoire avec une profondeur de mémoire de 2.

de l'AP et la complexité de la prédistorsion est investiguée.

En pratique, de nombreux amplificateurs, tels que ceux équipant les grandes stations de base, présentent des effets de mémoire potentiellement forts, principalement en raison de la réponse fréquentielle non plate, de la variation des réseaux de polarisation et de la charge harmonique de l'AP [VRM01b]. Pour cette raison, nous élargissons notre étude en tenant compte des effets de mémoire. Nous calculons donc l'EVM sur la base du modèle polynomial avec mémoire. Afin d'être exhaustif, ces expressions sont fournies lorsque l'écrêtage est activé ou non.

En se basant sur la Fig. 5 , on peut remarquer la différence significative entre l'EVM du signal amplifié utilisant un amplificateur avec effet mémoire et sans effet mémoire. Cette grande différence est naturellement due aux effets de mémoire de l'AP même dans la région linéaire, ce qui entraîne de fortes distorsions supplémentaires.

Il est intéressant de noter que nos analyses théoriques proposées pourraient être très utiles pour l'optimisation de l'efficacité et de la linéarité des futures stations de base et de la complexité de la technique de prédistorsion.

Chapitre 5

Dans le chapitre 5, nous nous concentrons sur l'étude théorique des distorsions hors de la bande de transmission. Nous dérivons analytiquement la Densité Spectrale de Puissance (DSP) du signal à porteuses multiples lorsque la prédistorsion est activée.

La Fig. 6 représente la DSP des signaux à porteuses multiples à l'entrée et à la sortie de l'amplificateur, comprenant 5 sous-porteuses modulées avec une constellation de type 16-QAM, en utilisant la technique de prédistorsion ou non. Tout d'abord, les courbes théoriques correspondent parfaitement aux simulations, ce qui prouve la précision des expressions proposées des DSP avec et sans prédistorsion. Comme prévu, la remontée spectrale dans le canal adjacent du signal amplifié sans prédistorsion est supérieure à la remontée spectrale lorsque la prédistorsion est activée.

Par conséquent, grâce à nos expressions analytiques, nous estimons la remontée spectrale à la sortie de l'AP qui provoque des interférences avec les canaux adjacents. Cette interférence est caractérisée par l'ACPR (Adjacent Chanel Power Ratio) qui est défini par le rapport entre la puissance du canal adjacent et le canal principal. L'ACPR est un facteur de mérite généralement utilisé pour décrire la linéarité des systèmes de télécommunications.

Par ailleurs, nous calculons l'ACPR en fonction de l'IBO lorsque la prédistorsion est

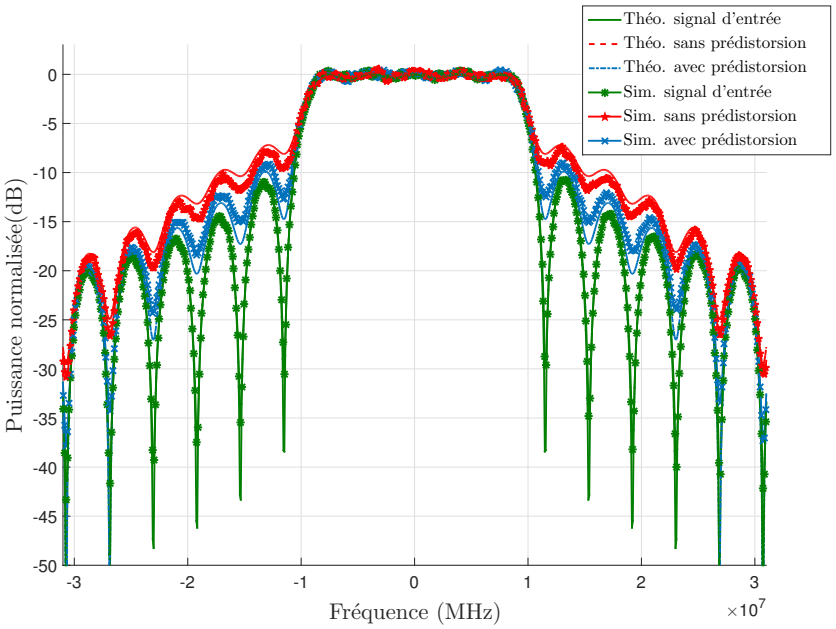

FIGURE 6 – PSD de signaux à porteuses multiples comprenant 5 sous-porteuses modulées avec une constellation de type 16-QAM et amplifiés lorsque la prédistorsion est activé ou non $IBO = 1\ dB$.

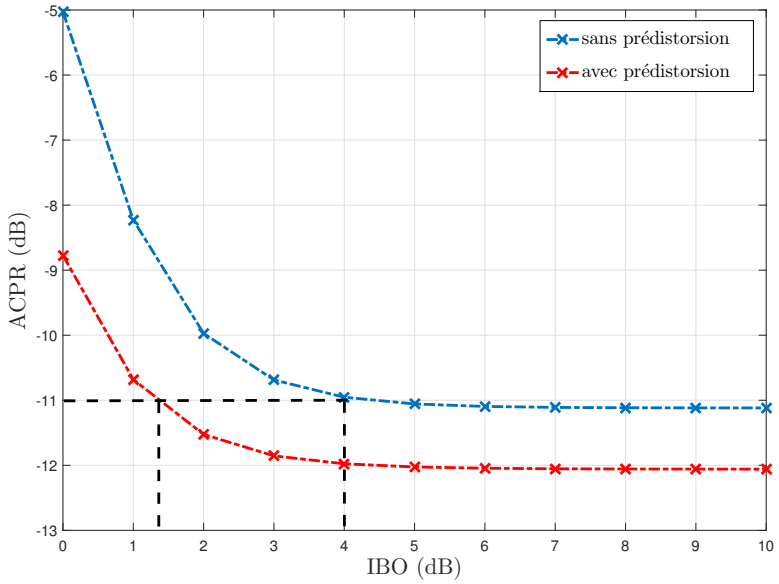

FIGURE 7 – ACPR en fonction de l'IBO pour des signaux à porteuses multiples modulées avec une constellation de type 16-QAM et amplifiés lorsque la prédistorsion est activée ou désactivée avec.

activée ou non. A partir des courbes de la Fig. 7, on peut voir que plus l'IBO diminue plus l'ACPR augmente, ce qui signifie que la remontée spectrale dans le canal adjacent augmente. Ainsi, supposons maintenant que l'on vise l'efficacité maximale de l'AP et que l'on veut connaître le minimum permis d'IBO par rapport à une contrainte ACPR. Notez que plus l'IBO diminue, plus l'efficacité de l'AP augmente. Dans ce cas, à partir des courbes données par la Fig. 7, on peut trouver l'IBO optimal qui maximise l'efficacité de l'AP et satisfait la contrainte d'ACPR lorsque la prédistorsion est activée ou non. Par exemple, si l'ACPR cible est égale à $-11dB$, nous remarquons que le minimum d'IBO qui satisfait l'ACPR est 1,3 dB et 4 dB lorsque la prédistorsion est activée ou non, respectivement.

De plus, pour aller plus loin dans l'analyse, l'étude de l'impact des effets mémoire de l'AP sur la DSP des signaux à porteuses multiples amplifiés a également été étudiée. Par la suite, en utilisant ces expressions analytiques, on peut trouver le point de fonctionnement optimal de l'AP, en tenant compte ou non des effets de mémoire et de la technique de prédistorsion, qui maximise l'efficacité de l'AP tout en satisfaisant les exigences de l'ACPR.

Perspectives

Pour faire suite à ces travaux de recherche menés pendant ces trois années de thèse, plusieurs axes d'étude peuvent être envisagés.

Dans cette thèse, nous avons considéré la technique d'écrêtage comme une technique de réduction du PAPR. Cette technique est largement utilisée dans la mise en œuvre pratique en raison de sa simplicité et son gain de réduction de PAPR. Par conséquent, nous avons dérivé les expressions EVM avec ou sans l'utilisation d'une technique d'écrêtage. En outre, nos expressions d'EVM sont également valables lorsqu'une technique de réduction du PAPR qui n'a pas d'impact sur la distribution d'amplitude du signal est utilisée. Un exemple de ces méthodes de réduction du PAPR sont les techniques probabilistes telles que le Selective Mapping (SLM) et le Partial Transmit Sequence (PTS), etc. Cependant, il pourrait être intéressant de dériver les expressions de l'EVM avec l'utilisation d'autres techniques de réduction de PAPR. En particulier la technique de Tone Reservation (TR) et Active Constellation Extension (ACE), qui sont proposées pour être utilisées dans les normes modernes de radiodiffusion telles que DVB-T2 et ATSC 3.0. Pour ce faire, une étude théorique de l'impact de ces techniques de réduction du PAPR sur la distribution de l'amplitude du signal doit être effectuée en premier lieu. Puis, en utilisant ces nouvelles distributions d'amplitude, on peut dériver les nouvelles expressions d'EVM avec la même méthodologie que celle utilisée dans cette thèse. À notre avis, il est intéressant de trouver de telles expressions qui donnent de nouvelles options pour le moteur de décision et améliorent le compromis global de linéarité-efficacité de l'AP.

Dans le chapitre 4, nous avons proposé une étude analytique de l'impact des effets mémoire de l'AP sur le signal à porteuses multiples amplifié. Par conséquent, nous avons dérivé les expressions de l'EVM en tenant compte ou non de la technique d'écrêtage. Nous avons montré par des simulations l'impact de la mémoire de l'AP sur la fidélité du signal. Notez que les concepteurs RF tentent de trouver une approche plus complète ces dernières années pour révéler le comportement exact des APs, y compris les effets de mémoire. Par conséquent, la prise en compte de la technique de prédistorsion pourrait être une extension très importante de nos expressions dérivées.

Dans le chapitre 5, nous avons proposé des expressions théoriques de la Densité spectrale de Puissance (DSP) des signaux à porteuses multiples amplifiés avec ou sans effets de mémoire. De plus, nous avons dérivé l'expression de la DSP du signal à porteuses multiples amplifié en prenant en compte la technique de prédistorsion. Au meilleur de nos connaissances, aucune expression analytique de la DSP prenant en compte la technique de prédistorsion n'existe dans la littérature. De telles expressions sont très utiles pour optimiser l'efficacité et la linéarité des futurs transmetteurs. Cependant, les techniques de réduction du PAPR ne sont pas prises en considération. Il pourrait donc être intéressant d'étudier l'impact de la technique de réduction du PAPR sur les expressions de la DSP. En outre, la mise en œuvre de ces expressions est complexe et la durée de la simulation

est aussi trop longue. Il convient de mentionner que même les expressions proposées de la DSP dans la littérature étaient aussi complexes et la durée de la simulation était aussi longue. Par conséquent, nous pensons qu'il est intéressant de faire une approximation de ces expressions afin de réduire la complexité de calcul. Par la suite, nous pensons que la dérivation de l'expression de l'ACPR en utilisant nos expressions dérivées de la DSP, est l'étape naturelle suivante.

L'une des questions les plus délicates qui pourraient être abordées dans les travaux futurs est d'étudier le lien entre les distorsions dans et hors de la bande de transmission. Autrement dit, le but est d'étudier analytiquement la relation entre les deux facteurs de mérite étudiés dans cette thèse à savoir l'EVM et l'ACPR. Nous pensons que ces deux caractéristiques sont liés à l'énergie globale du signal au-dessus d'un seuil donné. Par conséquent, il pourrait être intéressant d'aller plus loin dans cette analyse et d'étudier analytiquement le lien entre elle. Ensuite, il sera intéressant de trouver le métrique le plus critique, la contrainte EVM ou la contrainte ACPR. La réponse à cette question est très utile pour la mise en œuvre de notre moteur de décision ainsi que pour les concepteurs RF. De cette façon, l'accent pourrait être mis sur la contrainte la plus critique, une fois que nous l'avons vérifiée, la deuxième contrainte sera vérifiée automatiquement.

Table of Contents

Introduction

Context

After its invention, the telegram took 90 years to spread to four-fifths of developing countries. However, for the cell phone, the comparable diffusion was done in 16 years. In fact, the first mobile phone call using the Global System for Mobile Communications (GSM) took place in 1991 in Finland. Then, just 15 years later there were over two billion mobile subscriptions. Today, more than half of the population of the planet have already a mobile subscription. Thanks to the high-speed mobile data networks, such as 4G, the users are intensive consumers of internet, including video streaming i.e. Video on Demand (VoD), uploading and downloading files to/from cloud storage, but also surfing on the social networks (Facebook, Twitter, etc) and playing online games, etc. This continuous demand for high data rate wireless communication and ubiquitous access, comes at the cost of a sizable carbon footprint and a huge energy consumption. As a result, it is estimated that the whole Information and Communication Technology (ICT) produced 2% of the global CO_2 emission in 2007 which is equivalent to the aviation industry emission. Likewise, this amount of CO_2 emission is equivalent to one quarter of the emissions by all vehicles around the world [Gro08]. Moreover, if nothing is done, the overall ICT footprint might almost triple between 2007 and 2020 [FFMB11]. Besides, ICT sector is responsible for more than 2% of the worldwide primary energy consumption. Therefore, ICT energy consumption becomes a global crucial concern what industrials and researchers are trying to reduce. Hence, green metrics should be respected in future wireless communication systems to reduce the energy consumption, along with the associated CO_2 emission.

Currently, one of the biggest challenges is to reduce the energy consumption of Base Stations (BSs) which make up to about 80% in the total energy consumption of cellular infrastructure. In fact, in today's macro base stations, the high Power Amplifier (PA) efficiency plays a key role in the energy efficiency of the whole transmitter chain as the PA is one of the most power-consuming components. For example, the PA accounts for 55-60% of the overall power consumption at full load in an LTE macro base station [IP12]. On the other hand, although the PA energy efficiency is the major design metric, it conflicts with other traditional metrics such as linearity which ensure the quality of the transmitted signal. Considering the PA characteristics and the PA power efficiency, one can remark that while the PA linearity increases, the PA efficiency decreases and vice versa. Therefore, a trade-off between the PA efficiency and linearity must be carefully considered especially when multicarrier modulations are used. In fact, the multicarrier signal, which is used in most modern communication systems such as the Long Term Evolution (LTE), WiFi, DVB, etc, is characterized by high power fluctuations, measured

by the Peak-to-Average Power Ratio (PAPR). High PAPR value prevents radio-frequency designers to feed the signal at the optimal point of the PA characteristics which reduces its energy consumption.

In literature, the PAPR reduction and linearization techniques are the main approaches to solve the PAPR problem, the PA nonlinearities problem, as well as the low PA efficiency problem. On one hand, the PAPR reduction techniques aim at reducing the dynamic range of the transmitted signal, then the signal can be fed at the optimal point which increases the PA efficiency. On the other hand, the linearization techniques try to compensate for the PA nonlinearity to maintain the quality of the signal by satisfying the linearity requirements. Although the PAPR reduction and linearization techniques work in a complementary way, they have been designed separately and applied independently in conventional systems. However, one can remark that each of these two methods impacts both the linearity and the efficiency of the PA. Therefore, the optimization of each technique separately will not necessarily result in optimal PA linearity and efficiency because one technique can degrade the performance of the other. So, the study of the joint impact of the PAPR reduction and the linearization techniques on the PA linearity and efficiency should be well examined.

In this thesis, we propose to go a step beyond the conventional approach by introducing a new adaptive approach for future implementations. The adaptive approach would be to control the PAPR reduction and linearization stages in a flexible way according to some predefined parameters and transmission conditions so that they become adaptive and self-configurable. Our aim is to maximize the PA efficiency with respect to the linearity requirements. One can imagine a transmitter implementation that controls these two stages to meet various parameters target values related to different qualities of services. So, our objective is to derive a flexible transmitter model able to update its parameters according to incoming requirements and outside environment sensors in order to maximize its efficiency as much as possible while respecting the linearity constraint. Hence, this work is an important step in the study of the global optimization approach of the transmitter efficiency and linearity.

In that perspective, we are involved in this thesis in the analytical derivation of the Error Vector Magnitude (EVM) and the ACPR (ACPR) of multicarrier signals. EVM and ACPR are critical metrics and common figures of merit used to evaluate the quality of communication systems. While EVM measures the in-band distortion, ACPR measures the out-of-band distortion.

This thesis is a part of Toward Energy Proportional Networks (TEPN) project which is one of CominLabs excellence laboratory projects [2]. TEPN project includes various European partners, universities and institutes such as INSA Rennes, Centralesupélec, TelecomBretagne, IRISA, etc. This project aims at making the network energy consumption proportional to the actual charge of this network. An energy proportional network can be designed by taking intelligent decisions based on various constraints and metrics where our proposed adaptive approach is one implementation of this concept.

2. www.tepn.cominlabs.ueb.eu

Organisation of manuscript

This thesis is organized as follows.

Chapter 1 is devoted to introduce an overview of multicarrier concept, particularly the Orthogonal Frequency Division Multiplexing (OFDM) technique. Then, the PAPR problem is presented and some PAPR reduction technique are discussed. Finally, the criteria for PAPR reduction techniques selection are listed.

Chapter 2 deals with the non-linear power amplifier. Such aspect as the PA characteristics, the memory effects, and the PA efficiency are discussed. Then, some power amplifier models are presented. Also, in this chapter we address the figures of merit used to characterize the effect of nonlinearity on the performance of the communication systems. Next, several linearization techniques are detailed. Later, different approaches, existing in literature, combining the PAPR reduction and linearization are presented. Finally, our global approach that controls the PAPR reduction and linearization in a flexible way using a decision engine and based on the transmission conditions is proposed.

In chapter 3, the amplitude distribution of the OFDM signal is recalled. Afterwards, the impact of some PAPR reduction techniques on the amplitude distribution is studied. The EVM expression for nonlinear amplified multicarrier signals using Rapp PA is derived. We derive the EVM expression taking into account the PAPR reduction using a clipping technique. The impact of the predistortion technique, which is used as linearization technique, is analyzed. Finally, some practical scenarios are presented proving the importance of our proposed expressions in controlling the predistortion and the clipping techniques in order to optimize the efficiency with respect to the linearity constraint.

In chapter 4 the polynomial PA model is assumed. We derive the EVM expressions with or without the clipping and/or the predistortion techniques. Besides, a theoretical analysis of the trade-off between PA linearity-efficiency and predistortion complexity is investigated. Finally, we quantify the memory effects of the power amplifier by assuming a memory polynomial PA model.

In chapter 5, we focus on the theoretical study of the out-of-band distortions. We analytically derive the Power Spectral Density (PSD) of the multicarrier signal when predistortion is activated. Consequently, thanks to our analytical expression we predict the spectral regrowth at the PA output which in turn causes adjacent channel interference Adjacent Channel Interference (ACI). This interference is characterised by the Adjacent Channel Power Ratio (ACPR), which is a commonly used figure-of-merit to describe linearity in modem telecommunication systems. In addition, to go further in the analysis, the study of the impact of memory effects on the PSD of the amplified multicarrier signals has been also investigated. Thereafter, using this analytical expression, we can find the optimal operating point of the PA, taking into account or not the memory effects and the predistortion technique, which maximizes the PA efficiency and satisfies the ACPR requirements.

Finally, we conclude this thesis and give some potential directions in the future.

List of Publications of the author

International journals

The contributions of this work have been published in the following international journals and communications.

[J1] A. Cheaito, J.-F. Hélard, M. Crussière, and Y. Louët, "EVM Derivation of Multicarrier Signals to Determine the Operating Point of the Power Amplifier Considering Clipping and Predistortion", *to be published in EURASIP Journal on Wireless Communications and Networking.*

[J2] A. Cheaito, M. Crussière, J.-F. Hélard, and Y. Louët, "Quantifying the Memory Effects of Power Amplifiers: EVM Closed-Form Derivations of Multicarrier Signals", *to be published in IEEE Wireless Communications Letters.*

International communications

[C1] Ali Cheaito, Matthieu Crussière, Yves Louët, and Jean-François Hélard, "EVM Derivation for Multicarrier Signals: Joint Impact of Non-Linear Amplification and Predistortion", *2015 IEEE 81st Vehicular Technology Conference (VTC Spring), pages 1-6, Glasgow, United Kingdom, May 2015.*

[C2] Ali Cheaito, Jean-François Hélard, Matthieu Crussière, and Yves Louët, "Impact of Clipping on EVM of the Predistorted Non-Linear Amplified Multicarrier Signals", *Twelfth International Symposium on Wireless Communication Systems (ISWCS'15), pages 76-80, Bruxelles, Belgium, August 2015.*

[C3] Ali Cheaito, Matthieu Crussière, Jean-François Hélard, and Yves Louët, "Energy-Efficiency Optimization of the High Power Amplifier for Multicarrier Systems: Analytical EVM Derivation", *2016 IEEE International Conference on Computer Communications (INFOCOM), San Francisco, United States, April 2016. 6 pages,*(Best paper award).

[C4] Ali Cheaito, Yves Louët, Matthieu Crussière, and Jean-François Hélard, "Optimal Operating Point of the Power Amplifier with respect to the EVM for TV Broadcasting Applications", *11th Symposium on Broadband Multimedia Systems and Boradcasting (BMSB), Nara, Japan, June 2016. 4 pages.*

[C5] Ali Cheaito, Mohamed Saad Farah, Matthieu Crussière, Jean-François Hélard and Yves Louët, "Spectral Analysis of Predistorted Non-Linear Amplified Multicarrier Signals", *to be published in the IEEE Wireless Communications and Networking Conference (WCNC), San Fransisco, USA, March 2017.*

National communication

[NC1] Ali Cheaito, Matthieu Crussière, Yves Louët, and Jean-François Hélard, "Expression analytique de l'EVM pour les signaux multiporteuses: Impact conjoint des non-linéarités de l'amplificateur de puissance et de la fonction de prédistorsion", *GRETSI 2015, Lyon, France, September 2015. 4 pages.*

[NC2] Ali Cheaito, Jean-François Hélard, Yves Louët, and Matthieu Crussière, "Expression analytique du spectre pour les signaux multiporteuses : Impact conjoint des non-linéarités de l'amplificateur de puissance et de la fonction de prédistorsion", *submitted to GRETSI 2017, Juan-Les-Pins, France, Septembre 2017, 4 pages.*

Awards and honours

[A1] Best paper award at the 2016 IEEE International Conference on Computer Communications (INFOCOM), San Francisco, United States, April 2016, First international workshop on green and sustainable networking and computing (GSNC).

Chapter 1

PAPR problem in multicarrier systems

1.1 Introduction

Current communication systems are requesting high connectivity, reliable transmissions in mobility and increasing spectral efficiency. LTE, the Worldwide Interoperability for Microwave Access (WiMAx), WiFi, DVB and other communication systems today use multicarrier modulation which is considered as one of the key technologies able to fulfill all these demands. The basic principle of multicarrier systems relies on a parallel data transmission scheme where multiple data symbols are transmitted simultaneously. Therefore, each symbol occupy a part of the available bandwidth. Multicarrier systems have many advantages in comparison to the conventional single carrier systems, and they have found a wide range of applications in both wired as well as wireless communications systems. First, these systems exhibit the attractive feature of high spectral efficiency. Second, The Inter-Carrier Interference (ICI) and Inter-Symbol Interference (ISI) are mitigated by the insertion of guard intervals (i.e. Cyclic prefix). Besides, by dividing the channel into narrowband flat fading subchannels, multicarrier systems are more resistant to frequency selective fading than single carrier systems.

In this chapter, we first establish the principles of OFDM which is one of the most popular type of multicarrier systems. Then, the PAPR problem is investigated. Thereafter, we present some PAPR reduction techniques and the criteria for PAPR reduction techniques selection.

1.2 Orthogonal frequency multiplexing system

OFDM is a special form of multicarrier modulation, which transmit a single data stream over a number of lower rate subcarriers. It has long been studied and implemented to combat transmission channel impairments. Due to the advantages of OFDM, especially in the multipath propagation, interference, and fading environment, its applications have been extended from High Frequency (HF) radio communication to digital audio broadcasting, digital television terrestrial broadcasting and telephone networks [Pra98]. In fact, OFDM has already been adopted by many communication standards i.e. Asymmetric Digital Subscriber Line

(ADSL), European Digital Video Broadcasting Terrestrial Digital Video Broadcasting – Second Generation Terrestrial (DVB-T2), and Japanese Integrated Services Digital Broadcasting Terrestrial (ISDB-T), LTE as well as the network standards such as IEEE 802.11a/g/n, and WiMAx.

1.2.1 History of OFDM

Although OFDM system was standardized for the first time in 1993, it is reported that OFDM-based systems already existed during the Second World War. OFDM had been used by the US military in several high-frequency military systems such as KINEPLEX, ANDEFT, and KATHRYN [NP00].

In fact, the first fundamental contribution to OFDM was introduced by Robert W. Chang when he published in December 1966 a synthesis of band-limited orthogonal signals for multi-channel data transmission without ISI and ICI [CG68]. Then, in 1971 Weinstein and Ebert proposed an easier and efficient implementation by using a technique based on the Discrete Fourier Transform which eliminates the need for bank of subcarrier oscillators [WE71a].

Afterwards, another breakthrough in the history of OFDM came in 1980 when Peled and Ruiz introduced Cyclic Prefix (CP) [PR80]. Thus, the cyclic extension replaced the empty guard spaces in frequency domain. Hereafter, due to the substantial advancements in digital signal processing, the implementation of the modulation and demodulation in OFDM systems became simple and practical using the Fast Fourier Transform (FFT) and the Inverse Fast Fourier Transform (IFFT) pair, respectivelly, which made OFDM an important part of telecommunications landscape.

In 1993, the European Digital Audio Broadcasting (DAB) project adopted OFDM on its physical layer. The DAB standard was the first commercial use of OFDM technology. At the dawn of the $20th$ century, several communication standards such as Wireless Local Area Network (WLAN) standard, DVB standard, HIPERLAN/2 standard also adopted transmission techniques based on OFDM.

1.2.2 OFDM modulation principle

The principle of OFDM consists in transmitting data symbols in parallel on multiple subcarriers that share the available bandwidth. The idea behind this is to divide the system bandwidth into a large number of small orthogonal sub-bands that are supported by subcarriers. Therefore, the serial data stream is passed through a serial-to parallel converter which splits the serial data into a number of parallel channels. For each channel, the data is applied to a modulator carrier frequency f_p. Considering an OFDM system with N subcarriers, let $[X_0, X_1, ..., X_{N-1}]$ denote the input data symbols to be transmitted. Therefore, X_p, the p^{th} smbol, is carried by frequency f_p, thus the transmitted OFDM signal can be formed as

$$s(t) = \sum_{i=-\infty}^{+\infty} \sum_{p=0}^{N-1} X_{p,i}\ h(t - iT)\ e^{j2\pi f_p t}, \tag{1.1}$$

where T is the OFDM symbol duration. $h(t)$ is the real impulse response of the shaping filter. In standard OFDM, a rectangular time-limited window is used and

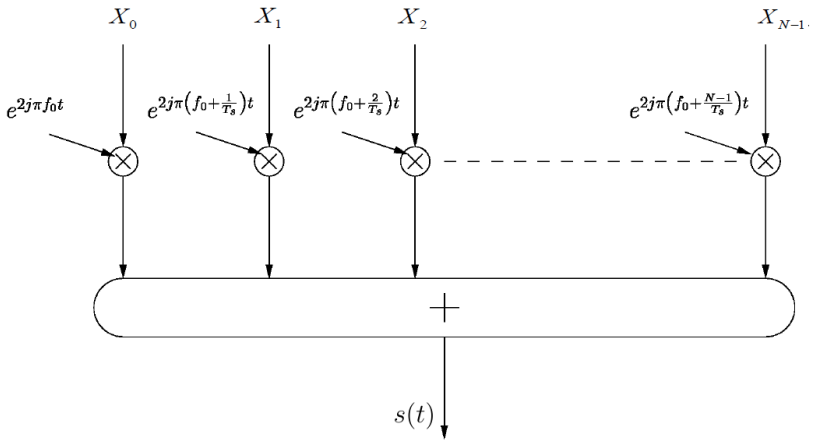

FIGURE 1.1 – Block diagram of OFDM modulator using N subcarriers, where X_p represent the data symbols.

given by

$$h(t) = \begin{cases} 1 & 0 < t < T \\ 0 & \text{otherwise.} \end{cases} \tag{1.2}$$

By omitting the time index i, the complex envelope of the transmitted signal with a rectangular time-limited window for each OFDM symbol is given by

$$s(t) = \sum_{p=0}^{N-1} X_p \, e^{j2\pi f_p t}. \tag{1.3}$$

The principle of OFDM transmitter systems is represented by Fig. 1.1. The frequency shift between adjacent channels is $\Delta f = \frac{1}{T}$, thus the overall bandwidth occupied by N carriers is $\frac{N}{T}$. Therefore,

$$f_p = f_0 + \frac{p}{T}, \qquad p = 0, 1, ..., N-1, \tag{1.4}$$

are the orthogonal frequencies, with f_0 the first carrier frequency. In fact, this orthogonality can be mathematically justified since each carrier is modulated by one symbol during a rectangular time window of duration T, is equivalent, in frequency domain, to a sinc function which is zero at all the multiple of $\frac{1}{T}$ as we can see in Fig. 1.2 .

1.2.3 Digital implementation of a baseband OFDM systems

In a digital system, the implementation complexity of OFDM systems is mitigated if the N sub channel modulators/demodulators are implemented using the pair of Discrete Fourier Transform (DFT) and Inverse Discrete Fourier Transform (IDFT), respectively [WE71b]. Therefore, the data constellations X_p are the frequency domain information carried over N orthogonal carriers, and the output of the IDFT is the time domain OFDM symbol (Fig. 1.3). Thus, the complex

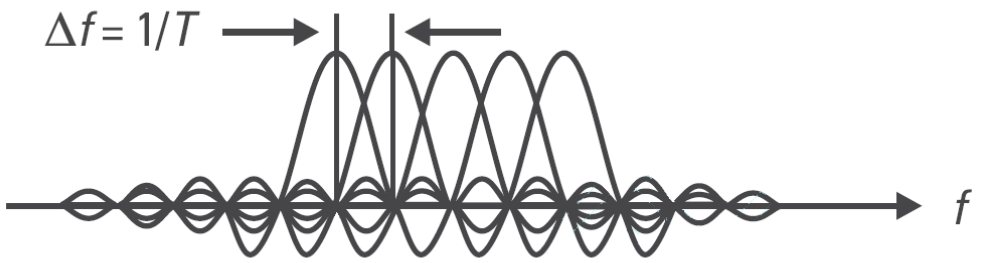

FIGURE 1.2 – Frequency spectra of overlapped orthogonal signals.

envelope of the baseband discrete-time OFDM signal $s(n)$ can be expressed as

$$s(n) = \sum_{p=0}^{N-1} X_p \, e^{j2\pi pn/N}, \quad n \in [0, N-1]. \tag{1.5}$$

One trick of the trade that makes OFDM transmitters low cost is the ability to be implemented via the use of the computationally efficient pair IFFT and FFT [ZWS+01]. In fact, the IFFT/FFT blocks are chosen due to their execution speed, flexibility and precision. Also, The IFFT/FFT algorithms provide orthogonality between adjacent subcarriers which makes the signal symbol relatively secure to the fading caused by natural multi-path environment. As a result, OFDM systems have became very popular in modern telecommunication systems.

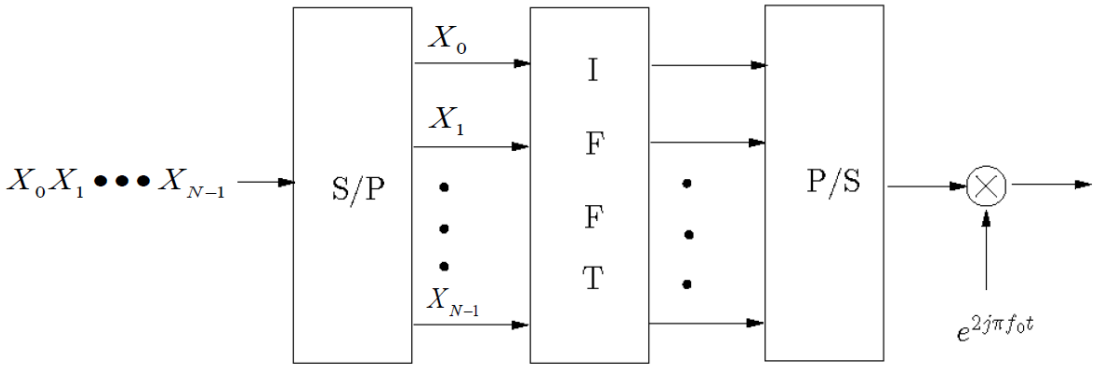

FIGURE 1.3 – Digital implementation of OFDM modulator using N subcarriers.

1.2.4 Zero padding and cyclic prefix OFDM

The efficiency in counteracting multipath delay spread is one of the main advantages that make OFDM systems attractive. However, the orthogonality of OFDM signals can be lost if the channel is time-dispersive. Therefore, a guard interval is normally inserted between OFDM symbols to prevent intersymbol interference (ISI). This interval is defined by a sub-set of zero-valued signals and serves as a buffer for the multipath reflection (the top part of Fig. 1.4). In practice, although ISI is prevented by the empty guard time with Zero Padding OFDM (ZP-OFDM), inter-carrier interference (ICI) may arise in presence of multi-path propagation, which

is crosstalk between different subcarriers, causing the loss of orthogonality [NP00]. Thence, to overcome this problem the OFDM symbol is cyclically extended along the guard time with Cyclic Prefix OFDM (CP-OFDM) in most of the standardized multicarrier systems. The generic idea consist in introducing cyclic extension of OFDM symbol instead of a simple zero padding, which is a copy of the last part of OFDM symbol, appended in front of the transmitted OFDM symbol [Mat01] (the bottom part of Fig. 1.4). The Cyclic Prefix (CP) length should be longer than the channel impulse response, such that multipath reflection from one symbol would not interfere with another. However, if the delay spread is larger than the CP length the orthogonality is lost. At the receiver side, the cyclic prefix is typically discarded before any processing. It is obvious that introducing CP causes loss of signal energy since it carries no information. Nevertheless, the fact that we get zero ICI and ISI pays off the loss.

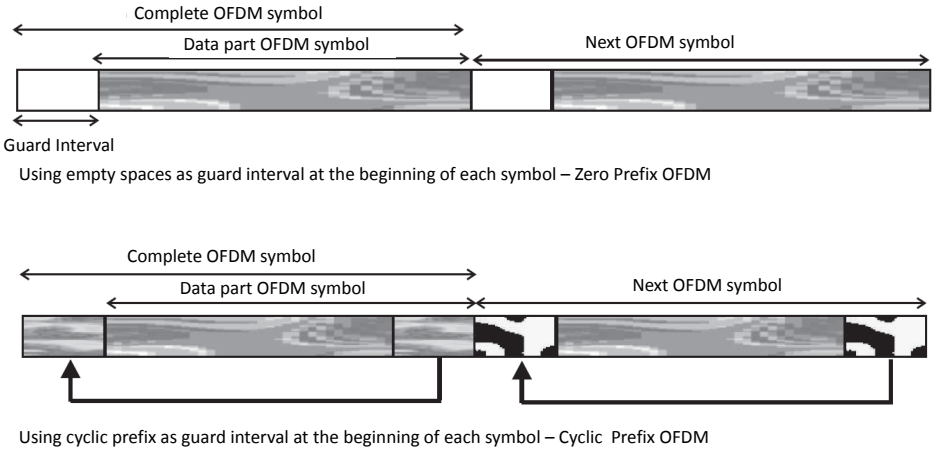

FIGURE 1.4 – Definition of the cyclic prefix and the guard interval in OFDM systems.

1.2.5 Applications of OFDM

In Europe, based on the successful results of the Digital Video Broadcasting Terrestrial (DVB-T) standard, DVB-T2 was standardized by the European Telecommunications Standards Institute (ETSI) in 2008. In 2010 DVB-T2 was first deployed in the UK. For the time being most of European countries are studying plan to switch from DVB-T to DVB-T2. In fact, both DVB-T and DVB-T2 use OFDM in their physical layers. Table 1.1 summarizes the specifications of DVB-T2 standard.

Also, the latest standard in the mobile network technology, Long Term Evolution (LTE), which has been adopted the OFDM modulation as downlink transmission scheme. The LTE standard is developed by the 3rd Generation Partnership Project (3GPP). The goal of LTE was to increase the capacity and speed of wireless data networks using new Digital Signal Processing (DSP) techniques and modulations. Therefore, Orthogonal Frequency Division Multiple Access (OFDMA), which is a multi-user version of OFDM, was chosen because of its high data rate

capacity, and its high spectral efficiency. Table 1.1 summarizes the specifications of LTE standard.

Despite both LTE and DVB-T2 standards use OFDM modulation, they have different OFDM parameters, e.g. different guard interval duration, different subcarrier spacing and symbol duration. For example, the subcarrier spacing in LTE standard is fixed, and the bandwith depends on the number of active subcarriers. However, in DVB-T2 the bandwidth is fixed, and the subcarrier spacing depends on the number of active subcarriers. These differences are due to the difference of coverage area size implying different channel effects on signals.

TABLE 1.1 – Comparison between LTE (downlink) and DVB-T2 standards specifications

Parameter Mode	LTE (downlink)	DVB-T2
Bandwidth (MHz)	1.4, 3, 5, 10, 15, 20	1.7, 5, 6, 7, 8, 10
FFT size	128, 256, 512, 1K, 2K, 4K	1K, 2K, 8K, 16K, 32K
Number of active subcarriers	76, 151, 301 601, 1201	853, 1705, 3409 6817, 13633, 27265
Useful OFDM symbol duration T_u (µs)	66.7	112, 224, 448, 896, 1792, 3584*
Subcarrier spacing (Hz)	15000	8929, 4464, 2232, 1116, 558, 279*
Sampling frequency (MHz)	1.92, 3.84, 7.68, 15.36, 23.04, 30.72	9.14*
Mapping	QPSK, 16QAM, 64QAM	QPSK, 16QAM, 64QAM, 256QAM
Guard interval / $T_u s$	1/4, 1/8, 1/16, 1/32	1/4, 19/128, 1/8, 19/256, 1/16, 1/32, 1/128
Typical data rate (Mbit/s)	25.2, 50.4, 100.8	40

* Only for a 8 MHz channel bandwidth.

1.2.6 Advantages and limitations

OFDM systems have several advantages, we list below the most important ones:

1. High spectral efficiency by employing overlapping orthogonal subcarriers which results almost rectangular frequency spectrum.
2. Robustness to inter-symbol interference since the parallel transmission of multiple symbols results in a longer OFDM symbol period.

3. Flexible adaptation of transmission parameters (i.e. modulation and power level) with respect to the channel condition on each subcarrier.
4. The Inter-Symbol Interference (ISI) and Inter-Channel Interference (ICI) may be efficiently mitigated by the insertion of cyclic prefix.
5. More resistant to the effects of frequency-selective fading than single-carrier systems.
6. The OFDM transmitter simplifies the channel effect, thus a simple channel estimation is enough for recovering transmitted data.
7. Simple implementation through the use of the Fast Fourier Transform and the Inverse Fast Fourier transform pair (FFT/IFFT) for modulation and demodulation, respectively. Such an implementation of OFDM has become very practical due the widespread availability of high speed Digital Signal Processors (DSPs).
8. Fragmented bands of available spectrum can be relatively easily aggregated to convey the secondary user's (SU's) (unlicensed user's) traffic, and that the spectrum utilization increases ...
9. The multi-user version of OFDM, the Orthogonal Frequency Division Multiple Access (OFDMA), which offers flexible subcarriers allocation. The multiple users access is achieved by subdividing the available bandwidth into multiple channels. Consequently, each channel is assigned to individual user. In fact, OFDMA was adopted by the 3GPP for the downlink of LTE systems and by the WiMAX Forum for mobile WiMAX systems.

On the other hand, the very attractive advantages of OFDM come at a cost.

1. Frequency synchronization between OFDM transmitter and receiver is crucial. In fact, any impairment that can destroy the system orthogonality characteristic generates detrimental effects, and can lead to inter-carrier interference. There are two main origins of frequency synchronization errors: Doppler spreading, carrier frequency and time offsets.
2. High PAPR is the major problem of OFDM systems. Since OFDM signal consists of a number of independent modulated subcarriers, that can cause a very large dynamic amplitude. Therefore, the focus of the next sections is on the PAPR and how to solve the problem of having high PAPR values.

1.3 Envelope fluctuation and PAPR problem

As explained above, OFDM signal is the sum of a number of independent modulated sub-carriers. Statistically speaking, OFDM can be viewed as a summation of many independent and identically distributed (i.i.d) random variables. Recalling the central limit theorem, when a large number of i.i.d random variables are added simultaneously, their distribution becomes Gaussian. Consequently, OFDM signal is characterized by a complex Gaussian process. Therefore, its magnitude converges to a Rayleigh distribution, which means that there is a very big gap between average and peak power as can be viewed in Fig 1.5, and then very high fluctuations of the signal amplitude. This gap is quantified by the PAPR metric.

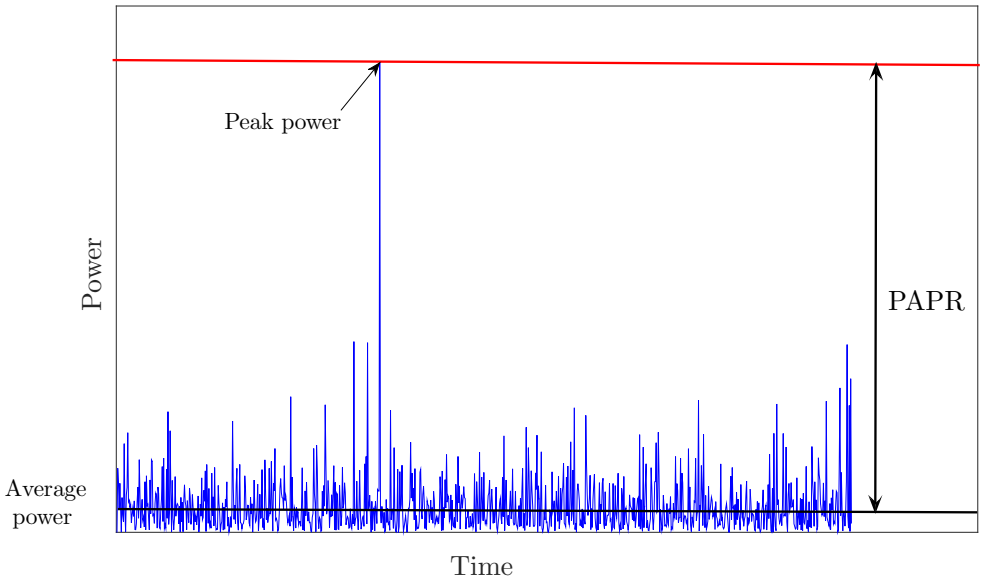

FIGURE 1.5 – The power fluctuation of the OFDM signal.

1.3.1 PAPR definition and distribution

The PAPR of a signal, $x(t)$, is defined as the ratio between the peak and the average power of the signal over a time interval T, and is given by

$$PAPR_{[x]} = \frac{\max_{t\in[0,T]} |x(t)|^2}{E\{|x(t)|^2\}}, \tag{1.6}$$

where $E\{.\}$ is the expectation function. Note that PAPR can be expressed for analog or digital signals. Besides, the relation between the PAPR of baseband signal, $PAPR_{BB}$, and the PAPR of RF signal, $PAPR_{RF}$, is given by [LP05],

$$PAPR_{RF} \approx PAPR_{BB} + 3dB, \tag{1.7}$$

[Tel01] provides an upper bound of the PAPR of OFDM signal with N active subcarriers associated to M-QAM modulation symbols which is given by:

$$PAPR_{max,M-QAM} = 3N\frac{\sqrt{M}-1}{\sqrt{M}+1}, \tag{1.8}$$

where M is the number of modulation states.

Another widely used characterization of the PAPR deals with its probabilistic distribution. Therefore, we introduce the Complementary Cumulative Distribution Function (CCDF) of PAPR which is the probability that the PAPR value of a randomly chosen OFDM symbol exceeds a predefined threshold ψ, $Pr(PAPR > \psi)$. In literature, we find either experimentally or analytically PAPR distribution functions. In [NP00], Nee proposes analytical CCDF expression of PAPR for a baseband OFDM signal which is only valid for an oversampling factor $L = 1$ (Nyquist rate), and it is expressed as

$$Pr(PAPR > \psi) = 1 - (1 - e^{-\psi})^N \tag{1.9}$$

However this analysis does not exactly reveal the signal fluctuations because some peaks are probably missed at this sampling rate. On the other hand, in the case of oversampling it is difficult to derive analytical CCDF expression as the condition of uncorrelated samples does not remain true. Therefore, an approximation of CCDF of oversampled signal has been presented in [vNdW98] and can be expressed by the following relation,

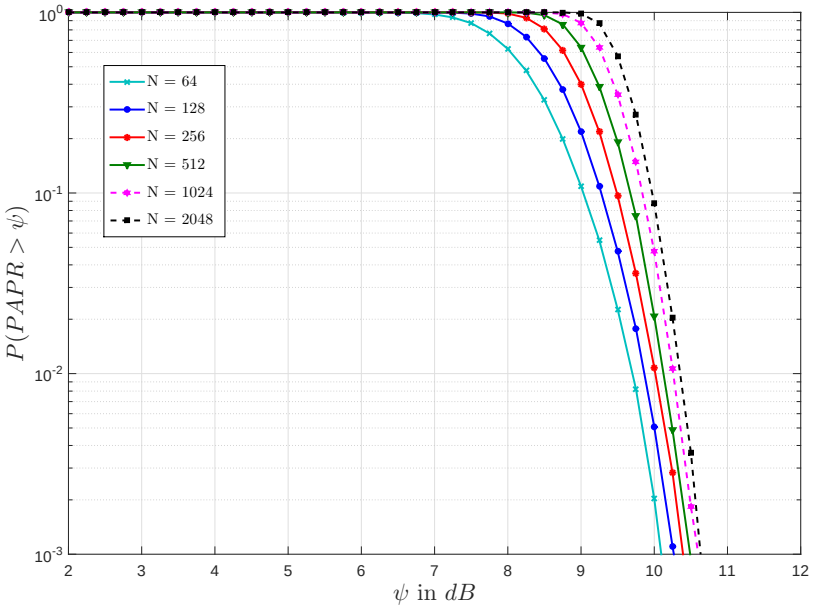

FIGURE 1.6 – CCDF of PAPR for a 16-QAM modulated baseband OFDM signal for different values of N (L =1).

$$Pr(PAPR > \psi) = 1 - (1 - e^{-\psi})^{2.8N} \tag{1.10}$$

In Fig. 1.6, different PAPR distribution functions of 16-QAM modulated OFDM signal are shown for different number of active subcarriers with $L = 1$. As expected, we see that as the number of subcarriers increases, the probability to find more peaks and thus larger PAPR values increases.

Besides a very interesting point to note about PAPR distribution function is that, if the number of subcarriers is large, it is independent of the mapping scheme of the OFDM symbols with $L = 4$. It is demonstrated in Fig. 1.7 by showing the PAPR CCDF for QPSK, 16-QAM, and 32-QAM modulated OFDM symbols. We see that all the differently mapped symbols show almost the same PAPR behavior. Actually, as the number of sub-carriers increases, the process becomes Gaussian following the central limit theorem and hides the PAPR dependence on mapped data. In addition, it is worthwhile to note that compared to the non-oversampled version with $L = 1$ (Fig. 1.6) oversampling with $L = 4$ (Fig. 1.7) leads to a PAPR CCDF gain of $1dB$ for $N = 1024$. As explained, when the signal is not oversampled ($L = 1$), some of the signal peaks may be missed a nd then the PAPR value will be less in this case.

In this work, the definition of PAPR in (1.6) is adopted taking a fairly wide time interval T. Thus, the PAPR of the signal is measured over T and has a

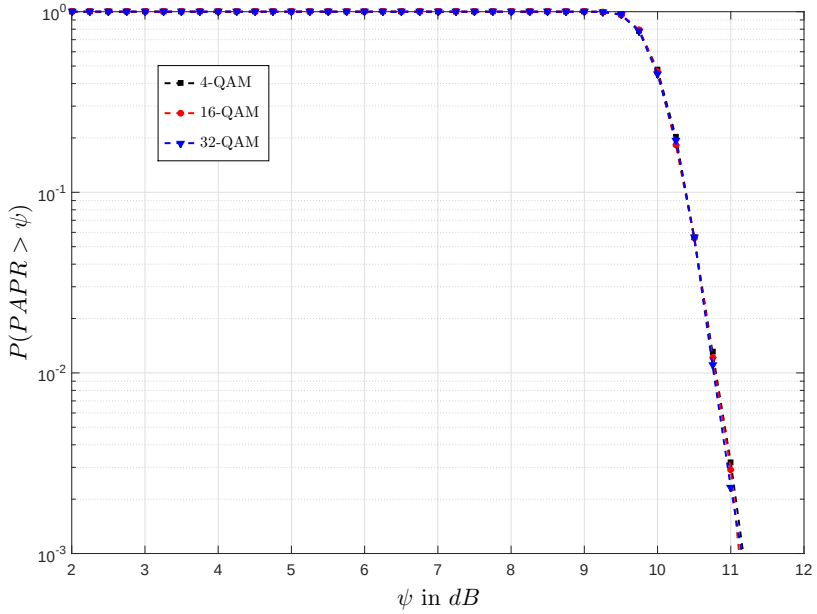

FIGURE 1.7 – CCDF of PAPR for a baseband OFDM signal with different modulation schemes ($L = 4$, $N = 1024$).

deterministic value which is bounded by the upper bound defined in (1.8). In addition, the probabilistic approach of PAPR is considered in some cases .

1.4 PAPR reduction techniques

As far as the PAPR problem is concerned, numerous PAPR reduction techniques have been proposed in literature. In fact, PAPR reduction techniques can be classified in three top categories which are coding methods, probabilistic methods and adding signal methods. This section is dedicated to briefly introduce each of these categories and the criteria for PAPR reduction techniques selection.

1.4.1 Coding methods

When N signals are added with the same phase, they produce a peak power, which is N times the average power. Coding methods consist in reducing the occurrence probability of the same phase value of these signals.

A simple block coding scheme was introduced in [JWB94], and it consists in finding out all possible codewords and then select those codewords of lowest PAPR. It maps 3 bits data into 4 bits codeword by adding a Simple Odd Parity Code (SOBC) at the last bit across the channels. It has been shown that using this scheme the PAPR of the signal can be reduced from 6.02 dB to 2.48 dB. This technique has two limitations. First, an exhaustive search is required to find the best suitable codeword. Second, it also suffers from complexity to store large lookup tables for encoding and decoding in the transmitter and receiver respectively.

In [Pop91], [JZZ04], authors used the Golay complementary sequences where more than 3 dB PAPR reduction has been obtained. In [DJ99], Davis et al. propo-

sed codes with error correcting capabilities to achieve more lower PAPR for OFDM signals by determining the relationship of the cosets of Reed-Muller codes to Golay complementary sequences. However, for OFDM systems with large number of subcarriers, these block codes significantly reduce the transmission rate.

In summary, the actual benefits of coding for PAPR reduction for practical multicarrier systems are limited, regarding the low coding rate, the intractable required search for a good code, as well as the prohibitively complexity for large number of subcarriers.

1.4.2 Probabilistic methods

The idea behind the probabilistic methods is to perform several copies of the initial signal by modifying the phase, amplitude and/or position of subcarriers and then select the copy with the minimum PAPR. These methods cannot guarantee the PAPR below a specified level. Moreover, it decreases the spectral efficiency, and the computational complexity increases as the number of subcarriers increases. The probabilistic methods include Selective Mapping (SLM), ands Partial Transmit Sequence (PTS) [MH97]. A block diagram of SLM technique is shown in Figure 1.8.

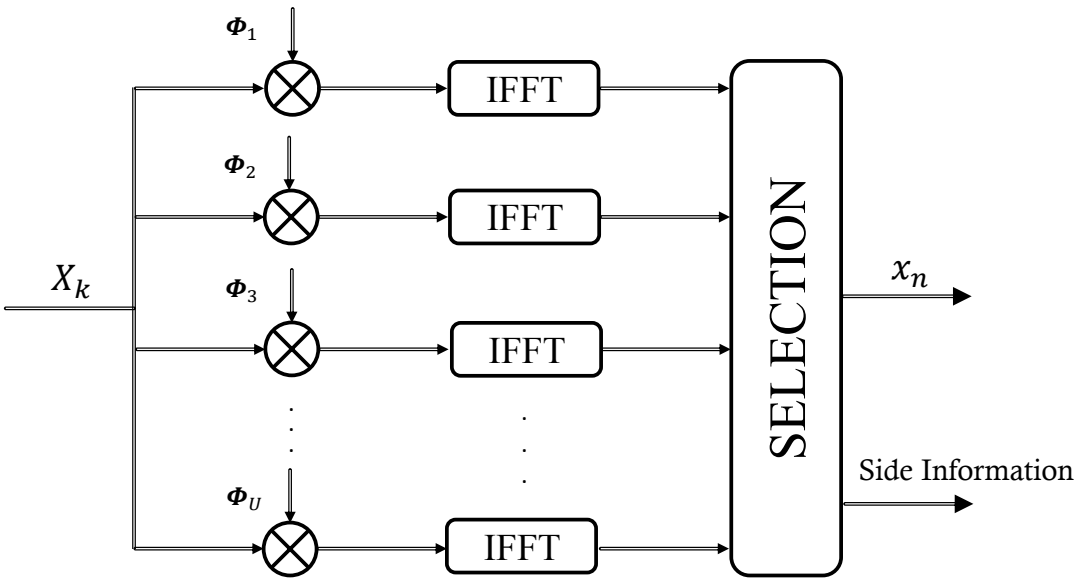

FIGURE 1.8 – Block diagram of Selective Mapping (SLM) technique.

In SLM, the input data sequences are multiplied by U different phase sequences to generate alternative input symbol sequences. Each of these alternative input data sequences are then applied to IFFT operation, and then the one with the lowest PAPR is selected for transmission [BFH96]. Therefore, its performance in reducing the PAPR directly depends on the number and the design of phase factors. The corresponding selected phase factor also needs to be transmitted to receiver as side information to properly extract the original information.

Its major drawback is the high computational complexity and loss of bandwidth efficiency, since it needs U IFFT operations and $ln\ U$ bits as side information. In

addition, in case of loss of the side information during transmission, the whole data block is lost which significantly degrades the error performance of the system. Note that a novel SLM method has proposed in [GASK+09] for which no side information needs to be sent.

1.4.3 Adding signal methods

This category, as its name suggests, includes all techniques of PAPR reduction that can be formulated as PAPR$(X + C_{papr})$ < PAPR (X), where X refers to the OFDM signal and C_{papr} refers to the peak-reduction signal. Indeed, X and C_{papr} could be in time or frequency domain. In the literature, we find a large number of adding signal techniques such as clipping [MR98], Tone Reservation (TR) [TMoEE99,TC98], Tone Injection (TI) [TMoEE99], and Active Constellation Extension (ACE) [KJ03a], etc.

1.4.3.1 Clipping

Clipping is one of the most used techniques for PAPR reduction due to its simplicity and its straightforward reduction gain. Its main objective is to constraint high amplitude peaks of a signal to a given threshold A_{max}, without affecting the phase $\phi(x)$. Thus, the clipped signal, $x_2(t)$, is represented as

$$x_2(t) = \begin{cases} x(t) & \text{if } |x(t)| \leq A_{max} \\ A_{max} e^{j\phi(x)} & \text{if } |x(t)| > A_{max} \ . \end{cases} \tag{1.11}$$

This technique results in both in-band and out-of-band distortions because of its nonlinear operation which degrades the system performance including Bit Error Rate (BER) and spectral efficiency. Filtering can reduce out of band radiation after clipping at the cost of peak re-growth so that, at some points, the signal after clipping and filtering will exceed the clipping threshold [LC97]. Additionally, it changes the amplitude probability distribution function of the signal and decreases the signal average power which will be discussed in the next chapter. To reduce the distortion effects of the clipping technique many other contributions were proposed to modify the clipping function, in the literature, such as deep clipping [KNSO08], and the Invertible Clipping [RPLL06a], etc.

1.4.3.2 Tone reservation

The TR concept was introduced by Tellado in 1997 [Pri14]. This method is based on reserving subcarriers that do not carry any useful information and are called peak reduction tones. These tones are used for generating a PAPR reduction signal which when added to the original multicarrier signal decreases its peaks. The peak reduction tones and data tones are orthogonal to each other which makes recovering the data trivial.

Let $\mathcal{R} = \{i_1, i_2, ..., i_W\}$ denote the ordered set of the positions of the reserved tones and $\mathcal{R}^C$ denote the complement set of $\mathcal{R}$ in $\mathcal{N} = \{0, 1, ..., N-1\}$, where N and W are the numbers of subcarriers and reserved tones, respectively. Thus, the transmitted signal is given by:

$$X_k + C_k = \begin{cases} C_k & \text{if } k \in \mathcal{R} \\ X_k & \text{if } k \in \mathcal{R}^C \end{cases}, \tag{1.12}$$

where C_k is the PAPR reduction symbol with 0 in the set $\mathcal{R}^C$ and X_k is the data symbol with 0 in the set $\mathcal{R}$ as shown in Fig. 1.9.

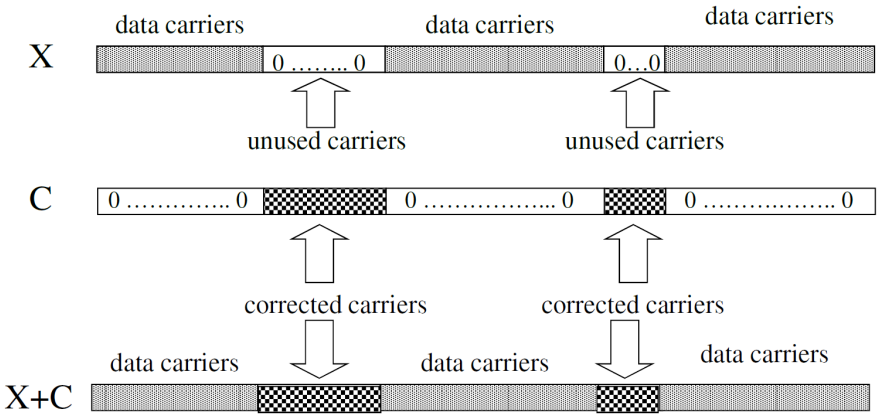

FIGURE 1.9 – Block diagram of Tone Reservation (TR) technique.

The performance of this technique depends on the number and the location of these reserved tones. While increasing the number of reserved tones improves the capability of PAPR reduction, the throughput proportionally reduces because of reduction in data bearing subcarriers. Consequently, since these dedicated tones are not used for data transmission, spectral efficiency will naturally decrease. Therefore, there is a trade-off to find between the PAPR reduction and the spectral efficiency.

To enhance the spectral efficiency, the non utilized tones of a standard are used as peak reduction carriers [ZPLL06]. For example, there are 12 tones out of 64 which are unused in WLAN standard and can be employed to reduce PAPR of the OFDM modulated standard. Besides, several broadcasting standards such as DVB for Nex Generation Handheld (DVB-NGH), the DVB-T2, and the recent version of Advanced Television Systems Committee Advanced Television Systems Committee (ATSC) 3.0 adopted the tone reservation as a PAPR reduction technique. Generally, in these broadcasting standards, only 1% of the subcarriers is dedicated to the PAPR reduction. For example, in the 32K mode of DVB-T2, which is today the most deployed mode by the terrestrial broadcasting, 288 tones out of 27265 active tones are used for the PAPR reduction.

The advantages of tone reservation include that there is no need nor side information neither special receiver oriented operation. While promising, up to the best of our knowledge tone reservation is not implemented in most of DVB-T2 transmitters, because the performance observed with TR algorithms proposed in the DVB-T2 standard do not offer a good performance-complexity trade-off.

1.4.3.3 Active constellation extension

ACE was introduced by Krongold and Jones in 1999 [Jon99, KJ03a, KJ03b] based on a Projection-Onto-Convex-Sets (POCS) approach to extend the outer

points of a given constellation and then minimize the PAPR. In 2003, Krongold and Jones proposed a simple implementation of the ACE for faster PAPR reduction which paved the way for ACE in modern telecommunication standards. ACE is now adapted to the European Computer Manufacturers Association (ECMA) standard that specifies an Ultra-Wideband UWB physical layer (PHY-UWB) for Wireless Personal Area Network (WPANs) [LJSO12]. In addition, like TR, ACE is proposed as an optional PAPR reduction technique for the DVB-T2, DVB-N5H and ATSC 3.0.

The basic principle of the scheme is easily explained by the following example of 16-QAM constellation shown in Fig. 1.10. The constellation point at the boundaries can be freely moved in the shaded region. Likewise, the other outer points can be dynamically extend away from the original constellation point (see Fig. 1.10). Consequently, additional co-sinusoidal and/or sinusoidal signals are added to the transmitted signal. Hence, these signals are used to reduce the time-domain peaks in the transmitted signal by intelligently adjusting the new constellation points.

The advantages of ACE are that no side information are needed and the BER performance and data rate are not affected. However, this comes at the cost of a moderate increase of the power of the transmitted signal. In addition, ACE has poor performance when the number of constellation points increases as the percentage of points that can be manipulated decreases.

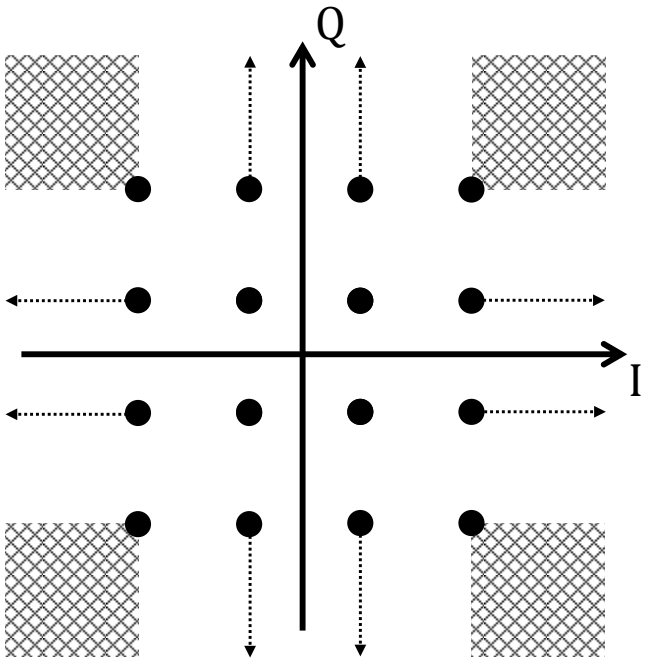

FIGURE 1.10 – Block diagram of Active Constellation Extension (ACE) technique.

1.5 Criteria for PAPR reduction techniques selection

Given the large number of PAPR reduction techniques proposed in the literature the last fifteen years [JW08, LHLM11, LP08a], it seems relevant to define some metrics that evaluate their performance.

PAPR-reduction performance

This metric seems trivial but it is, nevertheless, the most significant criterion. It quantifies the effectiveness of the technique in terms of the PAPR reduction. It is generally calculated using CCDF curves at a level of probability as shown in Fig. 1.11. Note that $x(t)$ is the original signal and $y(t)$ is the signal after the PAPR reduction. Thus, the PAPR-reduction gain denoted $\Delta PAPR(\phi)$ can be defined as

$$\Delta PAPR(\phi) = PAPR_{[x]}(\phi) - PAPR_{[y]}(\phi) \ , [dB] \tag{1.13}$$

where $PAPR_{[x]}(\phi)$ and $PAPR_{[y]}(\phi)$ are the PAPR of $x(t)$ and $y(t)$, respectively.

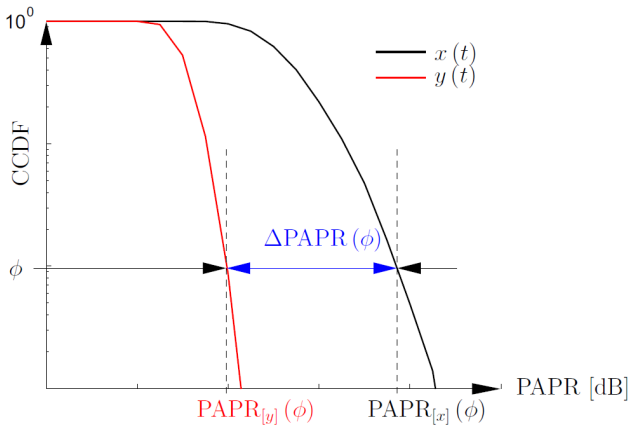

FIGURE 1.11 – Calculation of the PAPR-reduction gain for a particular value of the CCDF.

Average power variation

Some PAPR reduction techniques result in a decrease or an increase of the average power of the transmitted signal. For example, the average power of the transmitted signal decreases when clipping is applied, while using tone reservation or active constellation extension the average power increases. As a consequence, the variation in average power denoted by ΔE can be defined as

$$\Delta E = P_{[x]} - P_{[y]} \ , [dB] \tag{1.14}$$

where $P_{[x]}$ and $P_{[y]}$ are the average power of the signal before and after PAPR reduction, respectively.

In the literature, most studies of PAPR reduction techniques performance do not take into account the average power variation of the transmitted signal. Yet

this variation has a strong impact on the quality of the transmission. In the third chapter, we will discuss in detail the average power variation in the case of clipping technique.

In and out of band distortions

Some PAPR reduction techniques introduce in-band and/or out-of-band distortions because of its nonlinear operation. The in-band distortion is measured by the Error Vector Magnitude (EVM), while the out-of-band distortion is measured by the Adjacent Chanel Power Ratio (ACPR). These critical metrics are common figures of merit used to evaluate the quality of communication systems. Indeed, most of wireless communication standards such as the IEEE802.11a standard [EVM99], the IEEE802.16e, WiMAX standard [EVM05], and the LTE standard [LTE12] have already specified their requirements in of the EVM and ACPR. We note that these two metrics and the standards requirement described in details in the next chapter.

Indeed, PAPR reduction techniques can be also categorized in two groups. The first group which causes distortions like clipping. On the other hand, the second group includes the techniques which do not introduce any distortion like tone reservation, coding, and selective mapping.

Downward compatibility

A PAPR reduction techniqued is said to be downward compatible if it does not imply any change on the receiver side. This is the case of tone reservation and clipping technique. However, coding and partial transmit sequence are not downward compatible as they require post processing on the receiver side. In fact, this characteristic is very important in both mobile and broadcast communications if a method is implemented at the transmitter side (base station).

Data rate loss

The receiver, using some methods, needs additional information (side information) in order to recover useful data which degrades the capacity of the system. These methods need an increase of the bandwidth and consequently a decrease of the spectral efficiency. If the bandwidth has to be kept constant, this information transmission involves a data rate loss. This is the case of the selective mapping technique.

Complexity

Even though a method has powerful characteristics, for implementation on real systems computational complexity must be taken into account. In these circumstances, too much complex techniques will be impossible to implement. Therefore, there is a trade-off between the performance and complexity of the PAPR reduction technique which must be carefully considered.

1.6 Conclusion

This chapter provided the basic concepts of multicarrier modulations, and introduced the principles of OFDM systems. Then, the advantages and the limitations of OFDM are discussed. One of the most serious problem of OFDM is the very high signal fluctuations generally quantified by the term PAPR. In the last decade, many studies in the literature investigated the PAPR problem and hence several PAPR reduction methods have been proposed.

The next chapter will gives an overview of the non-linear Power Amplifier, especially its linearity and efficiency characteristics. In fact, signals with a high PAPR value may experience strong distortions in and out of the band when they pass through the PA. Indeed, the PA linearity-efficiency problematic will be discussed in a muticarrier context. Furthermore, the linearization techniques will be examined. Finally, a global approach for the PAPR reduction and linearization will be proposed.

Chapter 2

Power amplifier linearity and efficiency trade off

2.1 Introduction

The high Power Amplifier (PA) dominates the power consumption in base stations. Thus, it requests focusing the energy efficiency improvements on this device. Considering the PA characteristics and the PA power efficiency, we can notice that while the PA linearity increases, the PA efficiency decreases and vice versa. Therefore, a trade-off between the power amplifier efficiency and linearity must be carefully considered especially when multicarrier modulations are used, because they exhibit a high Peak-to-Average-Power Ratio (PAPR). Consequently, the PA efficiency and linearity are of primary concern due to the aforementioned reasons.

In this chapter, we will start by an overview of power amplifiers including their power consumptions and efficiencies, their nonlinear characteristics, as well as, the memory effects. Next, we will present some PA behavior models existing in the literature. Afterwards, to quantify the nonlinearities effects, we will define some figures of merit like the Error Vector Modulation (EVM) and the Adjacent Channel Power Ratio (ACPR). Later, the state of the art of the PA linearization techniques is presented. Then, we discuss the trade-off between the PA linearity and the PA efficiency, as well as the different approaches, exciting in the literature, to combine the PAPR reduction and linearization to improve this compromise. Finally, a global approach that controls the PAPR reduction and linearization in a flexible way and based on the transmission conditions is proposed.

2.1.1 Need for energy efficiency

It is estimated that the whole Information and Communication Technology (ICT) produced 2% of the global CO_2 emission in 2007, which is equivalent to the aviation industry emission or one quarter of the emissions by all vehicles around the world [Gro08]. Moreover, ICT sector is responsible for more than 2% of the worldwide primary energy consumption. For example, regarding Vodafone's business footprint, we can mention that Vodafone has a total annual emission of 1.45 million tonnes of CO_2 in 2007/2008 at worldwide level [Lis09]. Besides, the total energy consumption of Vodafone is estimated to 3,000 GWh. Also, the energy

demand is always increasing. Therefore, ICT energy consumption has became a crucial concern where industries and universities are trying to reduce it. Thence, 'Green Communication' has became one of the top areas in the field of ICT.

Currently, one of the biggest challenges is to reduce the energy consumption of base stations (BSs) which make up to about 80% in the total energy consumption of cellular infrastructure. In fact, in today's macro base stations, the high Power Amplifier (PA) efficiency plays a key role in the energy efficiency of the whole transmitter chain as the PA is one of the most power-consuming components. Based on different studies, the PA dominates the power consumption in base stations and requests focusing its energy efficiency improvements. For example, EARTH project reports an estimation of the power consumption of different LTE base station types for 2010 and 2012. Fig. 2.1 shows the power consumption of different sections in macro and micro LTE base stations. We can notice that, the PA power consumption account for 55- 60% of the overall power consumption at full load [IP12]. Under those circumstances, the power amplifier, in macro base stations, consumes at full load between 743 W and 810 W which is quite significant.

For digital terrestrial TV networks, the percentage of PA power consumption is even higher where transmission power can reach 100 dBm (compared to 43 dBm for a 4G LTE macro base station). As an example, at the French level, with 12,000 transmitters in operation (with radiated power ranging from a few watts to 5 kW), the French Digital terrestrial TV transmission network has a total radiated power of about 1,200 kW and consumes about 46 GWh electrical energy per year for the RF amplification part alone. The resulting yearly energy cost for the network operator is about 4,000 k€. Thus, improving the PA efficiency by 10 to 15% means saving 360 to 540 k€ a year. This highlights the vast potential for energy savings by improving the PA energy efficiency.

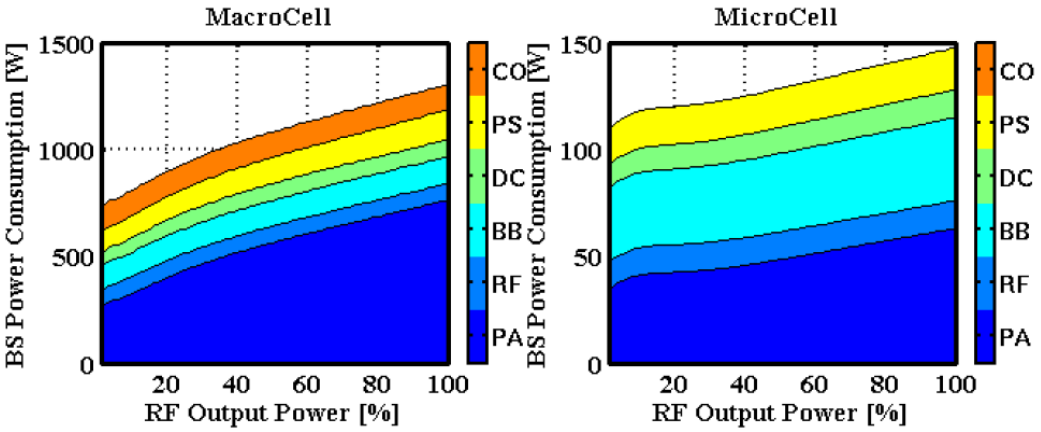

FIGURE 2.1 – Power consumption in all LTE base station types for a 10MHz bandwidth, based on the 2010 State-of-the-Art estimation. Legend: PA=Power Amplifier, RF=small signal RF transceiver, BB=Baseband processor, DC: DC-DC converters, CO: Cooling, PS: AC/DC Power Supply [IP12].

2.2 Overview of power amplifiers

The power amplifier is a key element of any communication system. In fact, the PA has to amplify the electrical radio signal before being transmitted so that the signal can reach the user up to tens of kilometers. Ideally, the amplified signal is multiplied by a gain factor and thus it has the same waveform as the original signal, i.e it is not deformed. However, the circuits of the amplifier are made of non-linear devices such as transistors (i.e. MOSFET, MESFET, or BJT) which have a non linear response under large-signal conditions. Therefore, power amplifiers have a major effect on the fidelity of wireless communications systems. This justifies the large number of studies undertaken to be aware of the PA limitations and then to optimize the PA performance.

2.2.1 PA classes

PAs are traditionally divided into several classes, depending on how the transistor is driven, and on the harmonic content or time behavior of the drain voltage [Crip99]. These classes are either very linear or very efficient, but both are not achieved simultaneously. Actually, modern communication systems use both amplitude and phase modulation of the RF carrier to increase the data rate. Hence, we focus in this section on the classes that have sufficient amplitude linearity which are commonly used in modern communications systems, namely A, B, and AB.

Class-A PAs are used when very low levels of distortion are tolerated. However, since the amplifier is always conducting with conduction angle 2π, the efficiency is very low. Therefore, the theoretical maximum efficiency of this class is 50%, and this occurs only at the maximum output power.

In Class B, the conduction angle is π. Therefore, the drain efficiency is significantly better than class-A amplifier (78.5%) at the cost of additional nonlinear distortion.

Class AB is the intermediate class between Class A and Class B. In fact, it is the most common used nonlinear mode of operation. Theoretically, the maximum efficiency of this class is 50% to 78.5% at the PA compression point.

2.2.2 Power amplifier characteristics

The power amplifier behavior impacts the linearity of the whole system. As mentioned previously, the output signal of an ideal power amplifier is proportional to the input signal. However, in practice, the output signal suffers from both amplitude and phase distortions. Therefore, we use the Amplitude to Amplitude (AM/AM) and Amplitude to phase (AM/PM) transfer characteristics to describe the PA behavior. The AM/AM transfer function represents the amplitude of the output signal as a function of input signal amplitude. On the other hand, the AM/PM transfer function describes the phase offset between the output and input signals as a function of the input signal amplitude. From Fig.2.2, one can divide the PA characteristics in three zones:

I. Linear Zone (Zone I): as the name says, the output power is proportional to the input power, so that the amplifier works like a linear device. Consequently, distortions are almost null in this region.

II. Compression Zone (Zone II): the gain is no longer linear, thus, the output power now is not proportional to the input power. Additionally, amplitude and phase distortions start appearing and they increase as we go deep in the Compression Zone. In this zone, there is an important PA characteristic, the so called 1 dB compression point. At this point, there is a gap of 1 dB between ideal and practical gain curves.

III. Saturation Zone (Zone III): from a certain point onwards, the gain decreases linearly. Therefore, in this region the output power becomes almost constant as the non-linearities become more and more evident.

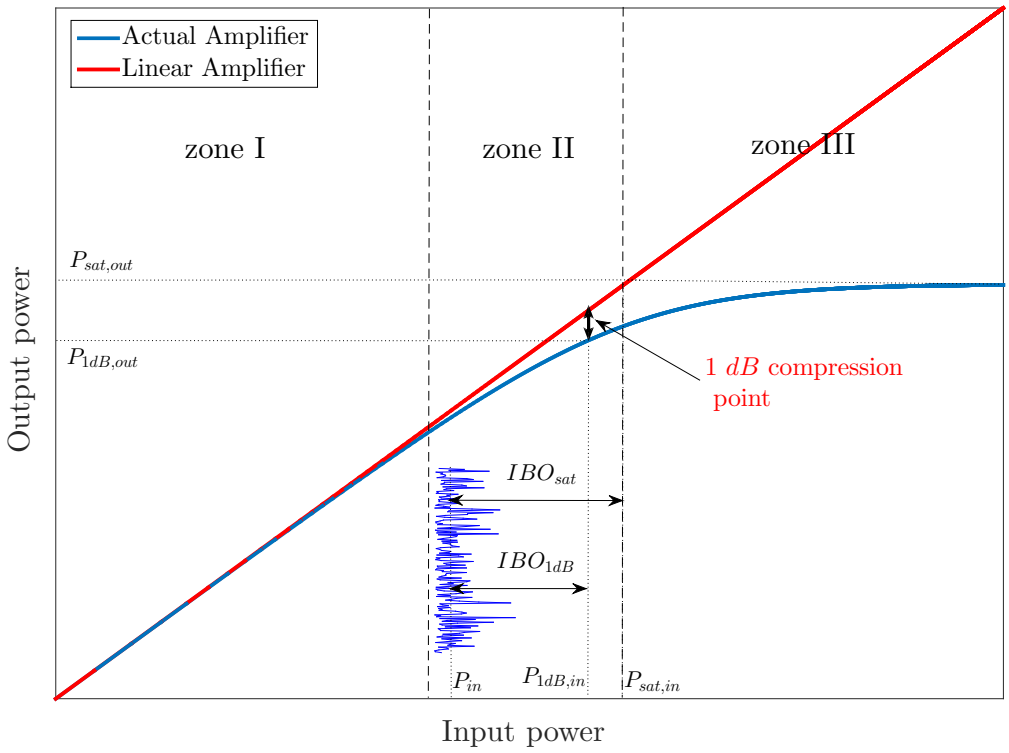

FIGURE 2.2 – Power amplifier characteristics: linear, compression and saturation zones.

2.2.3 Power back-off and 1 dB compression point

To avoid the PA saturation, normally the PA operation point is backed-off to the linear zone. This shift is measured with respect to the 1 dB compression point. The 1 dB compression point is a common figure of merit used to characterize the PAs linearity. It is the point for which the actual PA output power is 1 dB lower than what it would have been if the PA were linear.

This definition of the 1 dB compression point is graphically illustrated in Fig.2.2, which reports the AM/AM characteristic of the actual and ideal linear amplifier. Generally, the 1 dB compression point can be defined either with respect to the output power ($P_{1dB,out}$) or with reference to the input power ($P_{1dB,in}$).

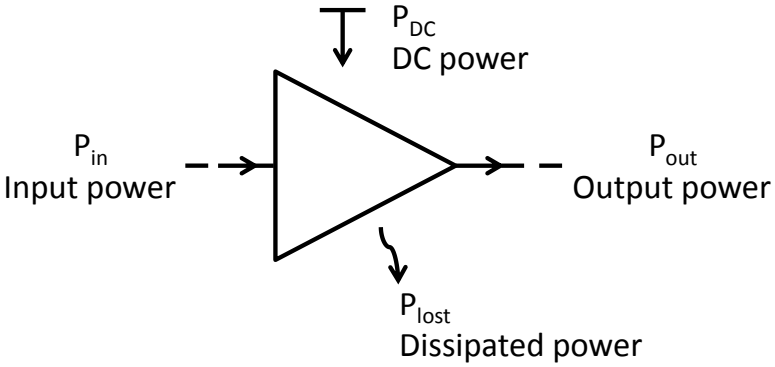

FIGURE 2.3 – Block diagram of the power amplifier.

Thus, to quantify the dimensioning of the amplifier we define the Input power Back-Off (IBO) term which is generally expressed in dB. In the literature we find two definitions of the IBO. The first definition is the ratio between the input power at the 1 dB compression point $P_{1dB,in}$ and the average input power P_{in} (eq.2.1).

$$IBO_{1dB} = \frac{P_{1dB,in}}{P_{in}}. \tag{2.1}$$

Likewise, the IBO can be defined by the ratio between the input power at the saturation point $P_{sat,in}$ and the average input power P_{in} (eq.2.2)

$$IBO_{sat} = \frac{P_{sat,in}}{P_{in}}. \tag{2.2}$$

In fact, the first definition is more widely used in the literature, that is why we adopted in our work. Thus, in the following the term IBO refers to IBO_{1dB} following Eq. (2.1). Similarly, the Output power Back-Off (OBO) could be defined as the ratio between the output power at 1 dB compression point and the average output power P_{out} (eq.2.3).

$$OBO = \frac{P_{1dB,out}}{P_{out}}. \tag{2.3}$$

Regarding Eq. 2.1 and Eq. 2.3, we remark that as the IBO (or the OBO) decreases, the input power decreases. Thus, we can notice that the larger the IBO, the less the distortions because the signal is amplified closer to the linear region (Fig. 2.2).

2.2.4 PA efficiency

An efficient power amplifier aims to deliver a certain amount of power to the load, without consuming too much power itself [RS06]. However, the actual DC power consumption, $P_{DC,PA}$, is always larger than the output power P_o. In fact, the PA dissipates a considerable amount of energy in the form of waste heat. Therefore, we find in the literature several definitions of the power amplifier efficiency.

- Drain efficiency : it is the ratio between the output power and the DC power, and is defined as

$$\eta_{DC} = \frac{P_o}{P_{DC,PA}}. \tag{2.4}$$

- Power Added Efficiency (PAE) : it takes into account the PA input power Pin, and is defined as

$$\eta_{PAE} = \frac{P_o - P_{in}}{P_{DC,PA}}. \tag{2.5}$$

In [Kaz08], the author proposed a relationship that gives the drain efficiency of the PA (classes A, B, and AB) as a function of the OBO. This relationship is given by

$$\eta_{DC} = \beta \, \frac{1}{OBO} \, , \tag{2.6}$$

where β equals 0.50, 0.66, and 0.78 for class A, AB, and B PAs, respectively. In Fig. 2.4, the power efficiency in (2.6) is plotted versus the OBO for class A, B, and AB PAs.

From Fig. 2.4, we see that the PA efficiency decreases when the back-off increases. However, we observed in Fig. (2.2) that the PA linearity increases when the back-off decreases. This means, therefore, that the linearity is degraded while the power efficiency is improved.

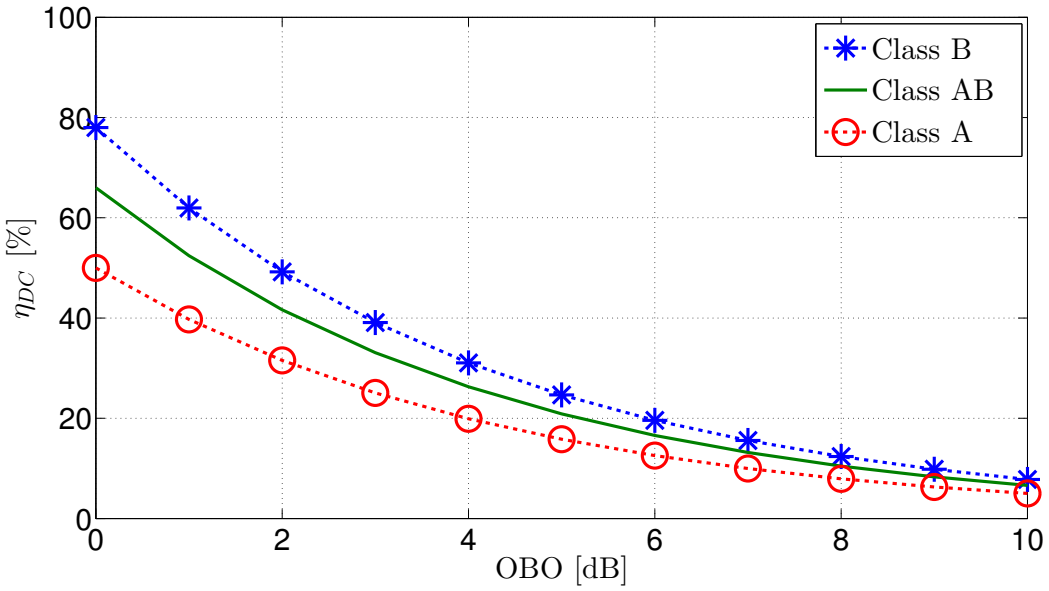

FIGURE 2.4 – Power efficiency depending on the OBO for class A, B, and AB PAs.

In this thesis, class A and class AB are considered as these types of PA are usually used in today base stations to insure the linearity of the transmitted signal especially because most modern communication standards use nonconstant envelope modulation which need linear amplification. In practice, the typical efficiency of a conventional power amplifier for digital terrestrial television signal in the UHF band is in the range of 15% to 25%. Thus, this means that the DC power consumption of a conventional power amplifier can be as much as 4 to 7 times the useful RF power delivered to the antenna. Furthermore, the PA efficiency in LTE macro, micro, pico, and femto base stations is 31.1%, 22.8%, 6.7%, and 4.4% respectively [AGG+11]. Also, referring to [DVT+10] the PA efficiency in WiMax and HSPA base stations do not exceed 12% while the power consumption is 100 Watts and 300 Watts, respectively.

Again, one can see that a significant portion of the total consumed power in base stations goes to the transmit power amplifier which has relatively a very

low efficiency. Secondly, we can remark from Fig. 2.4 that the most efficient PA operating point is close to the saturation point (OBO = 0). However, non-linear effects push the power amplifiers to operate in a more linear region because of the high fluctuations of the signal. Unfortunately, the PA efficiency in this region is relatively very low. This explains the reported weak PA efficiency in real base stations above.

2.2.5 Memory effects

Conventional static PA models, such as AM/AM and AM/PM characteristics, can represent, with reasonable accuracy, the PA behavior driven by narrowband input signals. However, in practice the actual amplitude and phase of the high PA output voltage are not only determined by the current input voltage. In reality, the output of High-Power Amplifiers (HPAs) such as those used in wireless base stations depend on the instantaneous inputs, but also on the previous inputs too. This kind of phenomenon is described as memory effects and it is illustrated in Fig. 2.5. Besides, wideband signals also tend to induce memory effects in the PA. In such cases, memoryless PA models can be ineffective. Thus, accurate representation of the PA memory effects is crucial. Vuolevi et al. [VRM01a] divided the memory effects into two class: electrical and thermal memory effects. Electrical memory effects are mainly caused by varying envelope, impact ionization, matching conditions at harmonic frequencies, and bias circuit design [BG89]. On the other hand, thermal memory effects are caused by the electrothermal coupling in the power transistor. It is a function of the power dissipated in the transistor, which directly affects the temperature of the transistor junction. As a result, the characteristics of the transistor in terms of gain and output power capability change versus these temperature variations.

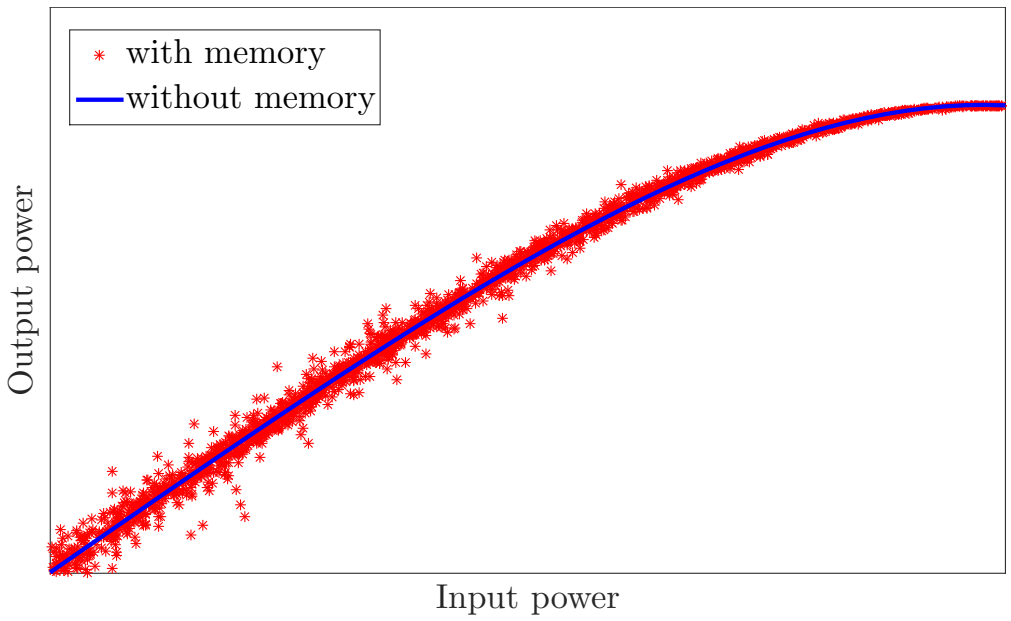

FIGURE 2.5 – Power amplifier characteristics with and without memory effects.

2.3 Power amplifiers modeling

In the past few decades, PAs modelling has been the focus of research as the PAs are the major source of nonlinearity in communication systems. Here, we present a literature review focusing on nonlinear PA behavioral models which can be divided into three types: memoryless and quasi memoryless nonlinear models, and nonlinear models with memory.

2.3.1 Memoryless nonlinear models

In memoryless power amplifier models the output signal is a nonlinear function of the instantaneous input amplitude only and not of the past one. In addition, memoryless PA models only consider AM-AM characteristics, and assume no phase distortion. In the following, some popular static behavioral PA models are presented.

2.3.1.1 Rapp model

The Rapp model introduced by Rapp in [Rap91] is well suited for amplifiers based on semiconductors Solid State Power Amplifiers (SSPA). This Rapp model is memoryless, i.e. its output at a determined time instant does not depend on the previous entries. In addition, it does not present any phase distortions. The AM-AM transfer curve of the PA is then given by

$$H_{PA}(r) = \frac{r}{\left(1 + \left(\frac{r}{A}\right)^{2b}\right)^{\frac{1}{2b}}} , \tag{2.7}$$

where r is the magnitude of the input voltage and A is the amplitude of the saturation output voltage of the amplifier. Parameter b is commonly referred to as the 'knee factor' of the PA characteristic and controls the smoothness of the transition between the linear and the saturation zones. Fig. 2.6 presents the AM/AM characteristic of the Rapp model for different knee factor values with a unitary amplification gain. It has to be noted that as the value of b increases, the Rapp model approaches to a soft envelope limiter model.

2.3.1.2 Memoryless polynomial model

Polynomial model uses a parametric Taylor series with reel coefficients to model the PA's nonlinear behavior. The PA output is expressed in baseband by the following odd order polynomial

$$H_{PA}(r) = \sum_{l=0}^{L_p-1} b_{2l+1}\, r^{2l+1}. \tag{2.8}$$

where L_p denotes the nonlinear model order, and b_{2l+1} are the nonlinear PA characteristics coefficients. Note that the odd order comes from the bandpass assumption [JBS00, p. 161]. Making the coefficients b_{2l+1} complex in (2.8) will result in a quasi memoryless polynomial PA model.

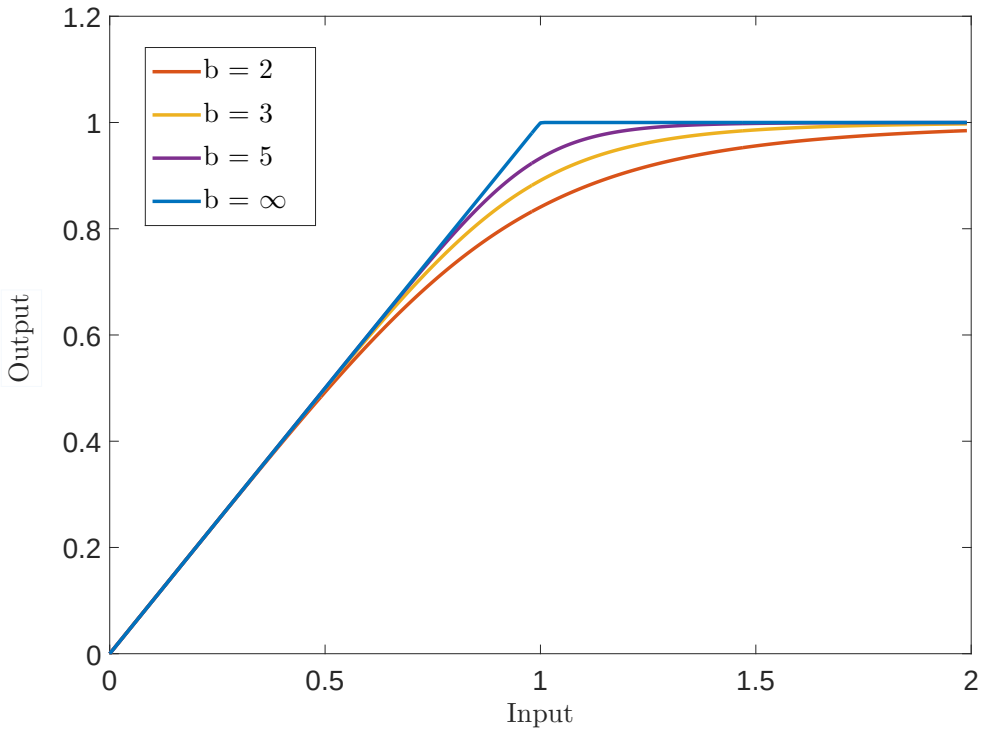

FIGURE 2.6 – AM/AM characteristic of Rapp model for different knee factor values.

2.3.2 Quasi memoryless nonlinear models

On the other hand, quasi memoryless PA models take into account both amplitude and phase distortions. Therefore, they are represented by the amplifier AM/AM as well as AM/PM characteristics.

2.3.2.1 Saleh model

The widely accepted Saleh model [Sal81] for memoryless Traveling Wave Tube Amplifiers (TWTA) is defined by two-parameter functions which represent the AM/AM and AM/PM characteristics. This model introduces more significant AM/PM distortion than most SSPA models. Its AM/AM and AM/PM conversion functions, F_a and F_p respectively, are described by the following equations

$$F_a(r) = \frac{\alpha_a \; r}{1 + \beta_a \; r^2} \; , \tag{2.9}$$

$$F_\theta(r) = \frac{\alpha_\theta \; r^2}{1 + \beta_\theta \; r^2} \; . \tag{2.10}$$

The constant parameters $\alpha_a, \beta_a, \alpha_\theta$ and β_θ characterize the behavior of the PA and are carefully chosen so that the model fit to the measurement data. Thus, the distorted output of the PA is expressed as

$$y(t) = F_a(|x(t)|) \; e^{j(arg(x(t)) + F_\theta(|x(t)|))}. \tag{2.11}$$

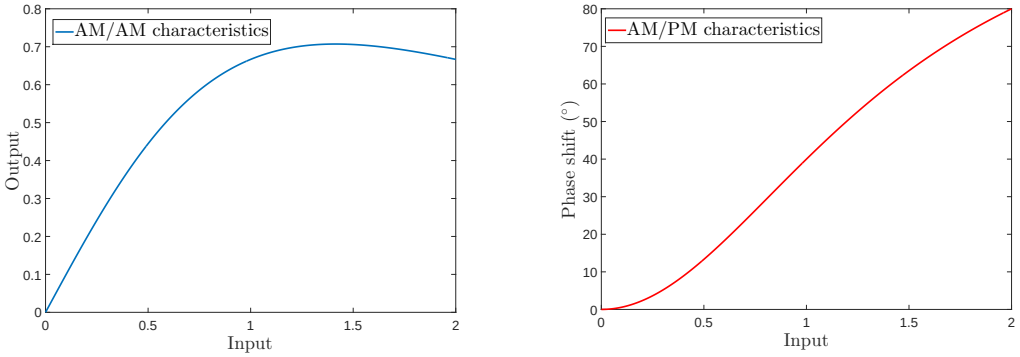

FIGURE 2.7 – AM/AM and AM/PM characteristics of Saleh model (α_a =2, β_a = 0.5, α_θ =$\pi/3$, β_θ =0.5)

The AM/AM and AM/PM characteristics of Saleh model are shown in Fig. 2.7. We note that appropriate values of the amplitude and phase coefficients also provide an accurate model for SSPA.

2.3.3 Nonlinear models with memory

In reality the PA output depends on both previous and current PA inputs what is called memory effects. These memory effects are due to thermal aspects, and long time constants in DC bias circuits. As the bandwidth of the signal increases, with for example wideband multicarrier systems, memory effects become even more severe and can no longer be ignored. Thus, PA memoryless models in this case are not accurate enough. Memory effects results in asymmetries between lower and upper sidebands, and bandwidth dependent variations in the magnitude of intermodulation products. In the next subsections we present some of the most common PA models with memory.

2.3.3.1 Volterra series model

A Volterra series is a combination of linear convolution and a nonlinear power series so that it can be used to describ any nonlinear stable system with fading memory [Sch06]. A truncated Volterra series in the discrete time domain can be expressed mathematically as follows

$$y(n) = \sum_{p=1}^{P} y_p(n), \tag{2.12}$$

where

$$y_p(n) = \sum_{i_1=0}^{N-1} \dots \sum_{i_P=0}^{N-1} h_p(i_1, \dots, i_p) \prod_{j=1}^{P} x(n - i_j). \tag{2.13}$$

$x(n)$ and $y(n)$ represent the input and the output respectively, P and M are the order of nonlinearities and the memory depth, respectively, and $h_p(i_1, \dots, i_p)$ is called the "Volterra kernel" of order n. The Volterra model can achieve higher accuracy in comparison with other PA memory models at the cost of very high computational complexity. In fact, its main disadvantage is that the number of

coefficients exponentially increases with respect to the memory length and/or the order of its kernels. This is the reason why it is unattractive and seldom used in practice. Therefore, the Wiener and the Hammerstein models, which will be presented in the next subsection, are simplified special cases of the Volterra model.

2.3.3.2 Wiener and Hammerstein models

As mentioned above, in real time applications, Volterra model is unpractical. To overcome the complexity issue associated to the Volterra series representation, special cases of Volterra series were investigated for modeling nonlinear power amplifiers with less complexity. The Wiener model, the Hammerstein model, and the Wiener-Hammerstein model are some of the category of Volterra special cases [BF82, GMB05, NG66].

The Wiener model is a Linear Time nvariant (LTI) system followed by a memoryless nonlinearity as illustrated in Fig. 2.8. The output $y(n)$ of a Wiener model is given by

$$y(n) = \sum_{i=1}^{N} b_i |u(n)|^{2i} u(n), \tag{2.14}$$

with

$$u(n) = \sum_{i=1}^{M} h_i \; x(n-i), \tag{2.15}$$

where Eq. 2.14 is the transfer function of the memoryless nonlinearity. b_i and h_i are the coefficients of the static nonlinearity and the impulse response of the LTI portion of the Wiener system, respectively. M represents the depth of the memory effects and N is the order of the nonlinearity.

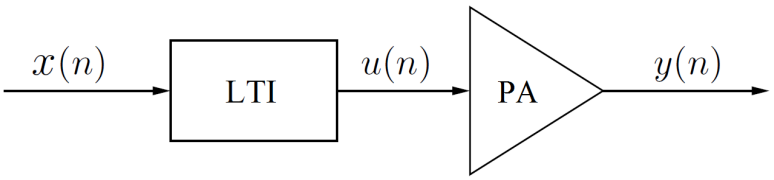

FIGURE 2.8 – Principle of Wiener model.

Hammerstein model is the inverse of the Wiener model. It is composed of a memoryless nonlinear polynomial followed by LTI filter. Its principle is illustrated in Fig. 2.9. The output of baseband polynomial PA is modeled as

$$v(n) = \sum_{i=1}^{N} b_i |x(n)|^{2i} x(n). \tag{2.16}$$

Therefore, the output $y(n)$ of a Hammerstein model is given by

$$y(n) = \sum_{i=1}^{M} h_i \; v(n-i). \tag{2.17}$$

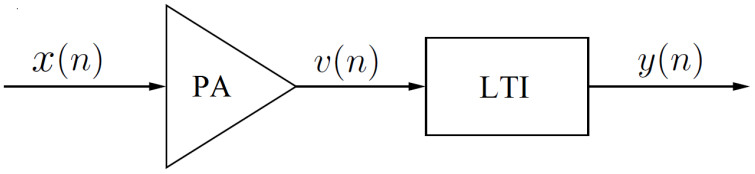

FIGURE 2.9 – Principle of Hammerstein model.

The Wiener-Hammerstein model is an LTI system followed by a memoryless nonlinearity, which in turn is followed by another LTI system (see Fig. 2.10). The subsystems in this model are described by

$$u(n) = \sum_{i=1}^{M_1} h_{1i}\, x(n-i), \tag{2.18}$$

$$v(n) = \sum_{i=1}^{N} b_i |u(n)|^{2i} u(n), \tag{2.19}$$

$$y(n) = \sum_{i=1}^{M_2} h_{2i}\, v(n-i). \tag{2.20}$$

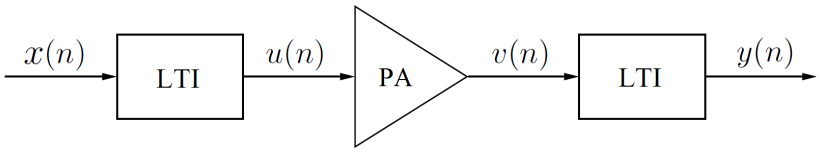

FIGURE 2.10 – Principle of Memory Polynomial model.

2.3.3.3 Memory polynomial model

Another popular and useful PA model is the memory polynomial model [KK01a] which is also a truncation of the general Volterra series, and it consists of only keeping the diagonal terms in the Volterra kernels. Thus, the number of parameters is significantly reduced compared to conventional Volterra model, and the computational complexity of the coefficients identification is remarkably decreased. The memory polynomial model can be viewed as parallel connected memoryless nonlinear models, each with individually delayed input signal so that the outputs of the nonlinear sub-models would be summed up, as shown in Fig. 2.11.

The relationship between the input and output of the memory polynomial model is given by the following equation

$$z(t) = \sum_{q=0}^{Q} \sum_{l=1}^{L} b_{lq}\, x(t-q\tau)\, |x(t-q\tau)|^{2(l-1)}, \tag{2.21}$$

where Q is the memory depth, τ is a delay parameter, L is the polynomial order and b_{lq} are complex coefficients. All these parameters reflect the nonlinearities

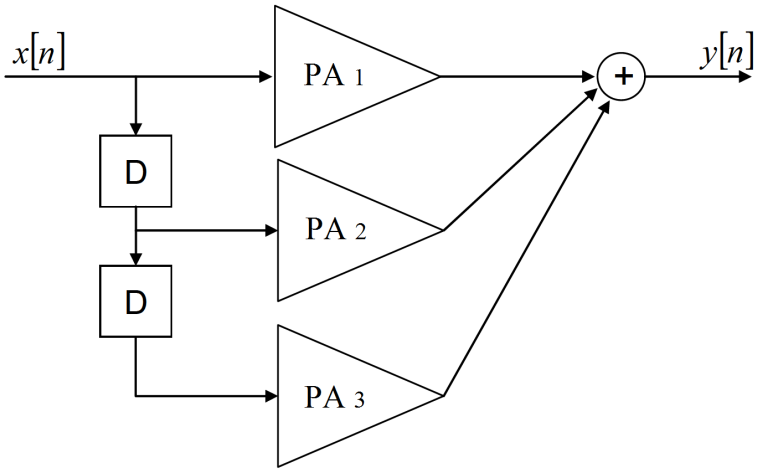

FIGURE 2.11 – Principle of memory polynomial model.

and memory effects of the PA and can be obtained through measurements and estimation algorithms for a particular PA [MMK+06].

2.4 Figures of merit

Signals may experience strong distortions due to the nonlinear components in the transceiver chain, such as the power amplifier, and other nonlinearities like the I/Q imbalance, oscillator phase noise and sampling jitter. As a result of these nonlinearities, in-band and out of band distortions are generated. The main effects are cloud-like shape of constellation points and the out-of-band radiation. To characterize the effect of nonlinearity on the performance of the communication system several figures of merit are used. This section focuses on some of these figures of merit which are the Error Vector Magnitude (EVM), Modulation Error Rate (MER), and Adjacent Channel Power Ratio (ACPR).

2.4.1 Error Vector Magnitude (EVM) and Modulation Error Rate (MER)

The Error Vector Magnitude is a metric which measures the in band distortion level of a signal. A signal sent by an ideal transmitter would have all constellation points precisely at their ideal locations. However, various imperfections in the implementation such as the nonlinearity of the PA function and the PAPR reduction stage, cause the actual constellation points to deviate from the ideal locations. Thus, a little cloud of demodulated symbols, located near from the ideal constellation points is created. Fig. 2.12 represents X_k and Z_k the kth complex symbols of the reference and amplified signals, $x(t)$ and $z(t)$, respectively. In this figure, a unitary amplification gain is assumed for the clarity of the representation.

By definition, the EVM is the ratio of the Root Mean Square (RMS) of the difference between a collection of measured symbols and ideal symbols to the square root of the mean signal power. Therefore, the EVM of the amplified signal $z(t)$ is

expressed in percentage and Decibel as follows

$$\mathrm{EVM}_{(\%)} = \sqrt{\frac{E\left\{|z(t)-x(t)|^2\right\}}{E\left\{|x(t)|^2\right\}}} \times 100, \tag{2.22}$$

$$\mathrm{EVM}_{(dB)} = 10\,\log\left(\sqrt{\frac{E\left\{|z(t)-x(t)|^2\right\}}{E\left\{|x(t)|^2\right\}}}\right), \tag{2.23}$$

where

$$E\left\{|z(t)-x(t)|^2\right\} = \int_0^{R_{max}} |\epsilon\,(r)|^2\, f_x\,(r)\; dr, \tag{2.24}$$

where $\epsilon\,(r) = z(t) - x(t)$ is a stationary random variable modeling the signal error, and R_{max} is the maximum amplitude of $x(t)$. Eq. (2.24) represents the second order moment of the magnitude error $|\epsilon\,(r)\,|$ and $E\{|x(t)|^2\}$ is the average signal power. Note that the signal amplitude in practice does not tend to infinity and is limited to a maximum value R_{max}.

Likewise, the Modulation Error Rate is a measure used to quantify the performance of a digital transmitter or receiver of a communications system. MER is a similar measurement to EVM but expressed differently. In literature, there are several MER definitions. Based on the technical report of the ETSI [ETS01], the MER is the ratio of the power of the signal to the power of the error vectors, generally expressed in dB, and it is given by

$$\mathrm{MER}_{(dB)} = 10\,\log\left(\frac{E\left\{|z(t)-x(t)|^2\right\}}{E\left\{|x(t)|^2\right\}}\right). \tag{2.25}$$

Therefore, the straightforward relationship between EVM and MER in Decibel is

$$\mathrm{MER}_{(dB)} = 2 \times \mathrm{EVM}_{(dB)} \tag{2.26}$$

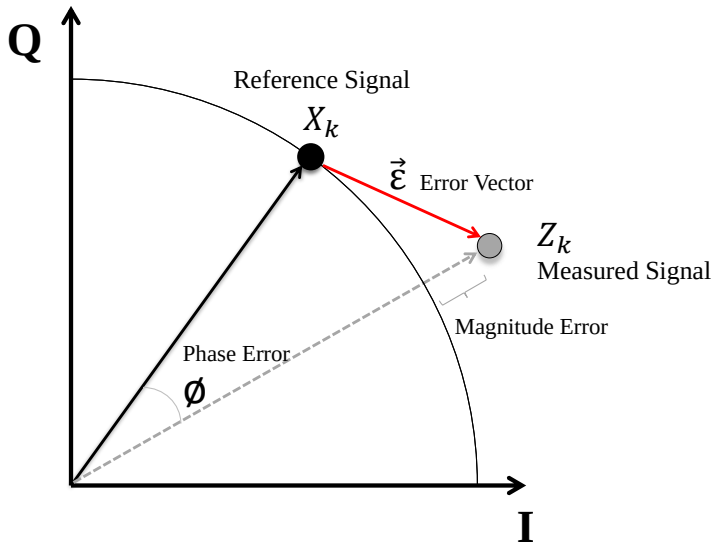

FIGURE 2.12 – Error vector magnitude representation.

2.4.1.1 EVM and MER requirements

In general, MER is a figure of merit analysis typically defined in the broadcasting industry. However, EVM is a figure of merit analysis typically defined in wireless industry. Therefore, most of wireless communication standards such as the IEEE 802.11ac standard [EVM99], the IEEE 802.16e WiMAX standard [EVM05], and the LTE standard [LTE12] have already specified their requirements in terms of EVM.

In the case of LTE standard, for all bandwidths, the EVM measurement shall be performed over all allocated resource blocks and downlink subframes within 10 *ms* measurement periods. The EVM for different modulation types on Physical Downlink Shared Channel (PDSCH) shall be better than the limits in Table 2.1.

TABLE 2.1 – Allowed EVM versus constellation size for LTE standard [LTE12].

Modulation	Required EVM (%)
QPSK	17.5 %
16QAM	12.5 %
64QAM	8 %

Likewise, the allowed EVM versus constellation size and coding rate for the IEEE 802.11ac standard are presented in Table 2.2.

TABLE 2.2 – Allowed EVM versus constellation size and coding rate for IEEE 802.11ac standard [EVM99].

Modulation	Coding rate	Required EVM (%)
BPSK	1/2	56%
QPSK	1/2	32 %
QPSK	3/4	22%
16-QAM	1/2	16 %
16-QAM	3/4	11 %
64QAM	2/3	8 %
64QAM	3/4	6 %
64QAM	5/6	5 %
256QAM	3/4	3 %
256QAM	5/6	2.5 %

On the other hand, there are no specifications for MER in broadcasting standards such as DVB-T2 and ATSC. Therefore, based on different transmission conditions like coverage area, broadcasting channel, etc, and after different measurements, the manufacturers of broadcast equipments adjust their parameters with an empirical MER in order to guarantee an acceptable quality of service. Generally, the MER constraint imposed by these manufacturers is between -32 dB and -36 dB which corresponds to an EVM value between 1.5 % and 2.5 %.

2.4.2 Adjacent Channel Power Ratio (ACPR)

The spectral mask is a crucial linearity requirement used to ensure that the transmitter does not interfere with the spectrum of neighboring channels. For this reason, all communication standards specify the minimal required Adjacent Channel Power Ratio (ACPR) i.e. the maximal allowable out of band distortion. Indeed, ACPR (also referred to as Adjacent Channel Leakage Ratio (ACLR)) characterizes undesirable spectral regrowth and it is one of the most important and critical figures of merit. ACPR is defined by the ratio between the average power transmitted in the desired band compared to the power transmitted in the right or left lateral bands and it is given by

$$\mathrm{ACPR}(dB) = 10 \log \frac{\int_{f_{ch}} PSD(f)df}{\int_{f_{adj}} PSD(f)df}, \tag{2.27}$$

where $PSD(f)$ is the power spectral density of the transmitted signal. f_{ch} and f_{adj} specify the frequency bands of the main channel and of the adjacent channel respectively.

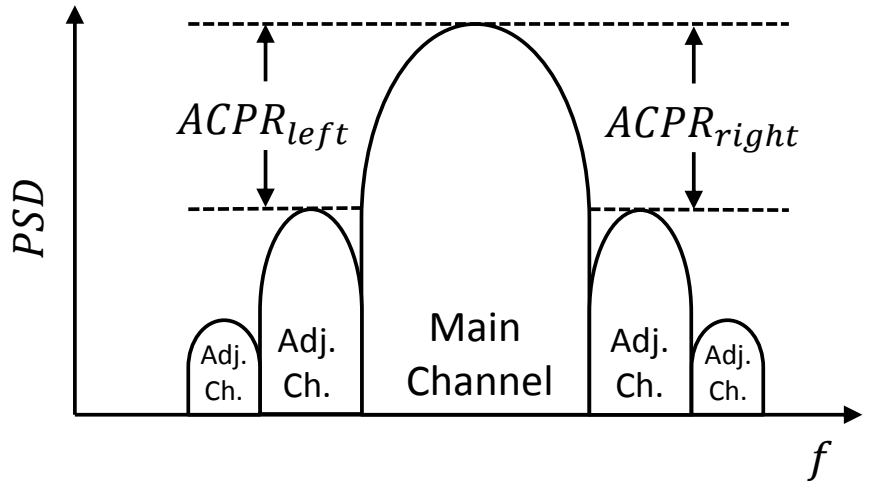

FIGURE 2.13 – Adjacent channel power ratio representation.

2.4.2.1 ACPR requirements

To verify that the transmitted signal does not cause unacceptable interference to adjacent channels in terms of ACPR, standards impose a minimum ACPR requirement and spectrum emission mask. Table 2.3 presents the minimum requirements to be applied to base stations in 3G and LTE standards for different adjacent channel offset [ACP]. Besides, Fig. 2.14 and Fig. 2.15 depict the spectrum emission mask used for DVB-T and IEEE 802.11ac standards [spe]. Also, Fig. 2.14 presents the critical and the uncritical masks to be used for the lowest and highest channels in the allocated band to protect neighboring radio services.

TABLE 2.3 – Minimum requirements of ACPR limits in 3G and LTE standards [ACP, LTE12].

Standard	Adjacent channel offset	ACPR limit (dB)
3G	± 5 MHz	45 dB
	± 10 MHz	55 dB
LTE	± 5, ± 10, ± 15, ± 20 MHz	45 dB

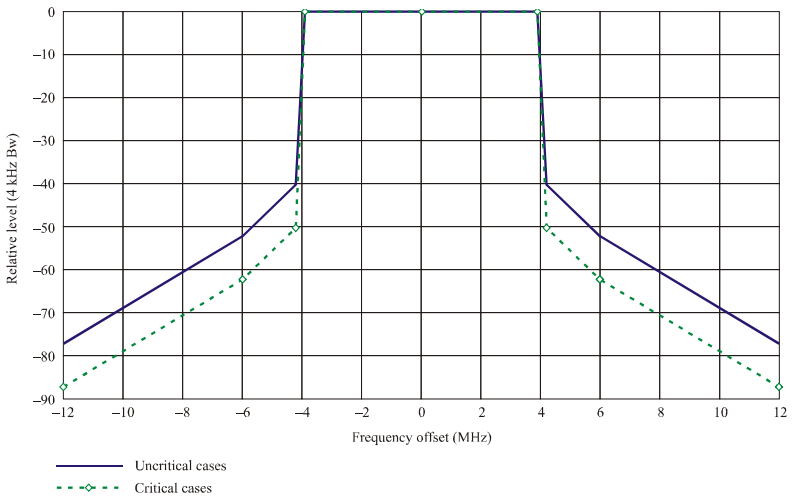

FIGURE 2.14 – Transmit spectral mask for 8 MHz DVB-T system.

2.5 Linearization techniques

The PA nonlinear characteristics result in harmful distortions which deteriorate the linearity response of the whole transmission chain especially when its operating point is closed to saturation. To overcome this problem, several techniques have been proposed for the compensation of the PA nonlinearities. In the following subsections, we present some of the widely used linearization techniques.

2.5.1 Feedback

Feedback is a widespread linearization technique due to its lower cost and lower complexity [AW71, Ken00a]. It can be applied in either baseband or RF parts. The basic concept of feedbacl is that the amplified signal should be fed back and compared with the input signal. Thus, the difference between these signals gives the error signal. Then, the error signal is used to compensate for the nonlinearity of the power amplifier. There are various types of this technique such as the polar feedbacl, the envelope feedbacl, and the cartesian feedbacl. Fig. 2.16 presents an example of cartesian loop feedback scheme where the input and amplified signals are separated into in-phase and quadrature components. After the comparison, the correction of I/Q signal shift are performed. The main advantage of feedback is that it can compensate effects due to aging and memory effects. Besides, it can overcome non-linear distortions originating from sources external to the PA e.g.

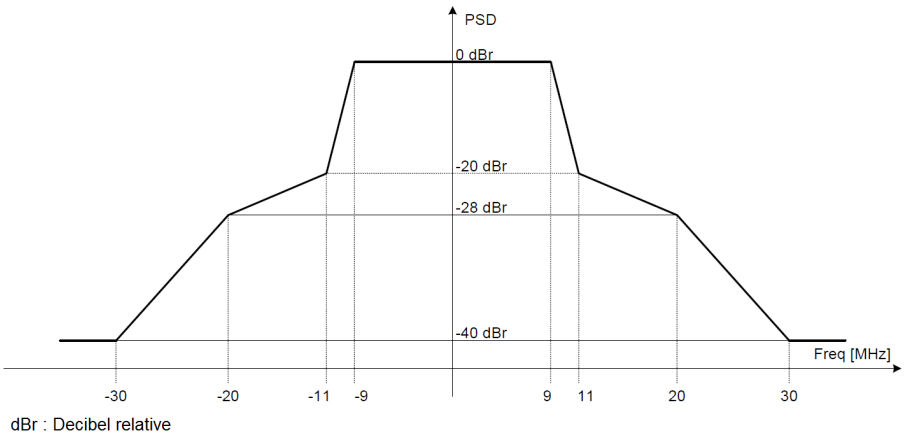

FIGURE 2.15 – Transmit spectral mask used by IEEE 802.11ac standard [spe].

mixers and filters. Furthermore, the closed loop gain can also make the PA gain less sensitive to variations in circuit components, i.e. due to temperature effects. On the other hand, the main disadvantage is the delay between the input and copied output signals. Also, the stability of the feedback loop is hard to maintain over the large dynamic range of modern communication systems.

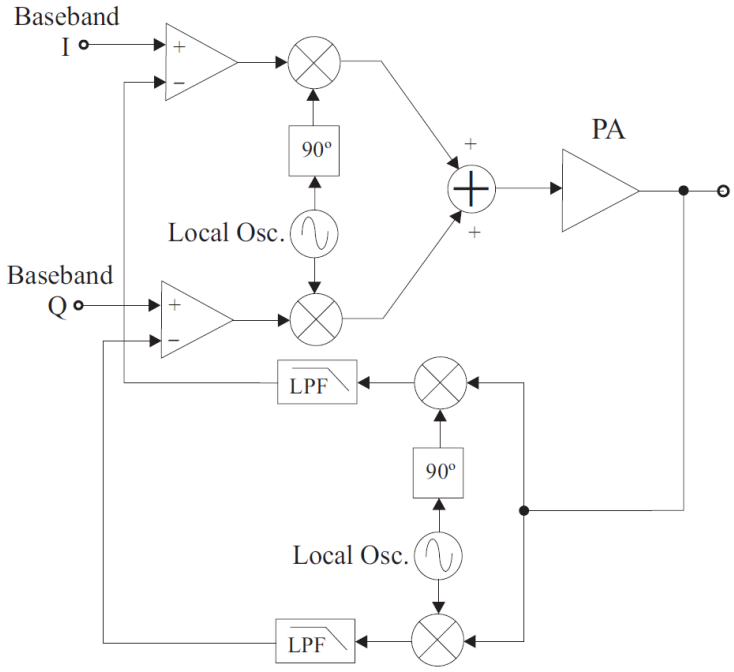

FIGURE 2.16 – Basic scheme for cartesian loop feedback.

2.5.2 Feedforward

The principle of feedforward technique is to employ an auxiliary path for non-linear distortion cancellation [Ken00b, S28]. In a first loop, an error signal is generated by subtracting the input PA signal from the attenuated output signal. Then, the error signal is amplified with highly linear PA and combined finally with the

output signal of the main PA after a 180 degree phase shift. Theoretically, we obtain a non distorted output spectrum.

Main advantages of feedforward technique over feedback technique are that the gain of the amplifier is not reduced, the system is unconditionally stable, as well as the bandwidth can be very high.

However, major disadvantages of the feedforward technique are the power efficiency loss due to the linear PA, complexity of time aligning adjustments as well as the system is not adaptive. As a result, the change of PA characteristics with respect to aging, temperature or any other change in circuitry can not be compensated.

Therefore, the cost and complexity of the practical implementation of this technique limit the use of this technique.

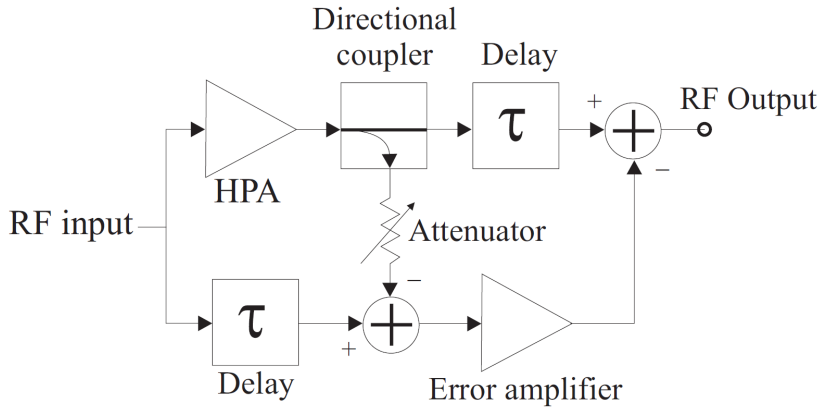

FIGURE 2.17 – Basic scheme for feedforward linearization technique.

2.5.3 Predistortion

PreDistortion (PD) is by far one of the most extended linearization techniques. The main principle of this technique is to apply the inverse function of the PA transfer function to cancel the nonlinearities at the PA output [INM89, SC92]. Therefore, the cascade of the predistorter and the PA gives a linear response. The advantage of predistortion is that it is relatively easy to implement at a low cost. As such, predistortion is frequently applied, not also in research, but also in commercially available products [SSS03].

2.5.3.1 Predistortion types

Generally, the predistortion is applied before the signal is presented to the nonlinear PA as shown in the block diagram of Fig. 2.18. However, there are two types of predistortion which are analogue predistortion and Digital PreDistortion (DPD) depending on where PD is performed, in RF part via analogue signal processing or in baseband part via DSPs. In practice, because of its highly cost effective and its relative implementation simplicity, DPD overrides other implementation approaches thanks to the increased performance involved in DSP. In fact, DPD is one of the most popular linearization techniques [Fra, Din04, Was04]. In addition, according to the latest research results due to the improvement of the hardware

components, e.g. FPGA and DAC of higher operating frequency, the operation bandwidth of a DPD can be extended over 60 MHz [DPD].

2.5.3.2 DPD modeling

We consider H_{PA} and H_{PD} the PA and predistortion baseband transfer functions. Theoretically, these two transfer functions should satisfy the following relationship

$$H_{PA} \circ H_{PD} = I_d, \tag{2.28}$$

where $\circ$ is the composite function and the I_d is the identity. Even though the predistortion modeling and PA modeling are two different applications, the working principles of both are almost identical to each other. In fact, the PA modeling aims at finding the exact PA transfer function, while the intention of the predistortion is to estimate the inverse transfer function of PA characteristics. Nonetheless, both the PA characteristics and its inverse transfer function can be based on the same mathematical models. That is why most of PA models previously mentioned in Section 2.3 can be used in the predistortion modeling such as the polynomial model, the Wiener and Hammerstein models and so on. In this work we adopted the well known polynomial model which is a good compromise between compensation performance and complexity. Thus, the predistorted signal can be expressed as follows

$$x_{PD}(t) = \sum_{k=0}^{K_p-1} a_{2k+1} x(t)^{2k+1}, \tag{2.29}$$

with a_{2k+1} the nonlinear polynomial coefficients and K_p the parameter which determine the nonlinear model order.

The objective of the conventional DPD modeling is to find the inverse transfer characteristics of PA to compensate the static nonlinearity of PAs without consideration of memory effects. In practice, one is able to estimate the inverse PA characteristic using a special training signal. Consequently, the resulted DPD transfer function does not need to be adapted since the PA characteristics are assumed to be unchanged during the operating time. The simplest open loop memoryless DPD is depicted in Fig. 2.18. In terms of stability and bandwidth capacities, open loop DPD is similar to feedforward, in addition, it does not present most limitations of feedback technique. In particular, it does not require any hardware or software resources.

Unfortunately, the PA characteristics do change during the operating time, depending on the signal statistics, device temperature, the PA aging and so on. Therefore, a static predistortion characteristic is inappropriate in practice as it will gradually tend to become misaligned with the PA nonlinearity. In order to adjust the DPD model during the operating time, close loop DPD was developed. In the following two adaptation algorithms to update the DPD characteristics are presented.

2.5.3.3 Direct and indirect learning architectures

There are two conventional learning structures of adaptive algorithm, named direct and indirect learning structure. On one hand, the indirect learning architecture compares the predistorted signal $x_{DPD}(n)$ and feedback signal $z(n)$ in order

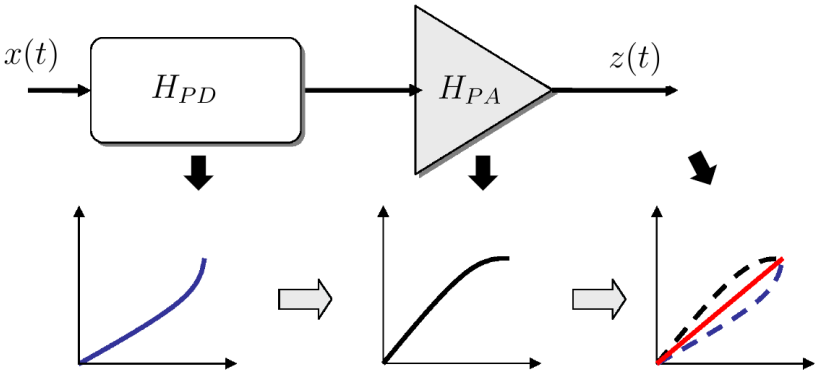

FIGURE 2.18 – Principle of the predistortion technique.

to derive a postdistorter of the nonlinear PA. Then, the postdistorter characteristics are copied to the predistorter block. Fig. 2.19 depicts the indirect learning architecture principle.

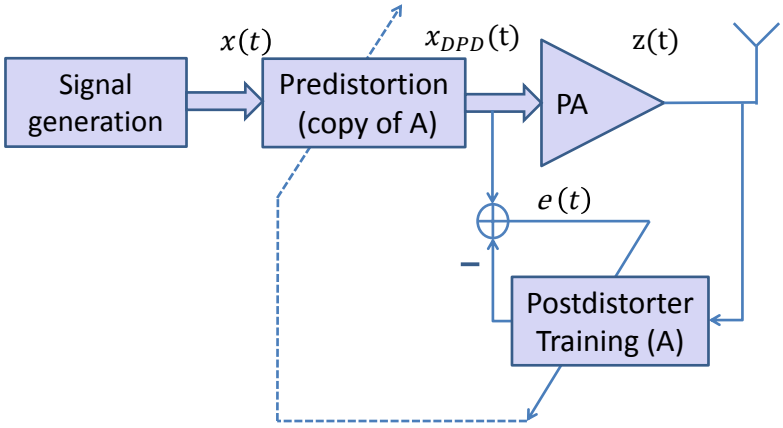

FIGURE 2.19 – Principle of the indirect learning.

On the other hand, the direct learning extract the PA nonlinear characteristics through the comparison between the input and output signals of the PA. Then, it tries to estimate the inverse characteristics which are copied to the predistortion block. The direct learning architecture principle is presented in Fig. 2.20.

In general, indirect learning and direct learning architectures exhibit similar performance. Nevertheless, since the original input signal $x(n)$ is free from any measurement noise, the direct learning architecture is much less sensitive to the measurement noise in comparison to the indirect learning architecture. However, regarding the computing issue, we can notice that the indirect learning architecture is more convenient, because the PA inverse transfer function is directly derived by solving a system of equations. In fact, the DPD coefficients a_{2k+1} can be calculated by solving the following equations

$$x_{DPD}(n) = \sum_{k=0}^{K_p-1} a_{2k+1} z(n)^{2k+1}. \tag{2.30}$$

It is worthwhile to note that equation (2.30) is nothing else than equation (2.29)

after substituting the input signal $x(n)$ by the amplified signal $z(n)$. Assuming a polynomial predistortion order of 5, in this case, we have to estimate three coefficients a_1, a_3, and a_5. Theoretically, we need only three pairs of feedforward and feedback samples to identify three unknowns. However, three points can not perfectly estimate a nonlinear model. In addition, using only few samples will lead to instable and unreliable model especially in presence of noise effect and signal accidental error. This is why much higher samples are used to perform the inverse transfer function.

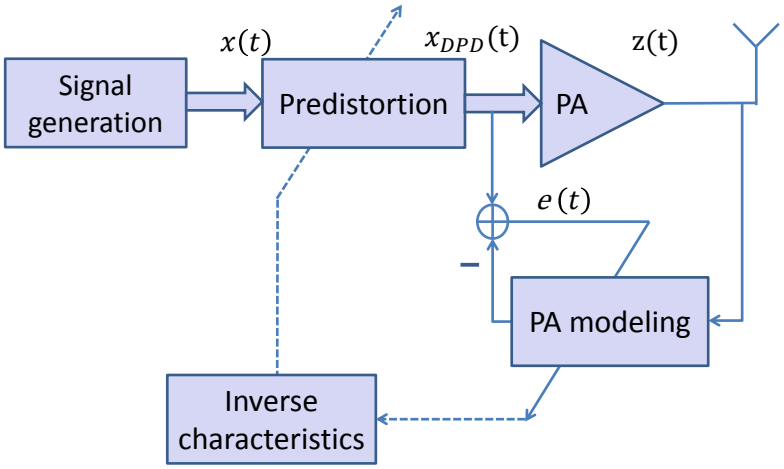

FIGURE 2.20 – Principle of the direct learning.

Referring to equation (2.30), it can be rewritten in a matrix format as an over-determined system of equations with N samples and K coefficients, and it is given by

$$\mathbf{X}_{PD} = \mathbf{M}_{\mathbf{z}} \,.\, \mathbf{A} \tag{2.31}$$

where

$$\mathbf{X}_{PD} = \begin{bmatrix} \mathbf{X}_{PD}[0] & \mathbf{X}_{PD}[1] & \dots & \mathbf{X}_{PD}[N-1] \end{bmatrix}^T, \tag{2.32}$$

$$\mathbf{M}_{\mathbf{z}} = \begin{bmatrix} z[0] & z[0]^3 & z[0]^5 & \dots & z[0]^{2k+1} \\ z[1] & z[1]^3 & z[1]^5 & \dots & z[1]^{2k+1} \\ \vdots & \vdots & \vdots & \dots & \vdots \\ \vdots & \vdots & \vdots & \ddots & \vdots \\ z[N-1] & z[N-1]^3 & z[N-1]^5 & \dots & z[N-1]^{2k+1} \end{bmatrix} \tag{2.33}$$

and

$$\mathbf{A} = \begin{bmatrix} a_1, a_3, a_5, \dots, a_{2k+1} \end{bmatrix}^T, \tag{2.34}$$

where $()^T$ denotes the transpose of a matrix. The coefficients estimation can be performed by solving an over-determined system of equations by Least Squares (LS) algorithm [DMM+06]

$$\mathbf{A} = \left[(\mathbf{M_z})^H \ \mathbf{M_z}\right]^{-1} (\mathbf{M_z})^H \mathbf{X}_{PD}, \tag{2.35}$$

where $()^{-1}$ and $()^H$ return the inverse value and conjugate transposed value, respectively.

2.5.3.4 Online DPD and offline DPD

DPD can be also categorized depending on how often the predistortion characteristics are updated. Therefore, we find two groups entitled online DPD (or real-time DPD) and offline. In the former category, the DPD characteristics are updated per each pair of feedforward and feedback samples. Hence, the required hardware resources are extremely low and the updating speed is very high. However, the implementation efforts of online DPD are very complex as the adaptation algorithm must be written in hardware language, such as VHDL, and implemented with the DPD system in one block. Apart from the implementation complexity, online DPD requires some other signal processes in baseband to support its work, e.g. the synchronization and power normalization of the feedforward and feedback data which yield the implementation efforts even higher.

The second category is the offline DPD which has been widely used in PA linearization because it requires less implementation efforts in comparison to online DPD. It consists in estimating the DPD model separately in a DSP after collecting feedforward and feedback data. Therefore, the implementation complexity is extremely reduced with offline DPD.

2.6 Power amplifier and non-constant envelope signals: linearity-efficiency problematic

Traditionally, an input power back-off (IBO) is applied to the signal in order to minimize the saturation effects. As we can see in Fig. 2.2 and Fig 2.21, larger the back-off, lower the PA distortions. However, this solution is not practical since the PA efficiency dramatically decreases as the back-off increases.

In Fig. 2.21, we present an actual PA characteristic. It is designed for Digital Video Brodcasting-Terrestrial in the 174 MHz to 230 MHz VHF broadcast band, where it can deliver 50 W [Tec10]. Fig. 2.21 depicts the gain and power efficiency of a real DVB-T PA as a function of the output power at 202 MHz. We note that this DVB-T PA will be used in our simulations later. We can clearly see that as the PA operates at power levels below saturation, the PA efficiency degrades. Therefore, one can remark that while the PA linearity increases, the PA efficiency decreases and vice versa. So, a trade-off between the PA linearity and the efficiency should be carefully considered.

Furthermore, this problem is more complicated when we use signals with non-constant envelope such as multicarrier signals which are characterized by high PAPR value. In fact, if we have to avoid the saturation of high peaks of the signal, then the average power level will be significantly away from saturation zone. Consequently, this will result in very low PA efficiency. On the other hand, if we drive the PA with average power near from saturation to keep the maximum

power efficiency, then peak power levels will drive the amplifier into saturation zone, creating larger nonlinearities.

In the next subsection, we will present how the PAPR reduction and linearization techniques are used in literature. Afterwards, we will introduce our global approach which enhance the interoperability of the PAPR reduction and linearization and establish the best compromise between linearity and efficiency.

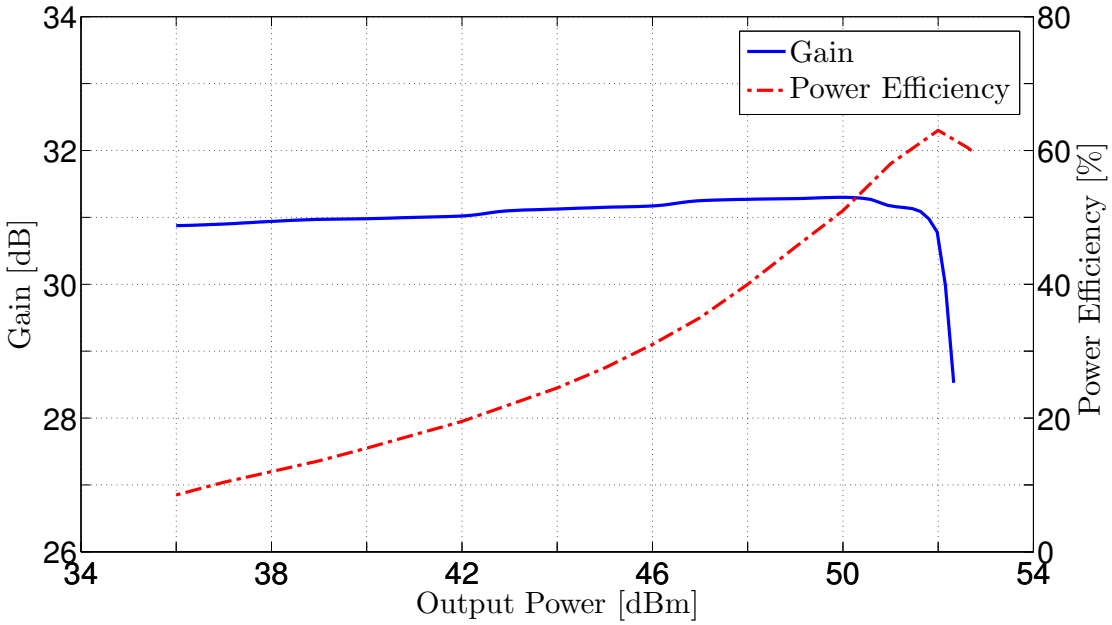

FIGURE 2.21 – The gain and power efficiency of the DVB-T PA as a function of the output power [Tec10].

2.7 Global approach for PAPR reduction and linearization

As explained in the previous sections, the two main methods usually advocated in literature to solve the problems of the PAPR and the PA non-linearity are the PAPR reduction and linearization techniques, respectively. The PAPR reduction techniques are used to decrease the high fluctuations of the signal amplitude, consisting in reducing the dynamics of the signal by means of dedicated signal processing. On the other hand, the linearization techniques try to compensate for the PA non-linearity. Aside from reducing the PAPR and improving the linearity, the PAPR reduction and linearization techniques play an important role in improving the PA efficiency. Indeed, the PAPR of the input signal, the PA linearity, and the PA efficiency are three closely related parameters.

Considering Fig. 2.22 we can present the relationship between the PAPR of the input signal, the PA-nonlinearity and the PA efficiency. In fact, the top and bottom of the figure depict the input signal before and after the PAPR reduction, respectively. In addition, the PA characteristics are given before and after the linearization by the red and blue curves respectively. Also, the PA efficiency as a function of the input power are presented by the green curve.

As we can see before applying the PAPR reduction, the fluctuation of the signal amplitude is very high, which results in high PAPR value. Consequently, a high IBO must be applied to mitigate the saturation effects. Then, referring to the PA efficiency curve, we remark that the PA efficiency in this operating point is very low. However, when the PAPR reduction is applied, the dynamic range of the input signal decreases and then the PAPR of the signal is lower. Therefore, thanks to the PAPR reduction, it possible to reduce the IBO and thus to increase the efficiency.

Likewise, the PA characteristics before linearization are non-linear. To mitigate distortions, one has to choose an operation point far away from the saturation zone which reduces the PA efficiency. However, after linearization the combined transfer function of the linearization and the power amplifier have a wider linearity range. Consequently, the operating point can be closer to saturation where the PA efficiency is greater.

In literature, many studies propose to combine the PAPR reduction and the linearization seen that they improve the PA efficiency and linearity [DJK05,YWC+02, RL03,RHL+04]. Based on the classification in [GOU13], there are two approaches for the combination of the PAPR reduction and linearization techniques namely non-collaborative approach and joint approach.

2.7.1 Non-collaborative approach

The non-collaborative approach consists of a combination of a PAPR reduction technique and a linearization technique. The idea of a non-collaborative approach is intuitive. On one hand, the linearization increases the PA linearity. On the other hand, the PAPR reduction improves the PA efficiency. So, in principle the cascade of a PAPR reduction technique and a linearization technique will increase the linearity and the efficiency of the power amplifier.

The block diagram of the non-collaborative approach is illustrated in Fig. 2.23. In this approach, the PAPR reduction and linearization are separated and independent from each others. Indeed, the PAPR reduction parameters are optimized and adjusted independently from the linearization and vice versa.

Thanks to the complementarity of these two treatments, the performance of the power amplifier is improved. In fact, the performance in terms of linearity (EVM, ACPR, etc.) is better if we consider only one processing (either PAPR reduction or linearization). Likewise, it is the same for PA efficiency. Moreover, numerous simulation results exist in the literature focusing on the performance in terms of PA linearity and efficiency after the association of PAPR reduction and linearization [SPCK04,KC06,HCVG09,RL03,RHL+04,BAT+11,KJ03c,Mir08, CY09]. The advantage of the non-collaborative approach is that numerous PAPR reduction and linearization techniques already exist in the literature. Most of these techniques are already implemented in real systems. This offer therefore many possibilities of combination.

However, even if the performance of each technique has been separately optimized according to its own criteria, the overall performance after the combination is not necessarily optimal because of the possible opposite effects. Generally, linearization increases the PAPR of the signal, and the PAPR reduction may distort the signal such as the clipping technique. Indeed, it has been shown that PAPR reduction and linearization have mutual effects, and, therefore, each technique impacts

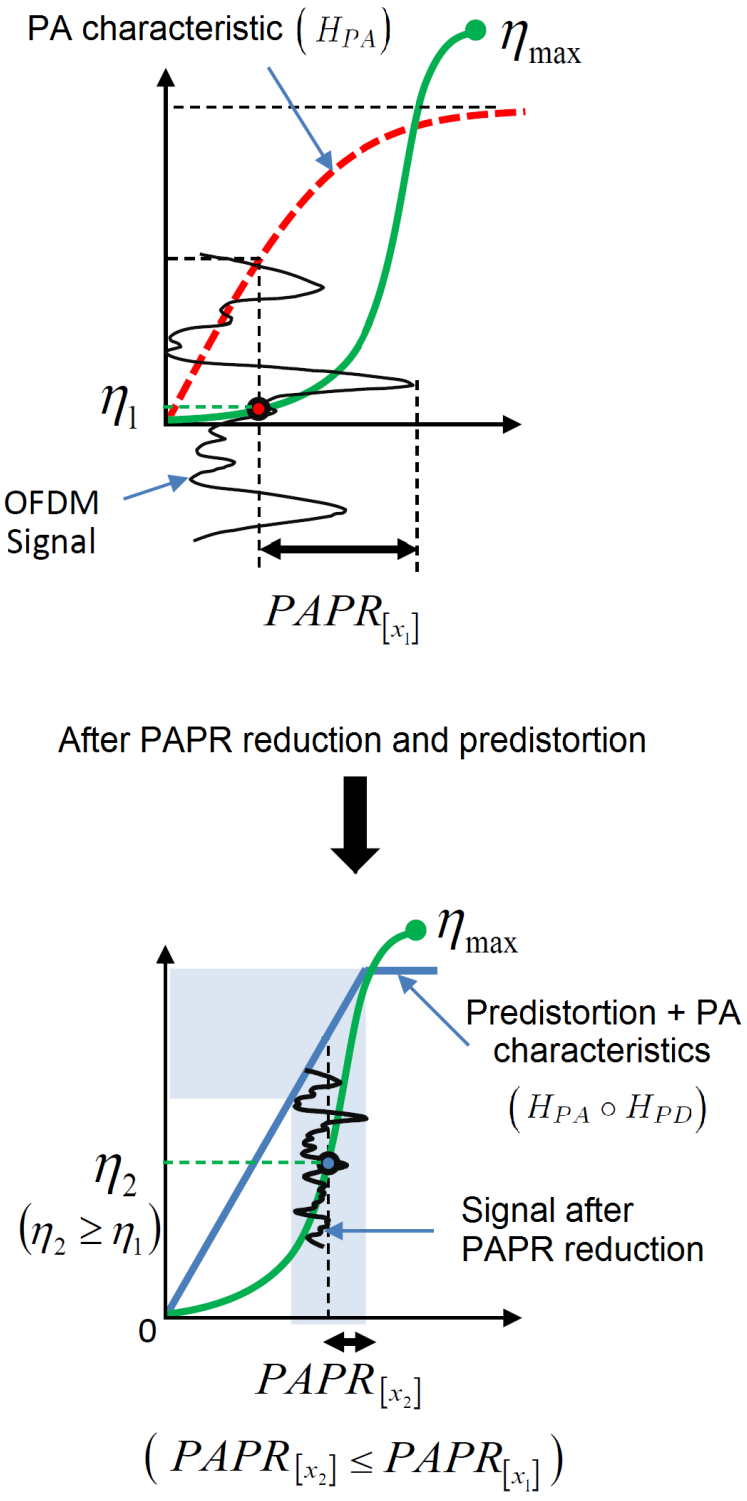

FIGURE 2.22 – The relationship between the PA efficiency, PA nonlinearity and the PAPR reduction. The top of the figure depicts the input signal and the PA characteristic before the PAPR reduction and presdistortion. The bottom of the figure depicts the input signal and the PA characteristic after the PAPR reduction and the presdistortion.

both the linearity and efficiency.

As a result, it is not excluded that the opposite effects of one technique impair the performance of the other. And since these treatments are independent, this results in either an over-dimensioning of the PA, thus unnecessary processing complexities and less PA efficiency, or in a saturation of the signal which will result important degradation of linearity. For example, if the linearization process is not enough efficient and we are amplifying near from the compression point with a high PAPR value, this may yield a saturation of the signal. Also, if the IBO is much larger than the PAPR of the signal, this may cause unnecessary processing complexities of the linearization process.

To avoid this, it makes sense to make a collaborative and adaptive treatment that it is called the joint collaborative approach [GOU13].

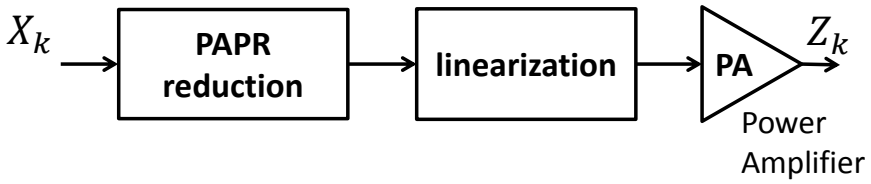

FIGURE 2.23 – Block diagram of the non-collaborative approach for the PAPR reduction and linearization..

2.7.2 Joint approach

The joint approach consists of an active and collaborative combination of the PAPR reduction and linearization. The idea is to benefit from the complementarity between these two treatments by taking into account their mutual effects. The diagram in Fig 2.24 illustrates the principle of the joint approach.

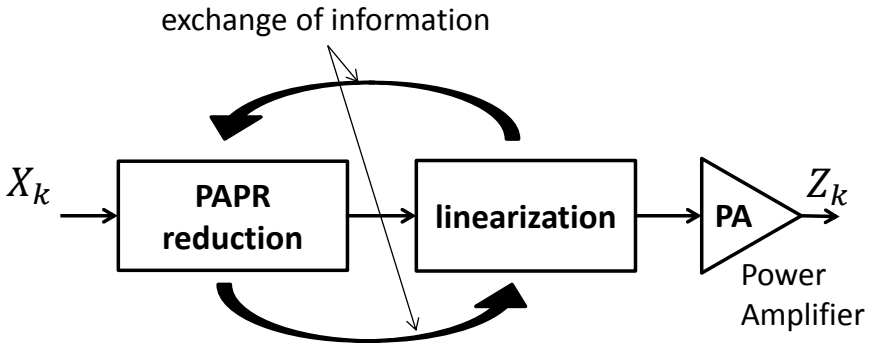

FIGURE 2.24 – Block diagram of the joint approach for the PAPR reduction and linearization.

Collaboration between these two treatments is done through exchanges of informations. The exchanged informations may be, for example, the PAPR of the

signal after the PAPR reduction or the 1_{dB} compression point of the PA after linearization. In fact, the linearization extends the linear zone of the PA which changes the PA characteristics, particularly the 1_{dB} compression point. Thus, the new 1_{dB} compression point should be sent to the PAPR reduction process to adapt its performance. Similarly, after the PAPR reduction, the linearization must also adjust its performance as a function of the new PAPR value. This adaptation of the PAPR reduction as a function of the linearization and/or vice versa makes it possible to avoid, on the one hand, the over-dimensioning of the PA and unnecessary processing complexities and on the other hand the saturation of the amplified signal which may result from a simple association (non-collaborative approach).

In the literature, references dealing with the collaborative approach can be found, for example, in [HWW+10, Bra12, HWPL08, RPLL06b, DJK05].

2.7.3 Global approach

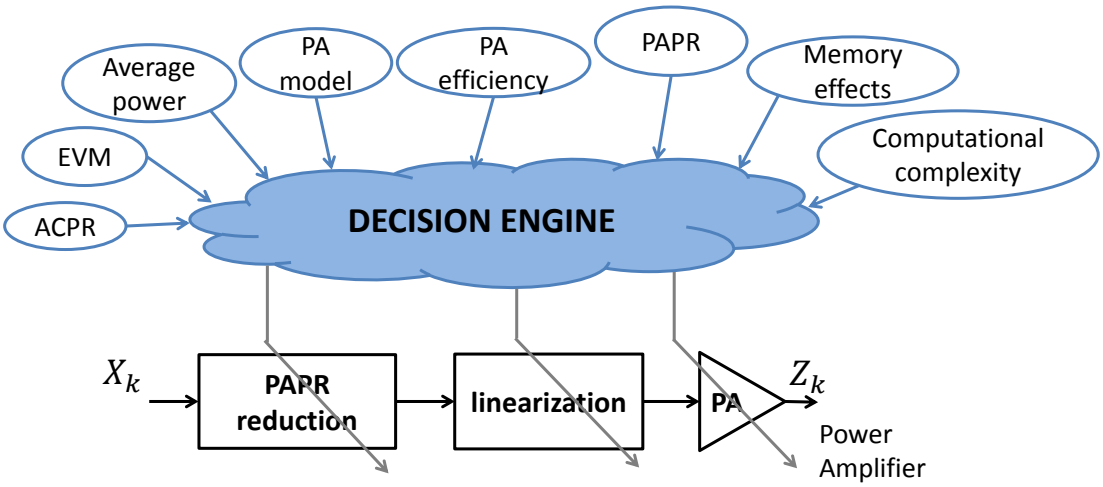

FIGURE 2.25 – Block diagram of the decision engine which controls the clipping and predistortion.

As shown above, recent communications and broadcasting systems use increased PAPR signals which lead to poor efficiency and degrade the linearity. However, while the linearity is mandatory to ensure the quality of the communication, the efficiency is a serious need and has became a issue that is widely investigated in the world of telecommunications today. As shown above, the PAPR reduction and linearization techniques directly impact both the linearity as well as the efficiency of the transmitter. At the same time, these techniques come at the cost of an additional computational complexity. Thus, it is worth to study these two treatments with a more global approach. In such an approach, the PAPR reduction and the linearization have to be jointly optimized and dynamically adapted subject to more generic metrics such as the PA efficiency, the computational complexity, and other predefined parameters and some transmission conditions.

Accordingly, we propose to go a step beyond the previously mentioned approaches by introducing a new adaptive approach which controls the PAPR reduction and linearization techniques in a flexible way. Our aim is to maximize the

PA efficiency and minimize the computational complexity with respect to predefined linearity parameters and according to some transmission conditions.

These parameters are metrics widely used to measure the performance of the transmitter linearity. Adjacent channel power ratio and error vector magnitude are examples of these parameters. In particular, EVM and ACPR are common figures of merit for assessing the quality of digital modulated telecommunication signals. While EVM measures the in-band distortions generated by the nonlinear components of the transmitter chain, ACPR characterizes the adjacent channel interference mainly caused by the spectral regrowth at the PA output. Indeed, most of wireless communication standards such as the IEEE802.11a standard [EVM99], the IEEE802.16e WiMAX standard [EVM05], and the LTE standard [LTE12] have already specified their requirements in terms of EVM and ACPR.

The principle of the global approach is illustrated in Fig. 2.25. It can be explained in the following steps

- First, informations on the transmission conditions are collected from a set of sensors.
- Accordingly, a decision engine analyzes these informations and adapts its parameters for a given environment.
- Finally, the decision engine configures the PAPR reduction and linearization techniques, and may controls the PA power in order to maximize the PA efficiency and respect the linearity requirements imposed by the standard.

Assuming a transmitter implementation with this global and adaptive approach for PAPR reduction and linearization processes, one can imagine controlling these techniques to meet a various EVM and ACPR target values related to different qualities of service and standard requirements. Such implementation can for example be found in high or medium power transmit base stations using OFDM at the physical layer, e.g. DVB-T2 towers or LTE nodes.

To summarize, our objective is to derive a flexible transmitter model able to update its parameters according to incoming requirements and outside environment. Therefore, this work is an important step in the analytical study of the global optimization approach of the transmitter efficiency and linearity.

In that perspective, we are involved in this thesis in the analytical derivation of the EVM and ACPR of multicarrier signals which are detailed in the next chapters. In particular, Chapter 3 will investigate the EVM of multicarrier using a clipping technique as PAPR reduction technique and/or a predistortion as a linearization technique using a Rapp PA model. Then, some practical scenarios are proposed to prove the importance of our theoretical expressions in optimizing the linearity and the efficiency of the transmitter.

2.8 Conclusion

In this chapter, the technical background of the power amplifier was reviewed. More specifically, we detailed the nonlinear characteristics of the PA and then we discussed the PA linearity efficiency problematic. Thereafter, a description of different figures of merit used to quantified the PA linearity was done. Further, some PA behavior models with and without memory effects were presented. Afterwards, some linearization methods used to improve the linearity of the RF power amplifier

was described. Moreover, the PA linearity-efficiency problematic in a multicarrier context was investigated. Finally, the global approach for PAPR reduction and linearization was proposed. This approach is based on the fact that these two techniques are complementary and have to be dynamically controlled based on generic metrics. In order to realize this approach, a theoretical study of the impact of the linearization on the PAPR reduction and vice versa must first be made. Moreover, it is important to analyze the impact of the combination of the PAPR reduction and linearization on the linearity criteria. Indeed, in the next chapter, the analytical EVM expression for nonlinear amplified multicarrier signal using Rapp model is derived with the use of a clipping as a PAPR reduction technique and the predistortion as a linearization technique. Also, some practical scenarios are proposed to show how we can control the PAPR reduction and the linearization techniques subject to improve the linearity and the efficiency simultaneously.

Chapter 3

EVM derivations using memoryless Rapp PA model

3.1 Introduction

In the previous chapter, we showed that the PAPR reduction and linearization are complementary. However, their simple combination may result in opposite effects. To mitigate this, we proposed to control the PAPR and the linearization subject to some generic metrics such as the EVM and the ACPR. In this context, the linearity will obviously depend on the performance of both the PAPR reduction and linearization techniques. In this chapter, we mathematically analyze the linearity using the EVM metric, and considering the predistortion as a linearization technique and the clipping as PAPR reduction technique.

This chapter is organized as follows, the distribution of the OFDM signal is recalled. Afterwards, the impact of some PAPR reduction techniques on the signal distribution is studied. Then, the EVM expression for the nonlinear amplified multicarrier signal using Rapp PA model is derived with the use or not of a clipping technique. Also, the impact of the predistortion technique is analyzed. Finally, some practical scenarios are presented proving the importance of our proposed expressions in controlling the predistortion and the clipping techniques in order to ensure the linearity requirements and mitigate the computational complexity.

3.2 State of the art of EVM derivations with memoryless power amplifier

As far as the theoretical EVM derivations are concerned, some contributions can be found in the literature. However, note that there are very few analytical EVM derivations in a scenario where PAPR reduction and linearization techniques are used, although the large number of studies that propose the joint approach for PAPR reduction and linearization. In fact, such studies are very interesting especially for improving the PA linearity and efficiency.

In [GL12a] and [GL12b], the authors study the linearity of the high power amplifier in OFDM context. The PA linearity is measured by the Error Vector Magnitude (EVM) metric. Therefore, they derived an upper bound of the EVM of the amplified signal using memoryless Rapp model. The derivations are done

taking into account the use of a PAPR reduction technique followed by a predistortion technique. The EVM is evaluated with the use of a clipping technique and Selective Mapping (SLM) technique. Then, an analytical trade-off between the PA efficiency and linearity is proposed based on these derived EVM expressions. It is worthwhile to mention that these contributions are pioneers who proposed to explore the theoretical analysis of the PA linearity when both PAPR reduction and linearization techniques are used. However, although the importance of these studies, the proposed EVM expression is just an upper bound. Thus, the theoretical value in some cases are so far from the real EVM value. Consequently, this will actually result in some problems when we seek the optimal trade-off between the PA linearity and efficiency as the linearity is not well estimated. Therefore, this EVM expression might be in some practical scenarios inefficient.

Other contributions, as [KHNSL12, KHNSL10], give closed-form EVM expressions. However, these computations rely on simplifying the PA model as a simple clipping making it inaccurate for any practical implementation. A comparison between the EVM results taking into account ideal linear PA and an actual PA will be proposed in this chapter. One can clearly remark the significant difference which could not be neglected. Particularly, since we focus in our context on the trade-off between the PA linearity and efficiency, the EVM expression should be as a function of the PA characteristics.

In [OI02, SO16] the performance analysis of clipped OFDM signals is proposed. However, the power amplifier is omitted from this study too. In addition, the authors do not consider any linearization technique.

So, the following chapter will present some new EVM expressions of the OFDM signal amplified with a Rapp model and taking into account or not the use of predistortion and clipping techniques.

3.3 System Model

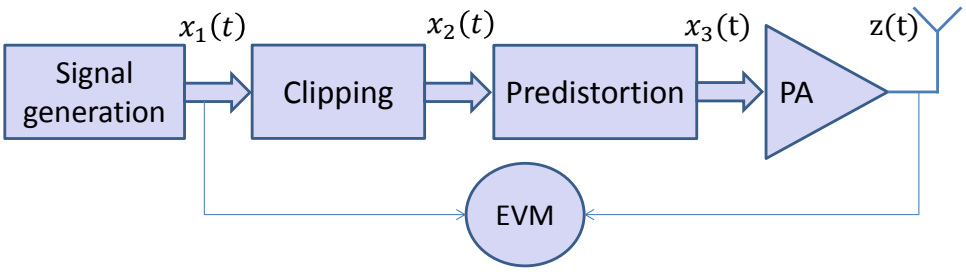

Figure 3.1 – Transmitter block diagram.

A simplified block diagram of the transmission chain with clipping and predistortion stages preceding the PA is presented in Fig.3.1. The multicarrier signal $x_1(t)$, generated by the system, becomes $x_2(t)$ after clipping, and $x_3(t)$ after the predistortion operation. The output of the PA is $z(t)$.

As mentioned in chapter 1 the relationship between the input and the clipped signal is given by

$$x_2(t) = \begin{cases} x_1(t) & \text{if } |x_1(t)| \leq A_{max} \\ A_{max} e^{j\phi(x)} & \text{if } |x_1(t)| > A_{max} \end{cases} . \tag{3.1}$$

Fig. 3.2 presents the transfer function of the clipping technique. We can clearly see how the clipping technique clip the signal peaks that are above the threshold A_{max}.. This technique slightly reduces the average power of the signal especially when the threshold is sufficiently low.

Besides, the amplifier model considered in this chapter is the memoryless SSPA (Solid State Power Amplifier) model given by Rapp [Rap91]. We recall the AM/AM (amplitude-to-amplitude) characteristics $H_{PA}(r)$ which is expressed as

$$H_{PA}(r) = \frac{r}{\left(1 + \left(\frac{r}{A}\right)^{2b}\right)^{\frac{1}{2b}}} , \tag{3.2}$$

The applied linearization technique is the predistortion which should have exactly the inverse function of the PA transfer function. It is straightforward to get the predistortion function corresponding to Rapp model previously introduced

$$H_{PD}(r) = \frac{r}{\left(1 - \left(\frac{r}{A}\right)^{2a}\right)^{\frac{1}{2a}}} , \tag{3.3}$$

where a is the predistortion knee factor (transition factor). A perfect linearization is performed when $a = b$, but in practice, this situation is difficult to achieve because of modeling problems of the PA.

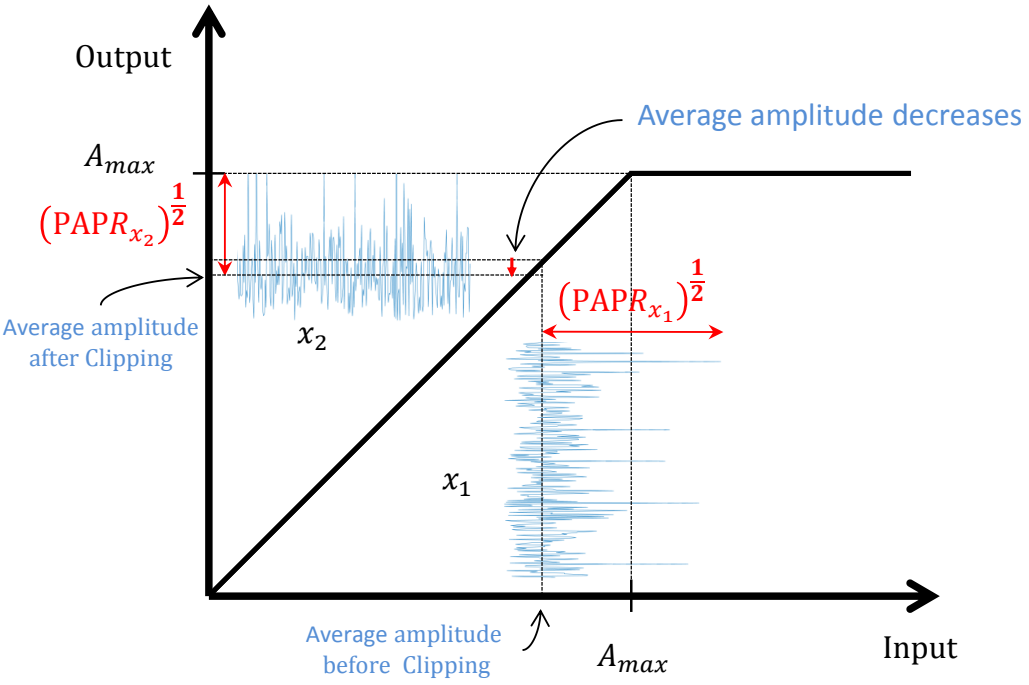

FIGURE 3.2 – Transfer function of the clipping technique.

3.3.1 The amplitude distribution of the OFDM signal

Thanks to central limit theorem, it has been shown that when the number of sub-carriers N is large, the OFDM signal can be approximated by a complex Gaussian random processes with zero mean [BLG02]. Therefore, its amplitude converges to a Rayleigh distribution whose the Probability Density Function (PDF) can be written as

$$f_{x_1}(r) = \frac{2r}{P_{x_1}} e^{-\frac{r^2}{P_{x_1}}} , \tag{3.4}$$

where P_{x_1} is the average power of the input signal $x_1(t)$ and r is the magnitude of the input voltage, i.e. $r = |x_1(t)|$.

3.3.2 Impact of the PAPR reduction technique on the amplitude distribution of OFDM signal

As stated before, the amplitude of the OFDM signal before PAPR reduction is approximated by a Rayleigh distribution. However, the distribution of the signal may change after PAPR reduction. Although the significant number of proposed PAPR reduction techniques [LP08b], there are very few studies about the distribution of the signal amplitude after PAPR reduction [BLG02]. In fact, the new distribution knowledge is necessary to estimate the distortions, and then to reach the optimal PA linearity-efficiency trade-off.

In the first chapter, we have seen that there are three main categories of PAPR reduction methods. In the following, we present the impact of each category on the amplitude distribution of OFDM signals.

First, we consider the case of coding methods which consist in finding out all possible codewords and then select those codewords that have the lowest PAPR values. Accordingly, a new mapping technique is established using codewords. Therefore, the new symbols are no longer i.i.d. (independent identically distributed) random variables and then the resulted signal is not complex Gaussian anymore but depends on the used coding method. Hence, the amplitude distribution of the signal in this case is not Rayleigh.

In the case of probabilistic methods, the data symbols are multiplied by deterministic vectors to perform several copies of the initial signal and then select the copy with the minimum PAPR. For SLM [BFH96] and PTS [MH97] techniques, only the phase of the symbols are modified, thus the amplitude distribution of the time domain signal after PAPR reduction remains the same (i.e. Rayleigh) [BP08]. This characteristic is important, nevertheless, as these techniques are generally not downward compatible, so that it requires post processing on the receiver side, they will not be investigated in this work.

Finally, the last category is the adding signal methods which are the most promising methods. Under this category, a huge number of methods are regularly published. Besides, these methods are very diverse and depend on the peak-reduction signal $c(t)$ which is generated differently. Accordingly, the distribution of the signal after PAPR reduction is different in each method depending on the additive signal $c(t)$. Therefore, an exhaustive study is impossible because of the diversity and the large number of PAPR reduction methods under this category. For this reason, we focus in our study on the clipping technique due to its popularity and its straightforward reduction gain.

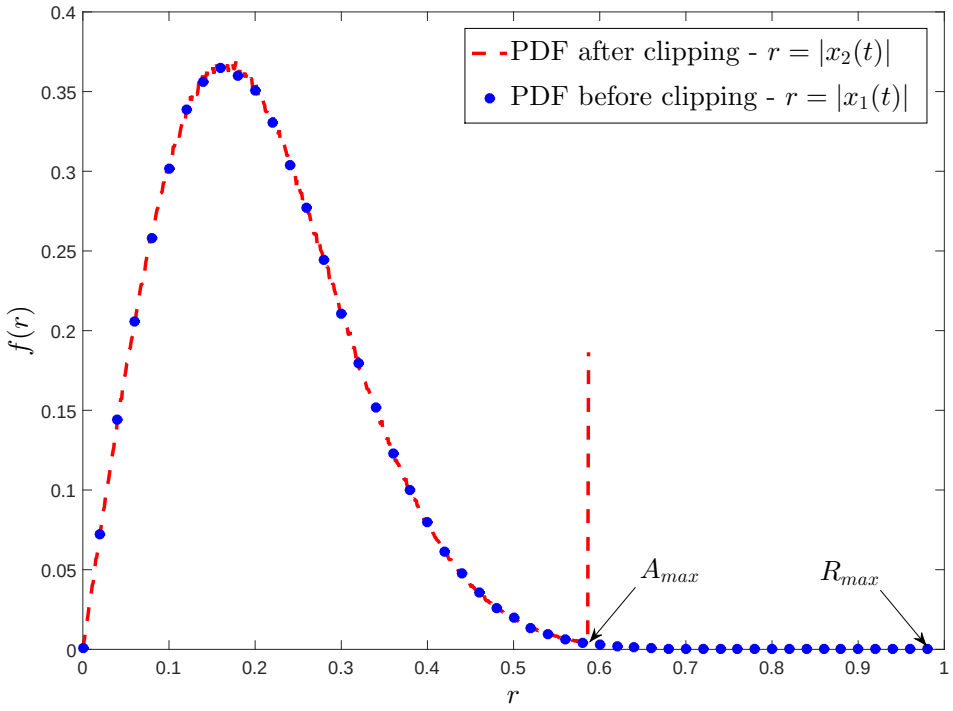

FIGURE 3.3 – Probability density function of the signal amplitude before and after Clipping.

Considering the clipping function eq.(3.1), the amplitude PDF of the clipped signal can be written as [BLG02]

$$f_{x_2}(r) = \begin{cases} f_{x_1}(r) & \text{if } r < A_{max} \\ P\{r \geq A_{max}\}\,\delta(r - A_{max}) & \text{if } r = A_{max} \end{cases} \tag{3.5}$$

where $\delta(r)$ is the Dirac impulse and $P\{r \geq A_{max}\}$ to be the probability that r, the amplitude of $x_1(t)$, to be larger or equal than the clipping threshold A_{max}. Hence, its expression is given by

$$\begin{aligned} P\{r > A_{max}\} &= \int_{A_{max}}^{R_{max}} f_{x_1}(r)\,dr \\ &= e^{\frac{-A_{max}^2}{P_{x_1}}} - e^{PAPR_{[x_1]}}\,, \end{aligned} \tag{3.6}$$

where R_{max} and $\text{PAPR}_{[x_1]}$ are the maximum magnitude and the PAPR of the input signal $x_1(t)$, respectively. Fig. 3.3 presents the amplitude distribution of the input signal $x_1(t)$, and the clipped signal $x_2(t)$. Undoubtedly, the average power of the clipped signal, P_{x_2}, is different from P_{x_1} as we can see in Fig. 3.2. Therefore, the ratio λ between the average power after and before clipping is given by

$$\lambda = \frac{P_{x_2}}{P_{x_1}} = 1 - e^{\frac{-A_{max}^2}{P_{x_1}}} - \frac{-A_{max}^2}{P_{x_1}}\, e^{-PAPR_{[x_1]}}\,. \tag{3.7}$$

Note that the PAPR of the clipped signal, $\text{PAPR}_{[x_2]}$, is $\frac{A_{max}^2}{P_{x_2}}$. Thus, the ratio $\frac{A_{max}^2}{P_{x_1}}$, which will be used in the following analytical derivations, is equal to $\lambda\ \text{PAPR}_{[x_2]}$.

3.4 Proposed EVM expressions without predistortion

In this section, we propose to calculate the EVM for amplified multicarrier signal as a function of the knee factor b of the PA, and, when activated, as a function of the clipping threshold R_{max}, and the PAPR of the input and clipped signal.

3.4.1 Without clipping

Firstly, let us treat the case of the EVM without clipping. In that case, using (3.2), (2.24) and (3.4), the second order moment of the error magnitude expresses as

$$E\left\{|Z_k - X_k|^2\right\} = \int_0^{R_{\max}} \left| r - \frac{r}{\left(\left(\frac{r}{A}\right)^{2b} + 1\right)^{\frac{1}{2b}}} \right|^2 \frac{2r}{P_{x_1}} e^{-\frac{r^2}{P_{x_1}}} dr. \tag{3.8}$$

Then, expanding the squared term in (3.8) and letting $u = \frac{r^2}{P_{x_1}}$ we get

$$E\left\{|Z_k - X_k|^2\right\} = \underbrace{\int_0^{\mathrm{PAPR}_{[x_1]}} P_{x_1} u e^{-u} du}_{I_1} - \underbrace{2P_{x_1} \int_0^{\mathrm{PAPR}_{[x_1]}} \left(1 + \left(\frac{P_{x_1} u}{A^2}\right)^b\right)^{\frac{-1}{2b}} u\, e^{-u} du}_{I_2}$$
$$+ \underbrace{P_{x_1} \int_0^{\mathrm{PAPR}_{[x_1]}} \left(1 + \left(\frac{P_{x_1} u}{A^2}\right)^b\right)^{\frac{-1}{b}} u\, e^{-u} du}_{I_3}, \tag{3.9}$$

in which the upper bound of the integrals results from the PAPR definition. The computation of I_1 is easily obtained applying integration by parts

$$I_1 = -P_{x_1}\left(e^{-\mathrm{PAPR}_{[x_1]}}\left(\mathrm{PAPR}_{[x_1]} + 1\right) - 1\right). \tag{3.10}$$

Then, since I_2 and I_3 looks similar, we will use the same manipulations for both as explicitly detailed hereafter for I_2. Let us first recall the Newton's binomial theorem [Coo49]

$$(1+x)^\alpha = \sum_{i=0}^{+\infty} \binom{\alpha}{i} x^i, \tag{3.11}$$

where $\binom{\alpha}{i}$ is the binomial coefficient and $|x|$ should be less than one. In our case, x is given as

$$x = \left(\frac{P_{x_1} u}{A^2}\right)^b = \left(\frac{r^2}{A^2}\right)^b. \tag{3.12}$$

Then, imposing $|x| < 1$ means that $\frac{A^2}{R_{\max}^2} > 1$. Such a situation corresponds to a sufficient IBO. However, this condition is not valid when we amplify near from the saturation zone. We can hence obtain an expansion of I_2 as

$$I_2 = -2P_{x_1} \sum_{i=0}^{+\infty} \binom{\frac{-1}{2b}}{i} \left(\frac{P_{x_1}}{A^2}\right)^{bi} \int_0^{\mathrm{PAPR}_{[x_1]}} u^{bi+1}\, e^{-u} du. \tag{3.13}$$

The final step then consists in using the following integral identity [Zwi]

$$\int_0^u x^{\alpha-1}\, e^{-\mu x} dx = \mu^{-\alpha}\gamma\left(\alpha, \mu u\right), \tag{3.14}$$

where γ represents the incomplete gamma function defined as

$$\gamma\left(\alpha, u\right) = \int_0^u x^{\alpha-1}\, e^{-x} dx. \tag{3.15}$$

This yields to the following expression for I_2

$$I_2 = -2P_{x_1} \sum_{i=0}^{+\infty} \binom{\frac{-1}{2b}}{i} \left(\frac{P_{x_1}}{A^2}\right)^{bi} \gamma\left(bi+2, \mathrm{PAPR}_{[x_1]}\right). \tag{3.16}$$

Similarly, I_3 can be computed as

$$I_3 = \; P_{x_1} \sum_{i=0}^{+\infty} \binom{\frac{-1}{b}}{i} \left(\frac{P_{x_1}}{A^2}\right)^{bi} \gamma\left(bi+2, \mathrm{PAPR}_{[x_1]}\right). \tag{3.17}$$

Finally, compiling (3.10), (3.13) and (3.17), the EVM expression can be written as (3.18).

Theorem 1: *The EVM of an amplified multicarrier signal using Rapp model is expressed as follows*

$$EVM = \Bigg[-\left(e^{-PAPR_{[x_1]}}\left(PAPR_{[x_1]}+1\right)-1\right) + \sum_{i=0}^{+\infty}\left[\binom{\frac{-1}{b}}{i} - 2\binom{\frac{-1}{2b}}{i}\right]\left(\frac{P_{x_1}}{A^2}\right)^{bi}\gamma\left(bi+2, PAPR_{[x_1]}\right)\Bigg]^{1/2} \tag{3.18}$$

Eventually, we obtain an EVM expression in the form of a series expansion involving Gamma functions and depending on the knee factor b and the saturation power A^2 of the PA, as well as on the signal PAPR and average power P_{x_1}.

3.4.2 With clipping

Let us now investigate the EVM calculation when clipping is activated. Using (3.2) and (3.5), the second order moment of the magnitude error is expressed as

$$E\left\{|Z_k - X_k|^2\right\} = \underbrace{\int_0^{A_{max}} |r - H_{PA}(r)|^2 f_{x_1} dr}_{I_4} + \underbrace{\int_{A_{max}}^{R_{max}} |r - H_{PA}(A_{max})|^2 f_{x_1} dr}_{I_5}. \tag{3.19}$$

The derivation of I_4 is similar to the second order moment of the magnitude error derivation without PAPR reduction which is previously presented. Hence, I_4

can be computed as

$$I_4 = -P_{x_1}\left(e^{-\lambda \mathrm{PAPR}_{[x_2]}}\left(\lambda \mathrm{PAPR}_{[x_2]}+1\right)-1\right) + P_{x_1}\sum_{i=0}^{+\infty}\left[\binom{\frac{-1}{b}}{i}-2\binom{\frac{-1}{2b}}{i}\right]\left(\frac{P_{x_1}}{A^2}\right)^{bi}\gamma\left(bi+2,\lambda \mathrm{PAPR}_{[x_2]}\right). \tag{3.20}$$

As far as I_5 is concerned, after expanding the squared term and setting $u=\frac{r^2}{P_{x_1}}$, we get

$$\int_{A_{max}}^{R_{max}}|r-H_{PA}(A_{max})|^2 f_{x_1}dr = P_{x_1}\underbrace{\int_{\lambda \mathrm{PAPR}_{[x_2]}}^{\mathrm{PAPR}_{[x_1]}} ue^{-u}du}_{I_6} - 2H_{PA}\left(A_{max}\right)\sqrt{P_{x_1}}\underbrace{\int_{\lambda \mathrm{PAPR}_{[x_2]}}^{\mathrm{PAPR}_{[x_1]}}\sqrt{u}\,e^{-u}du}_{I_7} + H_{PA}\left(A_{max}\right)^2\underbrace{\int_{\lambda \mathrm{PAPR}_{[x_2]}}^{\mathrm{PAPR}_{[x_1]}} e^{-u}du}_{I_8}. \tag{3.21}$$

Then, integration by parts is applied to I_6 and I_8

$$I_6 = P_{x_1}\,e^{-\lambda \mathrm{PAPR}_{[x_2]}}\left(\lambda \mathrm{PAPR}_{[x_2]}+1\right) - P_{x_1}\,e^{-\mathrm{PAPR}_{[x_1]}}\left(\mathrm{PAPR}_{[x_1]}+1\right), \tag{3.22}$$

$$I_8 = H_{PA}\left(A_{max}\right)^2\left(e^{-\lambda \mathrm{PAPR}_{[x_2]}}-e^{-\mathrm{PAPR}_{[x_1]}}\right), \tag{3.23}$$

and using the integral identity in [Zwi], I_7 can be calculated as

$$I_7 = -2\sqrt{P_{x_1}}H_{PA}\left(A_{max}\right)\left(\gamma\left(\frac{3}{2},\mathrm{PAPR}_{[x_1]}\right)-\gamma\left(\frac{3}{2},\lambda \mathrm{PAPR}_{[x_2]}\right)\right). \tag{3.24}$$

Finally, the EVM expression is expressed in the following theorem.

Theorem 2: *The EVM of an amplified multicarrier signal using Rapp model when clipping is activated can be written as follows*

$$\begin{aligned} EVM = \Bigg[& -\left(e^{-\lambda PAPR_{[x_2]}}\left(\lambda PAPR_{[x_2]}+1\right)-1\right) \\ & + \sum_{i=0}^{+\infty}\left[\binom{\frac{-1}{b}}{i}-2\binom{\frac{-1}{2b}}{i}\right]\left(\frac{P_{x_1}}{A^2}\right)^{bi}\gamma\left(bi+2,\lambda PAPR_{[x_2]}\right) \\ & + e^{-\lambda PAPR_{[x_2]}}\left(\lambda PAPR_{[x_2]}+\frac{H_{PA}\left(A_{max}\right)^2}{P_{x_1}}+1\right) \\ & - e^{-PAPR_{[x_1]}}\left(PAPR_{[x_1]}+\frac{H_{PA}\left(A_{max}\right)^2}{P_{x_1}}+1\right) \\ & - \frac{2H_{PA}\left(A_{max}\right)}{\sqrt{P_{x_1}}}\left(\gamma\left(\frac{3}{2},PAPR_{[x_1]}\right)-\gamma\left(\frac{3}{2},\lambda PAPR_{[x_2]}\right)\right)\Bigg]^{1/2}. \end{aligned} \tag{3.25}$$

As for (3.18), we obtain an EVM expression in the form of a series expansion involving Gamma functions and depending on several parameters. These parameters are the knee factor b, the PA saturation power A^2, the PAPR of the signal $x_1(t)$ and $x_2(t)$, as well as λ the ratio between P_{x_2} and P_{x_1}.

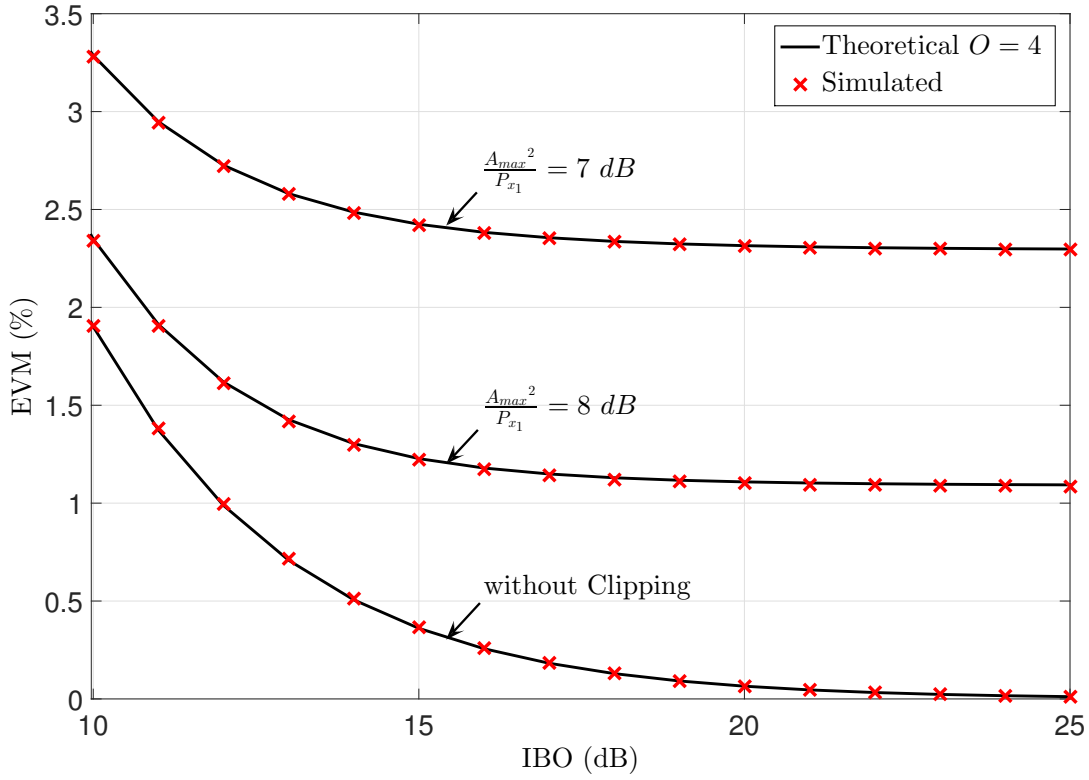

FIGURE 3.4 – Derived and simulated EVM with clipping and without predistortion (b=1.5).

3.4.3 Simulation results and analysis

In this subsection we present a comparison between the theoretical EVM given by (3.18) and (3.25) and the simulated EVM when clipping is activated or not. Note that each simulation considers 10^5 randomly generated OFDM symbols with 1024 sub-carriers associated to 16-QAM modulation. The approximation order in (3.25) is $O = 4$, i.e. $i \in [0...4]$. Fig. 3.4 and Fig. 3.5 depict the theoretical and simulated EVM as a function of the IBO when clipping is activated or not with knee factor, b, values of 1.5 and 5, respectively. We note that (3.18) and (3.25) can be expressed as a function of the IBO, by replacing the average power by $\frac{P_{1dB,in}}{IBO}$ according to the IBO definition in (2.1). In practice, a high IBO is commonly applied to the input signal to mitigate distortions. We consider clipping ratio $\frac{A_{max}{}^2}{P_{x_1}}$ of 7 dB and 8 dB. As expected, without clipping, the EVM tends to zero for very large IBO. On the contrary, with clipping, the more the clipping threshold decreases, the more the EVM increases. Moreover, we notice that our proposed equation of the EVM perfectly matches the exact and the simulated EVM starting for $O \geq 4$. This proves the accuracy of our proposed EVM expression. Besides, by comparing the EVM in Fig. 3.4 and Fig. 3.5, we clearly remark that the EVM of the amplified

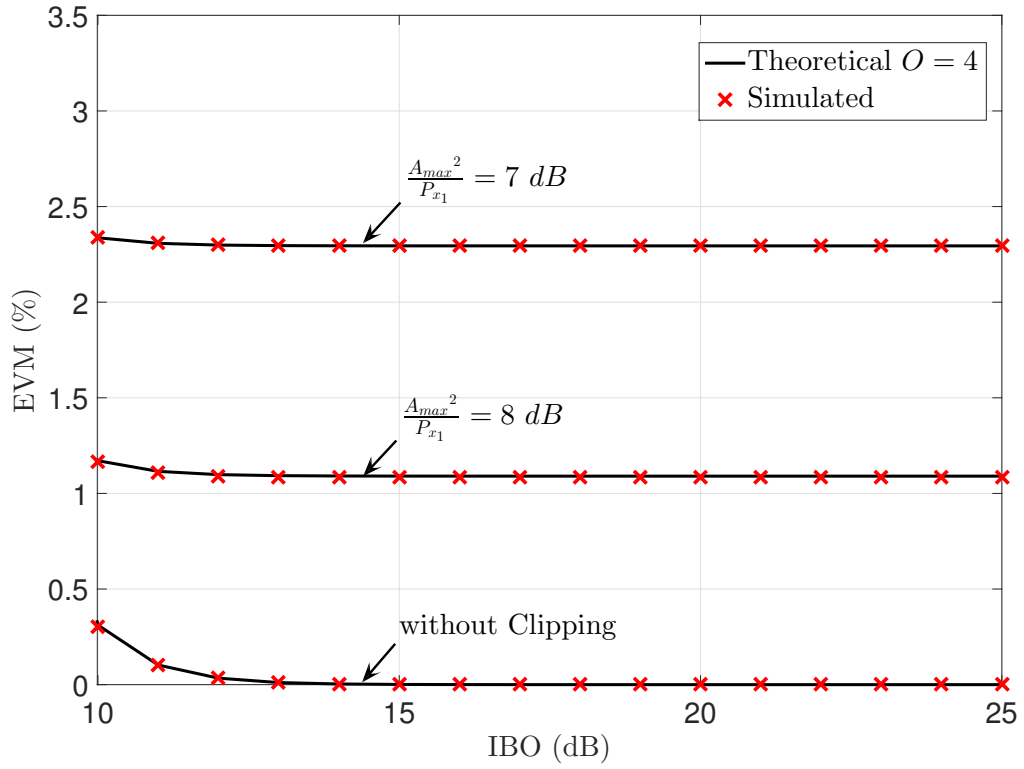

FIGURE 3.5 – Derived and simulated EVM with clipping and without predistortion (b=5).

signal with the knee factor $b = 5$ is smaller than the EVM when $b = 1.5$ due to the fact that as the knee factor of the PA increases, the PA model becomes more linear. To go further in the analysis, we plot in Fig. 3.6 the EVM as a function of the knee factor b with and without clipping and an IBO $= 12\ dB$. Likewise, we see that the EVM decreases as the knee factor increases which is in line with what we have seen in Fig. 2.6 that as the knee factor increases, the linearity zone of the PA becomes wider.

3.5 Proposed EVM expressions with predistortion

Let us now investigate the EVM calculation when the predistortion is activated. In this case, the equivalent transfer function combining the predistortion and amplification functions is simply obtained using (3.2), (3.3), and writes

$$H_{EQ}(r) = \frac{r}{\left(\left(1 - \left(\frac{r}{A}\right)^{2a}\right)^{\frac{b}{a}} + \left(\frac{r}{A}\right)^{2b}\right)^{\frac{1}{2b}}} \tag{3.26}$$

which can be used to get the second order moment of the error magnitude following the same approach as in Eq. (3.8).

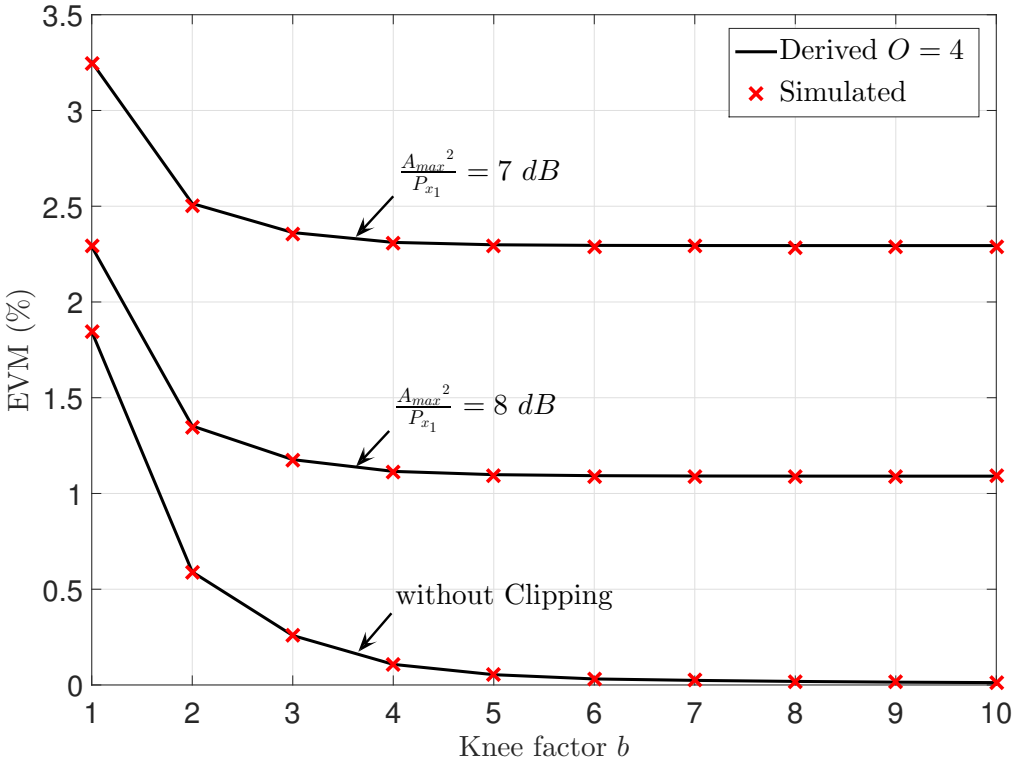

FIGURE 3.6 – Derived and simulated EVM as a function of the knee factor with and without clipping and an IBO = 12 dB.

3.5.1 Without clipping

After expansion, the second order moment of the magnitude error can be written as

$$E\left\{|Z_k - X_k|^2\right\} = \underbrace{\int_0^{\text{PAPR}_{[x_1]}} P_{x_1}\, u\, e^{-u} du}_{I_9} \tag{3.27}$$

$$\underbrace{-2\int_0^{\text{PAPR}_{[x_1]}} \left(\left(1-\left(\frac{uP_{x_1}}{A^2}\right)^a\right)^{\frac{b}{a}} + \left(\frac{uP_{x_1}}{A^2}\right)^b\right)^{\frac{-1}{2b}} uP_{x_1}e^{-u}du}_{I_{10}}$$

$$\underbrace{\int_0^{\text{PAPR}_{[x_1]}} \left(\left(1-\left(\frac{uP_{x_1}}{A^2}\right)^a\right)^{\frac{b}{a}} + \left(\frac{uP_{x_1}}{A^2}\right)^b\right)^{\frac{-1}{b}} uP_{x_1}e^{-u}du}_{I_{11}},$$

with once again $u = \frac{r^2}{P_{x_1}}$. Comparing (3.9) and (3.27), we note that $I_9 = I_1$, but that I_{10} and I_{11} are new integrals to calculate. Both can be expanded by applying the generalized Newton's binomial theorem [Coo49] which states as

$$(x+y)^\alpha = \sum_{i=0}^{+\infty} \binom{\alpha}{i} x^{\alpha-i} y^i, \tag{3.28}$$

with $|x| > |y|$. For I_{10}, the latter condition is obtained as long as $\left(\frac{A^2}{R^2_{\max}}\right) > 2^{1/a}$. Once again such a condition is true if a sufficient IBO is applied to the signal at the input of the PA, i.e. $P_{x_1} < A^2 - \left[\frac{3}{a}\right]_{dB}$. Let us consider this as an assumption for the rest of the calculation and discuss it when analyzing the simulation results. Such a condition is valid using a sufficient IBO, however, it will not be valid when the peaks of the signal coincides with the saturation power which will limit the utility of this expression in this zone. Integral I_5 can then be expressed as

$$\begin{aligned} I_{10} = & - 2P_{x_1} \int_0^{\mathrm{PAPR}_{[x_1]}} \sum_{i=0}^{+\infty} \binom{\frac{-1}{2b}}{i} \left(1 - \left(\frac{u\, P_{x_1}}{A^2}\right)^a\right)^{\frac{-b}{a}\left(\frac{1}{2b}+i\right)} \\ & \times \left(\frac{u\, P_{x_1}}{A^2}\right)^{bi} u\, e^{-u} du. \end{aligned} \tag{3.29}$$

Now by applying the binomial theorem (3.11) to the factor in (3.29) we have

$$\begin{aligned} I_{10} = & -2P_{x_1} \sum_{i=0}^{+\infty} \binom{\frac{-1}{2b}}{i} \sum_{j=0}^{+\infty} \binom{\frac{-b}{a}\left(\frac{1}{2b}+i\right)}{j} \left(\frac{P_{x_1}}{A^2}\right)^{aj+bi} \\ & \times (-1)^j \int_0^{\mathrm{PAPR}_{[x_1]}} u^{aj+bi+1}\, e^{-u} du. \end{aligned} \tag{3.30}$$

It is finally possible to compute the integral using (3.14) to get

$$\begin{aligned} I_{10} = & -2P_{x_1} \sum_{i=0}^{+\infty} \binom{\frac{-1}{2b}}{i} \sum_{j=0}^{+\infty} \binom{\frac{-b}{a}\left(\frac{1}{2b}+i\right)}{j} \left(\frac{P_{x_1}}{A^2}\right)^{aj+bi} \\ & \times (-1)^j \gamma\left(aj+bi+2, PAPR\right). \end{aligned} \tag{3.31}$$

The same methodology is used to calculate I_{11} so that the final EVM expression is given by Theorem 3.

Theorem 3: *The EVM of an amplified multicarrier signal using Rapp model when predistortion is activated can be written as follows*

$$\begin{aligned} EVM = & \Bigg[- \left(e^{-PAPR_{[x_1]}} \left(PAPR_{[x_1]} + 1\right) - 1\right) \\ & + \sum_{i=0}^{+\infty} \left[\binom{\frac{-1}{b}}{i} - 2\binom{\frac{-1}{2b}}{i} \right] \sum_{j=0}^{+\infty} \binom{\frac{-b}{a}\left(\frac{1}{2b}+i\right)}{j} \\ & \times \left(\frac{P_{x_1}}{A^2}\right)^{aj+bi} \cdot (-1)^j \gamma\left(aj+bi+2, PAPR_{[x_1]}\right) \Bigg]^{1/2}. \end{aligned} \tag{3.32}$$

As in the case without predistortion, the EVM is expressed as a series expansion based on Gamma functions. Note that it now depends on the both parameters b and a corresponding to the knee factors of the PA and the predistortion functions.

3.5.2 With clipping

In this subsection, we derive the EVM calculation when both clipping and predistortion are activated. Thus, we use H_{EQ} to get the second order moment of

the magnitude error which is presented as follows

$$E\left\{|Z_k - X_k|^2\right\} = \underbrace{\int_0^{A_{max}} |r - H_{EQ}(r)|^2 f_r dr}_{I_{12}} + \underbrace{\int_{A_{max}}^{R_{max}} |r - H_{EQ}(A_{max})|^2 f_r dr}_{I_{13}} . \tag{3.33}$$

We mention that the derivation of I_{12} is similar to the EVM derivation in the case with predistortion and without clipping which is previously presented. Likewise, the derivation of I_{13} is exactly the same as I_5.

***Theorem* 4:** *The EVM of an amplified multicarrier signal using Rapp model, when both clipping and predistortion are activated, can be written as follows*

$$\begin{aligned} EVM = \Bigg[& - \left(e^{-\lambda PAPR_{[x_2]}} \left(\lambda PAPR_{[x_2]} + 1\right) - 1\right) \\ & + \sum_{i=0}^{+\infty} \left[\binom{\frac{-1}{b}}{i} - 2\binom{\frac{-1}{2b}}{i}\right] \sum_{j=0}^{+\infty} \binom{\frac{-b}{a}\left(\frac{1}{2b} + i\right)}{j} \\ & \times \left(\frac{P_{x_1}}{A^2}\right)^{aj+bi} \cdot (-1)^j \gamma\left(aj + bi + 2, \lambda PAPR_{[x_2]}\right) \\ & + e^{-\lambda PAPR_{[x_2]}} \left(\lambda PAPR_{[x_2]} + \frac{H_{EQ}\left(A_{max}\right)^2}{P_{x_1}} + 1\right) \\ & - e^{-PAPR_{[x_1]}} \left(PAPR_{[x_1]} + \frac{H_{EQ}\left(A_{max}\right)^2}{P_{x_1}} + 1\right) \\ & - \frac{2H_{EQ}\left(A_{max}\right)}{\sqrt{P_{x_1}}} \left(\gamma\left(\frac{3}{2}, PAPR_{[x_1]}\right) - \gamma\left(\frac{3}{2}, \lambda PAPR_{[x_2]}\right)\right) \Bigg]^{1/2} . \end{aligned} \tag{3.34}$$

As in the case without clipping, the EVM is expressed as a series expansion based on Gamma function. Note that now it depends on both parameters $\text{PAPR}_{[x_1]}$ and $\text{PAPR}_{[x_2]}$, the PAPR of the signals before and after clipping, respectively.

3.5.3 Simulation results and analysis

In this subsection we present a comparison between the theoretical EVM given by (3.32) and (3.34) and the simulated EVM when predistortion is activated with or without clipping, with $a = 1.6$ and $b = 1.5$. Fig. 3.7 shows the theoretical and simulated EVM when predistortion is used with various clipping thresholds or without clipping, with $O = 6$.

To go further in the analysis, let us calculate the Absolute Percentage Error (APE) of the approximated EVM for various IBO values and for different orders O

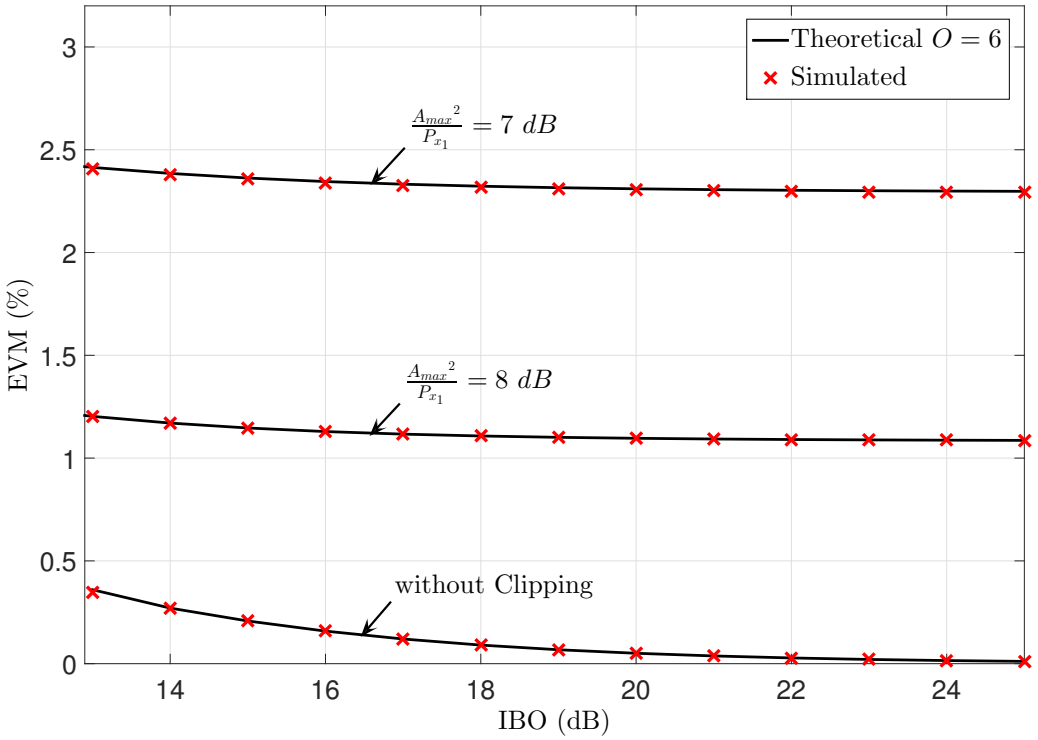

FIGURE 3.7 – Derived and simulated EVM with clipping and predistortion (a=1.6, b=1.5).

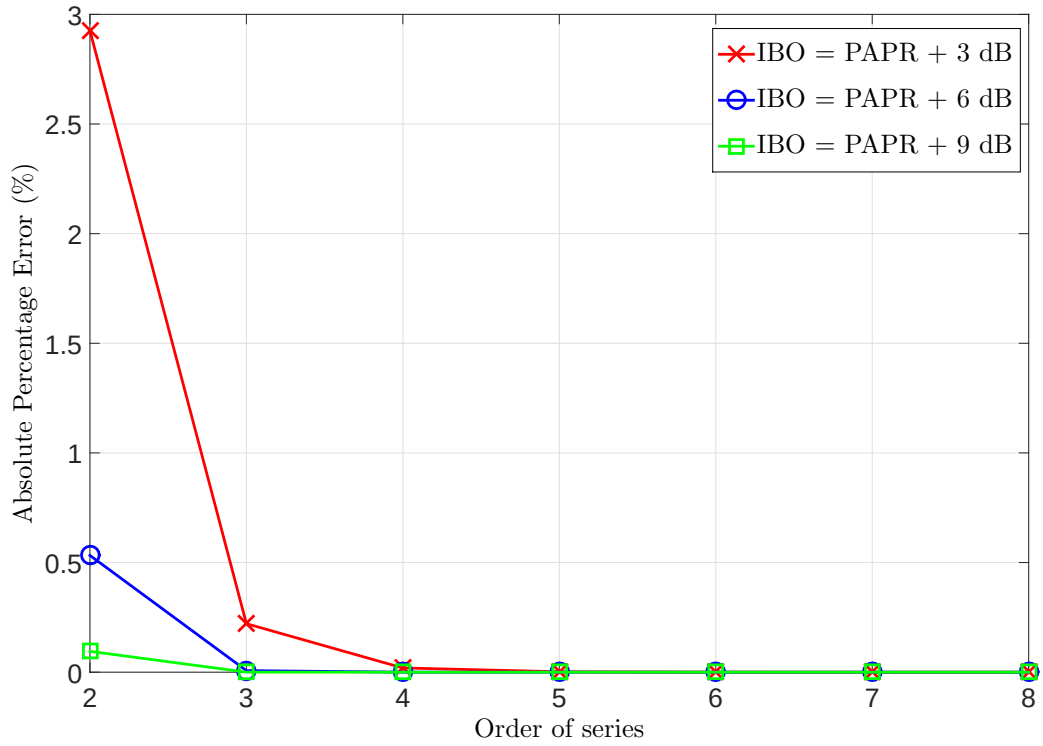

FIGURE 3.8 – Absolute Percentage Error of the approximated EVM with nonlinear amplification and without predistortion.

of the approximation. Note that a minimum IBO value equals to IBO = $\text{PAPR}_{[x_1]}$+

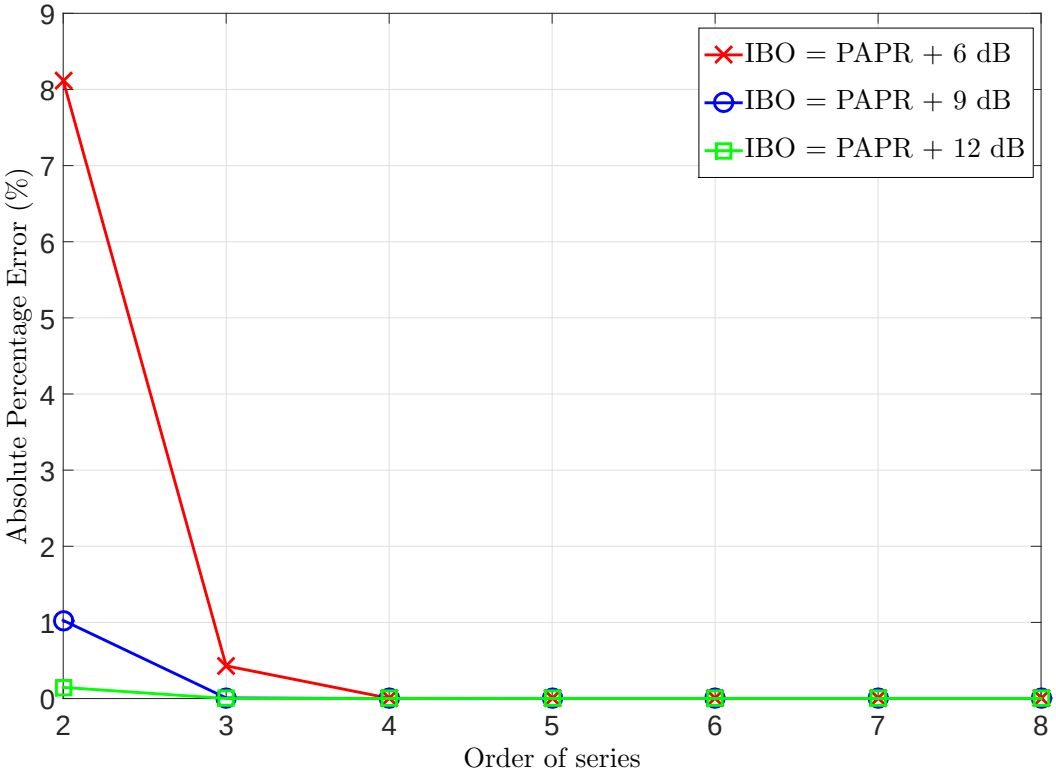

FIGURE 3.9 – Absolute Percentage Error of the calculated EVM with nonlinear amplification and with predistortion.

$3dB$ is considered which validates the assumption made in Eq. (3.11) and in Eq. (3.28) for the analytical derivation.

Fig. 3.8 and Fig. 3.9 give the APE obtained with and without predistortion. From these curves, it is concluded that an approximation of order $O = 4$ is highly sufficient to maintain the computation error far less than 1%. Recall that the exact EVM expression given by (2.22), based on integral forms, could not be implemented in practice in a system that would need to control its predistortion function in an adaptive manner. Yet, the proposed approximated EVM expressions can be used for such purpose.

3.6 Practical scenario

In this section, we present a simple scenario in which we show the importance of our proposed EVM expressions in controlling the transmitted power so that to respect the EVM constraint. Furthermore, we show that these expressions are useful in controlling the predistortion accuracy in order to mitigate as much as possible the linearization complexity. We consider that clipping and predistortion are activated. The clipping ratio is fixed to 10 dB. However, the estimation of the PA knee factor is not enough accurate in practice. Then, the value assigned to a is different from the exact value of b. Therefore, the key issue is to ensure that our transmitted power fulfils the linearity requirement despite the modelling error. For this reason, we plot the EVM of OFDM signals as a function of the a/b ratio for different IBO values as presented in Fig. 3.10. We assume an exact value of $b = 2$.

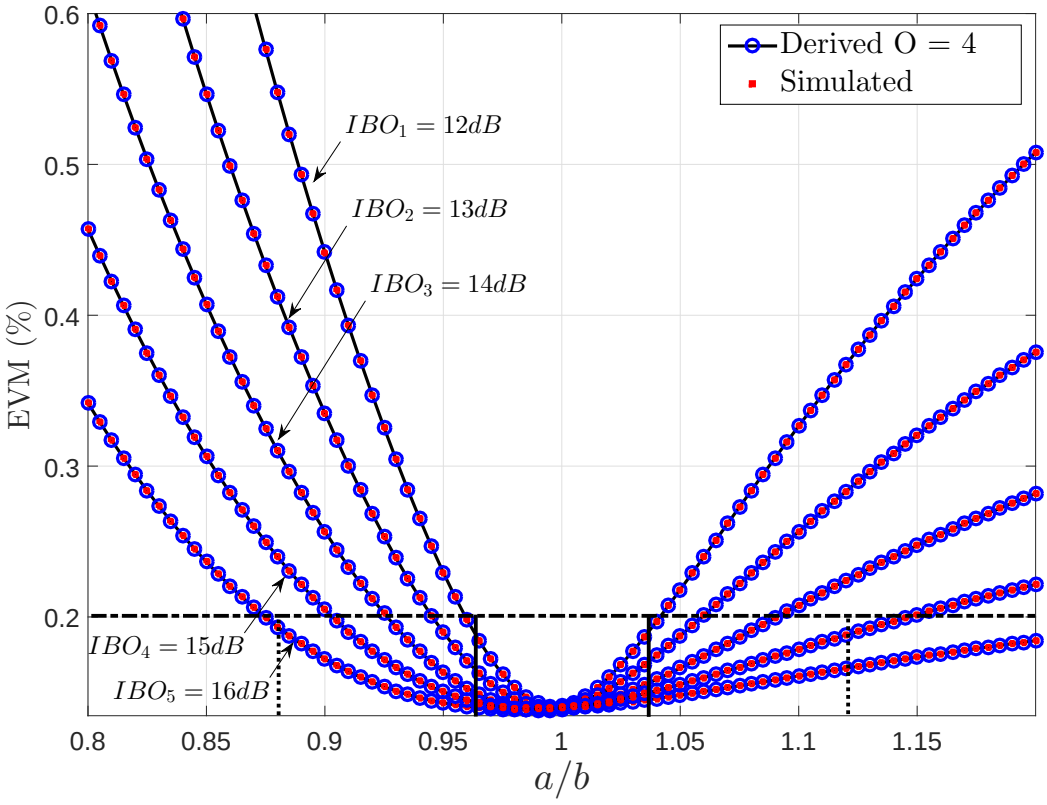

FIGURE 3.10 – EVM as a function of the 'knee factors' ratio a/b

As explained above, if $a = b = 2$, then the predistortion is perfect, so the EVM is minimized. Besides, when we move away from this point, the EVM increases as much as the estimation is inexact.

We now suppose that the EVM limit for our communication system is -27 dB (0.2%). In Fig. 3.10, with IBO_1, the predistortion should sufficiently accurate so that the range of a/b ratio varies from 0.96 to 1.04 (predistortion error less than $\pm 4\%$). Otherwise, however, the transmitter should use an IBO larger than IBO_1 in order to respect the EVM limit. In this way, we ensure that our transmitter is sufficiently linear and that the receiver on the other side has the lowest possible Bit Error Rate (BER). On the other hand, if the signal is amplified with IBO_5, the predistortion error could be acceptable with a tolerance of $\pm 12\%$ which does not require high precision in the estimation of the predistortion characteristics what implies a lower computational complexity.

More complex scenario can be analyzed. In particular several limitations and new constraints could be taken into account, e.g. Adjacent Channel Power Ratio, PA efficiency which will be discussed in next chapters. This will lead us to a global optimization approach of the transmitter efficiency and linearity.

3.7 Conclusion

In this chapter, the impact of the nonlinearities on the amplified multicarrier signal was analyzed considering Rapp PA model, PAPR reduction and PA lineari-

zation process. Therefore, we derived the expression of the Error Vector Magnitude (EVM) of the amplified signal with and without the use of predistortion and clipping techniques. It was concluded that an approximation of order $O = 4$ is highly sufficient to maintain the computation error far less than 1% with respect to the theoretical derivations. Therefore, the proposed EVM approximations can be favorably implemented in practice in a system that would need to control its clipping and predistortion functions in an adaptive manner. To go further in the analysis, some practical scenarios were proposed which demonstrate the importance of these analytical expressions in controlling the clipping and predistortion, to ensure the linearity and to mitigate the computational numerical distortions.

In the next chapter, more complex scenarios will be analyzed, in particular when new constraints are taken into account e.g. PA efficiency. Therefore, the polynomial PA model with or without memory effects is considered. Indeed, the derivation of the EVM for multicarrier signal is done using both clipping and predistortion. Hence, the PA linearity-efficiency trade-off is discussed in details.

Chapter 4

EVM derivations using polynomial PA model with and without memory effects

4.1 Introduction

In the previous chapter, we derived the EVM expressions using the Rapp model. In fact, on one hand, the derived EVM implies the calculation of infinite series. On the other, because of the convergence conditions of Binomial theorem, those analytical expressions are not valid in the compression zone where the PA efficiency is very high. However, there is a constant need to evaluate the EVM in both linear and compression zones to be able to handle the linearity-efficiency trade-off. Besides, it is well known that the Rapp PA model does not take into account neither the phase distortions nor the memory effects. Therefore, for all these reasons, we adopt in this chapter the polynomial PA model with and without memory. Thus, we derive the EVM expressions with or without the clipping and/or the predistortion techniques.

Moreover, we investigate the theoretical analysis of the PA linearity-efficiency and the predistortion complexity. We first examine the PA linearity-efficiency trade-off. Thereby, we provide an analytical expression which gives the optimal Input Back-Off (IBO) and clipping threshold which must be taken to maximize the PA efficiency for any EVM constraint. Secondly, we discuss the trade-off between the PA linearity-efficiency and the predistortion complexity aiming at reducing the predistortion complexity with respect to an EVM constraint. Therefore, we seek the optimal configuration of clipping and predistortion which maximizes the PA efficiency taking into account the predistortion complexity and satisfying the EVM constraint.

Next part deals with the analysis of the memory effects of the Power Amplifier (PA) on multicarrier signals. We analytically derive the expressions of the Error Vector Magnitude (EVM) of amplified signals jointly considering a memory polynomial PA model and clipping effects. We provide analytical EVM expressions that depend on the PA coefficients, PA order, and memory depth as well as the clipping threshold of the input signal. These analytical expressions are new general formulas which allow to predict in-band distortions at the PA output.

4.2 State of the art of EVM derivations taking into account the memory effects of the power amplifier

It is worthwhile to note that in literature, there are few studies that discuss the effect of the PA memory effects on the EVM. For example, in [GCW+13], an approximation expression for the EVM includes the effects of IQ imbalance, phase noise, and PA nonlinearities using Wiener PA model can be found. However, in this study the PAPR reduction is not considered. In addition, in [H+13], we can find an approximation of the symbol error rate in the presence of nonlinear PA with memory is presented. To the best of our knowledge, no analytical expression of the EVM taking into consideration the clipping technique and the memory effects through a memory polynomial model exists in the literature. Our contribution in this chapter is to propose such new expressions. In the previous sections, we already led the computation of the EVM of clipped multicarrier signals amplified by a memoryless PA model using Rapp or polynomial model. In this section, we expand our study accounting for the memory effects. We therefore compute the EVM on the basis of the aforementioned memory polynomial model. To be exhaustive in our study, these expressions are provided when clipping is activated or not prior to amplification. We eventually provide EVM expressions as a function of the PA characteristics, i.e. polynomial coefficients, as well as the clipping threshold of the input signal.

4.3 System model

In this chapter, we consider the PA polynomial model which is quasi-static model. Later, we extend our study to take into account the memory effects of the power amplifier using the memory polynomial model.

Thus, we first present the PA characteristics $H_{PA}(r)$ by the following odd order polynomial [1]

$$H_{PA}(r) = \sum_{l=0}^{L_p-1} b_{2l+1}\, r^{2l+1}, \tag{4.1}$$

where L_p denotes the nonlinear model order, b_{2l+1} are the nonlinear PA characteristics coefficients, and r is the amplitude of the input voltage. Since the PA model is a polynomial function, the inverse predistortion function can also be expressed as a polynomial. Therefore, the predistortion function is expressed as follows

$$H_{PD}(r) = \sum_{k=0}^{K_p-1} a_{2k+1} r^{2k+1}, \tag{4.2}$$

with K_p the nonlinear model order and a_{2k+1} the nonlinear polynomial coefficients.

1. Note that the odd order comes from the bandpass assumption as explained in [JBS00, p. 161].

4.4 Proposed EVM expressions without predistortion

In this section, we present the results of the EVM derivations when predistortion is not activated, in both cases with and without clipping, as a function of the PA characteristics, the average power and the PAPR of both input and clipped signals.

4.4.1 Without clipping

Firstly, we start by deriving the EVM expression when clipping and predistortion are deactivated. Using (2.22), (3.4), and (4.1), we derive a closed-form expression of the EVM.
In this case, using (2.24), (3.4), and (4.1), the second order moment of the magnitude error, denoted by m_2, can be expressed as follows

$$\begin{aligned} m_2 &= \int_0^{R_{max}} \left| H_{PA}(r) - r \right|^2 f_{x_1}(r)\, dr \\ &= \int_0^{R_{max}} \left| \sum_{l=0}^{L_p-1} C_{2l+1}\, r^{2l+1} \right|^2 \frac{2r}{P_{x_1}}\, e^{-\frac{r^2}{P_{x_1}}}\, dr\ , \end{aligned} \tag{4.3}$$

where

$$C_{2l+1} = \begin{cases} b_1 - 1 & \text{if } l = 0 \\ b_{2l+1} & \text{if } l \neq 0\ . \end{cases} \tag{4.4}$$

According to the multinomial theorem, it is possible to expand the squared term in (4.3) in the form of products of powers. In fact, for any positive integer m and any nonnegative integer n, the multinomial formula is given by

$$(x_1 + x_2 + ... + x_m)^n = \sum_{p_1+...+p_m=n} \binom{n}{p_1, p_2, ..., p_m} \prod_{i=1}^{m} x_i^{p_i} \tag{4.5}$$

where

$$\binom{n}{p_1, p_2, \ldots, p_m} = \frac{n!}{p_1! p_2! \ldots p_m!} \tag{4.6}$$

is a multinomial coefficient. The sum in (4.5) is taken over all combinations of nonnegative integer exponents p_1 through p_m such that the sum of all p_i is n. That is, for each term in the expansion, the exponents of x_i must be added up to n. Hence, we can obtain an expansion of m_2 as

$$m_2 = \sum_{p_1+...+p_{L_p-1}=2} \binom{2}{p_1, ..., p_{2L_p-1}} \times \prod_{l=0}^{L_p-1} (C_{2l+1})^{p_{2l+1}} \int_0^{R_{max}} \frac{2\, r^s}{P_{x_1}}\, e^{-\frac{r^2}{P_{x_1}}} dr \tag{4.7}$$

with

$$s = \sum_{l=0}^{L_p-1} (2l+1)\, p_{2l+1} + 1\ .$$

Then, using the integral identity in [Zwi, eq. (1) §3.381, pp. 346], the EVM expression can be written as (4.8).
Our main result is presented in the following theorem.

Theorem 5: *The EVM of an amplified multicarrier signal is expressed as follows*

$$EVM = \left[P_{x_1}{}^{\frac{s-3}{2}} \sum_{p_1+p_3+\ldots+p_{2L_p-1}=2} \binom{2}{p_1, p_3, \ldots, p_{2L_p-1}} \times \prod_{l=0}^{L_p-1} \left(C_{2l+1}\right)^{p_{2l+1}} \gamma\left(\frac{s+1}{2}, PAPR_{[x_1]}\right) \right]^{\frac{1}{2}}, \tag{4.8}$$

where γ represents the incomplete gamma function defined as

$$\gamma(\alpha, u) = \int_0^u x^{\alpha-1}\, e^{-x} dx, \tag{4.9}$$

with

$$s = \sum_{l=0}^{L_p-1} (2l+1)\, p_{2l+1} + 1 \ , \tag{4.10}$$

$$\binom{2}{p_1, p_3, \ldots, p_{2L_p-1}} = \frac{2!}{p_1! p_3! \ldots p_{2L_p-1}!} \ , \tag{4.11}$$

and

$$C_{2l+1} = \begin{cases} b_1 - 1 & \text{if } l = 0 \ , \\ b_{2l+1} & \text{if } l \neq 0 \ . \end{cases} \tag{4.12}$$

Note that the sum in (4.8) *is taken over all combinations of nonnegative integer exponents p_1 through p_{2L_p-1} such that the sum of all p_{2l+1} is equal to* 2.

This theorem provides an analytical EVM expression in the form of a series expansion involving Gamma functions and depending on different parameters. We can see that the in-band distortion of the amplified signal depends on the PA characteristics, as well as the PAPR of the signal $x_1(t)$ and the average power P_{x_1}. Note that this expression will be useful in the following analytical derivations of the EVM when considering clipping.

4.4.2 With clipping

We now lead the EVM calculation considering that the clipping is activated. In this case, using (3.5) and (4.45), the second order moment of the magnitude error is given by

$$m_2 = \underbrace{\int_0^{A_{max}} |r - H_{PA}(r)|^2 f_{x_1} dr}_{I_1} + \underbrace{\int_{A_{max}}^{R_{max}} |r - H_{PA}(A_{max})|^2 f_{x_1} dr}_{I_2} . \tag{4.13}$$

At first, the derivation of I_1 is similar to the derivation of m_2 in the case without clipping previously presented. Thus, using (3.7), I_1 can be computed as

$$I_1 = P_{x_1}{}^{\frac{s-1}{2}} \sum_{p_1+\ldots+p_{2L_p-1}=2} \binom{2}{p_1, \ldots, p_{2L_p-1}} \prod_{l=0}^{L_p-1} (C_{2l+1})^{p_{2l+1}} \gamma\left(\frac{s+1}{2}, \lambda \mathrm{PAPR}_{[x_2]}\right). \tag{4.14}$$

However, I_2 is an integral to be calculated. After expanding the squared term in I_2 and letting $u = \frac{r^2}{P_{x_1}}$ we get

$$\begin{aligned} I_2 = \; & P_{x_1} \underbrace{\int_{\lambda \mathrm{PAPR}_{[x_2]}}^{\mathrm{PAPR}_{[x_1]}} u\, e^{-u}\, du}_{I_3} \\ & - 2H_{PA}(A_{max}) \sqrt{P_{x_1}} \underbrace{\int_{\lambda \mathrm{PAPR}_{[x_2]}}^{\mathrm{PAPR}_{[x_1]}} \sqrt{u}\, e^{-u}\, du}_{I_4} \\ & + H_{PA}(A_{max})^2 \underbrace{\int_{\lambda \mathrm{PAPR}_{[x_2]}}^{\mathrm{PAPR}_{[x_1]}} e^{-u}\, du}_{I_5} . \end{aligned} \tag{4.15}$$

By applying integration by parts and using (3.7), I_3 and I_5 can be written as

$$I_3 = P_{x_1}\, e^{-\lambda \mathrm{PAPR}_{[x_2]}} \left(\lambda \mathrm{PAPR}_{[x_2]} + 1\right) - P_{x_1}\, e^{-\mathrm{PAPR}_{[x_1]}} \left(\mathrm{PAPR}_{[x_1]} + 1\right) ,$$

$$I_5 = H_{PA}(A_{max})^2 \left(e^{-\lambda \mathrm{PAPR}_{[x_2]}} - e^{-\mathrm{PAPR}_{[x_1]}}\right) . \tag{4.16}$$

Then, using the integral identity in [Zwi, eq. (1) §3.381, pp. 346], I_4 can be calculated as

$$I_4 = -2\sqrt{P_{x_1}} H_{PA}(A_{max}) \left(\gamma\left(\frac{3}{2}, \mathrm{PAPR}_{[x_1]}\right) - \gamma\left(\frac{3}{2}, \lambda \mathrm{PAPR}_{[x_2]}\right)\right). \tag{4.17}$$

Finally, compiling I_1 and I_2, the EVM expression can be written as (4.18).

In this case, using (2.22), (3.5), (3.7), and (4.1) we can derive a closed-form expression of the EVM which is presented in the following theorem.

Theorem 6: *The EVM of an amplified multicarrier signal, when clipping is activated, is expressed as follows*

$$
\begin{aligned}
EVM = \Bigg[& P_{x_1}{}^{\frac{s-3}{2}} \sum_{p_1+\ldots+p_{2L_p-1}=2} \binom{2}{p_1,\ldots,p_{2L_p-1}} \\
& \times \prod_{l=0}^{L_p-1} \left(C_{2l+1}\right)^{p_{2l+1}} \gamma\left(\frac{s+1}{2}, \lambda PAPR_{[x_2]}\right) \\
& + e^{-\lambda PAPR_{[x_2]}} \left(\lambda PAPR_{[x_2]} + \frac{H_{PA}\left(A_{max}\right)^2}{P_{x_1}} + 1\right) \\
& - e^{-PAPR_{[x_1]}} \left(PAPR_{[x_1]} + \frac{H_{PA}\left(A_{max}\right)^2}{P_{x_1}} + 1\right) \\
& - \frac{2H_{PA}(A_{max})}{\sqrt{P_{x_1}}} \left(\gamma\left(\frac{3}{2}, PAPR_{[x_1]}\right) - \gamma\left(\frac{3}{2}, \lambda PAPR_{[x_2]}\right)\right) \Bigg]^{1/2}, \qquad (4.18)
\end{aligned}
$$

with

$$
s = \sum_{l=0}^{L_p-1} (2l+1)\, p_{2l+1} + 1 \ , \qquad (4.19)
$$

Eventually, as in the case without clipping, Theorem 6 gives an EVM expression in the form of a series expansion composed of Gamma functions and depending on several parameters. These parameters are the PA order L_p, the PA coefficients b_{2l+1}, the average power and the PAPR of both input and clipped signals, as well as, the clipping threshold, and λ the ratio between P_{x_2} and P_{x_1}.

4.4.3 Simulation results and analysis

In this subsection, we present a comparison between the theoretical EVM expressions, given by Theorem 5 and Theorem 6, and the simulated EVM when clipping is activated or not. Note that each simulation considers 10^5 randomly generated OFDM symbols with 1024 sub-carriers modulated by 16-QAM symbols. The polynomial coefficients b_{2l+1} of the PA function have been derived by identification of two AM/AM characteristics. The first one is for a Rapp's SSPA model with knee factor $b = 2$ and the second one is a real PA for Digital Video Brodcasting-Terrestrial (DVB-T) which was previously presented in Chapter 2. Fig. 4.1 depicts the gain of the real DVB-T PA as a function of the output power at 202 MHz. We use a high-order polynomial function ($L_p = 6$) to achieve a satisfactory fitting accuracy. Fig. 4.2 and Fig. 4.3 depict the theoretical and simulated EVM as a function of the input power back-off when clipping is activated or not using a Rapp-modeled PA and DVB-T PA respectively. Note that (4.8) and (4.18) can be expressed as a function of the IBO, by replacing the average power by $\frac{P_{1dB,in}}{IBO}$ according to the IBO definition in (2.1). We consider clipping thresholds $\frac{A_{max}{}^2}{P_r}$ of 5 dB, 6 dB, 7 dB, and 8 dB. From the curves in Fig. 4.2 and Fig. 4.3, it can be verified that the EVM increases when the clipping threshold decreases. In addition, one can notice that using the Rapp-modeled PA, the EVM tends to zero

for high IBO when clipping is deactivated. However, such a behavior is not observed in the case of the DVB-T PA. This is due to the nonlinear characteristics of the DVB-T PA even within the expected linear region, which results in additional distortion.

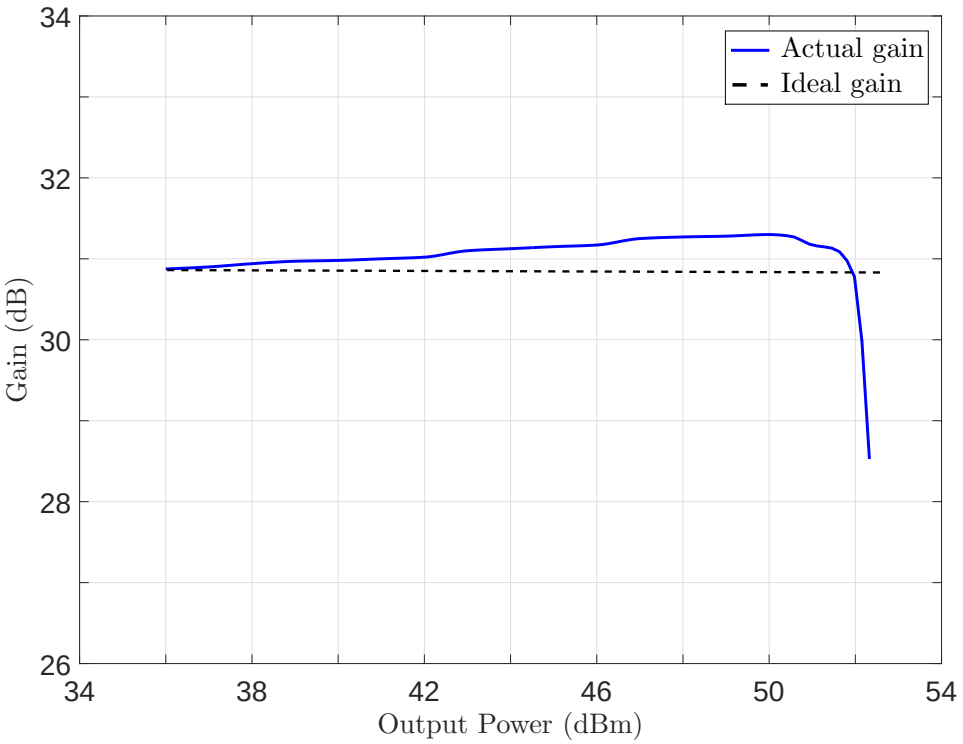

FIGURE 4.1 – The gain and power efficiency of the DVB-T PA as a function of the output power [Tec10].

4.5 Proposed EVM expressions with predistortion

In this section, we assume that the predistortion technique is activated. Hence, we investigate the EVM calculation, in both cases with and without clipping, based on the PA characteristics, the predistortion characteristics, and the clipping threshold, as well as, the average power and the PAPR of both input and clipped signals. Thus, the equivalent transfer function of the predistortion and amplification stages will be denoted by H_{EQ},

$$H_{EQ}(r) = H_{PA}(H_{PD}(r)) \ . \tag{4.20}$$

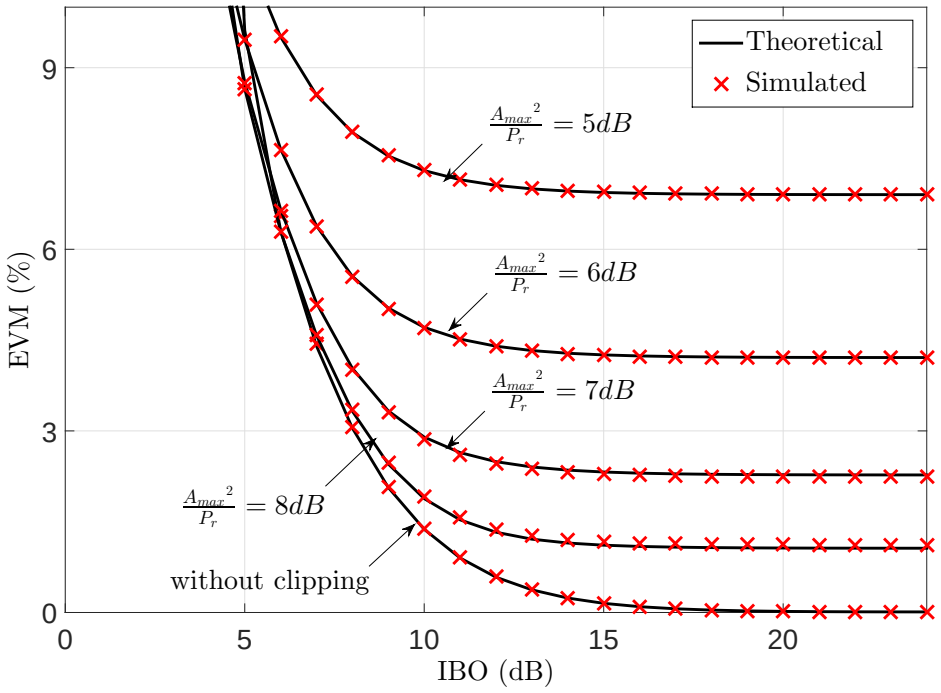

FIGURE 4.2 – Theoretical and simulated EVM without predistortion as a function of the IBO, when clipping is activated or not, using a Rapp modeled PA with a polynomial model ($L_p = 6$).

4.5.1 Without clipping

In this case, using (4.45) and (4.20) the second order moment of the magnitude error can be calculated as follows

$$\begin{aligned} m_2 &= \int_0^{R_{max}} \left| H_{EQ}(r) - r \right|^2 f_{x_1}(r)\, dr \\ &= \int_0^{R_{max}} \left| \sum_{l=0}^{L_p-1} b_{2l+1} \left[\sum_{k=0}^{K_p-1} a_{2k+1} r^{2k+1} \right]^{2l+1} - r \right|^2 f_{x_1}(r) dr. \end{aligned} \tag{4.21}$$

After expanding the squared term in (4.21), we get

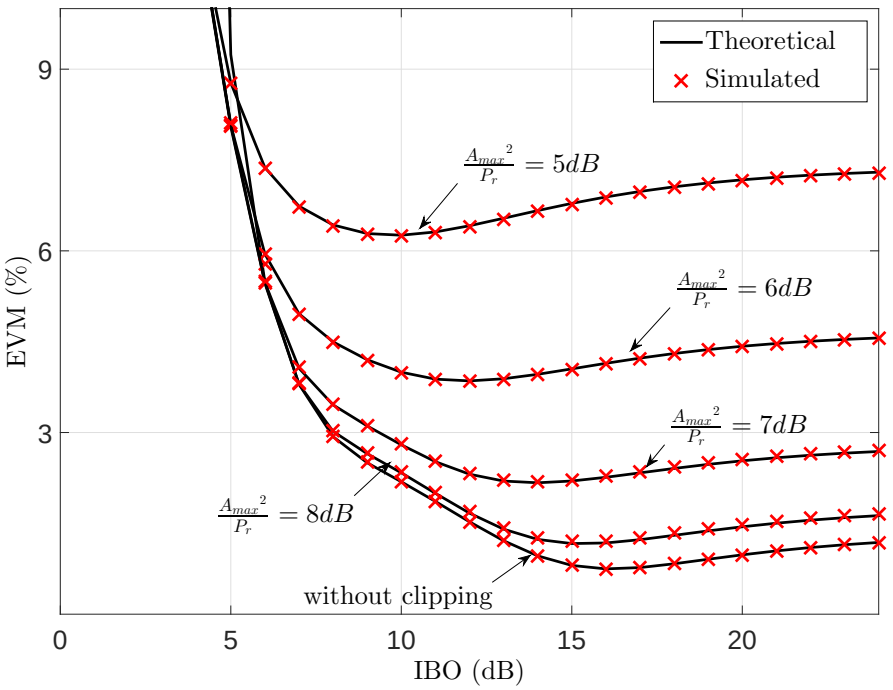

FIGURE 4.3 – Theoretical and simulated EVM without predistortion as a function of the IBO, when clipping is activated or not, using a DVB-T PA with $L_p = 6$ [Tec10].

$$
\begin{aligned}
m_2 \;=\; & \underbrace{\int_0^{R_{max}} r^2 \, \frac{2r}{P_{x_1}} e^{-\frac{r^2}{P_{x_1}}} dr}_{I_6} \\
& \underbrace{-2 \int_0^{R_{max}} r \sum_{l=0}^{L_p-1} b_{2l+1} \left[\sum_{k=0}^{K_p-1} a_{2k+1} r^{2k+1} \right]^{2l+1} \frac{2r}{P_{x_1}} e^{-\frac{r^2}{P_{x_1}}} dr}_{I_7} \\
& \underbrace{+ \int_0^{R_{max}} \left(\sum_{l=0}^{L_p-1} b_{2l+1} \left[\sum_{k=0}^{K_p-1} a_{2k+1} r^{2k+1} \right]^{2l+1} \right)^2 \frac{2r}{P_{x_1}} e^{-\frac{r^2}{P_{x_1}}} dr.}_{I_8}
\end{aligned}
\tag{4.22}
$$

In fact, the computation of I_6 is easily obtained by applying integration by parts

$$
I_6 = -P_{x_1} \left(e^{-\mathrm{PAPR}_{[x_1]}} \left(\mathrm{PAPR}_{[x_1]} + 1 \right) - 1 \right) \; . \tag{4.23}
$$

Then, using the multinomial theorem we can expand the power term in I_7, and after integration we have

$$I_7 = -2 \sum_{l=0}^{L_p-1} b_{2l+1} \sum_{q_1+q_3+\ldots+q_{2K_p-1}=2l+1} \binom{2l+1}{q_1, q_3, \ldots, q_{2K_p-1}} \times P_{x_1}{}^{\frac{s}{2}} \, \gamma\left(\frac{s}{2}+1, \mathrm{PAPR}_{[x_1]}\right) \prod_{k=0}^{K_p-1} (a_{2k+1})^{q_{2k+1}} , \tag{4.24}$$

with

$$s = \sum_{k=0}^{K_p-1} (2k+1)\, q_{2k+1} + 1 \ . \tag{4.25}$$

Likewise, we apply the multinomial theorem twice to the squared term in I_8, and after integration we get

$$I_8 = \sum_{p_1+p_3+\ldots+p_{2L_p-1}=2} \binom{2}{p_1, p_3, \ldots, p_{2L_p-1}} \prod_{l=0}^{L_p-1} (b_{2l+1})^{p_{2l+1}} \times \sum_{q_1+q_3+\ldots+q_{2K_p-1}=m} \binom{m}{q_1, q_3, \ldots, q_{2K_p-1}} \prod_{k=0}^{K_p-1} (a_{2k+1})^{q_{2k+1}} P_{x_1}{}^{\frac{n}{2}} \, \gamma\left(\frac{n}{2}+1, \mathrm{PAPR}_{[x_1]}\right), \tag{4.26}$$

where

$$m = \sum_{l=0}^{L_p-1} p_{2l+1}\,(2l+1)\,, \tag{4.27}$$

$$n = \sum_{k=0}^{K_p-1} (2k+1)\, q_{2k+1} \ . \tag{4.28}$$

Finally, after compiling these integrals, the EVM expression can be expressed as (4.29).

In this case, using (3.4), (2.22), and (4.20) we calculate the analytical EVM expression and the solution is given in Theorem 7.

Theorem 7: *The EVM of a predistorted amplified multicarrier signal is given*

by

$$EVM = \Bigg[-2 \sum_{l=0}^{L_p-1} b_{2l+1} \sum_{q_1+\ldots+q_{2K_p-1}=2l+1} \binom{2l+1}{q_1,\ldots,q_{2K_p-1}} \times {P_{x_1}}^{\frac{s}{2}-1} \gamma\left(\frac{s}{2}+1, PAPR_{[x_1]}\right) \prod_{k=0}^{K_p-1} (a_{2k+1})^{q_{2k+1}} + \sum_{p_1+\ldots+p_{2L_p-1}=2} \binom{2}{p_1,\ldots,p_{2L_p-1}} \prod_{l=0}^{L_p-1} (b_{2l+1})^{p_{2l+1}} \times \sum_{q_1+\ldots+q_{2K_p-1}=m} \binom{m}{q_1,\ldots,q_{2K_p-1}} {P_{x_1}}^{\frac{n}{2}-1} \times \gamma\left(\frac{n}{2}+1, PAPR_{[x_1]}\right) \prod_{k=0}^{K_p-1} (a_{2k+1})^{q_{2k+1}} - e^{-PAPR_{[x_1]}}\left(PAPR_{[x_1]}+1\right)+1 \Bigg]^{\frac{1}{2}}, \tag{4.29}$$

where

$$s = \sum_{k=0}^{K_p-1} (2k+1)\, q_{2k+1} + 1, \tag{4.30}$$

$$m = \sum_{l=0}^{L_p-1} (2l+1)\, p_{2l+1}, \tag{4.31}$$

$$n = \sum_{k=0}^{K_p-1} (2k+1)\, q_{2k+1}\ . \tag{4.32}$$

As in the case without predistortion, this theorem provides an EVM expression in the form of a series expansion based on Gamma functions. Besides, it now depends on the order and coefficients of both the predistortion and the amplifier, as well as the PAPR of the input signal $x_1(t)$ and its average power P_{x_1}.

4.5.2 With clipping

In this subsection, we derive the EVM expression when both clipping and predistortion techniques are activated using (2.22), (3.5), (3.7), and (4.20).

Using (3.5), (4.45), and (4.20), the second order moment of the magnitude error can be written as

$$m_2 = \underbrace{\int_0^{A_{max}} |H_{EQ}(r) - r|^2 f_{x_1} dr}_{I_9} + \underbrace{\int_{A_{max}}^{R_{max}} |H_{EQ}(A_{max}) - r|^2 f_{x_1} dr}_{I_{10}} . \tag{4.33}$$

However, the derivation of I_9 is similar to the derivation of (4.21). Moreover, the derivation of I_{10} is exactly the same calculation of I_2 previously presented. Hence, the EVM expression can be expressed as (4.34).

***Theorem* 8:** *The EVM of an amplified multicarrier signal when clipping and predistortion are activated is expressed as follows*

$$\begin{aligned} EVM = \Bigg[& e^{-\lambda PAPR_{[x_2]}} \left(\frac{H_{EQ}(A_{max})^2}{P_{x_1}} \right) + 1 \\ & - \frac{2H_{EQ}(A_{max})}{\sqrt{P_{x_1}}} \left(\gamma \left(\frac{3}{2}, PAPR_{[x_1]} \right) - \gamma \left(\frac{3}{2}, \lambda PAPR_{[x_2]} \right) \right) \\ & - 2 \sum_{l=0}^{L_p-1} b_{2l+1} \sum_{q_1+\ldots+q_{2K_p-1}=2l+1} \binom{2l+1}{q_1, \ldots, q_{2K_p-1}} \\ & \times {P_{x_1}}^{\frac{s}{2}-1} \gamma \left(\frac{s}{2}+1, \lambda PAPR_{[x_2]} \right) \prod_{k=0}^{K_p-1} (a_{2k+1})^{q_{2k+1}} \\ & + \sum_{p_1+\ldots+p_{2L_p-1}=2} \binom{2}{p_1, \ldots, p_{2L_p-1}} \prod_{l=0}^{L_p-1} (b_{2l+1})^{p_{2l+1}} \\ & \times \sum_{q_1+\ldots+q_{2K_p-1}=m} \binom{m}{q_1, \ldots, q_{2K_p-1}} {P_{x_1}}^{\frac{s}{2}-1} \\ & \times \gamma \left(\frac{s}{2}+1, \lambda PAPR_{[x_2]} \right) \prod_{k=0}^{K_p-1} (a_{2k+1})^{q_{2k+1}} \\ & - e^{-PAPR_{[x_1]}} \left(PAPR_{[x_1]} + \frac{H_{EQ}(A_{max})^2}{P_{x_1}} + 1 \right) \Bigg]^{1/2} . \end{aligned} \tag{4.34}$$

where

$$s = \sum_{k=0}^{K_p-1} (2k+1)\, q_{2k+1} + 1, \tag{4.35}$$

$$m = \sum_{l=0}^{L_p-1} (2l+1)\, p_{2l+1}, \tag{4.36}$$

$$n = \sum_{k=0}^{K_p-1} (2k+1)\, q_{2k+1}\ . \tag{4.37}$$

Eventually, as in the case without clipping, Theorem 8 gives an EVM expression in the form of a series expansion depending on the same parameters. In addition, it depends now on the PAPR of the clipped signal $x_2(t)$, the clipping threshold, and the ratio λ between P_{x_2} and P_{x_1}.

4.5.3 Simulation results and analysis

In this subsection, we present a comparison between the theoretical EVM, given by Theorem 3 and Theorem 4, and the simulated EVM when predistortion is activated. Fig. 4.4 and Fig. 4.5 depict the theoretical and simulated EVM as a function of the IBO when clipping is activated or not using the previously introduced Rapp-modeled and DVB-T PAs respectively. Please note here again that the Rapp and DVB-T PAs are modeled by a polynomial PA model with $L_p = 6$. We consider the predistortion order $K_p = 5$ and clipping thresholds $\frac{{A_{max}}^2}{P_r}$ of 5 dB, 6 dB, 7 dB, and 8 dB. Note that the in-direct learning is used to extract the coefficients a_{2k+1} [DRZ02]. First of all, we can see by comparing Fig. 4.5 and Fig. 4.3, that the EVM is lower when the predistortion is activated in both cases with and without clipping. Second, we can remark from the curves in Fig. 4.4 and Fig. 4.5 that the EVM of the predistorted and amplified signal in the case of DVB-T PA is similar to the EVM in the case of a modeled PA. This is due to the high linearization order which provides a linear response of the transmitter chain in both cases. In addition, we note also that the EVM increases rapidly when the IBO is lower than the clipping threshold. This is explained by the fact that the peaks of the signal are amplified in the saturation zone of the PA.

4.6 Theoretical analysis of the trade-off between PA linearity-efficiency and predistortion complexity

In the previous section, we have analytically proven that the linearity of the PA measured by the EVM metric depends on the performance of clipping and predistortion. In this section, we show that the performance of clipping and predistortion also impacts the PA's efficiency. Thus, we theoretically analyze the trade-off between the PA linearity and efficiency considering the clipping and predistortion techniques. Secondly, as far as the complexity and the power consumption of the digital signal processing in the baseband are concerned, we expand our study to

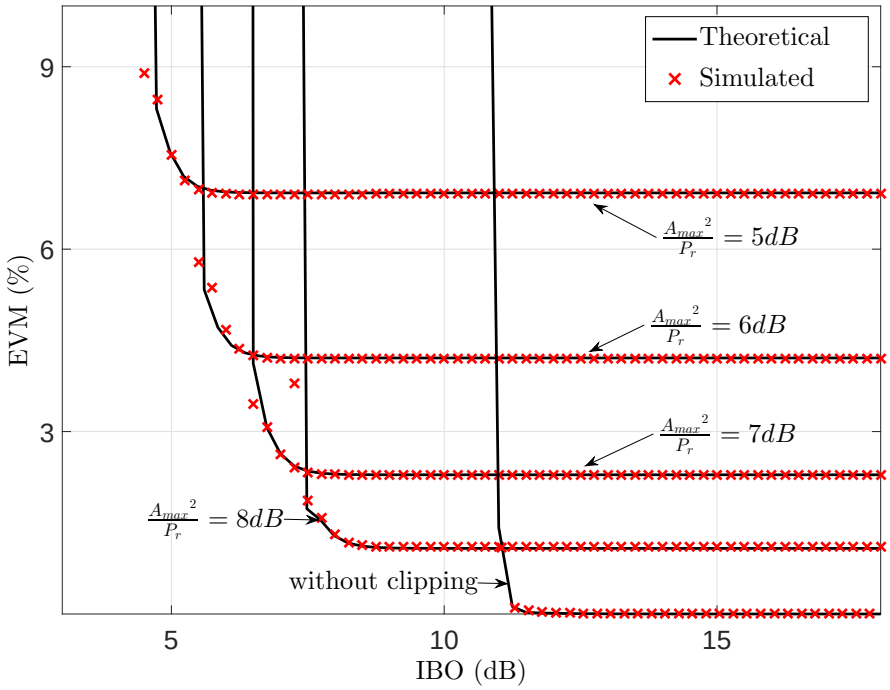

FIGURE 4.4 – Theoretical and simulated EVM with predistortion as a function of the IBO, when clipping is activated or not, using a modeled Rapp PA with a polynomial PA model ($L_p = 6$, $K_p = 5$).

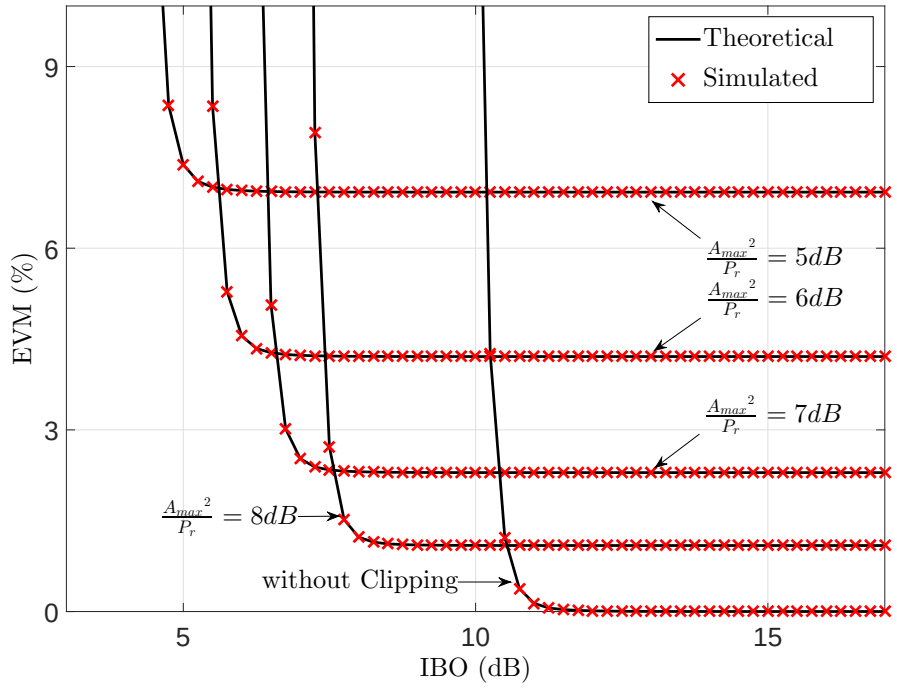

FIGURE 4.5 – Theoretical and simulated EVM with predistortion as a function of the IBO, when clipping is activated or not, using a DVB-T PA with $L_p = 6$ and $K_p = 5$ [Tec10].

minimize the complexity of the predistortion technique with respect to an EVM constraint. Therefore, we seek to provide a joint configuration of the predistortion and clipping techniques which maximizes the PA power efficiency taking into account the complexity of the predistortion technique and considering an EVM constraint.

4.6.1 Trade-off between PA linearity-efficiency and predistortion complexity considering clipping and predistortion

Wireless communication standards impose significant constraints on the transmitter's linearity, and at the same time require high efficiency. The EVM is a common figure of merit used to evaluate the linearity of communication systems and has became a mandatory part of some communication standards, e.g. [LTE12]. In the rest of this subsection, we seek to maximize the power efficiency of the PA while respecting an EVM limitation and considering a given predistortion complexity.

In the first part, we investigate the PA linearity-efficiency trade-off. For this reason, we propose to control the clipping technique and adapt the transmit power in order to maximize the PA efficiency with respect to an EVM constraint. Therefore, we provide an analytical expression which gives the optimal input power back-off and clipping threshold which must be taken to maximize the PA efficiency for any EVM constraint. In the next part, we investigate the complexity of the predistortion technique given that the complexity of the clipping technique is negligible compared to the complexity of the predistortion. So we propose to control the clipping and predistortion techniques in order to find the optimal configuration which maximizes the PA efficiency taking into account the predistortion complexity and satisfying the EVM constraint.

4.6.1.1 Control the clipping technique

As stated before, maximizing the efficiency is equivalent to minimizing the IBO. Consequently, we seek the minimum IBO and the corresponding clipping threshold with respect to a specific EVM constraint. For this reason we plot the EVM as a function of the IBO for different clipping thresholds using a DVB-T PA [Tec10].

From Fig. 4.6 we remark that the EVM of the signal is constant if the $IBO \geq PAPR_{[x_2]}$, however, it rapidly increases when the $IBO < PAPR_{[x_2]}$. According to the results of Theorem 4 represented in Fig. 4.6 and in agreement with [GL12a], we can propose the following corollary of theorem 4.

Corollary 9: *the input power back-off of the PA must be set identical to the PAPR of the signal after PAPR reduction in order to keep the maximum power efficiency gained by the PAPR reduction. Therefore, the analytical expression which gives the optimal input power back-off to maximize the PA efficiency with respect*

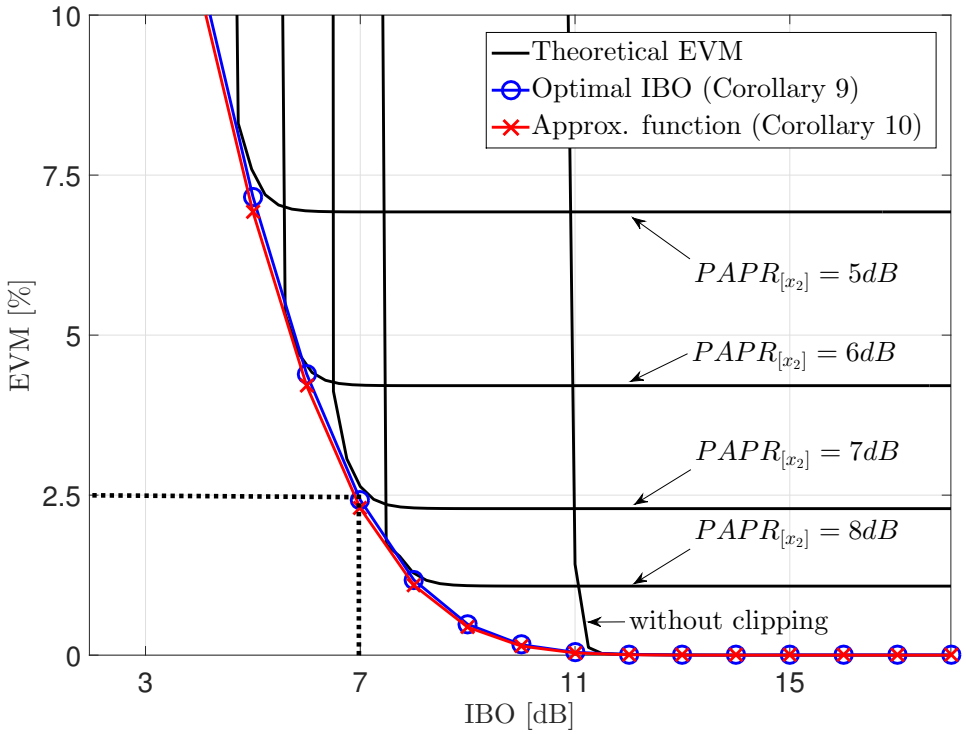

FIGURE 4.6 – Theoretical EVM with predistortion as a function of the IBO using a DVB-T PA with $L_p = 6$ and $K_p = 5$ [Tec10]. The analytical expression, which gives the optimal IBO for an EVM constraint given by Corollary 9, and the approximated one, given by Corollary 10, are also ploted.

to an EVM constraint is given by

$$
\begin{aligned}
EVM = \Bigg[& + e^{-\lambda IBO}\left(\frac{H_{EQ}(A_{max})^2}{P_{x_1}}\right) + 1 \\
& - \frac{2H_{EQ}(A_{max})}{\sqrt{P_{x_1}}}\left(\gamma\left(\frac{3}{2}, PAPR_{[x_1]}\right) - \gamma\left(\frac{3}{2}, \lambda IBO\right)\right) \\
& - 2\sum_{l=0}^{L_p-1} b_{2l+1} \sum_{q_1+\ldots+q_{2K_p-1}=2l+1} \binom{2l+1}{q_1, \ldots, q_{2K_p-1}} \\
& \times {P_{x_1}}^{\frac{s}{2}-1}\gamma\left(\frac{s}{2}+1, \lambda IBO\right) \prod_{k=0}^{K_p-1} (a_{2k+1})^{q_{2k+1}} \\
& + \sum_{p_1+\ldots+p_{2L_p-1}=2} \binom{2}{p_1, \ldots, p_{2L_p-1}} \prod_{l=0}^{L_p-1} (b_{2l+1})^{p_{2l+1}} \\
& \times \sum_{q_1+\ldots+q_{2K_p-1}=m} \binom{m}{q_1, \ldots, q_{2K_p-1}} {P_{x_1}}^{\frac{s}{2}-1} \\
& \times \gamma\left(\frac{s}{2}+1, \lambda IBO\right) \prod_{k=0}^{K_p-1} (a_{2k+1})^{q_{2k+1}} \\
& - e^{-PAPR_{[x_1]}}\left(PAPR_{[x_1]} + \frac{H_{EQ}(A_{max})^2}{P_{x_1}} + 1\right)\Bigg]^{1/2}. \qquad (4.38)
\end{aligned}
$$

Proof. According to the results of Theorem 4 represented in Fig. 4.6 and [GL12a], we can state that the maximum possible power efficiency, avoiding PA saturation, is achieved when peak power of the amplified signal coincides with the saturation power. So by replacing the $PAPR_{[x_2]}$ by the IBO in (4.34), we get (4.38). ■

Equation (4.38) provides the optimal IBO which maximizes the PA efficiency with respect to an EVM constraint. As shown in Fig. 4.6, equation (4.38) provides an exact fitting to the optimal IBO. Thus, suppose now that one targets the maximum PA efficiency and wants to identify which IBO is the optimal. However, there are two strategies to choose the optimal IBO. The first strategy aims at amplifying the transmit signal with no distortion which means that the EVM must be equal to zero. In this case, from the curve given by Fig. 4.6 according to Corollary 9, we remark that the optimal IBO which maximizes the PA efficiency and guaranties a null EVM is 11 dB. Thus, the clipping threshold should be also equal to 11 dB. On the other hand, the second strategy is to take advantage of the degree of freedom in the required EVM of the transmitted signal to boost the PA efficiency. Therefore, the key is to carefully manage the distortion, so we stay within the limits as specified in the communication standards [EVM99, EVM05, LTE12]. For example, if the EVM constraint of the communication system is equal to 2.5%, from the curve given by Fig. 4.6 according to Corollary 9, we remark that the optimal IBO is 7 dB. Thus, the clipping threshold should be also equal to 7 dB. Referring to the characteristics of the used DVB-T PA in Fig. 4.7, we can state that the efficiency increases from 19.5% to 31% [Tec10] by using the second strategy instead of the first one. So the efficiency gain is equal to 11.5% which is quite significant.

A simplification of (4.38) is given by the following corollary.

***Corollary* 10:** *The approximated analytical expression of (4.38), provided that the linearization process is sufficiently accurate, is given by*

$$EVM \approx \left[-2\sqrt{\lambda IBO}\left(\gamma\left(\frac{3}{2}, PAPR_{[x_1]}\right) - \gamma\left(\frac{3}{2}, \lambda IBO\right)\right) \right. \\ \left. e^{-\lambda IBO}\left(2\lambda IBO + 1\right) - e^{-PAPR_{[x_1]}}\left(PAPR_{[x_1]} + \lambda IBO + 1\right)\right]^{1/2}. \tag{4.39}$$

Proof. If the linearization technique is sufficiently accurate, the distortion of the PA could be negligible compared to the clipping distortion. Therefore, the expression of the EVM can be approximated by neglecting the integral I_9 in (4.33) and assuming that $\frac{H_{EQ}(A_{max})^2}{P_{x_1}} = \lambda \mathrm{PAPR}_{[x_2]}$. Moreover, according to Corollary 9, $\mathrm{PAPR}_{[x_2]} = \mathrm{IBO}$, so after doing some maths we obtain (4.39). ■

From Fig. 4.6, we show that Corollary 10 provides a perfect approximation of Corollary 9. We remark that the approximated EVM given by (4.39) is slightly less than the exact one given by (4.38). This is explained by the considered simplification of the PA distortion. Indeed, the importance of Corollary 10 is that it

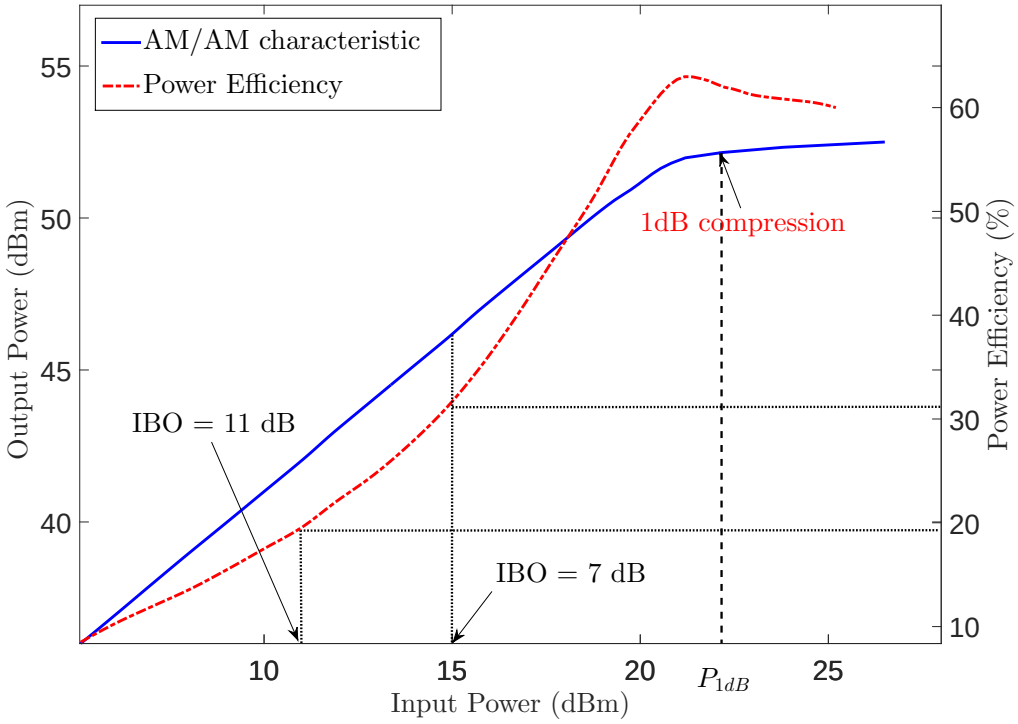

FIGURE 4.7 – The output power and power efficiency of the DVB-T PA versus the input power [Tec10].

does not depend on the linearization technique. So, for any linearization technique, using the clipping as a PAPR reduction, Corollary 10 is valid. However, the less accurate the used linearization technique is, the less correct the approximation is.

4.6.1.2 Control the clipping and predistortion techniques

In this part, we aim at jointly controlling the clipping and predistortion techniques in order to perform an optimal configuration which maximizes the PA efficiency taking into account the predistortion complexity and satisfying the EVM constraint. For this reason, we investigate the complexity of the predistortion, and seek a compromise between the complexity and linearity. Referring to (4.2), it can be rewritten in a matrix format as

$$\mathbf{X}_{N\times 1} = \mathbf{R}_{N\times K_p}\mathbf{A}_{K_p\times 1} \tag{4.40}$$

where $X_{N\times 1}$ represents the predistortion output vector and $\mathbf{R}_{N\times K_p}$ is the matrix which contains all linear and product terms of the amplitude signal $r, r^3, ..., r^{2k+1}$ for all the input data samples. Note that N represents the number of used input/output data samples and K_p is the number of involved predistortion coefficients. $\mathbf{A}_{K_p\times 1}$ represents the unknown coefficients vector.

To extract the coefficients, the in-direct learning [DRZ02] is used, where the predistorted output signal, $x_3(n)$, is used as the expected output, while the output of the PA, $z(n)$, is used as the input of the model. Using the Least Square

algorithm, the coefficients vector can be estimated from

$$\widehat{\mathbf{A}}_{K_p\times 1} = \left[\left(\mathbf{Z}_{N\times K_p}\right)^H \ \mathbf{Z}_{K_p\times N}\right]^{-1} \left(\mathbf{Z}_{N\times K_p}\right)^H \mathbf{X}_{N\times 1} \tag{4.41}$$

where $\mathbf{Z}$ is the PA output matrix in a similar form to the matrix $\mathbf{R}$, and $(.)^H$ represents the Hermitian transpose. Now, we have to compute the computational complexity of the matrix operations in (4.41). Indeed, there are one matrix inversion and three matrix-matrix multiplications. In fact, the inversion of a $K_p \times K_p$ matrix is approximately equivalent to ${K_p}^3$ number of multiplication operations. However, multiplying a $K_p \times N$ matrix by a $N \times K_p$ matrix requires $(N-1) \times K_p \times K_p$ additions and $K_p \times N \times K_p$ multiplications.

Therefore, the total number of multiplication operations and addition operations to be conducted in (4.41) are given respectively by

$$O^{\otimes}_{N,K_p} = N \times {K_p}^2 \times 2 + N \times K_p + {K_p}^3, \tag{4.42}$$

$$O^{\oplus}_{N,K_p} = (N-1) \times {K_p}^2 + N \times (K_p - 1) \times K_p + (N-1) \times K_p. \tag{4.43}$$

This leads to the conclusion that the computational complexity of model extraction actually depends on the nonlinear model order of the predistortion K_p and the number of the training samples N. Thereby, the more we decrease the number of predistortion coefficients and the training samples, the more we decrease the computational complexity. Consequently, thanks to our EVM expressions we can minimize the computational complexity of the predistortion technique by controlling K_p. Thus, we have to choose the minimum number of coefficients with respect to our EVM constraint.

To discuss this issue we plot (4.38) to find the optimal IBO for different predistortion orders. Note again that (4.38) gives the optimal input power back-off and clipping threshold which must be taken to maximize the PA efficiency for any EVM constraint. Based on the foregoing, the more we decrease the clipping threshold and the IBO, the more the PA efficiency increases. Furthermore, the more we decrease the predistortion order, the more the computational complexity decreases. On the other hand, we remark from Fig.4.8 that the more we decrease the predistortion order, the more the EVM increases. Consequently, assuming for example that the EVM should be less than 2.5%, we notice from Fig.4.8 that different solutions can be adopted according to the transmission constraints and limits. So, in terms of PA efficiency and without taking into account the predistortion complexity, the optimal IBO, with respect to the EVM constraint, is 7 dB which implies a $\text{PAPR}_{[x_2]} = 7$ dB. However, if we do not have sufficient computational capacity for the predistortion technique, we can decrease the predistortion order and choose for example $K_p = 2$ instead of choosing $K_p = 5$. In this case, the optimal IBO, that satisfies the computational complexity and respects the EVM constraint, becomes 7.6 dB. Although the PA efficiency decreases from 32% to 30%, we significantly mitigate the predistortion complexity. Therefore, the number of multiplication operations decreases from $55N + 125$ to $10N + 8$ and the number of addition operations decreases from $50N - 30$ to $8N - 6$. So thanks to our proposed theorems, we can decrease, in this scenario, the number of multiplication operations 5 times and the number of addition operations 6 times.

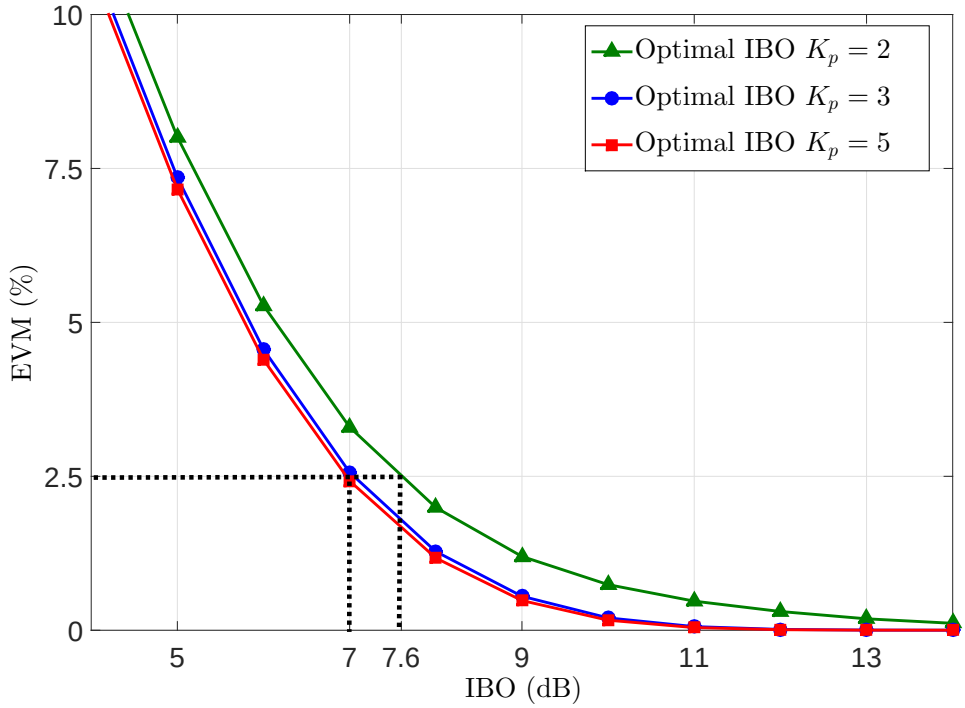

FIGURE 4.8 – The optimal IBO (Corollary 9) for $L_p = 6$ and $K_p = 2, 3$, and 5 using a DVB-T PA [Tec10].

4.7 Quantifying the memory effects of power amplifiers

Many Power Amplifier (PA) behavior models are based on the static AM/AM (Amplitude to Amplitude) and AM/PM (Amplitude to Phase) characteristics [DLR96] without taking into account any memory effects. It is thereby assumed that the output of the PA is a function of the instantaneous input signal amplitude only and not of the past ones. However, in practice, many high PAs such as those equipping wireless base stations exhibit potentially strong memory effects mainly due to the non-flat frequency response of the matching networks, the variation of the bias networks and the harmonic loading of the PA [VRM01b]. Moreover, as the bandwidth of the signal increases, with for example wideband multicarrier systems, memory effects become even more severe and can no longer be ignored. Hence, a more comprehensive approach to reveal the exact behavior of PAs in a communication chain is to use memory polynomial models which were proven to be effective for actual PAs under typical operating conditions [KK01b].

With such models however, any theoretical performance analysis turns out to be much more complex. For instance, deriving the analytical expression of the Error Vector Magnitude (EVM) at the output of the transmitter becomes tricky.

For this reason, we expand our study accounting for the memory effects. We therefore compute the EVM on the basis of the aforementioned memory polynomial model. To be exhaustive in our study, these expressions are provided when clipping is activated or not prior to amplification. We eventually provide EVM expressions

as a function of the PA characteristics, i.e. polynomial coefficients, as well as the clipping threshold of the input signal.

4.7.1 Proposed EVM derivations with PA memory effects

In this section, we consider the PA memory polynomial model which is a good model for the baseband behavior of the PA as shown in [KK01b]. Therefore, the amplified signal $z(t)$ is represented by the following memory polynomial model

$$z(t) = \sum_{q=0}^{Q} \sum_{l=1}^{L_p} b_{lq}\, x(t - q\tau)\, |x(t - q\tau)|^{2(l-1)}\,, \tag{4.44}$$

where b_{lq} are complex coefficients, Q is the memory depth, and L_p is the polynomial order. Note that τ is a parameter modeling the delay introduced by the memory effects.

Thus, using 2.21 the second order moment of the magnitude error $|\epsilon|$ is represented by the following equation

$$\begin{aligned} E\left\{|z(t) - x(t)|^2\right\} = & \int_0^R ... \int_0^{R_Q} \int_{-\pi}^{+\pi} ... \int_{-\pi}^{+\pi} |\epsilon|^2 \; f_x(r) \\ & ... f_{x_Q}(r_Q)\, f_\theta(\theta) ... f_{\theta_Q}(\theta_Q)\, dr ... dr_Q d\theta ... d\theta_Q. \end{aligned} \tag{4.45}$$

where $E\{|x(t)|^2\}$ is the average signal power and $E\{.\}$ is the expectation function. $R, R_1, ..., R_Q$ and $f_x, f_{x_1}, ..., f_{x_Q}$ are the maximum magnitude and the probability density function of $x(t)$, $x(t-\tau)$,..., $x(t-Q\tau)$, respectively. As $x(t-q\tau)$ is the time-shifted signal of $x(t)$, so $\forall q \in \{1, .., Q\}, R_q = R$ and $P_{[x_q]} = P_{[x]}$, then $PAPR_{[x_q]} = PAPR_{[x]}$. Note that $|\epsilon| = |z(t) - x(t)|$, is a stationary random variable modeling the signal error that depends on the magnitude and phase of input and output signals. In addition, we denote r_q and θ_q, the magnitude and the phase of the input complex baseband signal $x(t - q\tau)$, respectively.

4.7.1.1 Without clipping

First, we start by deriving the EVM expression when clipping is deactivated.

In order to simplify the notation, we denote $x(t - i\tau)$ by x_i. The squared magnitude error of the amplified signal can be written as

$$|\epsilon|^2 = \left| \sum_{q=0}^{Q} \sum_{l=1}^{L_p} b_{lq}\, x_q\, |x_q|^{2(l-1)} - x \right|^2 . \tag{4.46}$$

After applying this property $|\epsilon|^2 = \epsilon^* \epsilon$, and expanding these terms, we have

$$\begin{aligned}\left|\epsilon\right|^2 = & \underbrace{\sum_{q,q'=0}^{Q}\sum_{l,l'=1}^{L_p} b_{lq}b^*_{l'q'}\; x_q\; x^*_{q'}\,|x_q|^{2(l-1)}\,|x_{q'}|^{2(l'-1)}}_{i_1} \\ & \underbrace{-\sum_{q=0}^{Q}\sum_{l=1}^{L_p} b_{lq}\; x_q\,|x_q|^{2(l-1)}\,x^*}_{i_2} \;+\; \underbrace{xx^*}_{i_3} \\ & \underbrace{-\sum_{q'=0}^{Q}\sum_{l'=1}^{L_p} b^*_{l'q'}\; x^*_{q'}\,|x_{q'}|^{2(l-1)}\,x}_{i_4}\,. \end{aligned} \tag{4.47}$$

We denote I_1 through I_4 the integrals of the terms i_1 through i_4 in equation (4.47) respectively. First, i_3 depends only on r, so that the computation of I_3 is easily obtained by applying integration by parts with respect to r.

$$I_3 = P_x\left(1 - e^{-\mathrm{PAPR}_{[x]}}\left(\mathrm{PAPR}_{[x]} + 1\right)\right). \tag{4.48}$$

Secondly, I_1 can be written as

$$\begin{aligned} I_1 = & \sum_{q,q'=0}^{Q}\sum_{l,l'=1}^{L_p}\int_0^R ... \int_0^R \int_{-\pi}^{+\pi} ... \int_{-\pi}^{+\pi} \alpha_{(l,l',q,q')} f_x\left(r\right) \\ & ...f_{x_Q}\left(r_Q\right) f_\theta\left(\theta\right) ...f_{\theta_Q}\left(\theta_Q\right) dr...dr_Q d\theta...d\theta_Q, \end{aligned} \tag{4.49}$$

where

$$\alpha_{(l,l',q,q')} = \begin{cases} b_{lq}\; b^*_{l'q}\; r_q^{2(l+l'-1)} & \text{if } q' = q \\ b_{lq}\; b^*_{l'q'} e^{i(\theta_q - \theta_{q'})} r_q^{2l-1} r_{q'}^{2l'-1} & \text{if } q' \neq q. \end{cases} \tag{4.50}$$

If $q' \neq q$, then $I_1 = 0$, because

$$\int_{-\pi}^{+\pi} e^{j\theta_q} f_{\theta_q} d\theta_q = 0. \tag{4.51}$$

However, if $q' = q$, then I_1 depends only on r_q. Therefore, we have

$$I_1 = \sum_{q=0}^{Q}\sum_{l,l'=1}^{L_p} b_{lq}\; b^*_{l'q} \int_0^R r_q^{2(l+l'-1)} \frac{2r_q}{P_x} e^{-\frac{{r_q}^2}{P_x}} dr_q. \tag{4.52}$$

Then, using the integral identity in [Zwi, eq. (1) §3.381, pp. 346], I_1 can be written as (4.53).

$$I_1 = \sum_{q=0}^{Q}\sum_{l,l'=1}^{L_p} {P_x}^{l+l'-1} b_{lq}\; b^*_{l'q}\; \gamma\left(l + l', \mathrm{PAPR}_{[x_q]}\right). \tag{4.53}$$

Similarly, if $q \neq 0$ in i_2 and i_4, then I_2 and I_4 equal zero. Otherwise, using [Zwi, eq. (1) §3.381, pp. 346] we obtain

$$I_2 = -\sum_{l=1}^{L_p} b_{l1}\ P_x^l\ \gamma\left(l+1, \mathrm{PAPR}_{[x]}\right), \tag{4.54}$$

$$I_4 = -\sum_{l=1}^{L_p} b_{l1}^*\ P_x^l\ \gamma\left(l+1, \mathrm{PAPR}_{[x]}\right). \tag{4.55}$$

Finally, compiling these integrals and using (2.22), the EVM expression of an amplified multicarrier signal is given by the following theorem.

***Theorem* 11:** *The EVM expression of an amplified multicarrier signal, taking into account the memory effects, is expressed as follows*

$$\begin{aligned} EVM = \Bigg[& -\sum_{l=1}^{L_p} P_x^{l-1}\ \ \gamma\left(l+1, PAPR_{[x]}\right)\left(b_{l1}+b_{l1}^*\right) \\ & + \sum_{q=0}^{Q}\sum_{l,l'=1}^{L_p} \frac{b_{lq}\ b_{l'q}^*}{P_x}\ {P_x}^{l+l'-1}\ \gamma\left(l+l', PAPR_{[x]}\right) \\ & + 1 - e^{-PAPR_{[x]}}\left(PAPR_{[x]}+1\right)\Bigg]^{\frac{1}{2}}. \end{aligned} \tag{4.56}$$

This theorem provides an analytical EVM expression in the form of a series expansion involving Gamma functions and depending on different parameters. We can see that the in-band distortion of the amplified signal depends on the PA coefficients, PA order, and memory depth, as well as $PAPR_{[x]}$ and P_x, the PAPR and the average power of the signal $x(t)$.

4.7.1.2 With clipping

We now lead to the EVM calculation considering that the clipping is activated.

In this case, the squared magnitude error of an amplified signal can be expressed as follows

$$\left|\epsilon\right|^2 = \left|\sum_{q=0}^{Q}\sum_{l=1}^{L_p} b_{lq}\ \widetilde{x}_q\left|\widetilde{x}_q\right|^{2(l-1)} - x\right|^2. \tag{4.57}$$

In fact, the calculation of I_3 does not change after clipping. However, the integra-

tion of I_1 becomes as

$$\begin{aligned} I_1 =& \sum_{q=0}^{Q} \sum_{l,l'=1}^{L_p} b_{lq}\ b_{l'q}^{*} \Bigg(\int_0^A r_q^{2(l+l'-1)} \frac{2r_q}{P_x} e^{-\frac{{r_q}^2}{P_x}} dr_q \\ &+ A^{2(l+l'-1)} \int_A^{R_q} \frac{2r_q}{P_x} e^{-\frac{{r_q}^2}{P_x}} dr_q \Bigg) \\ =& \sum_{q=0}^{Q} \sum_{l,l'=1}^{L_p} b_{lq}\ b_{l'q}^{*} \Bigg({P_x}^{l+l'-1}\ \gamma\left(l+l', \lambda \mathrm{PAPR}_{[\widetilde{x}]}\right) \\ &+\ A^{2(l+l'-1)} \left(e^{-\lambda \mathrm{PAPR}_{[\widetilde{x}]}} - e^{-\mathrm{PAPR}_{[x]}}\right) \Bigg). \end{aligned} \tag{4.58}$$

Similarly, I_2 and I_4 are calculated as

$$\begin{aligned} I_2 =& -\sum_{l=1}^{L_p}\ b_{l1} \Bigg(P_x^l \gamma\left(l+1, \lambda \mathrm{PAPR}_{[\widetilde{x}]}\right) \\ &+ A^{2l-1}\sqrt{P_x} \left(\gamma\left(\frac{3}{2}, \mathrm{PAPR}_{[x]}\right) - \gamma\left(\frac{3}{2}, \lambda \mathrm{PAPR}_{[\widetilde{x}]}\right)\right) \Bigg), \end{aligned} \tag{4.59}$$

$$\begin{aligned} I_4 =& -\sum_{l=1}^{L_p}\ b_{l1}^{*} \Bigg(P_x^l \gamma\left(l+1, \lambda \mathrm{PAPR}_{[\widetilde{x}]}\right) \\ &+ A^{2l-1}\sqrt{P_x} \left(\gamma\left(\frac{3}{2}, \mathrm{PAPR}_{[x]}\right) - \gamma\left(\frac{3}{2}, \lambda \mathrm{PAPR}_{[\widetilde{x}]}\right)\right) \Bigg). \end{aligned} \tag{4.60}$$

Finally, compiling these integrals and using (2.22), the EVM expression of an amplified multicarrier signal, when clipping is activated, is given by the following theorem.

***Theorem* 12:** *The EVM of an amplified multicarrier signal, taking into account the memory effects, when clipping is activated, is expressed as follows*

$$\begin{aligned} EVM =& \Bigg[-\sum_{l=1}^{L_p} (b_{l1} + b_{l1}^{*}) \ \Bigg(P_x^{l-1}\ \gamma\left(l+1, \lambda PAPR_{[\widetilde{x}]}\right) \\ &+ \frac{A^{2l-1}}{\sqrt{P_x}} \left(\gamma\left(\frac{3}{2}, PAPR_{[x]}\right) - \gamma\left(\frac{3}{2}, \lambda PAPR_{[\widetilde{x}]}\right)\right) \Bigg) \\ &+ \sum_{q=0}^{Q} \sum_{l,l'=1}^{L_p} \frac{b_{lq}\ b_{l'q}^{*}}{P_x} \ \Bigg({P_x}^{l+l'-1}\ \gamma\left(l+l', \lambda PAPR_{[\widetilde{x}]}\right) \\ &+ A^{2(l+l'-1)} \left(e^{-\lambda PAPR_{[\widetilde{x}]}} - e^{-PAPR_{[x]}}\right) \Bigg) \\ &+\ 1 - e^{-PAPR_{[x]}} \left(PAPR_{[x]} + 1\right) \Bigg]^{\frac{1}{2}}. \end{aligned} \tag{4.61}$$

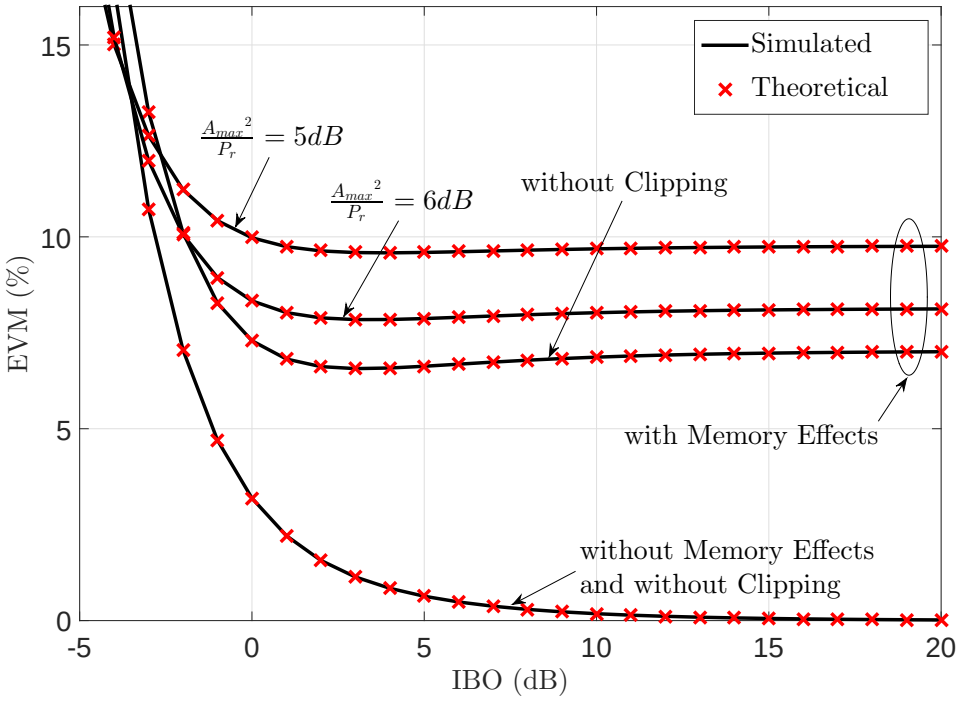

FIGURE 4.9 – Theoretical and simulated EVM as a function of the IBO, when clipping is activated or not, using memory and memoryless PA models with memory depth of 2 ($Q = 2$).

Eventually, as in the case without clipping, Theorem 12 gives an EVM expression in the form of a series expansion composed of Gamma functions depending on the same parameters. In addition, it now depends on $PAPR_{[\widetilde{x}]}$ the PAPR of the clipped signal $\widetilde{x}(t)$, as well as the clipping threshold A, and λ the ratio between $P_{\widetilde{x}}$ and P_x.

4.7.2 Simulation results and analysis

In this subsection, we present a comparison between the theoretical EVM expressions, given by Theorem 11 and Theorem 12, and the simulated EVM of amplified muticarrier signals, when clipping is activated or not. We use both memory and memoryless polynomial PA models, with memory depth of 2 ($Q = 2$). Note that each simulation considers 10^5 randomly generated OFDM symbols with 1024 sub-carriers associated to 16-QAM modulation symbols. The values of polynomial coefficients b_{lq}, in both cases, were taken from [D+04]. The theoretical and simulated EVM as a function of the Input power Back-Off (IBO), using memory and memoryless PA models, are shown in Fig. 4.9. As it is already stated te EVM formulas can be expressed as a function of the IBO, by replacing the average power by $\frac{P_{1dB,in}}{IBO}$ according to the IBO definition in (2.1). First, we can remark the significant difference between the EVM of the amplified signal using memory and memoryless PA models. This large difference is naturally due to the memory effects of the PA even within the expected linear region, which results in strong additional distortions. This prove that the memory effects are very severe, and cannot be ignored.

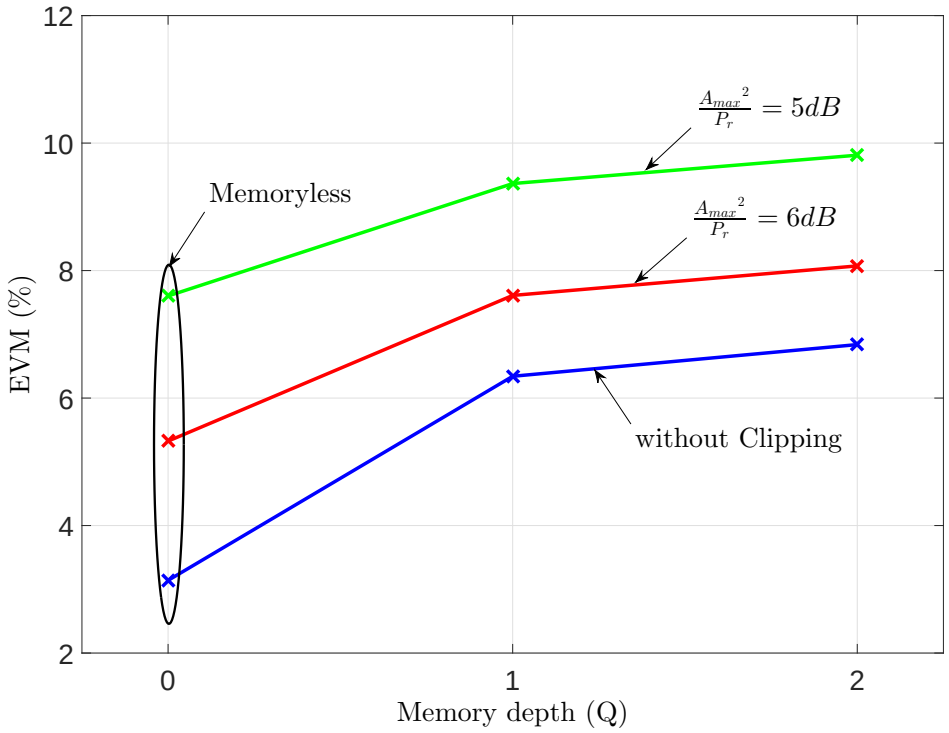

FIGURE 4.10 – EVM as a function of the memory depth when clipping is activated or not ($IBO = 10\ dB$).

Besides, we consider clipping thresholds $\frac{A^2}{P_x}$ of 5 and 6 dB. From the curves in Fig. 4.9, it is also verified that the EVM increases when the clipping threshold decreases as the case of memoryless PA model.

To quantify the amount of PA memory effects, the EVM of amplified multicarrier signals is plotted as a function of the memory depth, for an $IBO = 10\ dB$ and different clipping thresholds (Fig. 4.10). As expected, the more the memory depth of the memory polynomial model increases, the more the EVM increases. Therefore, we can remark that the memoryless polynomial model is not sufficient for modeling the PA when the memory effects are present. For example, when clipping is deactivated, the EVM of amplified signals using memoryless polynomial model is 2.5%. However, using memory polynomial model with memory depth of 2, the EVM increases to 6.8% which is quite significant. Once again, we show that the memory effects of the power amplifier can not be neglected.

4.8 Conclusion

In this chapter, the EVM expression of a multicarrier signal distorted by a polynomial PA model has been derived with or without the use of a clipping technique. Then, the impact of a polynomial predistortion on the EVM expressions has been investigated. The provided analytical expressions of the EVM are based on finite series expansions, and depend on the PA characteristics, the predistortion characteristics, as well as, the PAPR and the average power of both input and clipped signals. Simulation results compared to our proposed model confirm the accuracy

of our derived analytical expressions. Therefore it is no more necessary to realize a PA prototype to know if it respects the EVM standard. This analytical expression could be favorably integrated in simulation models to validate the PAs behavior. Moreover, the trade-off between the PA linearity and efficiency has been discussed. We showed that our theoretical EVM expressions are very useful for optimizing transmitter efficiency and linearity. Indeed, an analytical expression which gives the optimal IBO maximizing the PA efficiency with respect to any EVM constraint has been provided. Then, the complexity of the predistortion technique has been investigated aiming at reducing it. It is worthwhile to note that our proposed theoretical analyses could be very useful for optimizing future transmitter efficiency and linearity and the computational complexity of the predistortion technique. These analytical results are very interesting and could be applied in the field of broadcasting for the deployment of DVB-T2 transmitters as well as in LTE cellular networks. Next chapter will investigate out of band distortions, e.g. Adjacent Channel Power Ratio.

Chapter 5

Spectral analysis using polynomial PA model with and without memory effects

5.1 Introduction

In the last two chapters, we already quantified the in-band distortion of the power amplifier measured by the Error Vector Magnitude (EVM). In this chapter, we are involved in the theoretical study of the out-of-band distortion. Therefore, we are interested by the analytical derivation of the Probability Spectral Density (PSD) of the multicarrier signal. In particular, we first propose a generalization of the closed-form expression for PSD of the amplified multicarrier signal for any type of modulation. Then, as far as the memory effects are concerned, we derive the PSD expression with a memory polynomial PA model. Thereafter, we extend the study to the derivation of the PSD expression of the amplified multicarrier signal taking into account the predistortion technique. Consequently, thanks to our analytical expression we predict the spectral regrowth at the PA output which in turn causes ACI. This interference is characterised by the Adjacent Channel Power Ratio (ACPR), which is a commonly used figure-of-merit to describe linearity in modem telecommunication systems. Indeed, most of wireless communication standards such as LTE, DVB, CDMA, IEEE 802.11 and Bluetooth have already specified their requirements in terms of ACPR. Suppose now that one targets the maximum PA efficiency with respect to a specific ACPR constraint. Based on our expression, we can find the optimal operating point of PA and the optimal configuration of predistortion which maximize the PA efficiency and satisfy the ACPR requirements.

The remainder of this chapter is organized as follows. Next section presents the state of the art of the spectral regrowth of non-Linear amplified multicarrier signals. Then, we introduce our system model. Afterwards, the generalization of the PSD expression for any type of modulation is introduced. In addition, a novel PSD expression is derived taking into account the memory effects of the PA. Further, a theoretical derivation of the PSD of the PA output taking into account the predistortion technique is presented. Finally, the simulation results are discussed.

5.2 State of the art of the spectral regrowth of non-Linear amplified multicarrier signals

As far as theoretical PSD derivations are concerned, PSD of the PA output signal can be found in [GGS99, CP02, ZR] but assuming the input signal of the PA as a complex Gaussian random process. Considering the central limit theorem, this assumption is reasonable for OFDM signals with a large number of subcarriers, but it is not valid for all communication signals. On the other hand, some works like [Zho00, RZ04, RZ01] have calculated the PSD of amplified signals using higher order statistics of the signal but these methods can be extremely complicated as the polynomial order is high. Besides, another limitation of these works is that they assume the stationarity of the input signal which is usually not the case. Even if the sequence of source symbols is stationary, the signal after the shaping filter and modulation may be non stationary. Moreover, to the best of our knowledge, no analytical PSD expression taking into account the predistortion technique exists in literature.

This is for all these reasons, we use in our study the methodology presented in [BB99] which perfectly fits our problem. In fact, using this method, we can derive the spectrum of a signal whatever stationary, non stationary or cyclostationary and it avoids to make hypotheses on the source signals statistics. In addition, using this methodology the analytic expressions of the spectrum could be expressed as a function of the predistortion characteristic and the impulse response of shaping filter.

In [CWT08], a PSD expression of multicarrier signal, amplified by a memoryless PA, has been derived using the methodology in [BB99]. However, the presented closed-form expression does not take into account neither the PA memory effects nor the predistortion and it is only limited to phase modulation. In this study, we first propose a generalization of the closed-form expression for PSD of the amplified signal for any type of modulation. Then, we extend the study taking into account the memory effects of the PA. Thereafter, a novel derivation of the PSD expression of the amplified multicarrier signal taking into account the predistortion technique is done.

Thanks to our proposed expressions, we can find the optimal configuration of the predistortion and the optimal operating point of the PA which maximizes the PA efficiency and satisfying the adjacent channel interference constraint. Therefore, this work is an important step in the analytical study of the global optimization approach of the transmitter efficiency and linearity, and could be favorably integrated in simulation models to validate the PA behavior.

5.3 System model

5.3.1 Signal model

In general case, the mathemathical model of a modulated signal can be described as [BB99]

$$x(t) = \Re[\tilde{x}(t)e^{j(2\pi f_0 t+\theta_0)}] \tag{5.1}$$

with the complex envelope, $\tilde{x}(t)$, given by

$$\tilde{x}(t) = \sum_{n=-\infty}^{+\infty} h(t-nT) \sum_{p=1}^{N} B_{p,n} e^{j2\pi\Delta_{f_p} t} \tag{5.2}$$

where $\Delta_{f_N} = (p - 1 - \frac{N-1}{2})\Delta_f$ and $B_{p,n} = A_{p,n}e^{j\Phi_{p,n}}$. In (5.2), N is the number of carriers, p is the carrier index, n is the symbol index, Δ_f is the frequency shift between two successive carriers, f_0 is the central frequency, θ_0 is the initial phase of the central carrier, and $h(t)$ is the real impulse response of the shaping filter. Note that Δ_{fp} gives the position of the $p-th$ carrier with respect to the central frequency and $B_{p,n}$ is the n-th symbol on the p-th carrier (modulus $A_{p,n}$, phase $\Phi_{p,n}$).

5.3.2 Predistortion model

Predistortion is based on the following simple idea that the non-linearity of the PA may be counteracted by applying to the input signal a function H_{PD} which is exactly the inverse of the PA transfer function. With perfect predistortion, the whole chain is expected to present a linear response. The predistortion function can be expressed as a polynomial model and it is given by

$$H_{PD}(\tilde{x}(t)) = \sum_{k=0}^{K} a_{2k+1} |\tilde{x}(t)|^{2k} \tilde{x}(t) \tag{5.3}$$

with K being nonlinear model order and a_{2k+1} being the nonlinear polynomial coefficients.

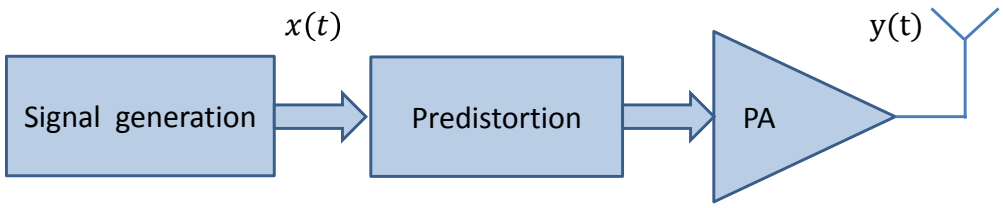

FIGURE 5.1 – Transmitter block diagram.

5.3.3 Nonlinear behavioral model of the power amplifier

In this chapter, we consider the Solid State Power Amplifier (SSPA) type for a mobile transmitter and assume that it is memoryless. The AM/AM (amplitude-to-amplitude) and the AM/PM (amplitude-to-phase) characteristics of the PA are represented by a Taylor's series of odd order [BB99]. Thus, the complex envelope function $H_{PA}(r)$ is given by

$$H_{PA}(\tilde{x}(t)) = \sum_{l=0}^{L} b_{2l+1} |x(t)|^{2l} x(t) \tag{5.4}$$

where L denotes the nonlinear model order and b_{2l+1} are the non linear PA characteristic coefficients.

5.3.4 ACPR definition

The Adjacent Chanel Power Ratio (ACPR) is one of the most popular and critical figure of merit used to characterize the undesirable spectral regrowth. Indeed, most of wireless communication standards such as LTE, DVB, CDMA, IEEE 802.11 and Bluetooth have already specified the maximal allowable amount of power in the adjacent-channels to mitigate the adjacent channel interference.

ACPR is defined by the ratio between the average power transmitted in the lateral bands compared to the power transmitted in the desired band and it is given by

$$\text{ACPR}(dB) = 10 \log \frac{\int_{f_{adj}} PSD(f)df}{\int_{f_{ch}} PSD(f)df}, \tag{5.5}$$

where $PSD(f)$ is the power spectral density of the transmitted signal. f_{ch} and f_{adj} specify the frequency bands of the main channel and of the adjacent channel respectively.

5.3.5 Method used to calculate the PSD

The method proposed in [BB99, pp. 36-41] to calculate the PSD of a signal $\tilde{y}$ consists in the following steps

- A two-dimensional power density function, $\Gamma(f_1, f_2) = E[\tilde{Y}(f_1)\tilde{Y}^*(f_2)]$, is first calculated where $\tilde{Y}(f) = \mathcal{F}(\tilde{y}(t))$. $()^*$ denotes the complex conjugate. Note that $\Gamma(f_1, f_2)$ is also the Fourier transform of the autocorrelation function $R(\tau_1, \tau_2) = E[\tilde{y}(\tau_1)\tilde{y}^*(\tau_2)]$.

- Then, $\Gamma(f_1, f_2)$ is written in the following form

$$\Gamma(f_1, f_2) = P_{\tilde{y}}(f)\delta(f_1 - f_2) + \Delta(f_1, f_2) \tag{5.6}$$

where $\Delta(f_1, f_2) = 0$ for $f_1 = f_2$ and the PSD of $\tilde{y}$ is given by $P_{\tilde{y}}(f)$.

5.4 Generalization of the PSD expression for any type of modulation

In [CWT08], an analytical expression of the power spectral density of the amplified multicarrier signal, $P_{\tilde{y}}$, is given by

$$\begin{aligned} P_{\tilde{y}}(f) = \frac{1}{T} \sum_{l,l'=0}^{L} & b_{2l+1} b_{2l'+1}^{*} \; l!\; l'!\; (l+1)!\; (l'+1)! \\ & \times \sum_{\substack{\alpha_1+\ldots+\alpha_N=l+1 \\ \alpha'_1+\ldots+\alpha'_N=l \\ \alpha_j,\alpha'_j\geq 0}} H_{2l+1}\left(f - \sum_{p=1}^{N} (\alpha_p - \alpha'_p)\Delta_{f_p}\right) \\ & \times \sum_{\substack{\beta_1+\ldots+\beta_N=l'+1 \\ \beta'_1+\ldots+\beta'_N=l' \\ \beta_j,\beta'_j\geq 0 \\ \beta_p-\beta'_p=\alpha_p-\alpha'_p}} H_{2l'+1}^{*}\left(f - \sum_{p=1}^{N} (\beta_p - \beta'_p)\Delta_{f_p}\right) \\ & \times \sum_{d=-\infty}^{+\infty} g(d)\; e^{-j2\pi dT\left(f-\sum_{p=1}^{N}(\beta_p-\beta'_p)\Delta_{f_p}\right)}, \end{aligned} \tag{5.7}$$

where

$$g(d) = E\left[\prod_{p=1}^{N} \frac{B_{p,n}^{\alpha_p} B_{p,n}^{*\alpha'_p} B_{p,n-d}^{\beta_p} B_{p,n-d}^{*\beta'_p}}{\alpha_p!\alpha'_p!\beta_p!\beta'_p!}\right], \tag{5.8}$$

and

$$\begin{aligned} H_{2k+1}(f) &= \mathcal{F}[h^{2k+1}(t)] \\ &= H(f) \text{ convoluted } 2k+1 \text{ times}, \end{aligned} \tag{5.9}$$

and $\mathcal{F}$ represents the Fourier transform operator. Note that the second sum (resp. the third sum) in (5.7) is taken over all combinations of nonnegative integer exponents α_1 and α'_1 (resp. β_1, β'_1) through α_N and α'_N (resp. β_N, β'_N) such that the sum of all α_i and α'_i (resp. β_i, β'_i) is $l+1$ and l respectively (resp. $l'+1$, l').

In [CWT08], $g(d)$ was simplified considering a phase modulation. In this specific case, we have constant modulus symbols i.e. $|B_{p,n}| = A$ for all (p,n). Given that the symbols are uncorrelated and zero mean, $g(d)$ can be written as (please refer to [CWT08] for more details)

$$g(d) = \begin{cases} \frac{A^{2(l+l'+1)}}{\prod_{p=1}^{N} \alpha_p!\alpha'_p!\beta_p!\beta'_p!} & \text{if } d = 0 \\ 0 & \text{otherwise.} \end{cases} \tag{5.10}$$

However, most modern commu nication standards use quadrature amplitude modulation which limits the utility of this expression. In the following we present a generalization of the PSD expression of the amplified signal so that it can be used for any types of modulation.

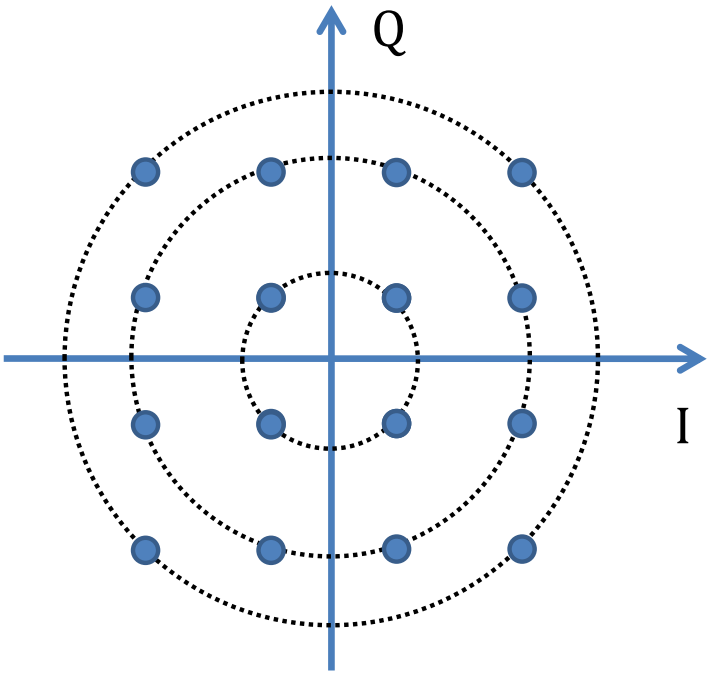

FIGURE 5.2 – 16-QAM modulation

We present the principle of the generalization by an example for 16-QAM. Fig. 5.2 represents a 16-QAM constellation. We can simply remark that a 16-QAM constellation is composed of three M-PSK constellations with different values of M and different amplitudes of A. Therefore, we have

$$g(0) = \prod_{p=1}^{N} \left[\frac{P_{r_1} {A_1}^{\psi} + P_{r_2} {A_2}^{\psi} + P_{r_3} {A_3}^{\psi}}{\alpha_p! \alpha'_p! \beta_p! \beta'_p!} \right] \tag{5.11}$$

where $\psi = \alpha_p + \alpha'_p + \beta_p + \beta'_p$, A_i are the amplitude of each PSK constellation, and P_{r_i} are the probability of having symbols from each PSK constellation. Thus, the general expression of $g(d)$ which is valid for any M-QAM is given by

$$g(d) = \begin{cases} \prod_{p=1}^{N} \left[\frac{\sum_{i=1}^{N_{psk}} P_{r_i} \ {A_i}^{\psi}}{\alpha_p! \alpha'_p! \beta_p! \beta'_p!} \right] & \text{if } d = 0 \\ 0 & \text{otherwise ,} \end{cases} \tag{5.12}$$

where N_{psk} is the number of PSK. Then, using (5.12), the PSD expression of the amplified multicarrier using any type of modulation can be expressed as

$$
\begin{aligned}
P_{\tilde{y}}(f) = \frac{1}{T} \sum_{l,l'=0}^{L} & b_{2l+1} b_{2l'+1}^{*}\ l!\ l'!\ (l+1)!\ (l'+1)! \\
& \times \sum_{\substack{\alpha_1+\ldots+\alpha_N=l+1 \\ \alpha'_1+\ldots+\alpha'_N=l \\ \alpha_j,\alpha'_j\geq 0}} \frac{H_{2l+1}\left(f-\sum_{p=1}^{N}(\alpha_p-\alpha'_p)\Delta_{f_p}\right)}{\prod_{p=1}^{N}\alpha_p!\alpha'_p!} \\
& \times \sum_{\substack{\beta_1+\ldots+\beta_N=l'+1 \\ \beta'_1+\ldots+\beta'_N=l' \\ \beta_j,\beta'_j\geq 0 \\ \beta_p-\beta'_p=\alpha_p-\alpha'_p}} \frac{H_{2l'+1}^{*}\left(f-\sum_{p=1}^{N}(\beta_p-\beta'_p)\Delta_{f_p}\right)}{\prod_{p=1}^{N}\beta_p!\beta'_p!} \\
& \times \prod_{p=1}^{N}\left[\sum_{i=1}^{Np} P_{p_i}\ {A_i}^{\psi}\right]
\end{aligned}
\tag{5.13}
$$

This closed-form expression for the PSD is valid for any linear modulation, which allows us to get some insight of the mechanisms of the spectral regrowth process at the output of the power amplifier. We can see that the PSD of the amplified signal depends on the PA characteristics and on the type of the shaping filter. In the following section, we assume that the predistortion is activated so that we will analytically evaluate the impact of the predistortion on the PSD of the signal.

5.5 Proposed analytical PSD expression taking into account the PA memory effects

In this section, we derive the PSD expression of the amplified multicarrier signals taking into account the memory effects of the PA. Thus, the memory polynomial PA model, presented in (2.21), is considered. From equations (2.21), and (5.2), the complex envelope of the output signal of the power amplifier when the memory effects are taken into account, can be written as

$$
\begin{aligned}
\tilde{y}(t) &= \sum_{q=0}^{Q}\sum_{l=0}^{L} b_{2l+1,q}|\tilde{x_q}(t)|^{2l}\tilde{x_q}(t) \\
&= \sum_{q=0}^{Q}\sum_{l=0}^{L} b_{2l+1,q}\left[\tilde{x}_q(t)\right]^{l+1}\left[\tilde{x}_q^{*}(t)\right]^{l} \\
&= \sum_{q=0}^{Q}\sum_{l=0}^{L} b_{2l+1,q}\left[\sum_{n=-\infty}^{+\infty} h(t-nT)\sum_{p=1}^{N} B_{p,n,q}e^{j2\pi\Delta_{f_p}t}\right]^{l+1} \\
&\quad \times \left[\sum_{n=-\infty}^{+\infty} h(t-nT)\sum_{p=1}^{N} B_{p,n,q}^{*}e^{j2\pi\Delta_{f_p}t}\right]^{l}.
\end{aligned}
\tag{5.14}
$$

In order to simplify the derivation, we assume that the duration of the impulse response of the shaping filter $h(t)$ is limited to $[-T/2; T/2]$. Under this condition the amplified signal can be expressed as

$$\begin{aligned}\tilde{y}(t) = &\sum_{q=0}^{Q}\sum_{l=0}^{L} b_{2l+1,q} \sum_{n=-\infty}^{+\infty} h^{2l+1}(t-nT) \\ &\times \left[\sum_{p=1}^{N} B_{p,n,q} e^{j2\pi\Delta_{f_p}t}\right]^{l+1} \left[\sum_{p=1}^{N} B^{*}_{p,n,q} e^{-j2\pi\Delta_{f_p}t}\right]^{l}. \end{aligned} \tag{5.15}$$

Applying the general Binomial formula, we get

$$\begin{aligned}\tilde{y}(t) = &\sum_{q=0}^{Q}\sum_{l=0}^{L} b_{2l+1,q} l!(l+1)! \sum_{n=-\infty}^{+\infty} h^{2l+1}(t-nT) \\ &\times \sum_{\substack{i_0+\ldots+i_L=l+1 \\ i_l\geq 0}} \left[\prod_{p=1}^{N} \frac{B^{i_p}_{p,n,q} e^{j2\pi i_p\Delta_{f_p}t}}{i_p!}\right] \sum_{\substack{i'_0+\ldots+i'_L=l \\ i'_l\geq 0}} \left[\prod_{p=1}^{N} \frac{B^{*}_{p,n,q} i'_p e^{-j2\pi i'_p\Delta_{f_p}t}}{i'_p!}\right], \\ = &\sum_{q=0}^{Q}\sum_{l=0}^{L} b_{2l+1,q} l!(l+1)! \sum_{n=-\infty}^{+\infty} h^{2l+1}(t-nT) \\ &\times \sum_{\substack{i_0+\ldots+i_L=l+1 \\ i'_0+\ldots+i'_L=l \\ i_l,i'_l\geq 0}} e^{j2\pi t\left(\sum_{p=1}^{N} i_p\Delta_{f_p} - i'_p\Delta_{f_p}\right)} \left[\prod_{p=1}^{N} \frac{B^{i_p}_{q,n} B^{*i'_p}_{q,n}}{i_p! i_p!}\right]. \end{aligned} \tag{5.16}$$

Then, the Fourier Transform of this signal at the output of the power amplifier is

$$\begin{aligned}\tilde{Y}(f) = &\sum_{q=0}^{Q}\sum_{l=0}^{L} b_{2l+1,q}\ l!\ (l+1)! \sum_{n=-\infty}^{+\infty} [H_{2l+1}(f) e^{-j2\pi fnT}] \\ &\otimes \mathcal{FFT}\left\{\sum_{\substack{i_0+\ldots+i_L=l+1 \\ i'_0+\ldots+i'_L=l \\ i_l,i'_l\geq 0}} e^{j2\pi t\left(\sum_{p=1}^{N} i_p\Delta_{f_p} - i'_p\Delta_{f_p}\right)} \left[\prod_{p=1}^{N} \frac{B^{i_p}_{p,n,q} B^{*i'_p}_{p,n,q}}{i_p! i_p!}\right]\right\}, \end{aligned} \tag{5.17}$$

where

$$\begin{aligned} H_{2l+1}(f) &= \mathcal{F}[h^{2l+1}(t)] \\ &= H(f) \text{ convoluted } 2l+1 \text{ times}, \end{aligned} \tag{5.18}$$

and $\mathcal{F}$ represents the Fourier transform operator. Thereafter, developing the second term of the convolution product, we obtain

$$\tilde{Y}(f) = \sum_{q=0}^{Q}\sum_{l=0}^{L} b_{2l+1,q}\ l!\ (l+1)! \sum_{n=-\infty}^{+\infty} H_{2l+1}(f)e^{-j2\pi fnT} \otimes \sum_{\substack{i_0+\ldots+i_L=l+1 \\ i'_0+\ldots+i'_L=l \\ i_l,i'_l\geq 0}} \left[\prod_{p=1}^{N} \frac{B_{p,n,q}^{i_p} B_{p,n,q}^{*i'_p}}{i_p! i_p!}\right] \delta\left(f - \sum_{p=1}^{N}(i_p - i'_p)\Delta_{f_p}\right). \tag{5.19}$$

We can simplify the convolution and we have:

$$\begin{aligned}\tilde{Y}(f) = & \sum_{q=0}^{Q}\sum_{l=0}^{L} b_{2l+1,q}\ l!\ (l+1)! \\ & \times \sum_{n=-\infty}^{+\infty} \sum_{\substack{i_0+\ldots+i_L=l+1 \\ i'_0+\ldots+i'_L=l \\ i_l,i'_l\geq 0}} \left[\prod_{p=1}^{N} \frac{B_{p,n,q}^{i_p} B_{p,n,q}^{*i'_p}}{i_p! i_p!}\right] \\ & \times H_{2l+1}\left(f - \sum_{p=1}^{N}(i_p - i'_p)\Delta_{f_p}\right) e^{-j2\pi nT\left(f - \sum_{p=1}^{N}(i_p - i'_p)\Delta_{f_p}\right)}.\end{aligned} \tag{5.20}$$

Then we can calculate the two-dimensional power density function defined as:

$$\begin{aligned}\Gamma(f_1, f_2) &= E[\tilde{Y}(f_1)\tilde{Y}^*(f_2)] \\ &= \sum_{q,q'=0}^{Q}\sum_{l,l'=0}^{L} b_{2l+1,q} b^*_{2l'+1,q'}\ l!\ (l+1)!\ l'!\ (l'+1)! \sum_{n,n'=-\infty}^{+\infty} \\ &\quad \times \sum_{\substack{i_0+\ldots+i_L=l+1 \\ i'_0+\ldots+i'_L=l \\ i_l,i'_l\geq 0}} \sum_{\substack{u_0+\ldots+u_L=l'+1 \\ u'_0+\ldots+u'_L=l' \\ u_l,u'_l\geq 0}} E\left[\prod_{p,p'=1}^{N} \frac{B_{p,n,q}^{i_p} B_{p,n,q}^{*i'_p} B_{p',n',q'}^{u_p} B_{p',n',q'}^{*u'_p}}{i_p! i'_p! u_p! u'_p!}\right] \\ &\quad \times H_{2l+1}\left(f_1 - \sum_{p=1}^{N}(i_p - i'_p)\Delta_{f_p}\right) e^{-j2\pi nT\left(f_1 - \sum_{p=1}^{N}(i_p - i'_p)\Delta_{f_p}\right)} \\ &\quad \times H^*_{2l'+1}\left(f_2 - \sum_{p=1}^{N}(u_p - u'_p)\Delta_{f_p}\right) e^{-j2\pi nT\left(f_2 - \sum_{p=1}^{N}(u_p - u'_p)\Delta_{f_p}\right)}.\end{aligned} \tag{5.21}$$

Setting $n' = n - d$, and let us denote the expected value term of (5.21) by $g(d)$, we get

$$\Gamma(f_1,f_2)=\sum_{q,q'=0}^{Q}\sum_{l,l'=0}^{L} b_{2l+1,q}b^{*}_{2l'+1,q'}\; l!\;(l+1)!\;l'!\;(l'+1)!\sum_{\substack{i_0+\ldots+i_L=l+1\\ i'_0+\ldots+i'_L=l\\ i_l,i'_l\geq 0}}\;\sum_{\substack{u_0+\ldots+u_L=l'+1\\ u'_0+\ldots+u'_L=l'\\ u_l,u'_l\geq 0}}$$
$$\times H_{2l+1}\left(f_1-\sum_{p=1}^{N}(i_p-i'_p)\Delta_{f_p}\right)H^{*}_{2l'+1}\left(f_2-\sum_{p=1}^{N}(u_p-u'_p)\Delta_{f_p}\right)$$
$$\times\sum_{d=-\infty}^{+\infty} g(d)e^{-j2\pi dT\left(f_2-\sum_{p=1}^{N}(u_p-u'_p)\Delta_{f_p}\right)}$$
$$\times\sum_{n=-\infty}^{+\infty} e^{-j2\pi nT\left(f_1-f_2-\sum_{p=1}^{N}(i_p-i'_p-u_p+u'_p)\Delta_{f_p}\right)}. \tag{5.22}$$

Then, using the following property, (5.22) can then be written as (5.24).

$$\sum_{n=-\infty}^{+\infty} e^{-j2\pi fnT}=\frac{1}{T}\sum_{n=-\infty}^{+\infty}\delta(f-\frac{n}{T}) \tag{5.23}$$

$$\Gamma(f_1,f_2)=\frac{1}{T}\sum_{q,q'=0}^{Q}\sum_{l,l'=0}^{L} b_{2l+1,q}b^{*}_{2l'+1,q'}\; l!\;(l+1)!\;l'!\;(l'+1)!$$
$$\times\sum_{\substack{i_0+\ldots+i_L=l+1\\ i'_0+\ldots+i'_L=l\\ i_l,i'_l\geq 0}} H_{2l+1}\left(f_1-\sum_{p=1}^{N}(i_p-i'_p)\Delta_{f_p}\right)$$
$$\times\sum_{\substack{u_0+\ldots+u_L=l'+1\\ u'_0+\ldots+u'_L=l'\\ u_l,u'_l\geq 0}} H^{*}_{2l'+1}\left(f_2-\sum_{p=1}^{N}(u_p-u'_p)\Delta_{f_p}\right)$$
$$\times\sum_{d=-\infty}^{+\infty} g(d)e^{-j2\pi dT\left(f_2-\sum_{p=1}^{N}(u_p-u'_p)\Delta_{f_p}\right)}$$
$$\times\sum_{n=-\infty}^{+\infty}\delta\left(f_1-f_2-\sum_{p=1}^{N}(i_p-i'_p-u_p+u'_p)\Delta_{f_p}-\frac{n}{T}\right). \tag{5.24}$$

Finally, if $n=0$ and $i_p-i'_p=u_p-u'_p\;\forall p\in[1,N]$, and using (5.12) we get the PSD expression which is presented in the next Theorem 13.

***Theorem* 13:** *The PSD of an amplified multicarrier signal for any type of modulation, taking into account the memory effects, is expressed as follows*

$$
\begin{aligned}
P_{\tilde{y}}(f) = \frac{1}{T} \sum_{q,q'=0}^{Q} \sum_{l,l'=0}^{L} & b_{2l+1,q} b^{*}_{2l'+1,q'} \; l! \; (l+1)! \; l'! \; (l'+1)! \\
& \sum_{\substack{i_0+\ldots+i_L=l+1 \\ i'_0+\ldots+i'_L=l \\ i_l, i'_l \geq 0}} H_{2l+1} \left(f - \sum_{p=1}^{N} (i_p - i'_p) \Delta_{f_p} \right) \\
& \times \sum_{\substack{u_0+\ldots+u_L=l'+1 \\ u'_0+\ldots+u'_L=l' \\ u_l, u'_l \geq 0}} H^{*}_{2l'+1} \left(f - \sum_{p=1}^{N} (u_p - u'_p) \Delta_{f_p} \right) \\
& \times \sum_{d=-\infty}^{+\infty} g(d) e^{-j2\pi dT \left(f - \sum_{p=1}^{N} (u_p - u'_p) \Delta_{f_p} \right)} \\
& \times \prod_{p=1}^{N} \left[\frac{\sum_{\alpha=1}^{N_{psk}} P_{r\alpha} \; {A_\alpha}^{i_p + i'_p + u_p + u'_p}}{i_p! i'_p! u_p! u'_p!} \right] .
\end{aligned}
\tag{5.25}
$$

where Q is the memory depth, N_{psk} is the number of PSK, A_α are the amplitude of each PSK constellation, and P_{r_α} are the probability of having symbols from each PSK constellation.

Eventually, we obtain a closed-form expression for the PSD of the amplified multicarrier signal when the predistortion is activated. This analytical expression is also valid for any linear modulation and allows us to predict the spectral regrowth at the PA output. We can see that the PSD of the predistorted non-linear amplified signal depends on the PA and predistortion characteristics as well as the type of the shaping filter.

5.6 Proposed analytical PSD expression when predistortion is activated

In this section, we derive the PSD expression of the predistorted nonlinear amplified multicarrier signals. From equations (5.2), (5.3) and (5.4), the complex

envelope of the output signal of the power amplifier can be written as

$$\begin{aligned}\tilde{y}(t) &= \sum_{l=0}^{L} b_{2l+1} \left| \sum_{k=0}^{K} a_{2k+1} |\tilde{x}(t)|^{2k} \tilde{x}(t) \right|^{2l} \\ &\quad \times \left[\sum_{k=0}^{K} a_{2k+1} |\tilde{x}(t)|^{2k} \tilde{x}(t) \right] \\ &= \sum_{l=0}^{L} b_{2l+1} \left[\sum_{k=0}^{K} a_{2k+1} \left[\tilde{x}(t)\right]^{k+1} \left[\tilde{x}^*(t)\right]^{k} \right]^{l+1} \\ &\quad \times \left[\sum_{k=0}^{K} {a^*}_{2k+1} \left[\tilde{x}(t)\right]^{k} \left[\tilde{x}^*(t)\right]^{k+1} \right]^{l}. \end{aligned} \tag{5.26}$$

Using the general multinomial theorem (see Appendix A), (5.26) can be written as

$$\begin{aligned}\tilde{y}(t) =& \sum_{l=0}^{L} b_{2l+1}\ l\ !\ (l+1)! \\ & \times \sum_{\substack{i_0+\ldots+i_K=l+1 \\ i_k \geq 0}} \left[\prod_{k=0}^{K} \frac{a_{2k+1}^{i_k}}{i_k!} \left[\tilde{x}(t)\right]^{(k+1)i_k} \left[\tilde{x}^*(t)\right]^{ki_k} \right] \\ & \times \sum_{\substack{i'_0+\ldots+i'_K=l \\ i'_k \geq 0}} \left[\prod_{k=0}^{K} \frac{{a^*}_{2k+1}^{i'_k}}{i'_k!} \left[\tilde{x}(t)\right]^{ki'_k} \left[\tilde{x}^*(t)\right]^{(k+1)i'_k} \right] \\ =& \sum_{l=0}^{L} b_{2l+1}\ l\ !\ (l+1)! \\ & \times \sum_{\substack{i_0+\ldots+i_K=l+1 \\ i'_0+\ldots+i'_K=l \\ i_k, i'_k \geq 0}} \left[\prod_{k=0}^{K} \frac{a_{2k+1}^{i_k} {a^*}_{2k+1}^{i'_k}}{i_k! i'_k!} \right] \left[\tilde{x}(t)\right]^{m} \left[\tilde{x}^*(t)\right]^{q}, \end{aligned} \tag{5.27}$$

where

$$m = \sum_{k=0}^{K} (k+1) i_k + k i'_k \tag{5.28}$$

$$q = \sum_{k=0}^{K} k i_k + (k+1) i'_k, \tag{5.29}$$

and

$$\begin{aligned}\left[\tilde{x}(t)\right]^{m} \left[\tilde{x}^*(t)\right]^{q} =& \left[\sum_{n=-\infty}^{+\infty} h(t-nT) \sum_{p=1}^{N} B_{p,n} e^{j2\pi\Delta_{f_p} t} \right]^{m} \\ & \times \left[\sum_{n=-\infty}^{+\infty} h(t-nT) \sum_{p=1}^{N} {B^*}_{p,n} e^{-j2\pi\Delta_{f_p} t} \right]^{q}. \end{aligned} \tag{5.30}$$

In order to simplify the derivation, we assume that the duration of the impulse response of the shaping filter $h(t)$ is limited to $[-T/2, T/2]$. Under this condition and using the general multinomial theorem (see Appendix A), the term $[\tilde{x}(t)]^m\,[\tilde{x}^*(t)]^q$ in (5.27) can be expressed as

$$\begin{aligned}
[\tilde{x}(t)]^m\,[\tilde{x}^*(t)]^q &= m!\;q! \sum_{n=-\infty}^{+\infty} h^{m+q}(t-nT) \\
&\quad \times \sum_{\substack{s_1+\ldots+s_N=m \\ s'_1+\ldots+s'_N=q \\ s_p,s'_{p'}\geq 0}} \left[\prod_{p=1}^{N} \frac{B_{p,n}^{s_p} B_{p,n}^{*s'_p} e^{j2\pi(s_p\Delta_{f_p}-s'_p\Delta_{f_p})t}}{s_p!s'_p!}\right] \\
&= m!\;q! \sum_{n=-\infty}^{+\infty} h^{m+q}(t-nT) \\
&\quad \times \sum_{\substack{s_1+\ldots+s_N=m \\ s'_1+\ldots+s'_N=q \\ s_p,{s_p}'\geq 0}} e^{j2\pi t\left(\sum_{p=1}^{N} s_p\Delta_{f_p}-s'_p\Delta_{f_p}\right)} \left[\prod_{p=1}^{N} \frac{B_{p,n}^{s_p} B_{p,n}^{*s'_p}}{s_p!{s'}_p!}\right]. \qquad (5.31)
\end{aligned}$$

Substituting (5.31) into (5.27), we obtain

$$\begin{aligned}
\tilde{y}(t) &= \sum_{l=0}^{L} b_{2l+1}\;l\;!\;(l+1)! \\
&\quad \times \sum_{\substack{i_0+\ldots+i_K=l+1 \\ i'_0+\ldots+i'_K=l \\ i_k,i'_k\geq 0}} \left[\prod_{k=0}^{K} \frac{a_{2k+1}^{i_k} {a^*}_{2k+1}^{i'_k}}{i_k!i'_k!}\right]\; m!\;q! \sum_{n=-\infty}^{+\infty} h^{m+q}(t-nT) \\
&\quad \times \sum_{\substack{s_1+\ldots+s_N=m \\ s'_1+\ldots+s'_N=q \\ s_p,{s_p}'\geq 0}} e^{j2\pi t\left(\sum_{p=1}^{N} s_p\Delta_{f_p}-s'_p\Delta_{f_p}\right)} \left[\prod_{p=1}^{N} \frac{B_{p,n}^{s_p} B_{p,n}^{*s'_p}}{s_p!{s'}_p!}\right] \qquad (5.32)
\end{aligned}$$

Then, the Fourier Transform of this signal at the output of the power amplifier is

$$\begin{aligned}
\tilde{Y}(f) &= \sum_{l=0}^{L} b_{2l+1}\;l\;!\;(l+1)! \sum_{\substack{i_0+\ldots+i_K=l+1 \\ i'_0+\ldots+i'_K=l \\ i_k,i'_k\geq 0}} \left[\prod_{k=0}^{K} \frac{a_{2k+1}^{i_k} {a^*}_{2k+1}^{i'_k}}{i_k!i'_k!}\right] \\
&\quad \times m!\;q! \sum_{n=-\infty}^{+\infty} H_{m+q}(f) e^{-j2\pi fnT} \\
&\quad \otimes \mathcal{F}\left\{\sum_{\substack{s_1+\ldots+s_N=m \\ s'_1+\ldots+s'_N=q \\ s_p,{s_p}'\geq 0}} e^{j2\pi t\left(\sum_{p=1}^{N}(s_p-s'_p)\Delta_{f_p}\right)} \left[\prod_{p=1}^{N} \frac{B_{p,n}^{s_p} B_{p,n}^{*s'_p}}{s_p!{s'}_p!}\right]\right\} \qquad (5.33)
\end{aligned}$$

where

$$\begin{aligned} H_{m+q}(f) &= \mathcal{F}[h^{m+q}(t)] \\ &= H(f)\text{convoluted } m+q \text{ times} \end{aligned} \tag{5.34}$$

and $\mathcal{F}$ represents the Fourier transform operator. Thereafter, developing the second term of the convolution product, we obtain

$$\begin{aligned} \tilde{Y}(f) = & \sum_{l=0}^{L} b_{2l+1}\ l\ !\ (l+1)! \sum_{\substack{i_0+\ldots+i_K=l+1 \\ i'_0+\ldots+i'_K=l \\ i_k,i'_k\geq 0}} \left[\prod_{k=0}^{K} \frac{a_{2k+1}^{i_k} a^{*i'_k}_{2k+1}}{i_k! i'_k!}\right] \\ & \times q!m! \sum_{n=-\infty}^{+\infty} H_{m+q}(f)\ e^{-j2\pi fnT} \otimes \sum_{\substack{s_1+\ldots+s_N=m \\ s'_1+\ldots+s'_N=q \\ s_p,{s_p}'\geq 0}} \left[\prod_{p=1}^{N} \frac{B_{p,n}^{s_p} B_{p,n}^{*{s'}_p}}{s_p! {s'}_p!}\right] \\ & \times \delta\left(f - \sum_{p=1}^{N} (s_p - s'_p)\Delta_{f_p}\right) \end{aligned} \tag{5.35}$$

The convolution product of this expression can be simplified as follows

$$\begin{aligned} \tilde{Y}(f) = & \sum_{l=0}^{L} b_{2l+1}\ l\ !\ (l+1)! \sum_{\substack{i_0+\ldots+i_K=l+1 \\ i'_0+\ldots+i'_K=l \\ i_k,i'_k\geq 0}} \left[\prod_{k=0}^{K} \frac{a_{2k+1}^{i_k} a^{*i'_k}_{2k+1}}{i_k! i'_k!}\right] \\ & \times\ q!m! \sum_{n=-\infty}^{+\infty} \sum_{\substack{s_1+\ldots+s_N=m \\ s'_1+\ldots+s'_N=q \\ s_p,{s_p}'\geq 0}} e^{-j2\pi nT\left(f-\sum_{p=1}^{N}(s_p-s'_p)\Delta_{f_p}\right)} \\ & \times \left[\prod_{p=1}^{N} \frac{B_{p,n}^{s_p} B_{p,n}^{*{s'}_p}}{s_p! {s'}_p!}\right] H_{m+q}\left(f - \sum_{p=1}^{N} (s_p - s'_p)\Delta_{f_p}\right) \end{aligned} \tag{5.36}$$

Then, we calculate the two-dimensional power density function defined as

$$
\begin{aligned}
\Gamma(f_1,f_2) &= E[\tilde{Y}(f_1)\tilde{Y}^*(f_2)] \\
&= \sum_{l,l'=0}^{L} b_{2l+1}\; b^*_{2l+1}\; l\,!\;(l+1)!\;l'\,!\;(l'+1)! \\
&\quad\times \sum_{\substack{i_0+\ldots+i_K=l+1\\ i'_0+\ldots+i'_K=l\\ i_k,i'_k\geq 0}} \left[\prod_{k=0}^{K} \frac{a_{2k+1}^{i_k} {a^*}_{2k+1}^{i'_k}}{i_k!\,i'_k!}\right]\; m!\;q! \\
&\quad\times \sum_{n=-\infty}^{+\infty} \sum_{\substack{s_1+\ldots+s_N=m\\ s'_1+\ldots+s'_N=q\\ s_p,{s_p}'\geq 0}} e^{-j2\pi nT\left(f_1-\sum_{p=1}^{N}\beta_{s_p}\Delta_{f_p}\right)} \\
&\quad\times H_{m+q}\left(f_1-\sum_{p=1}^{N}\beta_{s_p}\Delta_{f_p}\right) \sum_{\substack{u_0+\ldots+u_K=l'+1\\ u'_0+\ldots+u'_K=l'\\ u_k,u'_k\geq 0}} \left[\prod_{k=0}^{K} \frac{{a^*}_{2k+1}^{u_k} a_{2k+1}^{u'_k}}{u_k!u'_k!}\right] \\
&\quad\times m'!\;q'! \sum_{n'=-\infty}^{+\infty} \sum_{\substack{v_1+\ldots+v_N=m'\\ v'_1+\ldots+v'_N=q'\\ v_p,{v_p}'\geq 0}} e^{+j2\pi n'T\left(f_2-\sum_{p=1}^{N}\beta_{v_p}\Delta_{f_p}\right)} \\
&\quad\times H^*_{m'+q'}\left(f_2-\sum_{p=1}^{N}\beta_{v_p}\Delta_{f_p}\right)\; E\left[\prod_{p=1}^{N} \frac{B_{p,n}^{s_p} B_{p,n^{'}}^{*{s'}_p} B_{p,n'}^{v_p} B_{p,n'}^{*{v'}_p}}{s_p!{s'}_p!v_p!{v'}_p!}\right]
\end{aligned}
\tag{5.37}
$$

where $\beta_{s_p} = s_p - s'_p$ and $\beta_{v_p} = v_p - v'_p$. Setting $n' = n - d$, and let us denote the expected value term of (5.37) by $g(d)$.

$$
\begin{aligned}
\Gamma(f_1, f_2) = & \sum_{l,l'=0}^{L} b_{2l+1}\ b^*_{2l+1}\ l\ !\ (l+1)!\ l'\ !\ (l'+1)! \\
& \times \sum_{\substack{i_0+\ldots+i_K=l+1 \\ i'_0+\ldots+i'_K=l \\ i_k, i'_k \geq 0}} \left[\prod_{k=0}^{K} \frac{a_{2k+1}^{i_k} a^{*\,i'_k}_{2k+1}}{i_k! i'_k!} \right] m!\ q! \\
& \times \sum_{\substack{s_1+\ldots+s_N=m \\ s'_1+\ldots+s'_N=q \\ s_p, {s_p}' \geq 0}} H_{m+q} \left(f_1 - \sum_{p=1}^{N} \beta_{s_p} \Delta_{f_p} \right) \\
& \times \sum_{\substack{u_0+\ldots+u_K=l'+1 \\ u'_0+\ldots+u'_K=l' \\ u_k, u'_k \geq 0}} \left[\prod_{k=0}^{K} \frac{a^{*u_k}_{2k+1} a^{u'_k}_{2k+1}}{u_k! u'_k!} \right] m'!\ q'! \\
& \times \sum_{\substack{v_1+\ldots+v_N=m' \\ v'_1+\ldots+v'_N=q' \\ v_p, {v_p}' \geq 0}} H^*_{m'+q'} \left(f_2 - \sum_{p=1}^{N} \beta_{v_p} \Delta_{f_p} \right) \\
& \times \sum_{d=-\infty}^{+\infty} g(d) e^{-j2\pi dT \left(f_2 - \sum_{p=1}^{N} \beta_{v_p} \Delta_{f_p} \right)} \\
& \times \sum_{n=-\infty}^{+\infty} e^{-j2\pi nT \left(f_1 - f_2 - \sum_{p=1}^{N} \left(\beta_{s_p} - \beta_{v_p} \right) \Delta_{f_p} \right)}
\end{aligned}
\tag{5.38}
$$

Then, using the following property, (5.38) can then be written as (5.40).

$$
\sum_{n=-\infty}^{+\infty} e^{-j2\pi fnT} = \frac{1}{T} \sum_{n=-\infty}^{+\infty} \delta(f - \frac{n}{T}) \tag{5.39}
$$

$$\Gamma(f_1,f_2) = \frac{1}{T}\sum_{l,l'=0}^{L} b_{2l+1}\; b^*_{2l+1}\; l\;!\;(l+1)!\;l'\;!\;(l'+1)!$$
$$\times \sum_{\substack{i_0+\ldots+i_K=l+1\\ i'_0+\ldots+i'_K=l\\ i_k,i'_k\geq 0}} \left[\prod_{k=0}^{K} \frac{a_{2k+1}^{i_k} {a^*}_{2k+1}^{i'_k}}{i_k! i'_k!}\right]\; m!\;q!$$
$$\times \sum_{\substack{s_1+\ldots+s_N=m\\ s'_1+\ldots+s'_N=q\\ s_p,{s_p}'\geq 0}} H_{m+q}\left(f_1-\sum_{p=1}^{N}\beta_{s_p}\Delta_{f_p}\right)$$
$$\times \sum_{\substack{u_0+\ldots+u_K=l'+1\\ u'_0+\ldots+u'_K=l'\\ u_k,u'_k\geq 0}} \left[\prod_{k=0}^{K} \frac{{a^*}_{2k+1}^{u_k} a_{2k+1}^{u'_k}}{u_k! u'_k!}\right] m'!\;q'!$$
$$\times \sum_{\substack{v_1+\ldots+v_N=m'\\ v'_1+\ldots+v'_N=q'\\ v_p,{v_p}'\geq 0}} H^*_{m'+q'}\left(f_2-\sum_{p=1}^{N}\beta_{v_p}\Delta_{f_p}\right)$$
$$\times \sum_{d=-\infty}^{+\infty} g(d)\; e^{-j2\pi dT\left(f_2-\sum_{p=1}^{N}\beta_{v_p}\Delta_{f_p}\right)}$$
$$\times \sum_{n=-\infty}^{+\infty} \delta\left(f_1-f_2-\sum_{p=1}^{N}\left(\beta_{s_p}-\beta_{v_p}\right)\Delta_{f_p}-\frac{n}{T}\right) \qquad (5.40)$$

Finally, if $n=0$ and $\beta_{s_p}=\beta_{v_p}\;\forall p\in[1,N]$, and using (5.12) we obtain the PSD expression and it is given by the next Theorem.

***Theorem* 14:** *The PSD expression of an amplified signal for any type of*

modulation, when predistortion is activated, is expressed as follows

$$
\begin{aligned}
P_{\tilde{y}}(f) =& \frac{1}{T} \sum_{l,l'=0}^{L} b_{2l+1}\ b^{*}_{2l+1}\ l\ !\ (l+1)!\ l'\ !\ (l'+1)! \\
&\times \sum_{\substack{i_0+\ldots+i_K=l+1 \\ i'_0+\ldots+i'_K=l \\ i_k,i'_k\geq 0}} \left[\prod_{k=0}^{K} \frac{a_{2k+1}^{i_k} {a^{*}}_{2k+1}^{i'_k}}{i_k! i'_k!} \right] m!\ q! \\
&\times \sum_{\substack{s_1+\ldots+s_N=m \\ s'_1+\ldots+s'_N=q \\ s_p,{s_p}'\geq 0}} H_{m+q} \left(f - \sum_{p=1}^{N} \beta_{s_p} \Delta_{f_p} \right) \\
&\times \sum_{\substack{u_0+\ldots+u_K=l'+1 \\ u'_0+\ldots+u'_K=l' \\ u_k,u'_k\geq 0}} \left[\prod_{k=0}^{K} \frac{{a^{*}}_{2k+1}^{u_k} a_{2k+1}^{u'_k}}{u_k! u'_k!} \right] m'!\ q'! \\
&\times \sum_{\substack{v_1+\ldots+v_N=m' \\ v'_1+\ldots+v'_N=q' \\ v_p,{v_p}'\geq 0 \\ \beta_{s_p}=\beta_{v_p}}} H^{*}_{m'+q'} \left(f - \sum_{p=1}^{N} \beta_{v_p} \Delta_{f_p} \right) \\
&\times \prod_{p=1}^{N} \left[\frac{\sum_{\alpha=1}^{N_{psk}} P_{r\alpha}\ {A_\alpha}^{s_p+{s'}_p+v_p+{v'}_p}}{s_p! {s'}_p! v_p! {v'}_p!} \right]
\end{aligned}
\tag{5.41}
$$

where N_{psk} is the number of PSK, A_α are the amplitude of each PSK constellation, and P_{r_α} are the probability of having symbols from each PSK constellation.

Eventually, we obtain a closed-form expression for the PSD of the amplified multicarrier signal when the predistortion is activated. This analytical expression is also valid for any linear modulation and allows us to predict the spectral regrowth at the PA output. We can see that the PSD of the predistorted non-linear amplified signal depends on the PA and predistortion characteristics as well as the type of the shaping filter.

5.7 Simulation Results and Analysis

This section presents a comparison between the theoretical PSD, given by (5.13) and (5.41), and the simulated PSD. Note that each simulation considers 10^5 randomly generated OFDM symbols with 1024 sub-carriers associated to 16-QAM modulation. Note that a third order polynomial is used to fit the behavior of an actual PA (class AB). Furthermore, the rectangular pulse is chosen as baseband pulse shaping filter. Note that the averaged periodogram algorithm is used as PSD estimation reference for amplified signals. For the clarity of the representation, the maximum value of each PSD is normalized to 0 dB. In a first step, simulations are led with 10^6 samples of QPSK and 16-QAM modulated signals with $N = 5$, and symbol rate equal to $Fb = 1/T = 3.84Ms/second$. The Input power Back-Off (IBO) is 4 dB.

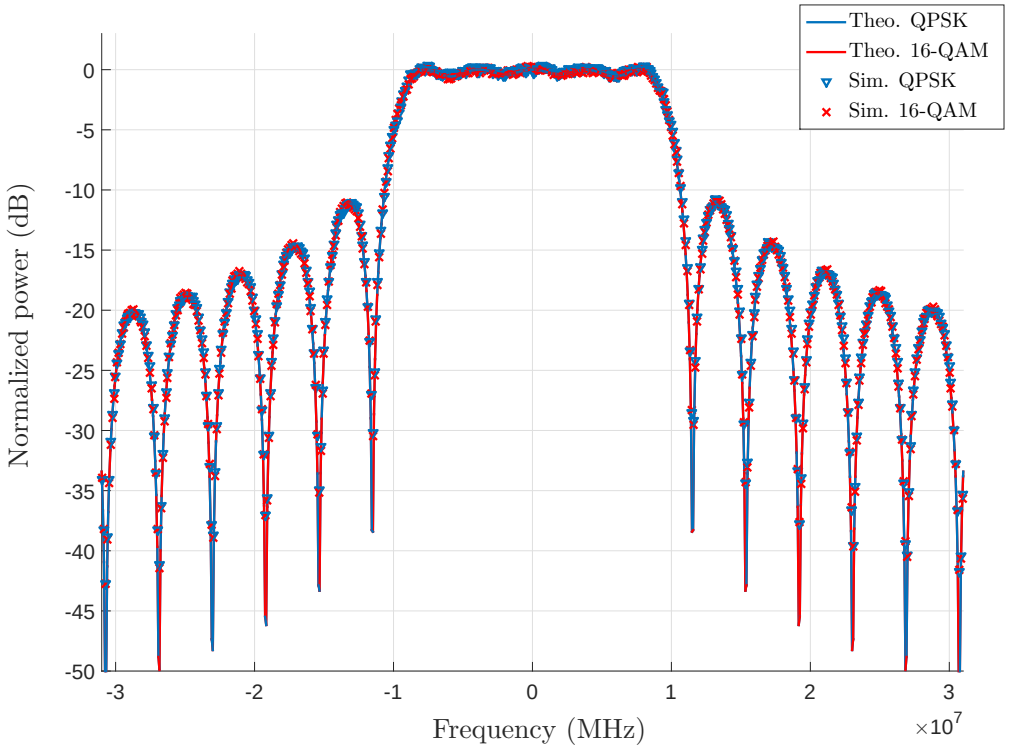

FIGURE 5.3 – PSD of amplified QPSK and 16-QAM modulated signals using rectangular pulse shaping filter with $IBO = 4\ dB$ and $N = 5$.

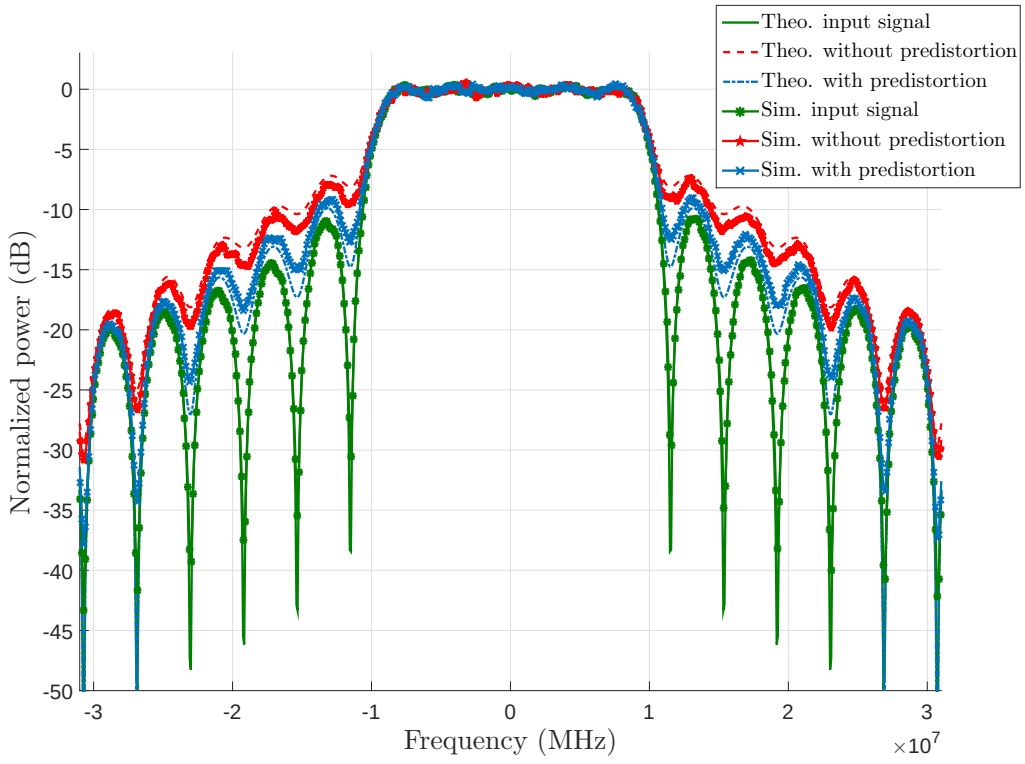

FIGURE 5.4 – PSD of amplified 16-QAM modulated signals with and without predistortion with $IBO = 1\ dB$ and $N = 5$.

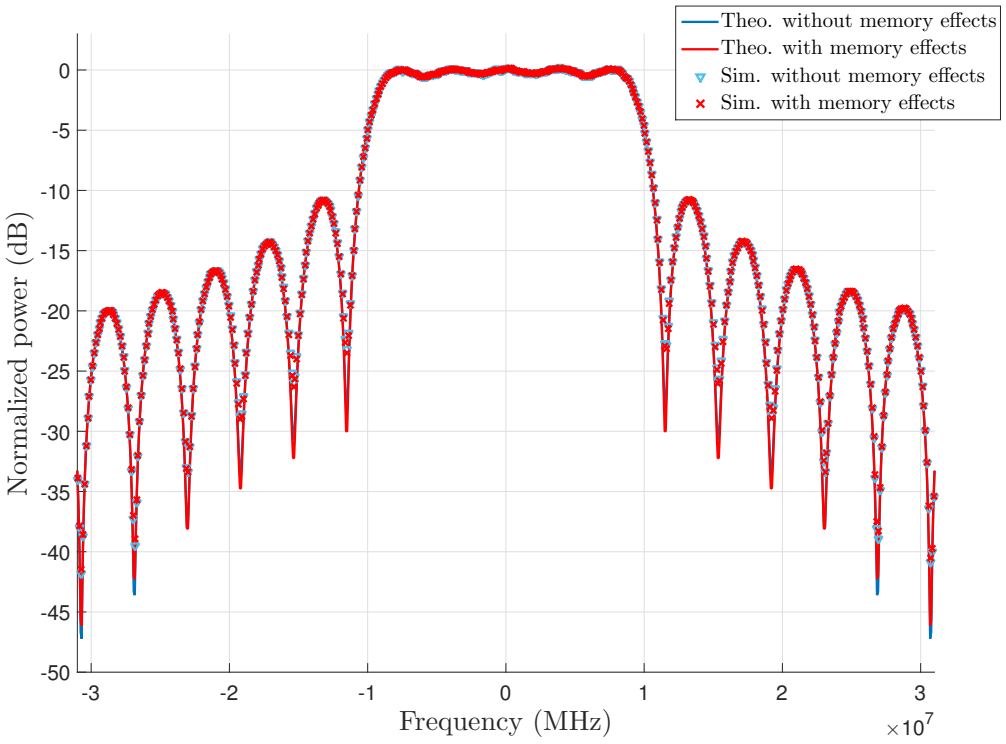

FIGURE 5.5 – PSD of amplified 16-QAM modulated signals with and without memory effects with $IBO = 6\ dB$ and $N = 5$.

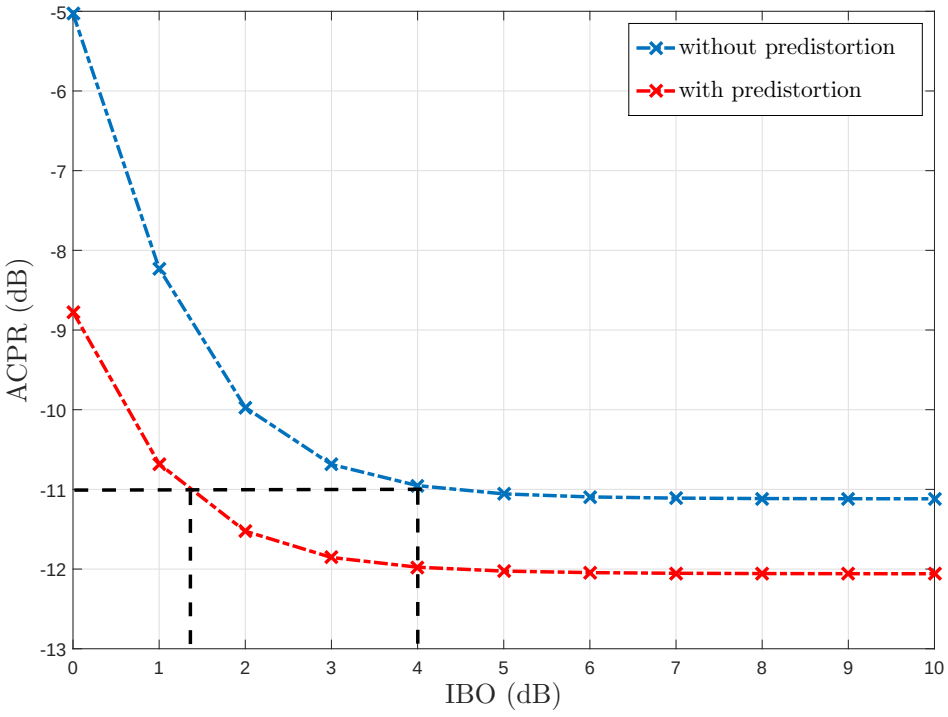

FIGURE 5.6 – ACPR as a function of the IBO for amplified 16-QAM modulated signals when predistortion is activated or deactivated with $N = 2$.

From the comparison between the theoretical and simulated PSD (Fig. 5.3), we conclude that our analytical results in (5.13) perfectly match the simulated PSD in both cases QPSK and 16-QAM modulations. This proves the accuracy of our proposed generalization of the PSD expression for any type of modulation. We can notice that the PSD of 16-QAM modulated signal, as expected, perfectly matches the PSD of QPSK modulated signal.

In a second step, simulations are led in both cases with and without predistortion with $N = 5$ and $IBO = 1\ dB$. To extract the predistortion coefficients, the in-direct learning and the least square algorithm are used. Fig. 5.4 depicts the PSD of the input and amplified 16-QAM modulated signals using the predistortion technique or not. As expected, the spectral regrowth in the adjacent channel of the amplified signal without predistortion is higher than the spectral regrowth when predistortion is activated.

Then, simulations are led in both cases with and without memory effects with $N = 5$ and $IBO = 6\ dB$ (Fig. 5.5). The values of polynomial coefficients b_{lq}, in both cases, were taken from [D$^+$04]. First of all, the theoretical curves perfectly match the simulated ones, proving the consistency of the proposed PSD expressions. Moreover, it is worth mentioning that the spectral regrowth when the memory effects are taking into account or not is almost the same.

Furthermore, we calculate the ACPR as a function of the IBO when predistortion is activated or not. From the curves in Fig. 5.6, we can see that the more the IBO decreases the more the ACPR increases which means that the spectral regrowth in the adjacent channel increases. Thus, suppose now that one targets the maximum PA efficiency and wants to know the minimum allowed IBO with respect to an ACPR constraint. Note that the more the IBO decreases, the more the PA efficiency increases. In this case, from the curves given by Fig. 5.6 according to (5.41) and (5.13), we can find the optimal IBO which maximizes the PA efficiency and satisfies the ACPR constraint when predistortion is activated or not. For example, if the ACPR constraint is equal to $-11\ dB$, we remark that the minimum IBO which satisfy the ACPR are $1.3\ dB$ and $4\ dB$ when predistortion is activated or not, respectively.

5.8 Conclusion

In this chapter, a generalization of the closed-form expression for the PSD of multicarrier signals for any type of modulation has been proposed. Then, to go further in the analysis, the study of the impact of memory effects on the PSD of the amplified multicarrier signals has been also investigated. Furthermore, we analytically derived the PSD expression of multicarrier signals distorted by non-linear PA taking into account the use of a predistortion step. We showed through simulations that the proposed expressions present very good accuracy. This work is then an important step in the analytical study of a global optimization approach of the transmitter efficiency and linearity. For example, with a given ACPR constraint, we can now analytically determine, in both cases with and without predistortion, the optimal IBO which maximizes the PA efficiency and satisfy the target ACPR. It is worthwhile to note that our proposed theoretical analyses could be very useful for optimizing future transmitter efficiency and linearity in the field of broadcasting applications for the deployment of DVB-T2 transmitters as well as for LTE

cellular networks.

Conclusion

Telecommunications pretty much runs our lives these days including our daily habits and our relationship with the world around us. From our work life to our home life, we have computers, smart phones, and gadgets helping us with our daily routine. Day after day, there is an increasing demand for faster transmission of voice, video, and multimedia applications. Nowadays, modern wireless and broadcast standards such as LTE and DVBT-2 with advanced modulation techniques are employed to offer a fast, reliable and secure transmission. However, these attractive services are not without its drawbacks. Indeed, the whole Information and Communication Technology (ICT) has a sizable carbon footprint and a huge energy consumption. As a consequence, it is estimated that the ICT produced 2% of the global CO_2 emission in 2007 which is equivalent to the aviation industry emission. Likewise, this amount of CO_2 emission is equivalent to one quarter of the emissions by all vehicles around the world [Gro08]. Besides, ICT sector is responsible for more than 2% of the worldwide primary energy consumption. As an example, it has been shown that around 3 million base stations consume 4.5 GW of power and cause approximately 20 Mt of CO_2 emission per year. Therefore, ICT energy consumption becomes a global crucial concern what industrials and researchers are trying to reduce.

Hence, one of the challenges for future communication systems is the reduction of energy consumption along with the associated CO_2 emission. In particular, the focus should be on minimizing base stations power consumption which consume about 80% of the total network energy and cause CO_2 emission very much more than mobile stations. In fact, the power consumption of a base station is mainly dominated by the radio equipment. Such radio equipment is especially critical as it provides a physical interface between the end users and the network. Therefore, it must guarantee a continuous flow of information while providing sufficient quality of service.

One of the most critical components in the wireless and broadcast communications systems implementation is the RF power amplifiers. In fact, the high PA accounts for 55-60% of the overall power consumption at full load in an LTE macro base station and requests focusing the energy efficiency improvements on this device [IP12]. Besides, due to the inherently nonlinear characteristics of the PA, another main concern in the PA design is the PA linearity. Unfortunately, the PA efficiency and the PA linearity are two conflicting requirements. Considering the PA characteristics and PA efficiency, one can remark that while the PA linearity increases, the PA efficiency decreases and vice versa especially when multicarrier modulations are used, because it exhibits a high Peak-to-Average-Power Ratio (PAPR). In fact, the high PAPR value of the multicarrier signals prevents radio-frequency designers to feed the signal at the optimal point of the PA characteristics

which reduces its energy consumption.

In literature, the two main approaches to solve the PAPR problem and the PA linearity-efficiency problematic are the PAPR reduction and linearization techniques. While the PAPR reduction techniques aim at reducing the dynamic range of the transmitted signal, the linearization techniques try to compensate for the PA nonlinearity. In this way, using the PAPR reduction and linearization techniques we can feed the signal at the most efficient PA operating point while respecting the linearity constraint. Indeed, one can remark that each of these two methods impacts both the linearity and the efficiency of the PA as they work in a complementary way.

However, unfortunately the PAPR reduction and linearization techniques have been designed separately and applied independently in conventional systems. With such implementation one technique can degrade the performance of the other. So, the study of the joint impact of the PAPR reduction and the linearization techniques on the PA linearity and efficiency should be well examined.

In this thesis, we propose to go a step beyond the conventional approach by introducing a new adaptive approach to control the PAPR reduction and linearization stages in a flexible way according to some predefined parameters. Our aim is to maximize the PA efficiency with respect to the linearity requirements. One can imagine a flexible transmitter model that controls these two stages according to incoming requirements and environment sensors to meet various target values related to different qualities of services.

In that perspective, we was involved in this thesis in the analytical derivation of the Error Vector Magnitude (EVM) and the Adjacent Chanel Power Ratio (ACPR) of multicarrier signals. EVM and ACPR are critical metrics and common figures of merit used to evaluate the quality of communication systems. While EVM measures the in band distortion, ACPR measures the out of band distortion. Consequently, novel analytical expressions were derived and a detailed theoretical study of the PA linearity-efficiency was proposed. Practical scenarios showed an interesting gain in term of PA efficiency while respecting the linearity requirements.

Hence, this analytical work is an important step in the study of the global optimization approach of the transmitter efficiency and linearity.

Contributions

Our contributions in this thesis are summarized as follows:

Firstly, we analyzed the impact of the in band nonlinearities of PAs on multicarrier signals, measured by the Error Vector Magnitude (EVM). We considered a transmitter structure in which clipping and predistortion techniques are available before the PA. The analytical EVM expressions of the output signal have been derived when the clipping and predistortion techniques are activated or not. Furthermore, the EVM expressions have been calculated for both Rapp and polynomial PA models. Simulation results compared to our proposed model confirm the accuracy of our analytical expressions. These analytical expressions could be favorably integrated in simulation models to validate the PAs behavior. Up to now, no analytical expression of the EVM, taking into account all the above mentioned nonlinearities, exists in the literature.

Secondly, we investigated the theoretical analysis of the PA linearity-efficiency trade off. Therefore, based on the EVM expressions, we provided an analytical expression which gives the optimal Input Power Back Off (IBO) and clipping threshold which must be taken to maximize the PA efficiency for any EVM constraint. Last but not least, we expanded our study to minimize the complexity of the predistortion technique with respect to an EVM constraint. Therefore, we sought to provide a joint configuration of the predistortion and clipping techniques which maximizes the PA efficiency taking into account the complexity of the predistortion technique and considering an EVM constraint.

Thirdly, since the PA memory effects become even more severe and can no longer be ignored, we quantified the PA memory effects by deriving closed-form EVM expressions of multicarrier signals distorted by a memory polynomial PA model with or without the use of a clipping technique. In fact, we provided analytical EVM expressions depending on the memory depth, PA coefficients, and PA order as well as the clipping threshold of the input signal.

Finally, we analyzed the impact of out of band nonlinearities of PAs on multicarrier signals. Indeed, we derived an analytical expression of the Power Spectral Density (PSD) of the predistorted nonlinear-amplified multicarrier signals. Consequently, thanks to our analytical expression we predict the spectral regrowth at the PA output which in turn causes adjacent channel interference (ACI). This interference is characterised by the Adjacent Channel Power Ratio (ACPR), which is a commonly used figure of merit to describe linearity in modem telecommunication systems. Suppose now that one targets the maximum PA efficiency with respect to a specific ACPR constraint. In addition, to go further in the analysis, the study of the impact of memory effects on the PSD of the amplified multicarrier signals has been also investigated. Based on our expression, we can find the optimal operating point of PA and the optimal configuration of predistortion which maximize the PA efficiency and satisfy the ACPR requirements taking into account or not the memory effects.

Perspectives

Many directions can be pursued to carry out some further researches. In our opinion, it would be interesting to consider the following listed aspects:

In this thesis, we considered the clipping technique as a PAPR reduction technique. This technique is widely used in practical implementation due to its simplicity and its straightforward reduction gain. Therefore, we derived the EVM expressions with the use or not of a clipping technique used as a PAPR reduction. In addition, our EVM expressions are also valid when a PAPR reduction which does not impact the amplitude distribution of the signal is used. An example of these PAPR reduction methods are the probabilistic techniques like Selective Mapping (SLM), and Partial Transmit Sequence (PTS), etc.... However, it could be interesting to derive the EVM expressions with the use of others PAPR reduction techniques especially the Tone Reservation (TR), and Active Constellation Extension (ACE) which are proposed to be optionally used in the modern wireless and broadcasting standards like DVBT-2, ATSC 3.0 and WiFi. To do so, a theoretical study of the impact of these PAPR reduction techniques on the distribution

of the amplitude signal should be done first. Then, using these new amplitude distributions, one can derive the new EVM expressions with the same methodology used in this thesis. In our opinion, it is worth to find such expressions which give new options for the decision engine and enhance the global PA linearity-efficiency compromise.

In Chapter 4, we proposed analytical study of the impact of the PA memory effects on the amplified multicarrier signal. Therefore, we derived the EVM expressions with the use or not of the clipping technique. We showed through simulations the impact of the PA memory on the signal fidelity. Note that the RF designers are trying to find more comprehensive approach to reveal the exact behavior of PAs including the memory effects in recent years. Therefore, the take into account of the predistortion technique could be a very important extension of our derived expressions.

In Chapter 5, we have proposed theoretical expressions of the Power Spectral Density (PSD) of the amplified multicarrier with or without memory effects. Moreover, we derived the PSD expression of the amplified multicarrier signal taking into account the predistortion technique. To the best of our knowledge, no analytical PSD expression taking into account the predistortion technique exists in literature. Such expressions are very useful for optimizing future transmitter efficiency and linearity. However, the PAPR reduction techniques are not considered. So it could be interesting to study the impact of the PAPR reduction technique on the PSD expressions. In addition, although the importance of these derived expressions, the implementation of these expressions was complex and the simulation duration was also too long. It is worth mentioning that even the proposed expressions of the PSD in literature were also so complex. Therefore, we think that it is interesting to make some approximation of these expressions in order to reduce the computational complexity. Thereafter, we think that the derivation of the closed-form expression of the Adjacent Channel Power Ratio (ACPR), defined by (5.5), using our derived expressions of the PSD, is the natural next step.

One of the challenging issue which could be addressed in future works is to study the link between the in band and the out of band distortions. In other word, the point is to analytically study the relationship between the two figures of merit investigated in this theses: EVM and ACPR. We think that these two characteristics are related to the global energy of the signal above a given threshold. Therefore, it could be interesting to go further in this analysis and analytically study the link between them. Then, it will be attractive if we find which is more critical, the EVM constraint or the ACPR constraint. The response on such question is very helpful and useful for the implementation of our decision engine as well as for radio frequency designers. In this way, the focus could be on one constraint, once we have verified the most critical constraint the other one will be automatically verified.

List of Figures

List of Tables

List of Acronyms

ACE Active Constellation Extension
ACI Adjacent Channel Interference
ACI Adjacent Channel Interference
ACLR Adjacent Channel Leakage Ratio
ACPR ACPRAdjacent Channel Power Ratio
ADSL Asymmetric Digital Subscriber Line
AM/AM Amplitude to Amplitude
AM/PM Amplitude to phase
ATSC Advanced Television Systems Committee
BER Bit Error Rate
BSs Base Stations
CCDF Complementary Cumulative Distribution Function
CP Cyclic Prefix
DAB Digital Audio Broadcasting
DFT Discrete Fourier Transform
DPD Digital PreDistortion
DSPs Digital Signal Processors
DVB-NGH DVB for Nex Generation Handheld
DVB-T2 Digital Video Broadcasting – Second Generation Terrestrial
ECMA European Computer Manufacturers Association
ETSI European Telecommunications Standards Institute
EVM Error Vector Magnitude
FFT Fast Fourier Transform
GSM Global System for Mobile Communications
HF High Frequency
HPAs High-Power Amplifiers
IBO Input power Back-Off
ICI Inter-Carrier Interference
ICT Information and Communication Technology
IDFT Inverse Discrete Fourier Transform
IFFT Inverse Fast Fourier Transform

i.i.d independent and identically distributed
ISDB-T Integrated Services Digital Broadcasting Terrestrial
ISI Inter-Symbol Interference
LTE Long Term Evolution
LTI Linear Time nvariant
MER Modulation Error Rate
OBO Output power Back-Off
OFDMA Orthogonal Frequency Division Multiple Access
OFDM Orthogonal Frequency Division Multiplexing
PAE Power Added Efficiency
PAPR Peak-to-Average Power Ratio
PA Power Amplifier
PDF Probability Density Function
PD PreDistortion
PDSCH Physical Downlink Shared Channel
PHY-UWB Ultra-Wideband UWB physical layer
POCS Projection-Onto-Convex-Sets
PSD Power Spectral Density
PSD Probability Spectral Density
PTS Partial Transmit Sequence
SLM Selective Mapping
SSPA Solid State Power Amplifiers
TEPN Toward Energy Proportional Networks
TI Tone Injection
TR Tone Reservation
VoD Video on Demand
WLAN Wireless Local Area Network
WPANs Wireless Personal Area Network
WiMAx Worldwide Interoperability for Microwave Access

Bibliography

[ACP] Universal mobile telecommunications system (umts) ; base station classification (tdd) (3gpp tr 25.952 version 5.0.0 release 5).

[AGG+11] G. Auer, V. Giannini, I. Godor, P. Skillermark, M. Olsson, M. A. Imran, D. Sabella, M. J. Gonzalez, C. Desset, and O. Blume. Cellular energy efficiency evaluation framework. In *Vehicular Technology Conference (VTC Spring), 2011 IEEE 73rd*, pages 1–6, May 2011.

[AW71] T. Arthanayake and H. B. Wood. Linear amplification using envelope feedback. *Electronics Letters*, 7(7) :145–146, April 1971.

[BAT+11] M. Brandon, M. Ariaudo, S. Traverso, J. Bouvier, I. Fijalkow, and J.L. Gautier. Linearity improvement thanks to the association of Active Constellation Extension and digital predistortion for OFDM. In *New Circuits and Systems Conference (NEWCAS), 2011 IEEE 9th International*, pages 293–296, June 2011.

[BB99] Sergio Benedetto and Ezio Biglieri. *Principles of Digital Transmission : With Wireless Applications*. Kluwer Academic Publishers, Norwell, MA, USA, 1999.

[BF82] S.A. Billings and S.Y. Fakhouri. Identification of systems containing linear dynamic and static nonlinear elements. *Automatica*, 18(1) :15 – 26, 1982.

[BFH96] Robert Bäuml, Robert Fischer, and Johannes Huber. Reducing the Peak to Average Power Ratio of Multicarrier Modulation by Selected Mapping. *Electronics Letters 32(22) :2056-2057*, 1996.

[BG89] W. Bosch and G. Gatti. Measurement and simulation of memory effects in predistortion linearizers. *IEEE Transactions on Microwave Theory and Techniques*, 37(12) :1885–1890, Dec 1989.

[BLG02] P. Banelli, G. Leus, and G.B. Giannakis. Bayesian estimation of clipped Gaussian processes with application to OFDM. In *Signal Processing Conference, 2002 11th European*, pages 1–4, Sept 2002.

[BP08] Kitaek Bae and E. J. Powers. Distribution of envelope power using selected mapping in ofdm systems with nonlinearity. In *2008 IEEE International Conference on Acoustics, Speech and Signal Processing*, pages 3065–3068, March 2008.

[Bra12] R.N. Braithwaite. Implementing crest factor reduction (CFR) by offsetting digital predistortion (DPD) coefficients. In *Integrated Nonlinear Microwave and Millimetre-Wave Circuits (INMMIC), 2012 Workshop on*, pages 1–3, Sept 2012.

[CG68] R. Chang and R. Gibby. A theoretical study of performance of an orthogonal multiplexing data transmission scheme. *IEEE Transactions on Communication Technology*, 16(4) :529–540, August 1968.

[Coo49] J. L. Coolidge. The Story of the Binomial Theorem. *The American Mathematical Monthly*, 1949.

[CP02] E. Costa and S. Pupolin. M-qam-ofdm system performance in the presence of a nonlinear amplifier and phase noise. *IEEE Transactions on Communications*, 50(3) :462–472, Mar 2002.

[CWT08] E. Cottais, Y. Wang, and S. Toutain. Spectral regrowth analysis at the output of a memoryless power amplifier with multicarrier signals. *IEEE Transactions on Communications*, 56 :1111–1118, July 2008.

[CY09] Li-Chung Chang and Chung-Ho Yang. A combined approach of MBAP/PR PAPR reduction and polynomial predistortion for performance enhancement. In *Information, Communications and Signal Processing, 2009. ICICS 2009. 7th International Conference on*, pages 1–5, Dec 2009.

[D+04] Lei Ding et al. A robust digital baseband predistorter constructed using memory polynomials. *Communications, IEEE Transactions on*, 52(1) :159–165, Jan 2004.

[Din04] Lei Ding. *Digital Predistortion of Power Amplifiers for Wireless Applications*. PhD thesis, School of Electrical and Computer Engineering, Georgia Institute of Technology, 2004.

[DJ99] J. A. Davis and J. Jedwab. Peak-to-mean power control in ofdm, golay complementary sequences, and reed-muller codes. *IEEE Transactions on Information Theory*, 45(7) :2397–2417, Nov 1999.

[DJK05] Ming Ding, Ben Jones, and Jaeweon Kim. Joint optimization of PAR reduction and digital predistortion for wireless LAN applications. In *Texas wireless symposium*. Citeseer, 2005.

[DLR96] A.N. D'Andrea, V. Lottici, and R. Reggiannini. Rf power amplifier linearization through amplitude and phase predistortion. *Communications, IEEE Transactions on*, 44(11) :1477–1484, Nov 1996.

[DMM+06] Lei Ding, Zhengxiang Ma, D. R. Morgan, M. Zierdt, and J. Pastalan. A least-squares/newton method for digital predistortion of wideband signals. *IEEE Transactions on Communications*, 54(5) :833–840, May 2006.

[DPD] Analog devices, 250 mhz bandwidth dpd observation receiver (ad6641).

[DRZ02] Lei Ding, Raviv Raich, and G.Tong Zhou. A hammerstein predistortion linearization design based on the indirect learning architecture. In *Acoustics, Speech, and Signal Processing (ICASSP), 2002 IEEE International Conference on*, volume 3, pages III–2689–III–2692, May 2002.

[DVT+10] M. Deruyck, W. Vereecken, E. Tanghe, W. Joseph, M. Pickavet, L. Martens, and P. Demeester. Comparison of power consumption of mobile wimax, hspa and lte access networks. In *Telecommunications*

Internet and Media Techno Economics (CTTE), 2010 9th Conference on, pages 1–7, June 2010.

[ETS01] ETSI. Digital Video Broadcasting (DVB) ; Measurement guidelines for DVB systems. Technical report, European Telecommunications Standards Institute V1.2.1, May 2001.

[EVM99] IEEE Standard for Telecommunications and Information Exchange Between Systems - LAN/MAN Specific Requirements , Dec 1999.

[EVM05] IEEE Standard for Local and Metropolitan Area Networks, Part 16, Amendment 2, 2005.

[FFMB11] A. Fehske, G. Fettweis, J. Malmodin, and G. Biczok. The global footprint of mobile communications : The ecological and economic perspective. *IEEE Communications Magazine*, 49(8) :55–62, August 2011.

[Fra] Marcelo Jorge Franco. *Wideband digital predistortion linearization of radio frequency power amplifiers with memory.* PhD thesis, Drexel University.

[GASK+09] S. Y. Le Goff, S. S. Al-Samahi, B. K. Khoo, C. C. Tsimenidis, and B. S. Sharif. Selected mapping without side information for papr reduction in ofdm. *IEEE Transactions on Wireless Communications*, 8(7) :3320–3325, July 2009.

[GCW+13] F. Gregorio, J. Cousseau, S. Werner, T. Riihonen, and R. Wichman. EVM Analysis for Broadband OFDM Direct-Conversion Transmitters. *IEEE Trans. Veh. Technol*, 62(7) :3443–51, 2013.

[GGS99] K. G. Gard, H. M. Gutierrez, and M. B. Steer. Characterization of spectral regrowth in microwave amplifiers based on the nonlinear transformation of a complex gaussian process. *IEEE Transactions on Microwave Theory and Techniques*, 47(7) :1059–69, 1999.

[GL12a] O. Abel Gouba and Yves Louet. Theoretical analysis of the trade-off between efficiency and linearity of the high power amplifier in OFDM context. In *European Wireless, 2012. EW. 18th European Wireless Conference*, pages 1–7, April 2012.

[GL12b] O.A. Gouba and Y. Louet. Predistortion performance considering peak to average power ratio reduction in ofdm context. In *Wireless Communications and Networking Conference (WCNC), 2012 IEEE*, pages 204–208, April 2012.

[GMB05] P. Gilabert, G. Montoro, and E. Bertran. On the wiener and hammerstein models for power amplifier predistortion. In *2005 Asia-Pacific Microwave Conference Proceedings*, volume 2, pages 4 pp.–, Dec 2005.

[GOU13] Oussoulare Abel GOUBA. *Approche conjointe de la reduction du facteur de crete et de la linearisation dans le contexte ofdm.* PhD thesis, Ecole Doctorale MATISSE, 2013.

[Gro08] The Climate Group. Smart2020 : Enabling the low carbon economy in the information age. Technical report, 2008.

[H+13] H. Hemesi et al. Analytical Modeling of MIMO-OFDM System in the Presence of Nonlinear Power Amplifier with Memory. *on IEEE Trans. Commun*, 61(1) :155–63, Jan. 2013.

[HCVG09] O. Hammi, S. Carichner, B. Vassilakis, and F. M. Ghannouchi. Effects of crest factor reduction on the predistortion performance for multi-carrier 3g rf power amplifiers. In *2009 IEEE MTT-S International Microwave Symposium Digest*, pages 1085–1088, June 2009.

[HWPL08] Su Hu, Gang Wu, Jing-Jing Ping, and Shao-Qian Li. HPA Nonlinearity Reduction by Joint Predistorter and Tone-Reservation with Null Subcarriers in WiMAX Systems. In *Circuits and Systems for Communications, 2008. ICCSC 2008. 4th IEEE International Conference on*, pages 187–190, May 2008.

[HWW+10] Su Hu, Gang Wu, Qingsong Wen, Yue Xiao, and Shaoqian Li. Nonlinearity Reduction by Tone Reservation with Null Subcarriers for WiMAX System. *Wireless Personal Communications*, 54(2) :289–305, 2010.

[INM89] N. Imai, T. Nojima, and T. Murase. Novel linearizer using balanced circulators and its application to multilevel digital radio systems. *IEEE Transactions on Microwave Theory and Techniques*, 37(8) :1237–1243, Aug 1989.

[IP12] M A Imran and Project Partners. Energy efficiency analysis of the reference systems, areas of improvements and target breakdown. Technical report, EARTH Project Report, Deliverable D2.3, 2012.

[JBS00] Michel C. Jeruchim, Philip Balaban, and K. Sam Shanmugan, editors. *Simulation of Communication Systems : Modeling, Methodology and Techniques*. Kluwer Academic Publishers, Norwell, MA, USA, 2nd edition, 2000.

[Jon99] D. L. Jones. Peak power reduction in ofdm and dmt via active channel modification. In *Conference Record of the Thirty-Third Asilomar Conference on Signals, Systems, and Computers (Cat. No.CH37020)*, volume 2, pages 1076–1079 vol.2, Oct 1999.

[JW08] T. Jiang and Y. Wu. An overview : Peak-to-average power ratio reduction techniques for ofdm signals. *IEEE Transactions on Broadcasting*, 54(2) :257–268, June 2008.

[JWB94] A. E. Jones, T. A. Wilkinson, and S. K. Barton. Block coding scheme for reduction of peak to mean envelope power ratio of multicarrier transmission schemes. *Electronics Letters*, 30(25) :2098–2099, Dec 1994.

[JZZ04] Tao Jiang, Guangxi Zhu, and Jianbin Zheng. Block coding scheme for reducing papr in ofdm systems with large number of subcarriers. *Journal of Electronics*, 21(6) :482–489, 2004.

[Kaz08] M.K. Kazimierczuk. *RF Power Amplifiers*. Wiley, 2008.

[KC06] J.S. Kenney and Jau-Horng Chen. Power Amplifier Linearization and Efficiency Improvement Techniques for Commercial and Military Applications. In *Microwaves, Radar Wireless Communications, 2006. MIKON 2006. International Conference on*, pages 3–8, May 2006.

[Ken00a] Peter B. Kenington. *High Linearity RF Amplifier Design*. Artech House, Inc., Norwood, MA, USA, 1st edition, 2000.

[Ken00b] Peter B. Kenington. *High Linearity RF Amplifier Design*. Artech House, Inc., Norwood, MA, USA, 1st edition, 2000.

[KHNSL10] I. Kotzer, S. Har-Nevo, S. Sodin, and S. Litsyn. An analytical approach to the calculation of evm in clipped ofdm signals. In *Electrical and Electronics Engineers in Israel (IEEEI), 2010 IEEE 26th Convention of*, pages 000193–000197, Nov 2010.

[KHNSL12] I. Kotzer, S. Har-Nevo, S. Sodin, and S. Litsyn. An Analytical Approach to the Calculation of EVM in Clipped Multi-Carrier Signals. *Communications, IEEE Transactions on*, 60(5) :1371–1380, May 2012.

[KJ03a] B. S. Krongold and D. L. Jones. Par reduction in ofdm via active constellation extension. In *Acoustics, Speech, and Signal Processing, 2003. Proceedings. (ICASSP '03). 2003 IEEE International Conference on*, volume 4, pages IV–525–8 vol.4, April 2003.

[KJ03b] B.S. Krongold and D.L. Jones. PAR reduction in OFDM via active constellation extension. *Broadcasting, IEEE Transactions on*, 49(3) :258–268, Sept 2003.

[KJ03c] B.S. Krongold and D.L. Jones. PAR reduction in OFDM via active constellation extension. *Broadcasting, IEEE Transactions on*, 49(3) :258–268, Sept 2003.

[KK01a] J. Kim and K. Konstantinou. Digital predistortion of wideband signals based on power amplifier model with memory. *Electronics Letters*, 37(23) :1417–1418, Nov 2001.

[KK01b] J. Kim and K. Konstantinou. Digital predistortion of wideband signals based on power amplifier model with memory. *Electronics Letters*, 37(23) :1417–1418, Nov 2001.

[KNSO08] Satoshi Kimura, Takashi Nakamura, Masato Saito, and Minoru Okada. Par reduction for ofdm signals based on deep clipping. In *Communications, Control and Signal Processing, 2008. ISCCSP 2008. 3rd International Symposium on*, pages 911–916, March 2008.

[LC97] Xiaodong Li and L.J. Cimini. Effects of clipping and filtering on the performance of OFDM. In *VTC, 1997, IEEE 47th*, volume 3, pages 1634–1638, May 1997.

[LHLM11] C. Langlais, S. Haddad, Y. Louet, and N. Mazouz. Clipping noise mitigation with capacity approaching fec codes for papr reduction of ofdm signals. In *Multi-Carrier Systems Solutions (MC-SS), 2011 8th International Workshop on*, pages 1–5, May 2011.

[Lis09] David Lister. An Operator's view on Green Radio. Technical report, Vodafone Group Research & Development, 2009.

[LJSO12] A. Louliej, Y. Jabrane, B. A. E. Said, and A. A. Ouahman. Reduction of power envelope fluctuations in ecma-368 ultra wideband communication system. In *2012 International Conference on Multimedia Computing and Systems*, pages 449–453, May 2012.

[LP05] Yves Louët and Jacques Palicot. Synthèse de la notion de facteur de crête et application aux modulations monoporteuse. In *20e Colloque*

GRETSI sur le traitement du signal et des Images, Louvain-la-Neuve, Belgium, September 2005.

[LP08a] Yves Louët and Jacques Palicot. A classification of methods for efficient power amplification of signals. *Annals of Telecommunications - annales des télécommunications*, 63(2008-08-07) :351–368, August 2008.

[LP08b] Yves Louët and Jacques Palicot. A classification of methods for efficient power amplification of signals. *annals of telecommunications - annales des télécommunications*, 63(7) :351–368, 2008.

[LTE12] LTE ; Evolved Universal Terrestrial Radio Access (E-UTRA) ; Base Station (BS) radio transmission and reception , 2012.

[Mat01] D. Matic. *OFDM Synchronization and Wideband Power Measurements at 60 GHz for Future Wireless Broadband Multimedia Communication.* PhD thesis, Aalborg University, Denmark, September 2001.

[MH97] S. H. Muller and J. B. Huber. Ofdm with reduced peak-to-average power ratio by optimum combination of partial transmit sequences. *Electronics Letters*, 33(5) :368–369, Feb 1997.

[Mir08] T. Miracco. Crest factor reduction and digital pre-distortion for wireless RF power amplifier optimization. In *Solid-State and Integrated-Circuit Technology, 2008. ICSICT 2008. 9th International Conference on*, pages 1357–1360, Oct 2008.

[MMK+06] D. R. Morgan, Z. Ma, J. Kim, M. G. Zierdt, and J. Pastalan. A generalized memory polynomial model for digital predistortion of rf power amplifiers. *IEEE Transactions on Signal Processing*, 54(10) :3852–3860, Oct 2006.

[MR98] T. May and H. Rohling. Reducing the peak-to-average power ratio in ofdm radio transmission systems. In *Vehicular Technology Conference, 1998. VTC 98. 48th IEEE*, volume 3, pages 2474–2478 vol.3, May 1998.

[NG66] K. Narendra and P. Gallman. An iterative method for the identification of nonlinear systems using a hammerstein model. *IEEE Transactions on Automatic Control*, 11(3) :546–550, Jul 1966.

[NP00] Richard van Nee and Ramjee Prasad. *OFDM for Wireless Multimedia Communications.* Artech House, Inc., Norwood, MA, USA, 1st edition, 2000.

[OI02] H. Ochiai and H. Imai. Performance analysis of deliberately clipped ofdm signals. *IEEE Transactions on Communications*, 50(1) :89–101, Jan 2002.

[Pop91] B. M. Popovic. Synthesis of power efficient multitone signals with flat amplitude spectrum. *IEEE Transactions on Communications*, 39(7) :1031–1033, Jul 1991.

[PR80] A. Peled and A. Ruiz. Frequency domain data transmission using reduced computational complexity algorithms. In *Acoustics, Speech, and Signal Processing, IEEE International Conference on ICASSP '80.*, volume 5, pages 964–967, Apr 1980.

[Pra98] Ramjee Prasad. *Universal Wireless Personal Communications*. Artech House, Inc., Norwood, MA, USA, 1st edition, 1998.

[Pri14] IT) Priotti, Paolo (Turin. Papr reduction in multi-carrier-carrier transmission, January 2014.

[Rap91] C. Rapp. Effects of HPA-nonlinearity on a 4-DPSK/OFDM-signal for a digital sound broadcasting signal. In P. S. Weltevreden, editor, *ESA Special Publication*, volume 332 of *ESA Special Publication*, October 1991.

[RHL+04] Heung-Gyoon Ryu, Tran Phuong Hoa, Kang Mi Lee, Sang-Woo Kim, and Jin-Soo Park. Improvement of power efficiency of HPA by the PAPR reduction and predistortion. *Consumer Electronics, IEEE Transactions on*, 50(1) :119–124, Feb 2004.

[RL03] Heung-Gyoon Ryu and Yun-Hee Lee. A new combined method of the block coding and predistortion for the nonlinear distortion compensation. *Consumer Electronics, IEEE Transactions on*, 49(1) :27–31, Feb 2003.

[RPLL06a] Salvatore Ragusa, Jacques Palicot, Yves Louët, and Christian Lereau. Invertible Clipping for Increasing the Power Efficiency of OFDM Amplification. In *ICT 2006*, Funchal (Madère), Portugal, 2006.

[RPLL06b] Salvatore Ragusa, Jacques Palicot, Yves Louët, and Christian Lereau. Invertible Clipping for Increasing the Power Efficiency of OFDM Amplification. In *ICT 2006*, pages 1–6, Funchal (Madère), Portugal, 2006.

[RS06] Patrick Reynaert and Michiel Steyaert. Rf power amplifiers for mobile communications, 2006.

[RZ01] R. Raich and G. T. Zhou. Analyzing spectral regrowth of QPSK and OQPSK signals. In *Acoustics, Speech, and Signal Processing, Proceedings. (ICASSP '01). IEEE International Conference on*, volume 4, pages 2673–2676 vol.4, 2001.

[RZ04] R. Raich and G. T. Zhou. Spectral analysis for bandpass nonlinearity with cyclostationary input. In *Acoustics, Speech, and Signal Processing,Proceedings. (ICASSP '04), IEEE International Conference on*, volume 2, pages 465–8, May 2004.

[S28] B.H. S. Translating system, October 9 1928. US Patent 1,686,792.

[Sal81] A. A. M. Saleh. Frequency-independent and frequency-dependent nonlinear models of twt amplifiers. *IEEE Transactions on Communications*, 29(11) :1715–1720, November 1981.

[SC92] S. P. Stapleton and F. C. Costescu. An adaptive predistorter for a power amplifier based on adjacent channel emissions [mobile communications]. *IEEE Transactions on Vehicular Technology*, 41(1) :49–56, Feb 1992.

[Sch06] Martin Schetzen. *The Volterra and Wiener Theories of Nonlinear Systems*. Krieger Publishing Co., Inc., Melbourne, FL, USA, 2006.

[SO16] J. Song and H. Ochiai. Performance analysis for ofdm signals with peak cancellation. *IEEE Transactions on Communications*, 64(1) :261–270, Jan 2016.

[SPCK04] R. Sperlich, Y. Park, G. Copeland, and J.S. Kenney. Power amplifier linearization with digital pre-distortion and crest factor reduction. In *Microwave Symposium Digest, 2004 IEEE MTT-S International*, volume 2, pages 669–672 Vol.2, June 2004.

[spe] Wireless lan medium access control (mac) and physical layer (phy) specifications.

[SSS03] W. B. Sander, S. V. Schell, and B. L. Sander. Polar modulator for multi-mode cell phones. In *Custom Integrated Circuits Conference, 2003. Proceedings of the IEEE 2003*, pages 439–445, Sept 2003.

[TC98] J. Tellado and J. M. Cioffi. Efficient algorithms for reducing par in multicarrier systems. In *Information Theory, 1998. Proceedings. 1998 IEEE International Symposium on*, pages 191–, Aug 1998.

[Tec10] AN10945 174 MHz to 230 MHz DVB-T power amplifier with the BLF881. Technical report, NXP Semiconductors, 2010.

[Tel01] C. Tellambura. Computation of the continuous-time par of an ofdm signal with bpsk subcarriers. *IEEE Communications Letters*, 5(5) :185–187, May 2001.

[TMoEE99] J. Tellado-Mourelo and Stanford University. Dept. of Electrical Engineering. *Peak to Average Power Reduction for Multicarrier Modulation*. Stanford University, 1999.

[vNdW98] R. van Nee and A. de Wild. Reducing the peak-to-average power ratio of ofdm. In *Vehicular Technology Conference, 1998. VTC 98. 48th IEEE*, volume 3, pages 2072–2076 vol.3, May 1998.

[VRM01a] J. H. K. Vuolevi, T. Rahkonen, and J. P. A. Manninen. Measurement technique for characterizing memory effects in RF power amplifiers. *IEEE Transactions on Microwave Theory and Techniques*, 49(8) :1383–1389, Aug 2001.

[VRM01b] J. H. K. Vuolevi, T. Rahkonen, and J. P. A. Manninen. Measurement technique for characterizing memory effects in RF power amplifiers. *IEEE Transactions on Microwave Theory and Techniques*, 49(8) :1383–1389, Aug 2001.

[Was04] Hugo Durney Wasaff. *Adaptive Pre-Distortion for Nonlinear High Power Amplifiers in OFDM Systems*. PhD thesis, Universitat Politècnica de Catalunya, 2004.

[WE71a] S. Weinstein and P. Ebert. Data transmission by frequency-division multiplexing using the discrete fourier transform. *IEEE Transactions on Communication Technology*, 19(5) :628–634, October 1971.

[WE71b] S. Weinstein and P. Ebert. Data transmission by frequency-division multiplexing using the discrete fourier transform. *IEEE Transactions on Communication Technology*, 19(5) :628–634, October 1971.

[YWC+02] Youngoo Yang, Young Yun Woo, Jeonghyeon Cha, Jaehyok Yi, and Bumman Kim. New linearization method for the modulated signals with high peak-to-average ratio : peak-to-average ratio reduction and expansion. In *2002 IEEE MTT-S International Microwave Symposium Digest (Cat. No.02CH37278)*, volume 2, pages 777–780 vol.2, June 2002.

[Zho00] G. T. Zhou. Analysis of spectral regrowth of weakly nonlinear power amplifiers. *IEEE Communications Letters*, 4 :357–9, Nov 2000.

[ZPLL06] S. Zabre, J. Palicot, Y. Louet, and C. Lereau. Socp approach for ofdm peak-to-average power ratio reduction in the signal adding context. In *2006 IEEE International Symposium on Signal Processing and Information Technology*, pages 834–839, Aug 2006.

[ZR] G. Tong Zhou and Raviv Raich. Spectral analysis of polynomial nonlinearity with applications to rf power amplifiers. *EURASIP Journal on Advances in Signal Processing*, 2004(12) :1–10.

[Zwi] Daniel Zwillinger. *Table of integrals, series, and products.* Elsevier (2014).

[ZWS+01] S. A. Zekavat, D. Wiegandt, S. Shattil, B. Natarajan, and Z. Wu. *Multi-Carrier Technologies for Wireless Communication.* Kluwer Academic Publishers, Norwell, MA, USA, 2001.

INSA de RENNES
Service des Formations

AVIS DU JURY SUR LA REPRODUCTION DE LA THESE SOUTENUE

Titre de la thèse:
Analytical analysis of in-band and out-of-band distortions for multicarrier signals: impact of non-linear amplification, memory effects and predistortion

Nom Prénom de l'auteur : CHEAITO ALI

Membres du jury :
- Madame BAUDOIN Geneviève
- Monsieur HELARD Jean-François
- Monsieur CRUSSIERE Matthieu
- Monsieur QUERE Raymond
- Madame FIJALKOW Inbar
- Monsieur ROS Laurent
- Monsieur LOUET Yves

Président du jury : R. QUÉRÉ

Date de la soutenance : 10 Mars 2017

Reproduction de la these soutenue

Thèse pouvant être reproduite en l'état
~~Thèse pouvant être reproduite après corrections suggérées~~

Fait à Rennes, le 10 Mars 2017

Signature du président de jury

Le Directeur,

M'hamed DRISSI

INSTITUT NATIONAL des SCIENCES APPLIQUÉES - RENNES -

Résumé

Les techniques multiporteuses de type OFDM sont aujourd'hui largement déployées dans tous les systèmes de communication sans fils notamment dans les réseaux cellulaires (LTE), les réseaux de diffusion (DVB) ou encore les réseaux WiFi. Cependant, les modulations multiporteuses se caractérisent par une très grande dynamique mesurée par le Peak to Average Power Ratio (PAPR), ce qui empêche d'alimenter l'amplificateur de puissance non linéaire (utilisé avant l'émission des signaux) à son point optimal et ainsi conduit à diminuer son efficacité énergétique. Des techniques de réduction du PAPR peuvent alors être mises en œuvre pour réduire le PAPR du signal et des techniques de pré-distorsion peuvent alors être utilisées pour compenser les non-linéarités de l'amplificateur de puissance.

L'approche développée dans le cadre de cette thèse a pour objectif d'étudier une solution intelligente pour les implémentations futures pour contrôler la réduction du PAPR et les étapes de linéarisation de manière flexible en fonction de certains paramètres prédéfinis afin qu'ils deviennent adaptatifs et auto-configurables. Plus précisément, notre travail a principalement porté sur l'analyse des différentes distorsions dans la bande (*in-band distortions*) mesurées par l'EVM ou Error Vector Magnitude et en dehors de la bande de transmission (*out-of-band distortions*) mesurées par l'ACPR ou Adjacent Channel Power Ratio de signaux à porteuses multiples.

En particulier de nombreux résultats analytiques complétés par des résultats de simulation permettant d'évaluer l'EVM et l'ACPR en fonction des caractéristiques de l'amplification non-linéaire en prenant en compte ou pas l'effet mémoire de l'amplificateur et la mise en œuvre de techniques d'écrêtage et de pré-distorsion ont été obtenus. Ces résultats constituent une étape importante dans l'optimisation globale de la complexité, de la linéarité et de l'efficacité énergétique des émetteurs aussi bien pour la diffusion de la télévision numérique que pour les réseaux cellulaires de 4ème génération (LTE) ou de 5ème génération.

Abstract

OFDM multicarrier techniques are now widely deployed in most wireless communication systems, in particular in cellular networks (LTE), broadcast networks (DVB) and WiFi networks. However, multi-carrier modulations are characterized by a very large dynamic amplitude measured by the Peak to Average Power Ratio (PAPR), which prevents radio frequency designers to feed the signal at the optimal point of the Power Amplifier (PA) which reduces the PA energy efficiency. In literature, the PAPR reduction and linearization techniques are the main approaches to solve the PAPR problem, the PA nonlinearities problem, as well as the low PA efficiency problem.

The approach developed in this thesis was to study an intelligent solution for future implementations to control the reduction of PAPR and the linearization steps in a flexible way according to some predefined parameters so that they become adaptive and self-configurable. More specifically, our work focused on the analytical analysis of in-band measured by the Error Vector Magnitude (EVM) and out-of-band distortions measured by the Adjacent Chanel Power Ratio (ACPR) for clipped multicarrier signals taking into account the impact of non-linear amplification, memory effects and predistortion.

In particular, many analytical results complemented by simulation results to evaluate the EVM and ACPR are proposed. These analytical expressions depend on the PA characteristics taking into account or not the PA memory effects and the use of clipping and pre-distortion techniques. It is worthwhile to note that our proposed theoretical analyses could be very useful for optimizing future transmitter efficiency and linearity in the field of broadcasting applications for the deployment of DVB-T2 transmitters as well as for LTE cellular networks.

INSA RENNES

N° d'ordre : **17ISAR 03 / D17 -03**

Institut National des Sciences Appliquées de Rennes
20, Avenue des Buttes de Coësmes - CS 14315 - F-35043 Rennes Cedex
Tél : 02 23 23 82 00 – Fax : 02 23 23 83 96